Advances
in Clinical and Experimental Medicine

Wroclaw
Medical University

Advances
in Clinical and Experimental
Medicine

Editorial Policy

Contents

Atrial functional mitral regurgitation: Insufficiently understood and recognized

Frank A. Flachskampf[1,2,B,D–F]

[1] Department of Clinical Physiology and Cardiology, Uppsala University Hospital, Sweden

[2] Department of Medical Sciences, Uppsala University, Sweden

A – research concept and design; B – collection and/or assembly of data; C – data analysis and interpretation;
D – writing the article; E – critical revision of the article; F – final approval of the article

Address for correspondence
Frank A. Flachskampf
E-mail: frank.flachskampf@medsci.uu.se

Abstract

Atrial functional mitral regurgitation (AFMR) is a form of functional mitral regurgitation that is still insufficiently recognized and characterized. The driving cause of AFMR is atrial, not ventricular dilatation, usually due to long-standing atrial fibrillation, and often in association with left ventricular diastolic dysfunction and heart failure with preserved ejection fraction (HFpEF). An increase in mitral annular area leads to a loss of central coaptation of the leaflets, often resulting in an "override" configuration and flattening of the annulus, as well as a loss of annular contraction. The left ventricle (LV) has a normal size; thus, there is usually only minor tenting of the leaflets. The regurgitant jet is mostly central, although posterior jet direction also occurs, frequently in a subform with posterior leaflet tethering and a marked localized dilatation of the posterior annulus. Because of the normal-sized and normally or nearly normally contracting LV, the amount of regurgitation is typically not more than moderate (or moderate-to-severe). Over time, functional mitral regurgitation may become mixed atrial and ventricular, with remodeling of the LV. However, the time course and the relation to symptoms have yet to be elucidated. This review presents current concepts and published insights into this form of mitral regurgitation.

Key words: mitral valve regurgitation, heart failure, valvular heart disease

Background

Mitral regurgitation (MR) is traditionally classified as:

(1) primary (acute or chronic), typically due to mitral valve prolapse, flail, endocarditis, papillary muscle rupture, cleft, or other diseases causing a structural abnormality of the leaflets or subvalvular apparatus; or

(2) secondary, due to chronic pathologic changes originating in non-valvular structures, most often eccentric remodeling of the left ventricle (LV) leading to changed mechanics of the subvalvular apparatus with an eccentric pull of the papillary muscles on the mitral leaflets, a constellation of the closed leaflets described as tenting, and the dilatation of the mitral annulus.

Another form of secondary or functional MR is atrial functional mitral regurgitation (AFMR), where the causative mechanism is atrial dilatation, typically due to atrial fibrillation. This form of MR is less common than ventricular secondary or functional MR (VFMR). Certainly, there are overlaps between atrial and ventricular forms of functional MR, and probably both can initiate vicious circles leading to mixed forms of functional MR. However, AFMR occurs without VFMR, and has received less attention and has been less clearly characterized than VFMR. In the following paper, we will briefly review the existing concepts and published data on AFMR.

Definition and mechanism

Atrial functional mitral regurgitation occurs due to atrial dilatation, and in the majority of cases due to long-standing atrial fibrillation, flutter or tachycardia. Atrial dilatation leads to mitral annular dilatation and flattening, pulling the mitral leaflets apart and causing central malcoaptation of the leaflet tips, often in the form of an "override" constellation, or a frank gap between the tips of the leaflets (Fig. 1). Decreased annular contraction during the cardiac cycle contributes to the leakage. Pronounced tenting is not typical for isolated AFMR, since there is no eccentric pull of the papillary muscles. The regurgitant jet is usually central, although posteriorly directed jets may also occur (see
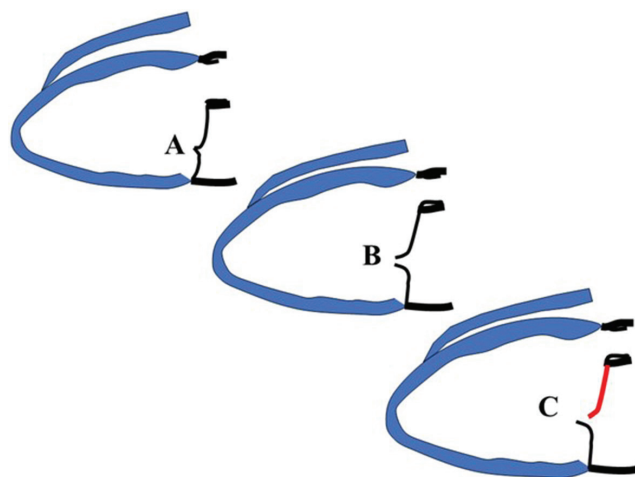
Fig. 1. Schematic drawing of hypothetic evolution of atrial functional mitral regurgitation (AFMR) with progressive dilatation of the left atrium (LA). Left (A) – normal anatomy in systole, no mitral regurgitation. Note slight concavity of mitral leaflet bodies towards left ventricle (LV), but no prolapse. Center (B) – dilated LA with central gap between the leaflets; loss of concavity of leaflets towards LV. There is functional atrial mitral regurgitation through the central gap due to disparity between leaflet size and annular orifice size. Right (C) – further enlargement of LA. There is an "anterior leaflet override" configuration of the mitral valve with tethering of the posterior leaflet and a systolic anterior leaflet (in red) tip position on the atrial side of the posterior leaflet, with further increase in mitral regurgitation

the last paragraph of this section). The LV by definition is not dilated in pure AFMR and shows normal or near-normal ejection fraction.[1–5] Since AFMR leads to a volume load of the left atrium (LA), it reinforces atrial dilatation in a vicious circle. Therefore, in its strict sense, AFMR requires a substantially dilated LA, mostly, but not always associated with atrial fibrillation or flutter, a normal sized LV with normal or slightly reduced ejection fraction, and a mitral valve without major structural abnormalities such as major tenting, prolapse or leaflet restriction; however, a small amount of tenting may be present (Table 1). The mechanism of regurgitation is a central leakage, often caused by an "override" configuration of the leaflets where the tip of one leaflet, mostly the posterior, is positioned on the atrial side of the other (mostly anterior), hence "overriding" the anterior leaflet without prolapsing beyond

Table 1. Defining features of isolated atrial functional mitral regurgitation (AFMR) compared to ventricular functional mitral regurgitation (VFMR) (adapted from Zoghbi et al.[5])

Features and parameters	AFMR	VFMR
Left atrial size	very dilated	dilated
LV size	normal	dilated
LV function	normal or mildly reduced (EF $\geq$ 40%)	mostly reduced
Mitral leaflet configuration	no or minor tenting, with a loss of concavity towards the LV; possible anterior leaflet override and posterior leaflet tethering	progressive tenting of both leaflets
Mitral annulus diameter/area	very dilated	dilated
Prevalence of atrial fibrillation	very high (>50%)	approx. 30%
Mitral regurgitant jet direction	central, sometimes posterior	central, sometimes posterior

LV – left ventricle; EF – ejection fraction. Note that the presence of mixed AFMR and VFMR is probably clinically not rare.
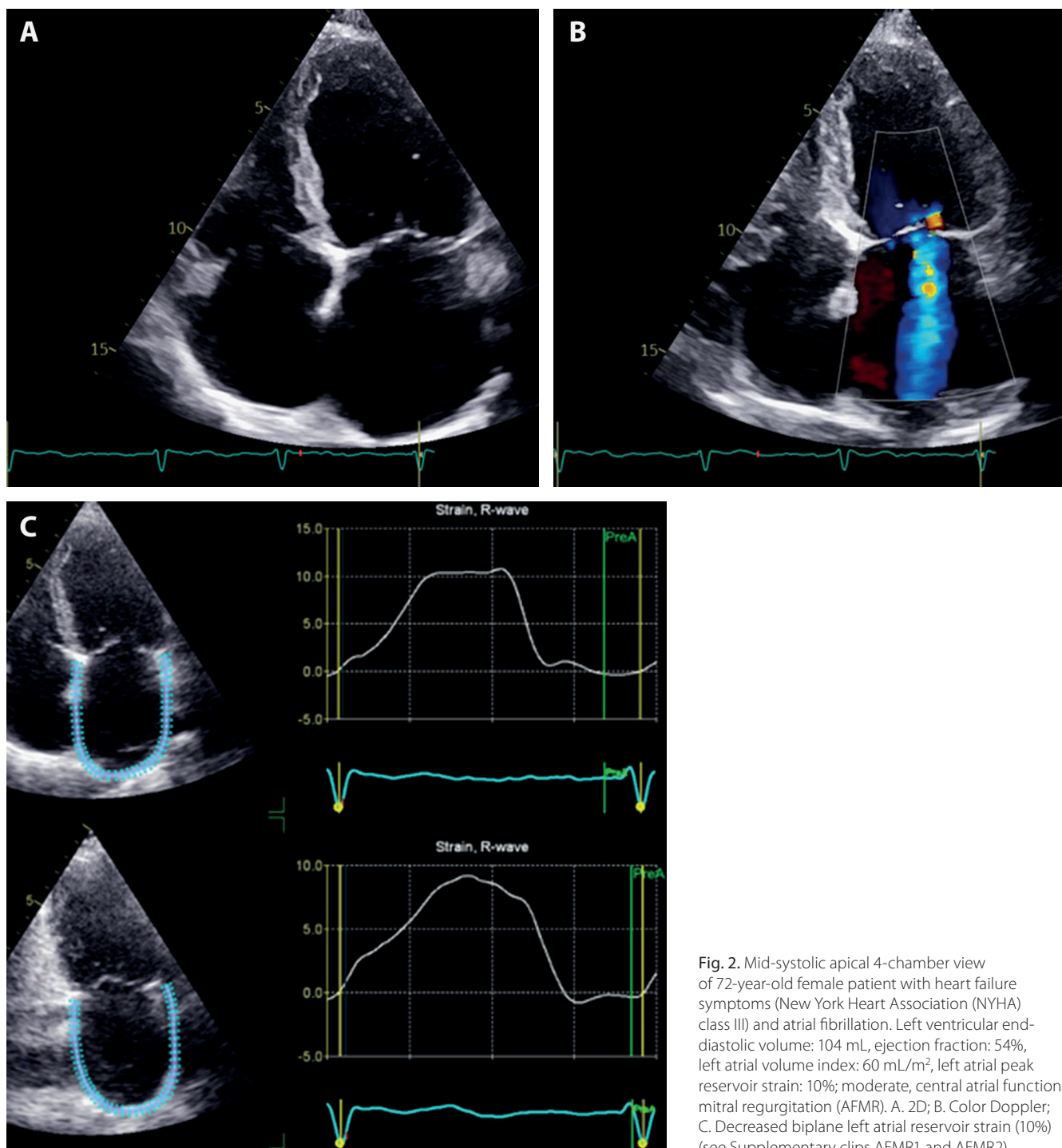
Fig. 2. Mid-systolic apical 4-chamber view of 72-year-old female patient with heart failure symptoms (New York Heart Association (NYHA) class III) and atrial fibrillation. Left ventricular end-diastolic volume: 104 mL, ejection fraction: 54%, left atrial volume index: 60 mL/m², left atrial peak reservoir strain: 10%; moderate, central atrial functional mitral regurgitation (AFMR). A. 2D; B. Color Doppler; C. Decreased biplane left atrial reservoir strain (10%) (see Supplementary clips AFMR1 and AFMR2)

the annular level. The resulting jet is mostly central, but can be posteriorly directed (see Fig. 2).

The initial causative mechanism of AFMR can be understood as a disparity between the enlarged and flattened mitral annulus and the disposable leaflet area to seal it during systole. The 3D echocardiography has shown that the amount of AFMR relates to the magnitude of this disparity.[2] The mitral apparatus is able to at least partially compensate for annular enlargement by initiating leaflet growth, and this compensatory growth can be inhibited in animal models of VFMR by cyproheptadine.[6] Hence,

it is possible that the described vicious circle of AFMR is amenable to beneficial modulation by drugs.

In the further course of the disease, the volume load of the regurgitant mitral volume likely affects the – initially normal – LV, leading to left ventricular dilatation and mixed atrial and ventricular FMR, with typical tenting configuration of the mitral valve. However, the time course of AFMR, and whether it inexorably leads to VFMR, has not been systematically studied.

The association of AFMR with atrial fibrillation, which analogously can lead on the right side of the heart

to functional tricuspid regurgitation, implies that AFMR is a relatively frequent finding in patients with risk factors for atrial fibrillation, or with heart failure with preserved – or mildly reduced – left ventricular ejection fraction (HFpEF). These patients have a high incidence of atrial tachyarrhythmias and elevated left ventricular diastolic pressures due to LV diastolic dysfunction. Both diastolic dysfunction and AFMR increase left atrial pressure, which in turn impairs atrial mechanical function, as evidenced by impaired left atrial strain. It is very difficult, if not impossible, in this scenario to tease out the relative contributions of diastolic dysfunction and of MR to symptoms, natriuretic peptide elevation, pulmonary congestion, and right-sided pressure increase, which are all affected by both pathophysiological mechanisms. Hence, AFMR and HFpEF often coexist and are difficult to separate clinically. A recent study showed that patients with HFpEF and AFMR display greater hemodynamic severity of disease and poorer functional capacity than in HFpEF without AFMR.[7]

Some authors have described a subform of AFMR that occurs as the result of a posteriorly located dilatation of the mitral annulus leading to a herniation of the annulus beyond the circumference of the ventricular myocardium, and a particularly strong tethering of the posterior leaflet, with the consequence of a posteriorly directed regurgitant jet.[4,8–10] Several terms, such as "hamstringing" or "atriogenic MR", have been used to describe this configuration.

Hemodynamic features of AFMR

By definition, the regurgitant volume of AFMR cannot be very large, because chronic occurrence of a large mitral regurgitant volume would lead to critical impairment of systemic stroke volume in the absence of left ventricular dilatation. Hence, as long as the LV is not dilated, AFMR is typically rather moderate than severe. However, this may change once the LV starts to dilate and produce a larger total stroke volume. It is also currently unclear whether the quantitative cutoffs of severe regurgitation used for primary and ventricular FMR (effective regurgitant orifice area (ERO) $\geq$0.4 cm^2, regurgitant volume > 50 mL, regurgitant fraction > 50–60 mL)[11] are adequate for AFMR.

Epidemiology

In a recent report on the etiology of all cases of moderate and severe MR seen at the Mayo Clinic over 10 years, functional MR made up 65% of a total of 727 MR cases, and about 40% of functional MR cases were diagnosed to be of atrial origin.[12] Survival curves in AFMR cases were similar to those in primary MR, with considerable excess mortality compared to expected survival of age- and sex-matched general population cohort. Given that atrial fibrillation is a chief driver of AFMR, the data provided by Abe et al. are of a great importance.[1] They show that in atrial fibrillation patients without other apparent heart disease and a LVEF $\geq$ 50%, the incidence of at least moderate AFMR increased from 3% (in patients with duration of atrial fibrillation <1 year) to 28% (in those with duration of atrial fibrillation >10 years).

Treatment and outcomes

Atrial functional mitral regurgitation is amenable to current surgical and interventional mitral repair techniques, apart from valve replacement. In the so far largest published cohort study of severe AFMR patients with follow-up, it has been shown that these patients had worse overall survival, more heart failure hospitalizations (and more diastolic dysfunction), and underwent valve surgery less often than similarly aged patients with severe primary MR and normal LV function.[10] Recently, the results of percutaneous edge-to-edge repair in 126 patients with AFMR were published, with good procedural success and symptomatic improvement[13]; however, whether this translates into improved prognosis cannot be currently determined.

Since atrial tachyarrhythmias are a key factor in the development of AFMR, the ablation of atrial arrhythmias is an appealing treatment option.[14] In a cohort of 136 AFMR individuals who underwent atrial fibrillation ablation, MR decreased in 64%, and only in those patients the LA volume also decreased.[15] Patients who had sinus rhythm restored had less MR and more reduction in LA volume than those who did not. The extent of low-voltage areas in the LA thought to reflect left atrial fibrosis and correlated with less reduction in MR and LA volume, suggesting that in the presence of extensive low-voltage areas AFMR may not be improved by ablation even if sinus rhythm is restored.

Areas of uncertainty in need for further research

Although the association of left atrial enlargement, atrial fibrillation and MR with a mitral leaflet without major visible abnormalities has been known for a long time, a more precise definition was lacking. Very recently, an expert panel viewpoint document has suggested a detailed framework for the definition of AFMR.[5] The most important open question related to AFMR is the time course of the disease and LA remodeling. Does AFMR develop to become mixed ventricular and atrial FMR over time, as we know it from functional tricuspid regurgitation? How to define severe AFMR when a normal-sized LV precludes large regurgitant volumes given that enough forward stroke volume must be preserved? Is a substantial proportion of what we call HFpEF in fact the consequence of AFMR? These questions await further research.

Conclusions

Atrial functional mitral regurgitation needs to be recognized as an important type of functional MR with morphological and pathophysiological characteristics that set it apart from other types of MR. Similar to functional atrial tricuspid regurgitation, the driver of this disease is neither a diseased valve nor the ventricle, but the remodeled atrium, in particular the dilated mitral annular area, with close association with the burden of atrial fibrillation over time. This is important not only for diagnosis, but also for the choice of therapy. The avoidance of major left atrial remodeling is crucial for the prevention of AFMR, and the induction of reverse remodeling is the ideal therapeutic principle. The time course of AFMR, its impact on the LV, the potential of reverse remodeling of the LA if sinus rhythm can be restored, and a bespoke therapeutic approach remain to be determined.

Supplementary material

The supplementary clips (AFMR1 and AFMR2) are available at https://doi.org/10.5281/zenodo.7273770.

ORCID iDs

Frank A. Flachskampf ● https://orcid.org/0000-0002-7401-278X

References

1. Abe Y, Akamatsu K, Ito K, et al. Prevalence and prognostic significance of functional mitral and tricuspid regurgitation despite preserved left ventricular ejection fraction in atrial fibrillation patients. *Circ J*. 2018;82(5):1451–1458. doi:10.1253/circj.CJ-17-1334
2. Kim DH, Heo R, Handschumacher MD, et al. Mitral valve adaptation to isolated annular dilation. *JACC Cardiovasc Imaging*. 2019;12(4):665–677. doi:10.1016/j.jcmg.2017.09.013
3. Deferm S, Bertrand PB, Verbrugge FH, et al. Atrial functional mitral regurgitation. *J Am Coll Cardiol*. 2019;73(19):2465–2476. doi:10.1016/j.jacc.2019.02.061
4. Kagiyama N, Mondillo S, Yoshida K, Mandoli GE, Cameli M. Subtypes of atrial functional mitral regurgitation. *JACC Cardiovasc Imaging*. 2020;13(3):820–835. doi:10.1016/j.jcmg.2019.01.040
5. Zoghbi WA, Levine RA, Flachskampf FA, et al. Atrial functional mitral regurgitation: A JACC cardiovascular imaging expert panel viewpoint. *JACC Cardiovasc Imaging*. 2022 [in press].
6. Marsit O, Clavel MA, Côté-Laroche C, et al. Attenuated mitral leaflet enlargement contributes to functional mitral regurgitation after myocardial infarction. *J Am Coll Cardiol*. 2020;75(4):395–405. doi:10.1016/j.jacc.2019.11.039
7. Tamargo M, Obokata M, Reddy YNV, et al. Functional mitral regurgitation and left atrial myopathy in heart failure with preserved ejection fraction. *Eur J Heart Fail*. 2020;22(3):489–498. doi:10.1002/ejhf.1699
8. Silbiger JJ. Mechanistic insights into atrial functional mitral regurgitation: Far more complicated than just left atrial remodeling. *Echocardiography*. 2019;36(1):164–169. doi:10.1111/echo.14249
9. Machino-Ohtsuka T, Seo Y, Ishizu T, et al. Novel mechanistic insights into atrial functional mitral regurgitation: 3-dimensional echocardiographic study. *Circ J*. 2016;80(10):2240–2248. doi:10.1253/circj.CJ-16-0435
10. Mesi O, Gad MM, Crane AD, et al. Severe atrial functional mitral regurgitation. *JACC Cardiovasc Imaging*. 2021;14(4):797–808. doi:10.1016/j.jcmg.2021.02.008
11. Zoghbi WA, Adams D, Bonow RO, et al. Recommendations for noninvasive evaluation of native valvular regurgitation. *J Am Soc Echocardiogr*. 2017;30(4):303–371. doi:10.1016/j.echo.2017.01.007
12. Dziadzko V, Dziadzko M, Medina-Inojosa JR, et al. Causes and mechanisms of isolated mitral regurgitation in the community: Clinical context and outcome. *Eur Heart J*. 2019;40(27):2194–2202. doi:10.1093/eurheartj/ehz314
13. Doldi P, Stolz L, Orban M, et al. Transcatheter mitral valve repair in patients with atrial functional mitral regurgitation. *JACC Cardiovasc Imaging*. 2022. doi:10.1016/j.jcmg.2022.05.009
14. Gertz ZM, Raina A, Saghy L, et al. Evidence of atrial functional mitral regurgitation due to atrial fibrillation. *J Am Coll Cardiol*. 2011;58(14):1474–1481. doi:10.1016/j.jacc.2011.06.032
15. Masuda M, Sekiya K, Asai M, et al. Influence of catheter ablation for atrial fibrillation on atrial and ventricular functional mitral regurgitation. *ESC Heart Fail*. 2022;9(3):1901–1913. doi:10.1002/ehf2.13896

Novel electroporation-based treatments for breast cancer

Zofia Łapińska[D,F], Jolanta Saczko[A,D–F]

Department of Molecular and Cellular Biology, Faculty of Pharmacy, Wroclaw Medical University, Poland

A – research concept and design; B – collection and/or assembly of data; C – data analysis and interpretation;
D – writing the article; E – critical revision of the article; F – final approval of the article

Abstract

Breast cancer (BC) is the most common cancer in women, and its incidence is increasing every year. Current treatment is based on surgical resection, chemotherapy (CT), radiotherapy, and hormone therapy (HT). Unfortunately, these methods are ineffective and are associated with a wide range of side effects (e.g., nausea, hair loss and fertility disorders). Electrochemotherapy (ECT), which exposes tumor cells to electric pulses (known as electroporation (EP)) in combination with cytostatic drugs, enables the reduction of cytotoxic drug doses while increasing their efficacy. Electroporation-based treatment methods are applied in breast carcinoma and are the subject of intensive research globally. Irreversible EP has shown promising therapeutic potential in the absence of cytotoxic drugs, as has EP associated with molecules such as calcium ions that are already present in the human body. The application of EP-based methods seems to be a safer and more effective treatment for BC in vitro and in vivo. Indeed, they have found applications in the treatment of BC and its metastases. Moreover, their palliative effects have also been established, and pain reduction has been noted in patients.

Key words: breast cancer, calcium ion, electroporation, electrochemotherapy

Introduction

Breast cancers (BCs) are the most common carcinomas in developing countries, and they consist of a wide range of heterogeneous diseases, both intertumorally and intratumorally. Existing morphological and molecular differences between the different types of BC affect their susceptibility to therapy.[1,2] Consequently, contemporary medicine is still facing the challenge of mounting an effective fight against BC, and this neoplasm remains one of the most common types of cancer and the leading cause of cancer-associated mortality in women.[3]

Conventional first-line treatment for BC includes surgery, radiation and chemotherapy (CT). While the first two treatments target the tumor region, CT involves the systemic administration of cytotoxic agents to either inhibit the growth of cancer cells or trigger their apoptosis.[4] However, default CT is noneffective due to the occurrence of multidrug resistance (MDR) against commonly used cytostatic agents, and the severe toxicities induced by them. Therefore, researchers started to look for new treatment strategies. One such strategy, endocrine therapy, exploits the fact that a wide group of BCs are characterized by the expression of estrogen and/or progesterone receptors. This adjuvant treatment reduces BC-associated mortality. Moreover, hormone therapy (HT) is the basic treatment in the advanced phases of BC. However, a subgroup of hormone receptor-positive (HR+) BCs do not benefit from endocrine therapy, and all HR+ metastatic BCs develop resistance to HT.[5,6] Due to the lack of efficiency in current methods, there is an urgent need to look for alternative, affordable and simple techniques to treat neoplasms refractory to conventional treatment standards.

Electroporation (EP) is a biophysical method based on the introduction of high-voltage electric pulses to cells in vitro or tissues in vivo, which results in permeabilization of the plasma membrane (PM). The occurrence of hydrophilic pores in the PM results in enhanced influx of a variety of molecules into the cell's cytosol. Pulse duration and electric field strength determine whether structural rearrangements in the cell membrane are reversible, enabling the re-establishment of the cell homeostasis, or irreversible, leading to cell death due to the loss of essential organelles through pores in the PM. Thus, 2 main types of EP may be distinguished: reversible EP (RE) and irreversible EP (IRE).[7–9]

The use of EP-based treatment methods can have a significant impact on increasing the amount of drug delivered into cells, which prevents the emergence of active drug efflux-based resistance mechanisms in cancer cells.[10] To this end, electrical pulse-mediated CT, known as electrochemotherapy (ECT), is a novel way to improve cancer treatment efficiency. Optimal EP parameters for use in clinical practice were defined as part of the European Standard Operating Procedures on Electrochemotherapy (ESOPE) multicenter trial,[11] and include the delivery of 8 rectangular pulses, each lasting 100 µs, with an electric field intensity ranging from 1.0 kV/cm to 1.5 kV/cm. Depending on whether a drug is administered locally or intravenously, pulses have to be delivered immediately following or a few minutes after the drug is delivered, respectively.[12,13] Hitherto, only 3 compounds have been used in clinical practice for ECT protocols: cisplatin, bleomycin, and recently, calcium chloride ($CaCl_2$). Moreover, it should be noted that ECT may be combined with immunotherapy[14,15] or radiotherapy.[16]

Studies on EP and ECT in breast cancer

Due to the phenomenon of MDR and other difficulties associated with BC (e.g., histological variety, hormonal dependence and resistance of cancer cells), EP has been highlighted as one of the methods that can increase the effectiveness of conventional treatment. Furthermore, EP decreases the number of side effects of conventional cancer treatments. Electroporation of BC cells may provide an efficient and feasible drug delivery system, enabling the reduction of dosage and drug exposure time. Electroporation and ECT have been investigated in BC in vitro, as well as in clinical studies.[17–20] Pehlivanova et al. examined the influence of electrical treatment on the cell adhesion of BC cells and fibroblasts. The application of suitable electric pulses triggered rearrangements in cytoskeleton organization and cell adhesiveness. Such variations could lead to the restriction of tumor metastasis rate, which contributes to the increased antitumor effect of EP-based therapy.[21] In other research, high-frequency irreversible EP (H-FIRE), an effective tumor ablation strategy, used bipolar bursts of ultrashort (0.25–5 µs) pulses characterized by different polarity.[22] It has been discovered that H-FIRE induced immune-mediated cell death and promoted systemic anti-tumor immunity. Cell death and tumor ablation following H-FIRE treatment activated the local innate immune system, causing the tumor microenvironment to change from an anti-inflammatory to a pro-inflammatory state.[23,24]

The analysis of the impact of EP without the use of anti-cancer drugs was conducted on human triple-negative BC (MDA-MB-231) and human colon cancer (SW-480 and HCT-116) cells, and these results were compared with studies investigated human fibroblast cell line (MRC-5), primary human aortic smooth muscle cells (hAoSMCs) and human umbilical vein endothelial cells (HUVECs).[25] The inhibition of cell proliferation was observed after EP was applied, and the intensity of this effect was dependent on the parameters of the protocol used. The use of a lower voltage (up to 0.5 kV/cm) induced a fast but temporary disturbance in viability of MDA-MB-231 cells, and apoptosis was the predominant type of cell death. However, the cells started to proliferate again after several hours. Only IRE with high voltages resulted in permanent BC cell

degradation. Different results were obtained for colon cancer cells, in which exposure to pulse intensities of up to 0.5 kV/cm caused permanent damage. Healthy cells (MRC-5s, hAoSMCs and HUVECs), similar to the MDA-MB-231 cell line, recovered after 72 h. This research indicates that EP might be a promising treatment method; however, more precise analyses are needed to develop an optimal EP protocol.[25]

Electrochemotherapy investigations on BC cell lines have mainly been conducted with the use of bleomycin or cisplatin. Increasing intracellular concentrations of these 2 drugs lead to cell death by apoptosis,[26] necrosis[27] or by other pathways, depending on the drug used.[26,28] A local inflammatory reaction has been observed within the area of the electric field application after ECT,[29,30] and the cytotoxicity of the anti-cancer agents used increased by 80–100-fold.[31,32]

Electroporation-based methods are a promising alternative for human breast adenocarcinoma therapy, especially in those resistant to drugs. Electroporation reduces the effective dose of the drug and drug exposure time; thus, it reduces the number of side effects. Rembiałkowska et al. conducted an in vitro investigation into the use of doxorubicin (DOX) as an anti-cancer drug alongside EP in the human estrogen receptor-positive (ER⁺) BC cell line (MCF-7/WT), which is sensitive to DOX. They also used a DOX resistance cell line (MCF-7/DOX), and an increased effectiveness of the drug was observed in these cells after ECT. Indeed, the resistant cell line was shown to be more sensitive to electric pulses. Furthermore, electron microscopic examination of both cell lines revealed some interesting results. Combining electric pulses with DOX led to the appearance of heterogeneous materials with irregular shapes characteristic of secondary lysosomes and vacuoles.[33]

Combining EP with calcium ions (Ca^{2+}) instead of cytotoxic agents has been investigated as a potential treatment modality, and is known as calcium EP (CaEP). An in vitro study demonstrated that an EP-driven influx of supraphysiological doses of Ca^{2+} into cells caused necrotic cell death associated with a severe energy reduction.[34,35] In another study, an enhanced antiproliferative effect on MCF-7 and MCF-7/DX cells electroporated using nanosecond pulsed electric field (nsPEF) protocols in combination with Ca^{2+} was noted.[36] In general, the use of CaEP revealed similar effects.[35,37]

Electrochemotherapy has a promising potential and can be used for inoperable, chemoresistant and radioresistant tumors that do not respond to the current standard of treatment.[38] Preliminary clinical studies on BC metastasis to the skin and subcutaneous tissue demonstrated the high effectiveness of ECT as a palliative treatment, with a significant improvement in the patient's quality of life.[19] However, such a small number of applicable drugs is a limiting factor of ECT, as its efficacy may be abolished by side effects such as pulmonary toxicity after the application of bleomycin,[39] or extensive tumor necrosis following EP with Ca^{2+}.[40]

Conclusions

The application of ECT, CaEP and IRE shows promising results as a safer and more effective treatment option for BC both in vitro and in vivo, with specific success seen for ECT in the treatment of BC and its metastases. Moreover, the palliative effects of ECT and pain reduction have been noted in patients.

ORCID iDs

Zofia Łapińska https://orcid.org/0000-0001-5070-2746
Jolanta Saczko https://orcid.org/0000-0001-5273-5293

References

1. Wesoła M, Jeleń M. The risk of breast cancer due to *PALB2* gene mutations. *Adv Clin Exp Med*. 2017;26(2):339–342. doi:10.17219/acem/59147
2. Maciejczyk A. New prognostic factors in breast cancer. *Adv Clin Exp Med*. 2013;22(1):5–15. PMID:23468257.
3. Sung H, Ferlay J, Siegel RL, et al. Global Cancer Statistics 2020: GLOBOCAN estimates of incidence and mortality worldwide for 36 cancers in 185 countries. *CA Cancer J Clin*. 2021;71(3):209–249. doi:10.3322/caac.21660
4. Heller R, Jaroszeski MJ, Glass LF, et al. Phase I/II trial for the treatment of cutaneous and subcutaneous tumors using electrochemotherapy. *Cancer*. 1996;77(5):964–971. doi:10.1002/(SICI)1097-0142 (19960301)77:5<964::AID-CNCR24>3.0.CO;2-0
5. Colleoni M, Gelber S, Coates AS, et al. Influence of endocrine-related factors on response to perioperative chemotherapy for patients with node-negative breast cancer. *J Clin Oncol*. 2001;19(21):4141–4149. doi:10.1200/JCO.2001.19.21.4141
6. Winer EP. Optimizing endocrine therapy for breast cancer. *J Clin Oncol*. 2005;23(8):1609–1610. doi:10.1200/JCO.2005.01.005
7. Neal RE, Singh R, Hatcher HC, Kock ND, Torti SV, Davalos RV. Treatment of breast cancer through the application of irreversible electroporation using a novel minimally invasive single needle electrode. *Breast Cancer Res Treat*. 2010;123(1):295–301. doi:10.1007/s10549-010-0803-5
8. Yarmush ML, Golberg A, Serša G, Kotnik T, Miklavčič D. Electroporation-based technologies for medicine: Principles, applications, and challenges. *Annu Rev Biomed Eng*. 2014;16(1):295–320. doi:10.1146/annurev-bioeng-071813-104622
9. Davalos RV, Mir LM, Rubinsky B. Tissue ablation with irreversible electroporation. *Ann Biomed Eng*. 2005;33(2):223–231. doi:10.1007/s10439-005-8981-8
10. Cadossi R, Ronchetti M, Cadossi M. Locally enhanced chemotherapy by electroporation: Clinical experiences and perspective of use of electrochemotherapy. *Future Oncol*. 2014;10(5):877–890. doi:10.2217/fon.13.235
11. Gehl J, Sersa G, Matthiessen LW, et al. Updated standard operating procedures for electrochemotherapy of cutaneous tumours and skin metastases. *Acta Oncol*. 2018;57(7):874–882. doi:10.1080/0284186X.2018.1454602
12. Miklavčič D, Serša G, Brecelj E, et al. Electrochemotherapy: Technological advancements for efficient electroporation-based treatment of internal tumors. *Med Biol Eng Comput*. 2012;50(12):1213–1225. doi:10.1007/s11517-012-0991-8
13. Kotulska M. Electrochemotherapy in cancer treatment. *Adv Clin Exp Med*. 2007;16(5):601–607. https://advances.umw.edu.pl/en/article/2007/16/5/601/. Accessed October 4, 2022.
14. Goggins CA, Khachemoune A. The use of electrochemotherapy in combination with immunotherapy in the treatment of metastatic melanoma: A focused review. *Int J Dermatol*. 2019;58(8):865–870. doi:10.1111/ijd.14314
15. Longo F, Perri F, Caponigro F, et al. Boosting the immune response with the combination of electrochemotherapy and immunotherapy: A new weapon for squamous cell carcinoma of the head and neck? *Cancers (Basel)*. 2020;12(10):2781. doi:10.3390/cancers12102781
16. Fiorentzis M, Sokolenko EA, Bechrakis NE, et al. Electrochemotherapy with bleomycin enhances radiosensitivity of uveal melanomas: First in vitro results in 3D cultures of primary uveal melanoma cell lines. *Cancers (Basel)*. 2021;13(12):3086. doi:10.3390/cancers13123086

17. Matthiessen LW, Johannesen HH, Hendel HW, Moss T, Kamby C, Gehl J. Electrochemotherapy for large cutaneous recurrence of breast cancer: A phase II clinical trial. *Acta Oncol*. 2012;51(6):713–721. doi:10.3109/0284186X.2012.685524

18. Telli ML, Nagata H, Wapnir I, et al. Intratumoral plasmid IL12 expands CD8+ T cells and induces a *CXCR3* gene signature in triple-negative breast tumors that sensitizes patients to anti–PD-1 therapy. *Clin Cancer Res*. 2021;27(9):2481–2493. doi:10.1158/1078-0432.CCR-20-3944

19. Wichtowski M, Murawa D, Czarnecki R, Piechocki J, Nowecki Z, Witkiewicz W. Electrochemotherapy in the treatment of breast cancer metastasis to the skin and subcutaneous tissue: Multicenter experience. *Oncol Res Treat*. 2019;42(1–2):47–51. doi:10.1159/000494093

20. Falk H, Matthiessen LW, Wooler G, Gehl J. Calcium electroporation for treatment of cutaneous metastases: A randomized double-blinded phase II study, comparing the effect of calcium electroporation with electrochemotherapy. *Acta Oncol*. 2018;57(3):311–319. doi:10.1080/0284186X.2017.1355109

21. Pehlivanova VN, Tsoneva IH, Tzoneva RD. Multiple effects of electroporation on the adhesive behaviour of breast cancer cells and fibroblasts. *Cancer Cell Int*. 2012;12(1):9. doi:10.1186/1475-2867-12-9

22. Sano MB, Fan RE, Xing L. Asymmetric waveforms decrease lethal thresholds in high frequency irreversible electroporation therapies. *Sci Rep*. 2017;7(1):40747. doi:10.1038/srep40747

23. Ringel-Scaia VM, Beitel-White N, Lorenzo MF, et al. High-frequency irreversible electroporation is an effective tumor ablation strategy that induces immunologic cell death and promotes systemic anti-tumor immunity. *EBioMedicine*. 2019;44:112–125. doi:10.1016/j.ebiom.2019.05.036

24. Rudno-Rudzińska J, Kielan W, Guziński M, Kulbacka J. Effects of calcium electroporation, electrochemotherapy, and irreversible electroporation on quality of life and progression-free survival in patients with pancreatic cancer: IREC clinical study. *Adv Clin Exp Med*. 2021;30(7):765–770. doi:10.17219/acem/139917

25. Cvetković DM, Živanović MN, Milutinović MG, et al. Real-time monitoring of cytotoxic effects of electroporation on breast and colon cancer cell lines. *Bioelectrochemistry*. 2017;113:85–94. doi:10.1016/j.bioelechem.2016.10.005

26. Mittal L, Aryal UK, Camarillo IG, Ferreira RM, Sundararajan R. Author Correction: Quantitative proteomic analysis of enhanced cellular effects of electrochemotherapy with Cisplatin in triple-negative breast cancer cells. *Sci Rep*. 2019;9(1):19124. doi:10.1038/s41598-019-55880-7

27. Esposito E, Siani C, Pace U, Costanzo R, di Giacomo R. Debulking mastectomy with electrochemotherapy: A case report of no surgery approach to recurrent breast cancer. *Transl Cancer Res*. 2021;10(2):1144–1149. doi:10.21037/tcr-20-2803

28. Batista Napotnik T, Polajžer T, Miklavčič D. Cell death due to electroporation: A review. *Bioelectrochemistry*. 2021;141:107871. doi:10.1016/j.bioelechem.2021.107871

29. Wichtowski M, Murawa D, Kulcenty K, Zaleska K. Electrochemotherapy in breast cancer: Discussion of the method and literature review. *Breast Care*. 2017;12(6):409–414. doi:10.1159/000479954

30. Sersa G, Cemazar M, Miklavcic D. Antitumor effectiveness of electrochemotherapy with cis-diamminedichloroplatinum(II) in mice. *Cancer Res*. 1995;55(15):3450–3455. PMID:7614485.

31. Mir LM, Orlowski S. Mechanisms of electrochemotherapy. *Adv Drug Deliv Rev*. 1999;35(1):107–118. doi:10.1016/S0169-409X(98)00066-0

32. Rols MP, Bachaud JM, Giraud P, Chevreau C, Roché H, Teissié J. Electrochemotherapy of cutaneous metastases in malignant melanoma. *Melanoma Res*. 2000;10(5):468–474. doi:10.1097/00008390-200010000-00009

33. Rembiałkowska N, Dubińska-Magiera M, Sikora A, et al. Doxorubicin assisted by microsecond electroporation promotes irreparable morphological alternations in sensitive and resistant human breast adenocarcinoma cells. *Appl Sci*. 2020;10(8):2765. doi:10.3390/app10082765

34. Frandsen SK, Gibot L, Madi M, Gehl J, Rols MP. Calcium electroporation: Evidence for differential effects in normal and malignant cell lines, evaluated in a 3D spheroid model. *PLoS One*. 2015;10(12):e0144028. doi:10.1371/journal.pone.0144028

35. Frandsen SK, Gehl J. Effect of calcium electroporation in combination with metformin in vivo and correlation between viability and intracellular ATP level after calcium electroporation in vitro. *PLoS One*. 2017;12(7):e0181839. doi:10.1371/journal.pone.0181839

36. Kulbacka J, Rembiałkowska N, Szewczyk A, et al. The impact of extracellular Ca2+ and nanosecond electric pulses on sensitive and drug-resistant human breast and colon cancer cells. *Cancers (Basel)*. 2021;13(13):3216. doi:10.3390/cancers13133216

37. Łapińska Z, Dębiński M, Szewczyk A, Choromańska A, Kulbacka J, Saczko J. Electrochemotherapy with calcium chloride and 17β-estradiol modulated viability and apoptosis pathway in human ovarian cancer. *Pharmaceutics*. 2020;13(1):19. doi:10.3390/pharmaceutics13010019

38. Esmaeili N, Friebe M. Electrochemotherapy: A review of current status, alternative IGP approaches, and future perspectives. *J Healthcare Eng*. 2019;2019:2784516. doi:10.1155/2019/2784516

39. Reinert T, Baldotto da R CS, Nunes FAP, Scheliga de S AA. Bleomycin-induced lung injury. *J Cancer Res*. 2013;2013:480608. doi:10.1155/2013/480608

40. Galant L, Delverdier M, Lucas MN, Raymond-Letron I, Teissie J, Tamzali Y. Calcium electroporation: The bioelectrochemical treatment of spontaneous equine skin tumors results in a local necrosis. *Bioelectrochemistry*. 2019;129:251–258. doi:10.1016/j.bioelechem.2019.05.018

Does a home-based exercise program play any role in the treatment of knee osteoarthritis? A meta-analysis

Jibing Wang[1,A,F], Dongfeng Xie[2,A], Zhijun Cai[3,C], Meimei Luo[4,C], Bo Chen[1,B], Yuguang Sun[5,E,F], Huixia Liu[5,E,F]

[1] Department of Rehabilitation Medicine, Northern Jiangsu People's Hospital, Yangzhou, China

[2] Department of Rehabilitation Medicine, The Third Affiliated Hospital, Sun Yat-Sen University, Guangzhou, China

[3] Department of Orthopedics, 920th Hospital of Joint Logistics Support Force of People's Liberation Army of China, Kunming, China

[4] Department of Orthopedics, Xijing Hospital, Air Force Medical University, Xi'an, China

[5] Department of Comprehensive Rehabilitation, Guangdong Industrial Injury Rehabilitation Hospital, Guangzhou, China

A – research concept and design; B – collection and/or assembly of data; C – data analysis and interpretation;
D – writing the article; E – critical revision of the article; F – final approval of the article

Abstract

Background. Knee-osteoarthritis is a very common joint disorder, affecting about 85% of the population worldwide. The effectiveness of home-based exercises is still debatable, with many studies indicating positive outcomes with few side effects, while others find them of limited utility.

Objectives. To assess the role of home-based exercise (HBE) programs in the treatment of knee osteoarthritis.

Materials and methods. Randomized controlled trials were included as per the predefined Population, Intervention, Comparison, Outcomes and Study (PICOS) criteria. Demographic summaries and event data for osteoarthritis therapy in the exercise and control groups were assessed, and comparative efficacy was evaluated using clustered graphs. The RevMan software was used to calculate the odds ratio (OR) and risk ratio of the included studies. The risk of bias was also evaluated and heterogeneity analysis was performed.

Results. Fifteen clinical trials performed from 2000 to 2022, with a total of 2922 osteoarthritis patients, were included in the study, according to the chosen inclusion criteria. We observed a reduction in Western Ontario and McMaster Universities Osteoarthritis Index (WOMAC) scores but a more marked improvement in clinical symptoms in the exercise group. The Knee Injury and Osteoarthritis Outcome Score (KOOS) increased only in the exercise group and not in the control group. We obtained a pooled OR of 0.59 (95% confidence interval (95% CI): 0.36–0.98), T^2 value of 0.88, χ^2 value of 185.41, degrees of freedom (df) value of 14, I^2 value of 92%, and p-value <0.00001. The overall Z effect was 2.04 with a p-value of 0.04. The pooled risk ratio was 0.81 (95% CI: 0.66–0.99) with a T^2 value of 0.14, χ^2 value of 191.53, df value of 14, I^2 value of 93%, and p-value <0.00001.

Conclusions. The data from the studies included in this meta-analysis are in favor of the use of HBEs for the treatment of knee osteoarthritis.

Key words: knee osteoarthritis, home-based exercises, Western Ontario and McMaster Universities Osteoarthritis Index (WOMAC) score, knee injury, Knee Injury and Osteoarthritis Outcome Score (KOOS)

Introduction

Knee osteoarthritis is a very common joint disorder that affects approx. 85% of the population worldwide, mostly adults over 50 years of age.[1] Knee osteoarthritis is a medical condition in which the flexible and slippery articular cartilage of the knee that normally protects the joint becomes degenerated.[2] Due to this degeneration, the joint undergoes friction and impaction, which ultimately leads to pain and stiffness.[3] The main clinical symptoms of knee osteoarthritis are joint stiffness, difficulty walking and swelling. Knee osteoarthritis can be hereditary or caused by increasing age, elevated weight, hormonal disturbances, and athletic injuries.[4] For its treatment, various pain-relieving medications, anti-inflammatory drugs, supporting braces, and exercises can be used. In extreme cases when knee osteoarthritis results from a fall, trauma, accident, or high impact motor vehicle collision, knee injuries occur to one or more tissues that make up the knee joint, including ligaments, cartilage, muscles, or knee bones; a knee replacement surgery is recommended in these cases.[5] Since medications are associated with adverse side effects, such as indigestion and dry mouth, as well as a high cost of supporting braces and complexity of surgical procedures, home-based exercises (HBEs) may be considered an effective alternative to alleviate the symptoms of knee osteoarthritis.[6]

For example, Thomas[7] and Thorstensson et al.[8] reported that exercise can significantly reduce the clinical symptoms associated with knee osteoarthritis. Thorstensson et al. suggested exercises such as one-leg hop, lateral step-up, one-leg semi-squatting, and heel-raising.[8] Similarly, Doi et al. concluded that quadricep strengthening HBEs can effectively improve knee osteoarthritis.[9] Knoop et al. recommend muscle strengthening exercises as an effective method to alleviate the symptoms of knee osteoarthritis.[10] Similarly, Williams et al. support an internet-based exercise training program.[11] Unlike Bennel et al.,[12] Kuntz et al.[13] advocate biomechanically-based yoga exercises. Shellington et al.[14] advocate the so-called square-stepping exercise, and Choi and Lee[15] recommend knee joint traction therapy. Nelligan et al. determined that lower limb strengthening exercise programs, such as seated knee extension, walk squats, hip abduction, and calf raises, are effective treatment methods.[16] Consistent with these studies, in the randomized controlled clinical trials by Allen et al., the authors described the effectiveness of a Stepped Exercise Program for Patients with Knee Osteoarthritis (STEP-KOA).[17] Rewald et al.[18] suggest aquatic cycling exercises and swimming, and Makarm et al.[19] support stretching for the hamstring and quadriceps muscles as effective strengthening HBE programs. Thiengwittayaporn et al.[20] support knee bending exercises, and Gohir et al.[21] mention hamstring and quadricep muscle-strengthening exercise programs as effective ways to reduce the symptoms associated with knee osteoarthritis.

Although there are numerous supporting studies, the effectiveness of HBEs is still debated, as some studies report that they have limited efficacy. Therefore, this study aimed to thoroughly analyze the available randomized controlled trials on the use of HBE programs for the treatment of knee osteoarthritis and to predict the outcome of the analysis.

Objectives

The goal of this meta-analysis was to assess the role of HBE programs in the treatment of knee osteoarthritis.

Materials and methods

We followed the guidelines of Preferred Reporting Items for Systematic Reviews and Meta-analyses (PRISMA) normative recommendations in this study with the registration No. SYSU//IRB//2021//554. All procedures performed in this study were according to the institutional and/or national research standards and followed the 1964 Declaration of Helsinki and its later amendments.

Search strategy

This meta-analysis was based on an extensive search conducted in the databases of MEDLINE (via PubMed), CINAHL (via EBSCO), Scopus, and Web of Science, and covered the years 2000–2022. The following key words were used for searching the relevant studies: [knee osteoarthritis], [joint disorder], [home-based exercises], [randomized controlled trial], [WOMAC score], [and KOOS score]. All the included articles were selected following the PRISMA guidelines. The studies were selected randomly irrespective of the language, publication status or type of study (prospective, retrospective or clinical trial). A demographic summary of the patients with event data extracted from the included studies is summarized in Table 1.[7–21]

To assess the efficacy and safety of HBEs for the treatment of mild to moderate knee osteoarthritis in comparison with various pain relievers, data from randomized controlled trials were extracted. In these studies, patients from different age groups were treated with different exercises or control treatments; their Western Ontario and McMaster Universities Osteoarthritis Index (WOMAC) and Knee Injury and Osteoarthritis Outcome Score (KOOS) were measured, and changes in clinical symptoms were observed. Statistical parameters, such as diagnostic odds ratio (OR) and risk ratio with 95% confidence intervals (95% CIs), were calculated with the help of RevMan software (Cochrane, London, UK), and their respective forest plots were drawn.

Two authors (JW and DX) separately scanned the relevant sources for related studies. The full-text articles of the sources were collected when possible, while abstracts were used only if they provided sufficient information for the meta-analysis. Obsolete references were excluded, and

Table 1. Demographic summary of the included studies

Study and year	Journal	Type of study	Sample size	Age of patients [years]	Gender F/M	Duration of study	Improvement of assessment parameter	Exercise group			Control group		
								intervention arm	pre-treatment score	post-treatment score	control arm	pre-treatment score	post-treatment score
Thomas 2002	*British Medical Journal*	randomized controlled trial	786	50–70	126/74	24 months	WOMAC	78/199	11.96 ±3.54	6.96 ±3.54	121/199	13.06 ±3.44	7.04 ±3.67
Thorstensson et al. 2005	*BMC Musculoskeletal Disorders*	randomized controlled trial	69	36–65	31/30	6 weeks	KOOS	31/61	60 ±18	61.8 ±18	30/61	64 ±19	62.7 ±19
Doi et al. 2008	*American Journal of Physical Medicine & Rehabilitation*	randomized controlled trial	142	50–80	90/31	8 weeks	WOMAC	58/121	22.85 ±16.79	13.69 ±13.47	63/121	25.95 ±15.88	18.59 ±16.38
Knoop et al. 2013	*Osteoarthritis and Cartilage*	randomized controlled trial	159	55–70	97/62	12 weeks	WOMAC	79/159	25.2 ±11.8	17.4 ±11.6	80/159	27.1 ±12.7	19.3 ±11.4
Williams et al. 2015	*BMC Musculoskeletal Disorders*	randomized controlled trial	350	>60	–	4 months	WOMAC	70/350	6.5 ±17.5	6.1 ±17.5	280/350	6.5 ±17.5	6.75 ±17.5
Bennell et al. 2016	*Arthritis Care & Research*	randomized controlled trial	222	52–70	89/60	52 weeks	WOMAC	74/149	34.3 ±7.2	18.1 ±11.2	75/149	35.0 ±7.4	21.30 ±9.8
Kuntz et al. 2018	*PLOS ONE*	randomized controlled trial	59	55–80	31 F	12 weeks	KOOS	10/31	48.8 ±12.4	70.3 ±12.8	21/31	52.0 ±17.9	49.9 ±24.7
Shellington et al. 2019	*Canadian Journal on Aging*	pilot randomized controlled trial	22	60–70	15/7	24 weeks	WOMAC	10/22	32.5 ±5.7	30.0 ±5.7	12/22	24.7 ±6.7	22.6 ±6.7
Choi and Lee 2019	*The Journal of Korean Physical Therapy*	randomized controlled trial	30	60–72	15/15	4 weeks	WOMAC	15/30	47.20 ±1.65	25.33 ±2.38	15/30	44.13 ±2.29	35.26 ±2.76
Nelligan et al. 2019	*BMC Musculoskeletal Disorders*	randomized controlled trial	206	>45	–	24 weeks	WOMAC	102/206	6.3 ±11.5	2.3 ±11.5	104/206	6.5 ±11.5	5.5 ±10.5
Allen et al. 2019	*BMC Musculoskeletal Disorders*	randomized controlled trial	345	>40	–	9 months	WOMAC	300/345	6.5 ±17.5	5.2 ±17.5	336/345	6.5 ±17.5	6.1 ±17.5
Rewald et al. 2020	*Archives of Physical Medicine and Rehabilitation*	randomized controlled trial	111	50–70	–	12 weeks	KOOS	47/111	56.96 ±12.96	63.55 ±15.33	55/111	57.89 ±15.26	57.24 ±19.16
Makarm et al. 2021	*Egyptian Rheumatology and Rehabilitation*	randomized controlled clinical study	210	40–65	161/49	6 months	VAS	104/210	58.29 ±17.4	41.4 ±14.2	106/210	61.2 ±13.7	60.9 ±14.7
Thiengwittayaporn et al. 2021	*Archives of Orthopaedic and Trauma Surgery*	randomized controlled trial	106	40–80	73/9	4 weeks	KOOS	40/82	67.3 ±13.3	70.7 ±11.0	42/82	65.3 ±4.1	62.0 ±5.2
Gohir et al. 2021	*JAMA Network Open*	randomized clinical trial	105	>45	71/34	6 weeks	WOMAC	48/103	8.0 ±3.9	5.1 ±3.8	57/103	7.8 ±3.7	6.0 ±3.7

WOMAC – Western Ontario and McMaster Universities Arthritis Index; KOOS – Knee Injury and Osteoarthritis Outcome Score; VAS – Visual Analogue Scale.

1190

J. Wang et al. Home exercise & knee osteoarthritis

useful studies were included as per the inclusion criteria. Event data with useful variables were collected independently by 2 researchers (ZC and ML).

Inclusion and exclusion criteria

Studies were included if they reported the safety and efficacy of HBEs for the treatment of patients with mild to moderate knee osteoarthritis. Studies were selected within the timeframe from 2000 to 2022 and abstracts were utilized only when they had provided the sufficient information for meta-analysis, while studies with insufficient data, studies reporting only the use of medicines and surgeries (without exercises), and studies published before 2000 were excluded, as shown in Fig. 1.

Evaluation of the analytical standard

Two reviewers (JW and DX) separately evaluated the methodological validity of the included studies and calculated the heterogeneity of the included experiments. One

author (BC) was responsible for resolving any disagreements between the authors. To evaluate heterogeneity, Cochran's Q statistic and the I^2 index in a random bivariate model were calculated with the help of RevMan software. The Deeks' funnel plot for publication bias was drawn with the help of MedCalc software (MedCalc Software Ltd., Ostend, Belgium). A risk of bias summary and a graph for the assessment of the risk of bias were made using RevMan software. To compare the changes in WOMAC and KOOS scores pre- and post-treatment with the exercise and control strategies, clustered bar graphs were plotted.

Sources of heterogeneity

The investigated heterogeneity sources included the use of full-text publications compared to abstracts, randomized controlled trials compared to retrospective studies, varied age groups and different numbers of patients, variable duration of treatment, different scales of analysis, and the comparison of HBEs with different control treatment methods.
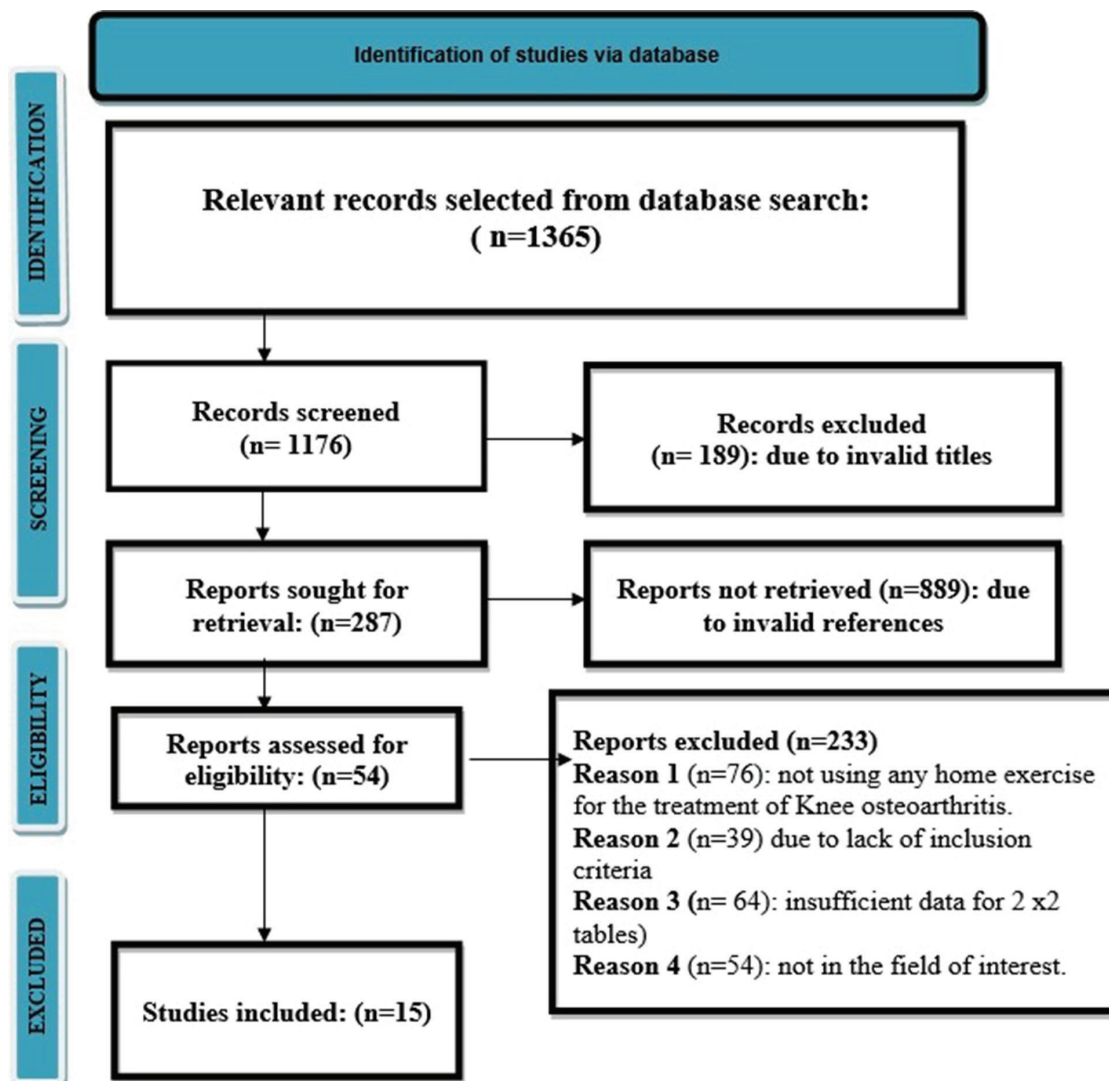
Fig. 1. Preferred Reporting Items for Systematic Reviews and Meta-Analyses (PRISMA) diagram of the study group

Statistical analyses

The diagnostic OR and relative risk were calculated using the DerSimonian–Laird technique. For this, a 2×2 table was created, and a meta-analysis was conducted using RevMan software. The pooled diagnostic OR value and pooled relative risk value were calculated with 95% CIs and respective forest plots. The heterogeneity of the studies was calculated in terms of the T^2 value, χ^2 value, Z value, and p-value using the Mantel–Haenszel method with random effects with RevMan software. The Deeks' funnel plot was constructed to assess the publication bias using MedCalc software, and the p-value was determined using Begg's test and Egger's test. The risk of bias summary and the risk of bias graph were assessed with RevMan software. To compare the changes in WOMAC and KOOS of patients who use either HBEs or any of the control methods, clustered bar graphs were plotted.

Results

Literature search results

A total of 1365 studies were found in the databases. Among these studies, we excluded 189 studies by reading their titles and abstracts, and thus 1176 records remained to be screened. Due to invalid references and duplicity, further 889 studies were excluded, leaving only 287 studies for the final screening. Of these 287 studies, 233 more were excluded: 76 on the basis of inadequate evidence, 39 due to the lack of inclusion criteria, 64 due to insufficient data, and 54 due to inappropriate data. Then, 2×2 tables were created for review. The eligibility of the remaining 54 studies was assessed further. Finally, 15 eligible studies that fulfilled the inclusion criteria (i.e., the use of different HBEs compared to control strategies) were used for the meta-analysis, as shown in Fig. 1.

Demographic details

The demographic details of the studies included in this meta-analysis are shown in Table 1. It provides the author of the study, year of publication, journal of publication, duration of the study, total sample size, age of the patients, gender of the patients, positive outcomes in the exercise and control groups, and mean values of pre- and post-treatment WOMAC and KOOS, along with their standard deviations (SDs). Fifteen randomized controlled clinical trials encompassing a total of 2922 knee osteoarthritis patients were included according to the inclusion criteria for the years 2000–2022. The included studies enrolled adult patients of different age groups who were chosen randomly and treated with either HBEs or control methods, such as placebo, pain relieving medications or joint supporters.

Risk of bias analysis

The meta-analysis was performed using RevMan software. The risk of bias for the included studies was assessed and is shown in Table 2. This study has a low risk of bias, as evident from the risk of bias graph shown in Fig. 2, and the resulting risk of bias is summarized in Fig. 3. The summarized values are suggestive of a random sampling of data and the use of categorical study variables. This meta-analysis has a low risk of publication bias, as apparent from the Deeks' funnel plot (Fig. 4). We obtained a significance level or p-value of 0.3 for Begg's test and 0.5 for Egger's test, indicating no evidence of publication bias.

Statistical parameters and heterogeneity

The OR was calculated using RevMan software to assess the effect of HBEs on knee osteoarthritis patients compared to the outcomes of standard control methods. The forest plot of the ORs and heterogeneity of the data are

Fig. 2. Risk of bias summary

1192

J. Wang et al. Home exercise & knee osteoarthritis
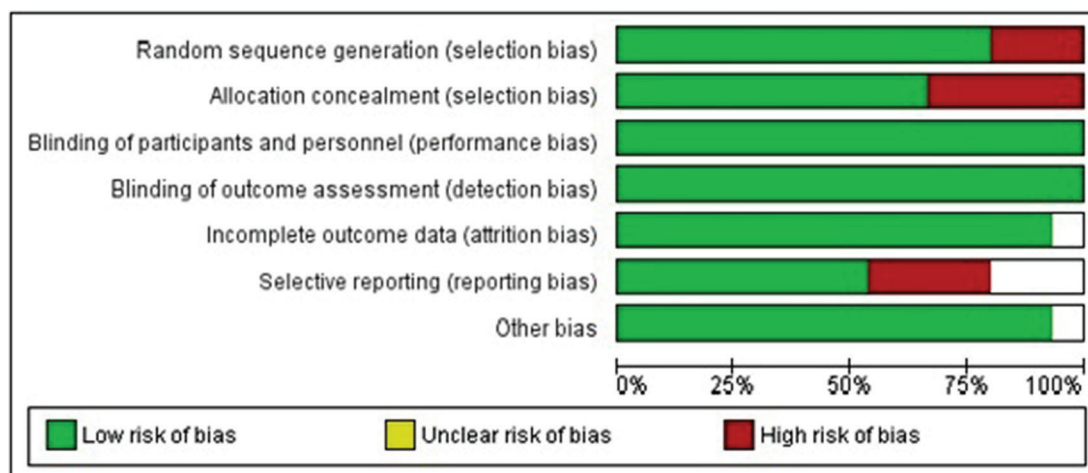
Table 2. Risk assessment for the included studies

Question	Thomas 2002	Thorstensson et al. 2005	Doi et al. 2008	Knoop et al. 2013	Williams et al. 2015	Bennell et al. 2016	Kuntz et al. 2018	Shellington et al. 2019	Choi and Lee 2019	Nelligan et al. 2019	Allen et al. 2019	Rewald et al. 2020	Makarm et al. 2021	Thiengwittayaporn et al. 2021	Gohir et al. 2021
Was the sample of enrolled patients consecutive or random?	Y	Y	Y	Y	Y	Y	Y	Y	Y	Y	Y	Y	Y	Y	Y
Did the study avoid inappropriate exclusions?	Y	Y	Y	Y	Y	Y	Y	Y	Y	Y	Y	Y	Y	Y	Y
Did all patients receive the same reference standard?	Y	Y	Y	Y	Y	Y	Y	Y	Y	Y	Y	Y	Y	Y	Y
Were all patients included in the analysis?	N	N	N	N	N	N	N	N	N	N	N	N	N	N	N
Was the sample frame appropriate to address the target population?	Y	Y	Y	Y	Y	Y	Y	Y	Y	Y	Y	Y	Y	Y	Y
Were study participants sampled in an appropriate way?	Y	Y	Y	Y	Y	Y	Y	Y	Y	Y	Y	Y	Y	Y	Y
Were the study subjects and the setting described in detail?	Y	Y	Y	Y	Y	Y	Y	Y	Y	Y	Y	Y	Y	Y	Y
Were valid methods used for the identification of the condition?	Y	Y	Y	Y	Y	Y	Y	Y	Y	Y	Y	Y	Y	Y	Y
Was the condition measured in a standard, reliable way for all participants?	Y	Y	Y	Y	Y	Y	Y	Y	Y	Y	Y	Y	Y	Y	Y
Was an appropriate statistical analysis conducted?	Y	Y	Y	Y	Y	Y	Y	Y	Y	Y	Y	Y	Y	Y	Y

presented in Fig. 5. We obtained a pooled OR value of 0.59 (95% CI: 0.36−0.98), T^2 value of 0.88, χ^2 value of 185.41, degrees of freedom (df) value of 14, I^2 value of 92%, and p-value <0.00001. The overall Z effect was 2.04, with a p-value of 0.04. A value of $p < 0.05$ indicates the statistical significance of the data, and a value of OR < 1 is indicative of the protective exposure of an HBE program for the treatment of knee osteoarthritis compared to control strategies; thus, it can be determined that HBEs are a worthwhile treatment method with minimal side effects.

The risk ratio of the included studies was also calculated using RevMan software, and the respective forest plot is shown in Fig. 6. The pooled risk ratio was 0.81 (95% CI: 0.66−0.99) with a T^2 value of 0.14, χ^2 value of 191.53, df value of 14, I^2 value of 93%, and p-value <0.00001.

The overall Z effect was 2.06, with a p-value of 0.04. A risk ratio value of less than 1 proves that the use of different HBEs is associated with low risk and is very protective and safe.

An I^2 value above 90% for both the OR and risk ratio is suggestive of substantial heterogeneity of the included studies with low bias. A value of $p < 0.05$ indicates a statistical significance and reflects the high treatment efficacy of HBEs for knee osteoarthritis.

Comparative efficacy of exercise compared to control methods

The patients were randomized into 2 arms: the exercise group and the control group. In both groups, the changes
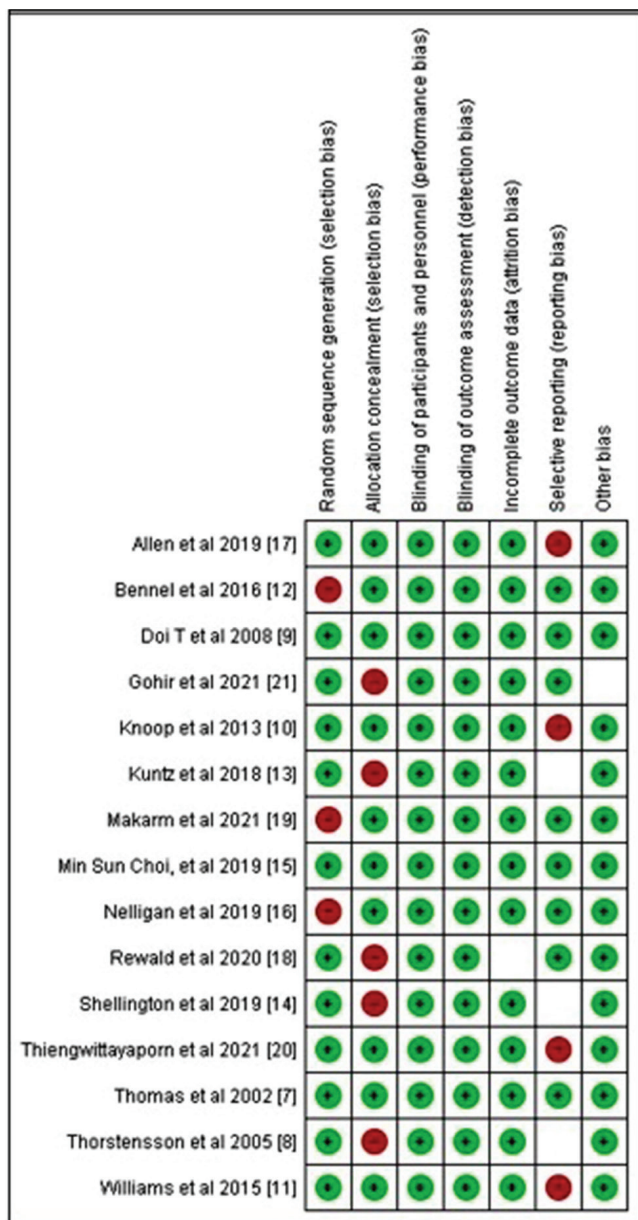
Fig. 3. Risk of bias graph

in KOOS and reductions in WOMAC were calculated, and comparative clustered graphs were designed. A low KOOS indicates extreme difficulty due to knee osteoarthritis, while a high KOOS represents no problems due to knee osteoarthritis. The clustered graph for KOOS (Fig. 7) showed that the score increased in the exercise groups but decreased in the control groups. This proves that exercise improves the pain and other clinical symptoms of knee osteoarthritis more effectively than control methods. Similarly, the clustered graph for reduced WOMAC scores (Fig. 8) showed a reduction in WOMAC scores in both groups, but the reduction was more pronounced in the exercise group. The higher the WOMAC score, the worse the pain, joint stiffness and functional ability limitations. When patients start performing a suitable HBE program, their WOMAC scores decrease (i.e., their pain and stiffness subside and their mobility improves). As shown in these plots, HBEs provide rapid and effective recovery from knee osteoarthritis, with minimal adverse side effects.

Combining all these results, it is clear that HBEs are safe, affordable and highly successful treatment strategies for knee osteoarthritis. Since they can reduce WOMAC scores and increase KOOS scores significantly, this study highly recommends the use of HBEs for the treatment of knee osteoarthritis.

Discussion

Knee osteoarthritis is a very common medical ailment affecting most of the adult population between 40 and 70 years of age. Due to an increased work stress and unhealthy lifestyles, weight gain and hormonal imbalances are common, leading to knee osteoarthritis or other joint disorders. This results in issues such as joint stiffness, difficulty walking and pain during movements. For

Fig. 4. Funnel plot for publication bias

95% CI – 95% confidence interval.

Publication bias

Egger's test	
Intercept	-1.3246
95% CI	-5.3767 to 2.7275
Significance level	P = 0.4925
Begg's test	
Kendall's Tau	-0.1923
Significance level	P = 0.3177

Study or Subgroup	Intervention Events	Total	Control Events	Total	Weight	Odds Ratio M-H, Random, 95% CI
Shellington et al 2019 [14]	12	22	10	22	5.3%	1.44 [0.44, 4.72]
Kuntz et al 2018 [13]	10	31	21	31	5.6%	0.23 [0.08, 0.66]
Min Sun Choi, et al 2019 [15]	15	30	15	30	5.8%	1.00 [0.36, 2.75]
Allen et al 2019 [17]	300	345	336	345	6.5%	0.18 [0.09, 0.37]
Thorstensson et al 2005 [8]	31	61	30	61	6.5%	1.07 [0.53, 2.17]
Thiengwittayaporn et al 2021 [20]	40	82	42	82	6.8%	0.91 [0.49, 1.67]
Gohir et al 2021 [21]	48	103	57	103	6.9%	0.70 [0.41, 1.22]
Bennel et al 2016 [12]	47	111	55	111	6.9%	0.75 [0.44, 1.27]
Rewald et al 2020 [18]	47	111	55	111	6.9%	0.75 [0.44, 1.27]
Doi T et al 2008 [9]	58	121	63	121	7.0%	0.85 [0.51, 1.40]
Knoop et al 2013 [10]	79	159	80	159	7.1%	0.98 [0.63, 1.51]
Thomas et al 2002 [7]	78	199	121	199	7.2%	0.42 [0.28, 0.62]
Nelligan et al 2019 [16]	102	206	104	206	7.2%	0.96 [0.65, 1.42]
Makarm et al 2021 [19]	104	210	106	210	7.2%	0.96 [0.66, 1.41]
Williams et al 2015 [11]	70	350	280	350	7.2%	0.06 [0.04, 0.09]
Total (95% CI)		**2141**		**2141**	**100.0%**	**0.59 [0.36, 0.98]**
Total events	1041		1375			

Heterogeneity: Tau² = 0.88; Chi² = 185.41, df = 14 (P < 0.00001); I² = 92%
Test for overall effect: Z = 2.04 (P = 0.04)

Fig. 5. Forest plot OR

OR – odds ratio; 95% CI – 95% confidence interval; M–H – Mantel–Haenszel method.

Study or Subgroup	Intervention Events	Total	Control Events	Total	Weight	Risk Ratio M-H, Random, 95% CI
Shellington et al 2019 [14]	12	22	10	22	4.7%	1.20 [0.66, 2.18]
Kuntz et al 2018 [13]	10	31	21	31	4.9%	0.48 [0.27, 0.84]
Min Sun Choi, et al 2019 [15]	15	30	15	30	5.3%	1.00 [0.60, 1.66]
Thorstensson et al 2005 [8]	31	61	30	61	6.4%	1.03 [0.72, 1.47]
Thiengwittayaporn et al 2021 [20]	40	82	42	82	6.7%	0.95 [0.70, 1.29]
Bennel et al 2016 [12]	47	111	55	111	6.8%	0.85 [0.64, 1.14]
Rewald et al 2020 [18]	47	111	55	111	6.8%	0.85 [0.64, 1.14]
Gohir et al 2021 [21]	48	103	57	103	6.9%	0.84 [0.64, 1.10]
Doi T et al 2008 [9]	58	121	63	121	7.0%	0.92 [0.72, 1.18]
Knoop et al 2013 [10]	79	159	80	159	7.2%	0.99 [0.79, 1.23]
Williams et al 2015 [11]	70	350	280	350	7.3%	0.25 [0.20, 0.31]
Thomas et al 2002 [7]	78	199	121	199	7.3%	0.64 [0.52, 0.79]
Nelligan et al 2019 [16]	102	206	104	206	7.4%	0.98 [0.81, 1.19]
Makarm et al 2021 [19]	104	210	106	210	7.4%	0.98 [0.81, 1.19]
Allen et al 2019 [17]	300	345	336	345	7.9%	0.89 [0.85, 0.93]
Total (95% CI)		**2141**		**2141**	**100.0%**	**0.81 [0.66, 0.99]**
Total events	1041		1375			

Heterogeneity: Tau² = 0.14; Chi² = 191.53, df = 14 (P < 0.00001); I² = 93%
Test for overall effect: Z = 2.06 (P = 0.04)

Fig. 6. Forest plot risk ratio

95% CI – 95% confidence interval; M–H – Mantel–Haenszel method.

the treatment of clinical symptoms associated with osteoarthritis, pain-relieving medications to alleviate pain, anti-inflammatory drugs to reduce swelling, and support braces for comfortable walking are available[22]; however, these can be expensive and may be associated with side effects.

Home-based exercise programs, including muscle strengthening and weight loss exercises, are safe, affordable and effective ways to substantially reduce the clinical symptoms of knee osteoarthritis. In a review published in 2005, Roddy et al. reported that home-based quadricep strengthening exercises and aerobic walking are the best treatment methods to reduce the pain and disability of knee

osteoarthritis.[23] Similarly, in their systematic review and meta-analysis, Li et al. preferred HBEs as an effective treatment strategy.[24] Swimming and pool exercises are considered highly advantageous for patients with knee osteoarthritis. However, in contrast to these supporting studies, Messier et al. in their randomized controlled trial reported that high-intensity muscle strengthening exercises did not reduce knee pain effectively.[25] In 2009, Bosomworth reported the potential benefits and hazards of HBEs, and asserted that patients with knee osteoarthritis should not perform activities that put extensive strain on their joints, such as running, jumping, and sports like tennis and basketball.[26]

Change in KOOS Score Control Group

Change in KOOS Score Excercise Group
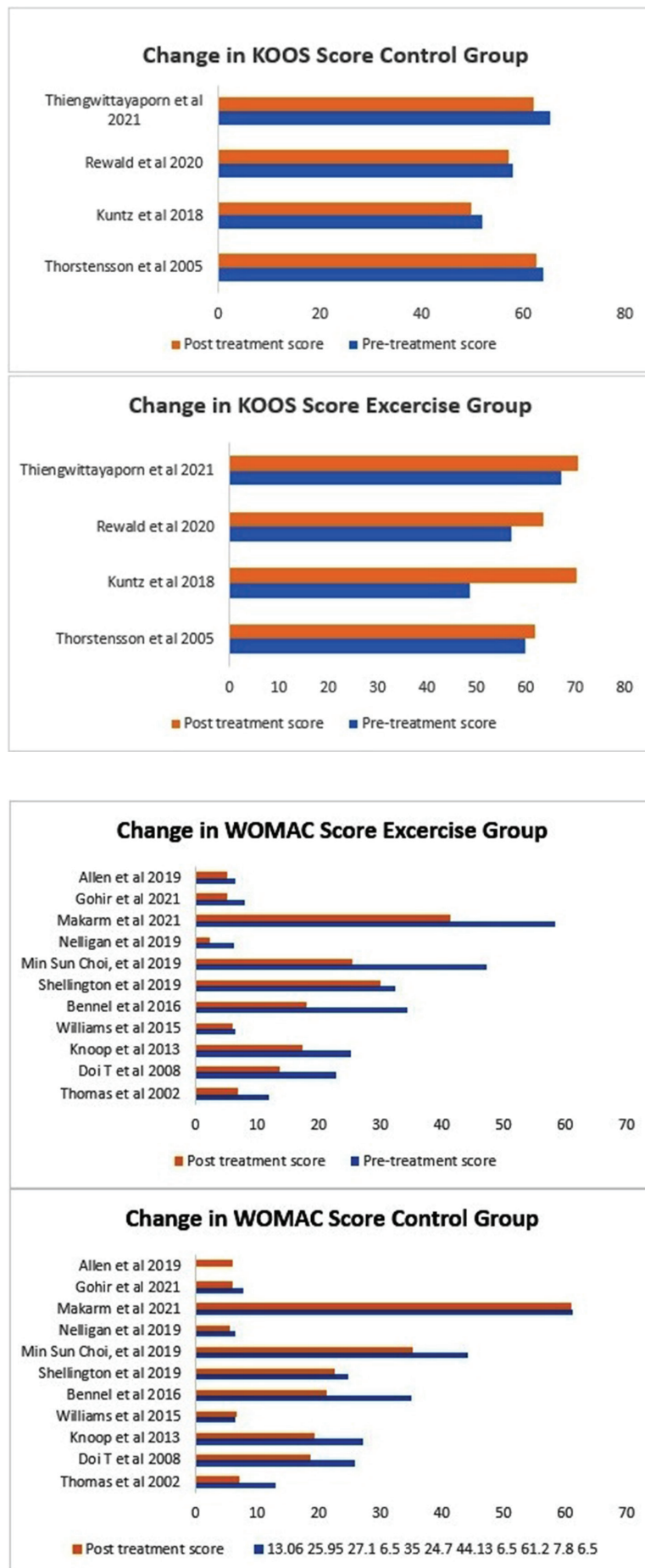
Fig. 7. Change in Knee Injury and Osteoarthritis Outcome Score (KOOS) pre- and post-treatment

To resolve these conflicting conclusions regarding the use of HBE programs for the treatment of knee osteoarthritis, this meta-analysis analyzed the available literature and performed a statistical meta-analysis. We obtained a pooled OR value of 0.59 (95% CI: 0.36−0.98), T^2 value of 0.88, χ^2 value of 185.41, df value of 14, I^2 value of 92%, and p-value <0.00001. The overall Z effect was 2.04, with a p-value of 0.04. The pooled risk ratio was 0.81 (95% CI: 0.66−0.99) with a T^2 value of 0.14, χ^2 value of 191.53, df value of 14, I^2 value of 93%, and p-value <0.00001. The overall Z effect was 2.06, with a p-value of 0.04. All these values are statistically significant. A value of p < 0.05 reflects the high treatment efficacy of HBEs for knee osteoarthritis. Similarly, the clustered graphs comparing the changes in WOMAC and KOOS scores also prove the superiority of exercise over the control treatment strategies.

Thus, based on the statistically significant meta-analysis results, this study highly recommends the use of HBE programs for the treatment of knee osteoarthritis. However, in the case of post-traumatic and severe knee damage, the knee replacement therapy is the most suitable option.

Limitations

There are certain limitations to this study. The first is the variability of exercises and control methods used for the treatment of knee osteoarthritis, which in turn skews the results. Similarly, the observation of WOMAC scores and clinical symptoms by different analytical tests performed by different people also increases the risk of false-negative results. Many studies do not report on the efficacy of exercise compared with a conventional pain reliever or anti-inflammatory drug; this may also affect the analysis to some extent. Data from other relevant studies that affirm the efficacy of HBEs in comparison with different medications could also include more results to guide their use more precisely. To observe the variability, detailed data on the case history of the patient, physical examination and pathological tests could further explain the results in order to recommend HBE programs as effective treatment for knee osteoarthritis.

Change in WOMAC Score Excercise Group

Change in WOMAC Score Control Group

Fig. 8. Change in Western Ontario and McMaster Universities Osteoarthritis Index (WOMAC) score pre- and post-treatment

1196

J. Wang et al. Home exercise & knee osteoarthritis

Conclusions

Surgery, pain relievers and anti-inflammatory drugs are some of the standard treatment strategies available for knee osteoarthritis; however, each strategy has its complexities and adverse effects. Since exercise has no adverse side effects, HBEs may be considered the best treatment strategy for knee osteoarthritis. Regular exercises can significantly improve the clinical symptoms, reduce the WOMAC scores and significantly increase the KOOS scores of knee osteoarthritis patients. Therefore, they can be considered a preferred, safe and inexpensive treatment method. In this study, we obtained an OR value of 0.59 and a risk ratio value of 0.81. Since both values are less than 1, it suggests that HBEs are safe and effective, and can reduce the clinical symptoms associated with knee osteoarthritis, without any adverse effects. We found substantial improvements in the KOOS and WOMAC scores of patients who performed HBEs for knee osteoarthritis. Based on our statistically significant meta-analysis results ($p < 0.05$) and a low risk of bias, we strongly support the use of HBEs for adults with knee osteoarthritis.

ORCID iDs

Jibing Wang https://orcid.org/0000-0002-3026-4424
Dongfeng Xie https://orcid.org/0000-0002-6541-439X
Zhijun Cai https://orcid.org/0000-0003-3728-8100
Meimei Luo https://orcid.org/0000-0001-6121-8036
Bo Chen https://orcid.org/0000-0003-2506-9875
Yuguang Sun https://orcid.org/0000-0002-6328-4835
Huixia Liu https://orcid.org/0000-0003-4472-3801

References

1. Oláh T, Reinhard J, Laschke MW, et al. Axial alignment is a critical regulator of knee osteoarthritis. *Sci Transl Med*. 2022;14(629):eabn0179. doi:10.1126/scitranslmed.abn0179
2. Vitaloni M, Botto-van Bemden A, Sciortino Contreras RM, et al. Global management of patients with knee osteoarthritis begins with quality of life assessment: A systematic review. *BMC Musculoskelet Disord*. 2019;20(1):493. doi:10.1186/s12891-019-2895-3
3. Katz JN, Arant KR, Loeser RF. Diagnosis and treatment of hip and knee osteoarthritis: A review. *JAMA*. 2021;325(6):568–578. doi:10.1001/jama.2020.22171
4. Nishigami T, Tanaka S, Mibu A, Imai R, Wand BM. Knee-related disability was largely influenced by cognitive factors and disturbed body perception in knee osteoarthritis. *Sci Rep*. 2021;11(1):5835. doi:10.1038/s41598-021-85307-1
5. Bartholdy C, Juhl C, Christensen R, Lund H, Zhang W, Henriksen M. The role of muscle strengthening in exercise therapy for knee osteoarthritis: A systematic review and meta-regression analysis of randomized trials. *Semin Arthritis Rheum*. 2017;47(1):9–21. doi:10.1016/j.semarthrit.2017.03.007
6. Luan L, El-Ansary D, Adams R, Wu S, Han J. Knee osteoarthritis pain and stretching exercises: A systematic review and meta-analysis. *Physiotherapy*. 2022;114:16–29. doi:10.1016/j.physio.2021.10.001
7. Thomas KS. Home based exercise programme for knee pain and knee osteoarthritis: Randomised controlled trial. *BMJ*. 2002;325(7367):752. doi:10.1136/bmj.325.7367.752
8. Thorstensson CA, Roos EM, Petersson IF, Ekdahl C. Six-week high-intensity exercise program for middle-aged patients with knee osteoarthritis: A randomized controlled trial [ISRCTN20244858]. *BMC Musculoskelet Disord*. 2005;6:27. doi:10.1186/1471-2474-6-27
9. Doi T, Akai M, Fujino K, et al. Effect of home exercise of quadriceps on knee osteoarthritis compared with nonsteroidal antiinflammatory drugs: A randomized controlled trial. *Am J Phys Med Rehabil*. 2008;87(4):258–269. doi:10.1097/PHM.0b013e318168c02d
10. Knoop J, Dekker J, van der Leeden M, et al. Knee joint stabilization therapy in patients with osteoarthritis of the knee: A randomized, controlled trial. *Osteoarthritis Cartilage*. 2013;21(8):1025–1034. doi:10.1016/j.joca.2013.05.012
11. Williams QI, Gunn AH, Beaulieu JE, et al. Physical therapy vs. internet-based exercise training (PATH-IN) for patients with knee osteoarthritis: Study protocol of a randomized controlled trial. *BMC Musculoskelet Disord*. 2015;16:264. doi:10.1186/s12891-015-0725-9
12. Bennell KL, Ahamed Y, Jull G, et al. Physical therapist-delivered pain coping skills training and exercise for knee osteoarthritis. Randomized controlled trial: Pain coping and exercise for knee OA. *Arthritis Care Res (Hoboken)*. 2016;68(5):590–602. doi:10.1002/acr.22744
13. Kuntz AB, Chopp-Hurley JN, Brenneman EC, et al. Efficacy of a biomechanically-based yoga exercise program in knee osteoarthritis: A randomized controlled trial. *PLoS One*. 2018;13(4):e0195653. doi:10.1371/journal.pone.0195653
14. Shellington EM, Gill DP, Shigematsu R, Petrella RJ. Innovative exercise as an intervention for older adults with knee osteoarthritis: A pilot feasibility study. *Can J Aging*. 2019;38(1):111–121. doi:10.1017/S0714980818000454
15. Choi MS, Lee DK. The effect of knee joint traction therapy on pain, physical function, and depression in patients with degenerative arthritis. *J Kor Phys Ther*. 2019;31(5):317–321. doi:10.18857/jkpt.2019.31.5.317
16. Nelligan RK, Hinman RS, Kasza J, Bennell KL. Effectiveness of internet-delivered education and home exercise supported by behaviour change SMS on pain and function for people with knee osteoarthritis: A randomised controlled trial protocol. *BMC Musculoskelet Disord*. 2019;20(1):342. doi:10.1186/s12891-019-2714-x
17. Allen KD, Bongiorni D, Caves K, et al. STepped exercise program for patients with knee OsteoArthritis (STEP-KOA): Protocol for a randomized controlled trial. *BMC Musculoskelet Disord*. 2019;20(1):254. doi:10.1186/s12891-019-2627-8
18. Rewald S, Lenssen AFT, Emans PJ, de Bie RA, van Breukelen G, Mesters I. Aquatic cycling improves knee pain and physical functioning in patients with knee osteoarthritis: A randomized controlled trial. *Arch Phys Med Rehabil*. 2020;101(8):1288–1295. doi:10.1016/j.apmr.2019.12.023
19. Makarm WK, Sharaf DM, Zaghlol RS. Impact of home exercise program on self-efficacy and quality of life among primary knee osteoarthritis patients: A randomized controlled clinical study. *Egypt Rheumatol Rehabil*. 2021;48(1):28. doi:10.1186/s43166-021-00073-2
20. Thiengwittayaporn S, Wattanapreechanon P, Sakon P, et al. Development of a mobile application to improve exercise accuracy and quality of life in knee osteoarthritis patients: A randomized controlled trial. *Arch Orthop Trauma Surg*. 2021;8:1–10. doi:10.1007/s00402-021-04149-8
21. Gohir SA, Eek F, Kelly A, Abhishek A, Valdes AM. Effectiveness of Internet-based exercises aimed at treating knee osteoarthritis: The iBEAT-OA randomized clinical trial. *JAMA Netw Open*. 2021;4(2):e210012. doi:10.1001/jamanetworkopen.2021.0012
22. Gay C, Chabaud A, Guilley E, Coudeyre E. Educating patients about the benefits of physical activity and exercise for their hip and knee osteoarthritis: Systematic literature review. *Ann Phys Rehabil Med*. 2016;59(3):174–183. doi:10.1016/j.rehab.2016.02.005
23. Roddy E, Zhang W, Doherty M. Aerobic walking or strengthening exercise for osteoarthritis of the knee? A systematic review. *Ann Rheum Dis*. 2005;64(4):544–548. doi:10.1136/ard.2004.028746
24. Li S, Ng WH, Abujaber S, Shaharudin S. Effects of resistance training on gait velocity and knee adduction moment in knee osteoarthritis patients: A systematic review and meta-analysis. *Sci Rep*. 2021;11(1):16104. doi:10.1038/s41598-021-95426-4
25. Messier SP, Mihalko SL, Beavers DP, et al. Effect of high-intensity strength training on knee pain and knee joint compressive forces among adults with knee osteoarthritis: The START randomized clinical trial. *JAMA*. 2021;325(7):646–657. doi:10.1001/jama.2021.0411
26. Bosomworth NJ. Exercise and knee osteoarthritis: Benefit or hazard? *Can Fam Physician*. 2009;55(9):871–878. PMID:19752252.

Tocilizumab treatment in COVID-19:
A prognostic study using propensity score matching

Özge Aydın Güçlü[A–F], Uğur Önal[A,B,E], Halıs Akalın[A,E,F], Nılüfer Aylın Acet Öztürk[B,E], Hazel Öztürk Belik[B,E], Ezgi Demirdöğen[D,E], Aslı Görek Dilektaşlı[D,E], Esra Kazak[D,E], Gökhan Ocakoğlu[C], İmran Sağlık[E], Funda Coşkun[D,E], Dane Ediger[D,E], Yasemin Heper[D,E], Ahmet Ursavaş[D,E], Emel Yılmaz[D,E], Esra Uzaslan[D,E], Mehmet Karadağ[D,E]

Faculty of Medicine, Bursa Uludağ University, Turkey

A – research concept and design; B – collection and/or assembly of data; C – data analysis and interpretation;
D – writing the article; E – critical revision of the article; F – final approval of the article

Address for correspondence
Özge Aydın Güçlü
E-mail: drozgeaydinguclu@gmail.com

Conflict of interest
None declared

Abstract

Background. The potential role of interleukin-6 (IL-6) in coronavirus disease 2019 (COVID-19) pneumonia provides the rationale for investigating IL-6 signaling inhibitors.

Objectives. To evaluate and report treatment responses to tocilizumab (TCZ) in COVID-19 patients and compare mortality outcomes with those of standard care.

Materials and methods. Patients hospitalized with a severe acute respiratory syndrome coronavirus 2 (SARS-CoV-2) infection, diagnosed with reverse transcription polymerase chain reaction (RT-PCR) between March 2020 and April 2021, were enrolled in this single-center retrospective cohort study. Propensity score matching was performed in order to reduce confounding effects secondary to imbalances in receiving TCZ treatment.

Results. A total of 364 patients were included in this study. Two hundred thirty-six patients received standard care, while 128 patients were treated with TCZ in addition to standard care (26 (20.3%) patients received a dose of 400 mg intravenously once, while 102 (79.7%) patients received a total dose of 800 mg intravenously). In the propensity score-matched population, less noninvasive mechanical ventilation ($p = 0.041$) and mechanical ventilation support ($p = 0.015$), and fewer deaths ($p = 0.008$) were observed among the TCZ-treated patients. The multivariate adjusted Cox regression model showed a significantly higher survival rate among TCZ patients compared to controls (hazard ratio (HR): 0.157, 95% confidence interval (95% CI): 0.026–0.951; $p = 0.044$). The hazard ratio for mortality in the TCZ group was 0.098 (95% CI: 0.030–0.318; $p = 0.0001$ using log-rank test).

Conclusions. This study determined that TCZ treatment in COVID-19 patients was associated with better survival, reduced need for mechanical ventilation and reduced hospital-associated mortality.

Key words: pneumonia, tocilizumab, COVID-19, cytokine storm, mortality

Background

In December 2019, a novel coronavirus was identified in Wuhan, China. It had clinical characteristics comparable to those of severe acute respiratory syndrome coronavirus 1 (SARS-CoV-1) and Middle East respiratory syndrome coronavirus (MERS-CoV).[1] This new coronavirus form, known as SARS-CoV-2, quickly spread around the globe, with the first case discovered in Turkey on March 11, 2020. As of September 12, 2021, there were 6,039,857 confirmed coronavirus disease 2019 (COVID-19) cases and 52,860 COVID-19-related deaths.[2]

Coronavirus disease 2019 begins with a period of rapid viral replication, followed by a 2nd phase controlled by the host immunological response.[1] Cytokine storms mediated by proinflammatory cytokine overproduction have been recognized in the vast majority of critically ill COVID-19 patients.[3] Cytokine storms cause cardiovascular collapse, multiple organ dysfunction and death. Patients at this stage have abnormal inflammatory markers, such as increased levels of serum ferritin, interleukin-6 (IL-6), and C-reactive protein (CRP).[4] Higher levels of serum IL-6 have been linked to increased SARS-CoV-2 viremia, extended viral RNA shedding, progression to mechanical ventilation, and death.[5,6] These findings led us to hypothesize that blocking the IL-6 receptor could terminate the inflammatory process at a critical point. As a result, early detection, treatment and prevention of cytokine storms may be vital for patients.

The significant role of IL-6 in COVID-19 pneumonia justifies further research into IL-6 signaling inhibitors.[7,8] Tocilizumab (TCZ) is a monoclonal antibody that targets the IL-6 receptor alpha and is used to treat inflamatory diseases such as rheumatoid arthritis, giant cell arteritis, and systemic sclerosis-associated interstitial lung disease.[9]

In cases of severe COVID-19 pneumonia, patients who received TCZ were shown to have better outcomes, and retrospective observational cohort studies revealed an immediate decrease in fever, decreased need for oxygen therapy and mechanical ventilation, as well as an improvement in lung symptoms.[10–14]

Objectives

The goal of this retrospective cohort study was to describe the therapeutic response to TCZ in COVID-19 patients and compare mortality outcomes to those associated with standard therapy.

Materials and methods

Between March 2020 and April 2021, adult patients (18 years and older) hospitalized with a positive SARS-CoV-2 reverse transcription polymerase chain reaction (RT-PCR) diagnosis at the Uludağ University Faculty of Medicine in Bursa, Turkey, were enrolled in this single-center retrospective cohort study. Pregnant women, patients enrolled in other clinical trials and patients receiving TCZ for chronic rheumatic disorders were excluded. The study protocol is summarized in Fig. 1.

Each patient provided written informed consent prior to the inclusion in the study. The study followed the principles of the Declaration of Helsinki and was approved by the Uludağ University Faculty of Medicine Clinical Research Ethics Committee (approval No. 2020-23/11), as well as the Ministry of Health's of the Republic of Turkey Ethical Committee.
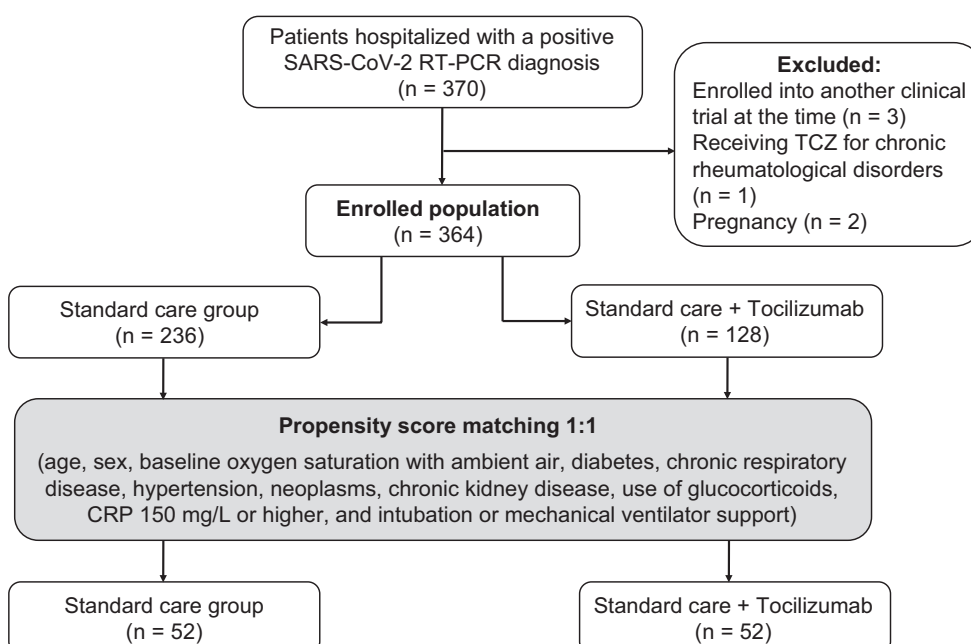

Fig. 1. Study flowchart

SARS-CoV-2 – severe acute respiratory syndrome coronavirus 2; RT-PCR – reverse transcription polymerase chain reaction; TCZ – tocilizumab; CRP – C-reactive protein.

Data collection

The electronic health records database at the hospital included sociodemographic information, clinical presentation, comorbid conditions, chest computed tomography (CT) findings, laboratory results, therapies, and their variables. Comorbidities were defined as those diagnosed prior to COVID-19 hospitalization.

Lymphocyte, eosinophil, ferritin, D-dimer, CRP, and procalcitonin parameters were recorded at baseline, before the TCZ treatment, and on the 1st, 3rd, 5th, 7th, and 14th day of treatment. The duration of hospitalization, number of days from hospitalization to death and secondary infection rates were recorded. The main endpoint was intubation or in-hospital mortality.

Definitions

Possible COVID-19 instances were diagnosed according to the national guidelines of Turkish Ministry of Health.[2,15] Nasopharyngeal swabs were taken for real-time RT-PCR when patients were admitted. Chest X-rays taken at admission were reviewed, and chest CT patterns and distributions characteristic of COVID-19 infection were carefully defined in accordance with the Radiological Society of North America's expert consensus statement, which proposes 4 categories for standardized COVID-19 reporting ("typical appearance," "indeterminate appearance," "atypical appearance," and "negative for pneumonia").[16] A chest radiologist and an experienced pulmonologist reviewed each probable COVID-19 patient's chest CT.

Hospital care and treatment of patients

From hospital admissions to treatment protocols, all clinical decisions adhered to the national guidelines published by the Turkish Ministry of Health.[2] Patients were observed until the completion of the clinical monitoring period, which was described as complete recovery, discharge from hospital with SpO_2 greater than 94% on room air, or death.

In the standard care group, the patients received favipiravir (1600 mg twice daily as a loading dose, followed by 600 mg twice daily as a maintenance dose); antibiotics were also administered as an initial treatment to account for the possibility of a bacterial etiology. Convalescent plasma was administered within 7 days of symptom onset in selected patients. Severely ill COVID-19 patients who required supplemental oxygen or ventilator support were administered 6 mg of dexamethasone daily for 10 days or until discharge.

Tocilizumab was added to standard therapy in patients who had clinical and laboratory findings such as persistent fever despite treatment, continuing to increase or constantly high proinflammatory cytokines and inflammatory markers, elevated ferritin, lymphopenia and thrombocytopenia, or elevated D-dimer.

Statistical analyses

The IBM SPSS Statistics for Windows, v. 23.0 software (IBM Corp., Armonk, USA) was used to conduct the statistical analyses. The Shapiro–Wilk test was used to ascertain the distribution of the variables. When the data were normally distributed, they were shown as mean and standard deviation (SD). When the data were not normally distributed, they were presented as median (interquartile range (IQR)). The categorical characteristics were given as numbers (%). To compare continuous outcome variables between the groups, we used the independent samples t-test for normally distributed data and the Mann–Whitney U test for non-normally distributed data. The Pearson's χ^2 test was used to compare categorical variables. The Friedman tests were employed to identify if significant changes in the lymphocyte, eosinophil, ferritin, D-dimer, CRP, and procalcitonin variables were observed due to incorrect parametric test assumptions (non-normal distribution).

We used propensity score matching to eliminate confounding effects caused by imbalances in TCZ treatment approval, inherent in a retrospective cohort analysis. To begin with, we calculated a propensity score for each patient in order to receive TCZ treatment using multivariable logistic regression with the confounding variables (age, sex, baseline oxygen saturation with ambient air, diabetes, chronic respiratory disease, hypertension, malignancy, chronic kidney disease, use of glucocorticoids, CRP 150 mg/L or higher, and intubation or mechanical ventilator support). The Hosmer–Lemeshow test was used to determine the multivariable logistic regression model's fit. Then, using NCSS 2019 statistical software (NCSS, Kaysville, USA), we employed nonparametric nearest neighbor matching of propensity scores to establish a matched cohort in a 1:1 ratio, pairing patients treated with TCZ with those who were not. To identify risk factors that are thought to be important in predicting mortality, the variables reported in the univariate studies were first investigated using univariate Cox regression. Then, the variables meeting the p < 0.25 threshold were included in the multivariate Cox regression model. When the relevant variables were analyzed using Cox regression, it was determined that age, hypertension, baseline SpO_2 in ambient air, need for intubation, and receiving TCZ met the p < 0.25 criterion.[17] The enter selection method was used to choose variables, and the results of the analysis were shown. The hazard ratios (HRs) and 95% confidence intervals (95% CIs) were summarized. The proportional hazard assumption was checked by producing a time variable (T-COV).

The survival rates of patients treated with TCZ in addition to standard therapy (TCZ group) and patients treated with standard therapy alone (standard treatment group) were determined using a Kaplan–Meier plot, with group (TCZ compared to standard treatment) as the between

factor, death as the event, and time to death or discharge as the time variable. To determine statistical significance, an overall 5% type I error threshold was applied.

Results

A total of 364 patients were included in this study. Two hundred thirty-six patients received standard care, while 128 patients were treated with TCZ in addition to standard care (26 (20.3%) patients received a dose of 400 mg intravenously once, while 102 (79.7%) patients received a total dose of 800 mg intravenously). Baseline demographic details, clinical characteristics, and laboratory and radiology findings are reported in Table 1 and Table 2, as unmatched and propensity score-matched.

Tocilizumab was used more frequently in male patients (93 (72.7%) compared to 124 (52.5%), p < 0.001). It was administered for a median of 12 (5–36) days after the start of patient-reported symptoms, a median of 6 days (1–23) from the date of hospitalization, and a median of 1 day (0–15) from the date of intensive care unit (ICU) support. Of the 364 patients, 78 (21.4%) died, including 52 (40.6%) of the 128 that received TCZ and 26 (11.0%) of the 236 that did not receive TCZ. Fifty-three (41.4%) of the 128 patients who received TCZ were started on it after intubation. Of these, 52 (98.1%) died, while 1 (1.9%) required extracorporeal membrane oxygenation (ECMO) support and was extubated during the follow-up.

In the unmatched population, patients who received TCZ had significantly longer symptom duration, longer hospital stay, lower baseline oxygen saturation, and more dyspnea than patients who did not receive TCZ (median (IQR): 5 (4) days) compared to 3 (5), p < 0.001; 16 11) compared to 7 (6), p < 0.001; 92 (7) compared to 96 (6), p < 0.001; 72 (56.3%) compared to 89 (36.9%), p < 0.001, respectively). In the propensity score-matched population, patients who received TCZ had significantly longer symptom duration and longer hospital stay than patients who did not (6 (3) compared to 3 (5), p = 0.002; 14 (9) compared to 8 (5), p < 0.001, respectively).

Among both the unmatched and propensity score-matched patients, there were significant differences between groups that did and did not receive TCZ in terms of typical chest CT images (p = 0.008 and p = 0.033, respectively). In addition, TCZ-treated patients had significantly lower lymphocyte, eosinophil and platelet levels than patients who were not treated with TCZ (Table 2).

In the unmatched population, patients who received TCZ had more noninvasive mechanical ventilation (NIMV), high-flow nasal oxygen (HFNO) and mechanical ventilation requirements, as well as more deaths than patients who did not recieve TCZ (p < 0.001 for each). In the propensity score-matched population, conversely, less NIMV (p = 0.041) and mechanical ventilation support (p = 0.015) and fewer deaths (p = 0.008) were observed among the TCZ-treated patients. Additionally, in the propensity score-matched population, more TCZ-treated patients required HFNO than non-TCZ-treated patients (17 (32.7%) compared to 5 (9.6%), p = 0.004).

The multivariate adjusted Cox regression model (adjusted for age, hypertension, baseline oxygen saturation with room air, and intubation) revealed that TCZ patients had a significantly higher survival rate than patients who did not receive TCZ (HR: 0.157, 95% CI: 0.026–0.951; p = 0.044; Table 3). Meanwhile, the risk of death was 5.3 times higher (p = 0.017) due to hypertension and 18.5 times higher (p < 0.001) when intubation was required.

The Kaplan–Meier curves for time to death are shown in Fig. 2. The hazard ratio for mortality in the TCZ group was 0.098 (95% CI: 0.030–0.318; p = 0.0001 using log-rank test).

Considering the pharmacodynamics of TCZ, an immediate effect on inflammatory indices is expected. Patients in the TCZ group were monitored for 14 days after the beginning of therapeutic interventions. Distributions of lymphocyte, eosinophil, ferritin, D-dimer, CRP, and procalcitonin parameters at baseline, before TCZ treatment, and on the 1st, 3rd, 5th, 7th, and 14th day of treatment are shown in Table 4.

Of the 128 patients who received TCZ, 35 (27.3%) developed a bacterial infection, 4 (3.1%) a fungal infection and 2 (1.6%) a viral infection (cytomegalovirus viremia) during hospitalization. Positive sputum cultures were identified in 25 (19.5%) patients.

Discussion

This single-center retrospective cohort study aimed to evaluate therapeutic responses to TCZ in COVID-19 patients and compare mortality outcomes to those associated with standard therapy. Receiving TCZ was associated with a decrease in hospital-related mortality in patients hospitalized with COVID-19. However, of the 53 patients who received TCZ after intubation, 52 died. Among the general population of the study, TCZ was only administered to clinically severe cases. Therefore, in unmatched analyses, the need for respiratory support and mortality rates were found to be higher in TCZ-treated patients compared to those who received standard care without TCZ. The propensity score-matched model adjusted for the factors such as age, gender, basal oxygen saturation with room air, diabetes, chronic lung disease, hypertension, malignancy, kidney failure, steroid use, CRP of 150 mg/L or more, and intubation or mechanical ventilator support determined that patients who received TCZ required less mechanical ventilation support and had lower mortality rates.

Cytokine storm is a term that refers to an out-of-control inflammatory response and impaired immune system function induced by infection, certain drugs and other

Table 1. Baseline characteristics of unmatched and propensity score-matched patients

Patient characteristics	Unmatched patients (n = 364)			Propensity score-matched patients (n = 104)		
	no tocilizumab (n = 236)	tocilizumab group (n = 128)	p-value	no tocilizumab (n = 52)	tocilizumab group (n = 52)	p-value
Age [years]	56 (27)	60 (19)	0.082[b] U: 13529	57.7 ±12.9	59.4 ±16.1	0.104[a] t: 1.639
Gender						
Female	112 (47.5%)	35 (27.3%)	<0.001[c]	11 (21.2%)	11 (21.2%)	>0.99[c]
Male	124 (52.5%)	93 (72.7%)		41 (78.8%)	41 (78.8%)	
Any comorbidity	94 (73.4%)	94 (73.4%)	>0.99[c]	32 (61.5%)	32 (61.5%)	>0.99[c]
Comorbidities						
Diabetes	52 (22%)	31 (24.2)	0.635[c]	9 (17.3%)	9 (17.3%)	>0.99[c]
Hypertension	83 (35.2%)	48 (37.5%)	0.658[c]	14 (26.9%)	14 (26.9%)	>0.99[c]
Cardiovascular disease	25 (19.5%)	25 (19.5%)	>0.99[c]	11 (21.2%)	11 (21.2%)	>0.99[c]
Chronic pulmonary disease	11 (4.7%)	6 (4.7%)	0.99[c]	1 (1.9%)	1 (1.9%)	>0.99[c]
Chronic renal insufficiency	11 (4.7%)	10 (7.8%)	0.243[c]	–	–	N/A
Cancer	25 (10.6%)	10 (7.8%)	0.390[c]	2 (3.8%)	2 (3.8%)	>0.99[c]
Disease duration						
Days from symptoms onset to hospitalization [days]	3 (5)	5 (4)	<0.001[b] U: 10534	3 (5)	6 (3)	0.002[b] U: 817
Hospital stay [days]	7 (6)	16 (11)	<0.001[b] U: 3891.5	8 (5)	14 (9)	<0.001[b] U: 412
Days from hospitalization to death [days]	9 (12)	16 (10)	0.003[b] U: 382.5	11.36 ±9.9	6.66 ±5.85	0.458[a] t: 0.767
Symptom severity at the time of hospital admission						
Mild	0 (0%)	35 (37.3%)	<0.001[c]	0 (0%)	9 (17.3%)	<0.001[c]
Moderate	0 (0%)	14 (10.9%)		0 (0%)	8 (15.4%)	
Severe	160 (67.8%)	59 (46.1%)		17 (32.7%)	27 (51.9%)	
Critical	76 (32.2%)	20 (15.6)		35 (67.3%)	8 (15.4%)	
Signs and symptoms						
Fever	100 (42.4%)	63 (49.2%)	0.210[c]	27 (48.1%)	27 (48.1%)	>0.99[c]
Cough	119 (50.4%)	61 (47.7%)	0.614[c]	23 (44.2%)	27 (51.9%)	0.432[c]
Sputum	20 (8.5%)	9 (7%)	0.627[c]	3 (5.8%)	4 (7.7%)	0.696[c]
Shortness of breath	89 (36.9%)	72 (56.3%)	<0.001[c]	20 (38.5%)	26 (50%)	0.236[c]
Myalgia	59 (20%)	22 (17.2%)	0.087[c]	8 (15.4%)	11 (21.2%)	0.446[c]
Fatigue	74 (31.4%)	44 (34.4%)	0.557[c]	14 (26.9%)	17 (32.7%)	0.520[c]
Vomiting	33 (14%)	12 (9.4%)	0.202[c]	5 (9.6%)	3 (5.8%)	0.462[c]
Diarrhea	26 (11%)	13 (10.2%)	0.861[c]	9 (17.3%)	5 (9.6%)	0.250[c]
Headache	21 (8.9%)	11 (8.6%)	0.922[c]	1 (1.9%)	5 (9.6%)	0.093[c]
Throat ache	21 (8.9%)	4 (3.1%)	0.039[c]	2 (3.8%)	1 (1.9%)	0.558[c]
Smell and taste dysfunction	15 (6.4%)	4 (3.1%)	0.186[c]	2 (3.8%)	2 (3.8%)	>0.99[c]
Initial vital signs						
Fever [°C]	36.6 (0.60)	36.8 (0.88)	0.027[b] U: 12982.5	36.8 (0.70)	36.7 (0.95)	0.321[b] U: 1264.5
Oxygen saturation with room air [%]	96 (6)	92 (7)	<0.001[b] U: 8336	92 (5)	92 (7)	0.572[b] U: 1336
Systolic blood pressure [mm Hg]	125 (20)	125 (26)	0.650[b] U: 14532	120 (30)	125 (20)	0.566[b] U: 1333
Diastolic blood pressure [mm Hg]	80 (15)	75 (10)	0.016[b] U: 12633	75 (10)	70 (14)	0.056[b] U: 1056
Heart rate [bpm]	88 (20)	90 (24)	0.967[b] U:14711	90.23 ±20.15	90.01 ±15.48	0.953[a] t: −0.059

Data are presented as mean ± standard deviation (SD), median (interquartile range (IQR)) and n (%). Statistical significance was determined with the two-sample t-test ([a]) for normally distributed continuous variables and the Mann–Whitney U test ([b]) for comparison of continuous non-normal data. Categorical variables were compared using the Pearson's χ² test ([c]). N/A – not applicable.

1202

Ö. Aydın Güçlü et al. Tocilizumab treatment in COVID-19

Table 2. Radiological and laboratory treatment and follow-up findings of unmatched and propensity score-matched patients

Patient characteristics	Unmatched patients (n = 364)			Propensity score-matched patients (n = 104)		
	no tocilizumab (n = 236)	tocilizumab group (n = 128)	p-value	no tocilizumab (n = 52)	tocilizumab group (n = 52)	p-value
Chest CT images, n [%]						
Typical	180 (77.3%)	112 (91.8%)	0.008[c]	40 (78.4%)	47 (95.9%)	0.033[c]
Indeterminate	26 (11.2%)	5 (4.1%)		6 (11.8%)	0 (0%)	
Atypical	18 (7.7%)	4 (3.3%)		3 (5.9%)	2 (4.1%)	
Negative	9 (3.9%)	1 (0.8%)		2 (3.9%)	0 (0%)	
Initial laboratory findings						
Leukocyte count [per mm³]	6470 (4630)	5570 (6810)	0.011[b] U: 12550.5	7340 (4822)	4970 (6965)	0.001[b] U: 852
Lymphocyte count [per mm³]	1350 (1004)	457 (1118)	<0.001[b] U: 5569	1197 (1027)	375 (906)	<0.001[b] U: 503
Neutrophil count [per mm³]	4205 (4134)	3635 (6983)	0.002[b] U: 12187.5	4310 (4081)	2898 (5391)	<0.001[b] U: 829
Eosinophil count [per mm³]	18 (76)	0.006 (0.01)	<0.001[b] U: 956	8.50 (42)	0.007 (0.01)	<0.001[b] U: 151.5
Hemoglobin [g/dL]	13.2 (2.7)	13.3 (2.3)	0.560[b] U: 14545	13.2 (2.2)	13.7 (1.9)	0.038[b] U: 1033
Platelet count [per 10⁹/L]	205500 (107600)	134750 (199235)	<0.001[b] U: 8316	196300 (130300)	132550 (180484)	<0.001[b] U: 700.5
D-dimer [mg/L]	0.73 (1.13)	0.72 (1.07)	0.624[b] U: 13800	0.78 (0.98)	0.64 (0.79)	0.603[b] U: 1164.5
ALT [U/L]	23 (21.7)	30 (20)	0.002[b] U: 12193	29 (26)	34 (35)	0.607[b] U: 1103.5
AST [IU/L]	26 (23.5)	36 (23.5)	<0.001[b] U: 10051	32 (22)	31 (24)	0.679[b] U: 1076.5
Creatinine [mg/dL]	0.85 (0.35)	0.98 (0.41)	0.884[b] U: 12591	0.98 (0.43–6.9)	0.93 (0.61–2.33)	0.241[b] U: 1226
Ferritin [ng/mL]	184 (500)	596 (883)	<0.001[b] U: 7193	376 (453)	531 (818)	0.035[b] U: 883.5
C-reactive protein [mg/L]	35.0 (88.5)	92.8 (120)	<0.001[b] U: 9059	73.7 (88.6)	65.3 (93.5)	0.840[b] U: 1316.5
Procalcitonin [ng/mL]	0.06 (0.18)	0.09 (0.21)	<0.001[b] U: 10639	0.10 (0.22)	0.08 (0.11)	0.139[b] U: 1008
Concomitant medications						
Hydroxychloroquine	129 (54.5%)	15 (14.6%)	<0.001[c]	20 (38.5%)	6 (15%)	0.013[c]
Remdesivir	3 (1.3%)	2 (1.7%)	0.728[c]	2 (3.8%)	0 (0%)	0.174[c]
Lopinavir/ritonavir	2 (0.8%)	2 (1.7%)	0.460[c]	1 (1.9%)	0 (0%)	0.339[c]
Favipiravir	171 (72.5%)	124 (96.9%)	<0.001[c]	44 (84.6%)	51 (98.1%)	0.015[c]
Dexamethasone	68 (28.8%)	90 (70.3%)	<0.001[c]	32 (61.5%)	32 (61.5%)	>0.99[c]
Pulse steroid	7 (3%)	70 (54.7)	<0.001[c]	4 (7.7%)	29 (55.8%)	<0.001[c]
Convalescent plasma	49 (20.8%)	80 (66.1%)	<0.001[c]	18 (34.6%)	36 (73.5%)	<0.001[c]
NIMV, yes	11 (4.7%)	22 (17.2%)	<0.001[c]	4 (7.7%)	0 (0%)	0.041[c]
HFNO, yes	13 (5.5%)	62 (48.4%)	<0.001[c]	5 (9.6%)	17 (32.7%)	0.004[c]
Mechanical ventilation, yes	22 (9.3%)	53 (41.4%)	<0.001[c]	8 (15.4%)	1 (1.9%)	0.015[c]
Death, yes	26 (11%)	52 (40.6%)	<0.001[c]	11 (21.2%)	2 (3.8%)	0.008[c]

CT – computed tomography; ALT – alanine transaminase; AST – aspartate aminotransferase; NIMV – noninvasive mechanical ventilation; HFNO – high-flow nasal oxygen. Data are presented as mean ± standard deviation (SD), median (interquartile range (IQR)) and n (%). Statistical significance was determined by the two-sample t-test ([a]) for normally distributed continuous variables and the Mann–Whitney U test ([b]) for comparison of continuous non-normal data. Categorical variables were compared using the Pearson's χ^2 test ([c]). Corticosteroid treatment: dexamethasone (DXM) 6 mg/day or methylprednisolone 40 mg/day; pulse steroid dose: 250 mg/day for 3 days; 500 mg/day for 3 days or 1000 mg/day for 3 days.

Table 3. Multivariable Cox regression model of mortality in propensity score-matched coronavirus disease 2019 (COVID-19) pneumonia

Variable	Multivariable model		
	HR	95% CI	p-value
Tocilizumab (yes/no)	0.157	0.026–0.951	0.044
Age [years]	1.014	0.943–1.057	0.505
Hypertension (yes/no)	5.283	1.344–20.757	0.017
Percentage oxygen saturation with room air, baseline	1.012	0.905–1.131	0.839
Intubation (yes/no)	18.524	3.874–88.568	<0.001

HR – hazard ratio; 95% CI – confidence interval.
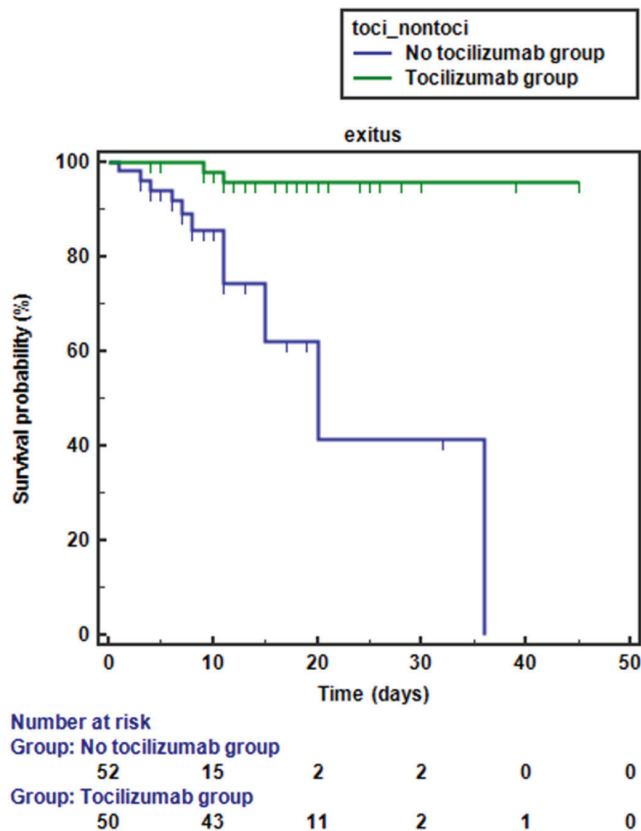
Fig. 2. Overall survival among propensity score-matched patients

Hazard ratio (HR) was 0.098, 95% confidence interval (95% CI) was 0.030–0.318 and log-rank p < 0.001.

reasons such as malignant tumors or rheumatic diseases. Severe acute respiratory syndrome coronavirus 2 attaches to alveolar epithelial cells and subsequently activates both the innate and adaptive immune systems, resulting in the release of a variety of cytokines, including IL-6. Additionally, these proinflammatory substances enhance vascular permeability, resulting in a flood of fluid and blood cells into the alveoli, which can lead to shortness of breath and potentially, respiratory failure.[18] Interleukin 6 is a critical component of the cytokine storm. It is typically reported in individuals with severe COVID-19 infection and found at significantly higher levels in these patients than in patients with less severe forms of the disease.[18] In the propensity score-matched population, patients who

received TCZ had significantly longer hospital stays than patients who did not receive it. Since TCZ is administered to clinically severe patients, longer durations of hospitalization in this patient population are expected.

In both the unmatched and propensity score-matched groups, patients who received TCZ had significantly lower lymphocyte, eosinophil and platelet levels than those who did not receive TCZ. The induction of cytokine storm by IL-6 results in a robust inflammatory response manifested by an increase in CRP and procalcitonin levels, a decrease in lymphocyte counts and stimulation of the coagulation pathway, as demonstrated by elevated D-dimer levels and hypoxia.[19] It has been observed that eosinophils undergo considerable changes during the early stages of COVID-19 and are more sensitive to disease diagnosis than lymphocytes. Additionally, recovered patients experience a dynamic eosinophil recovery process, and peripheral blood eosinophils are significantly lower in deceased patients.[20] Patients in the TCZ group were monitored for 14 days from the beginning of therapeutic interventions. Consistent with previous studies,[21,22] CRP, ferritin and D-dimer values decreased toward the normal range, while lymphocyte and eosinophil counts increased. In the groups of overall and discharged patients, a decrease was observed in procalcitonin levels at the follow-up after the TCZ treatment. Conversely, in the group of patients who died, there was an initial decrease followed by an increase in procalcitonin levels on the 14th day.

In a randomized clinical trial, TCZ administered with remdesivir did not shorten the time to hospital discharge in patients with severe COVID-19 pneumonia compared to placebo plus remdesivir group.[23] It was reported that in subjects with severe COVID-19, the use of both TCZ and systemic corticosteroid therapy compared to no TCZ treatment reduced the risk of mortality.[24] For severe COVID-19 patients, the addition of TCZ to the standard of care may reduce mortality and the need for mechanical ventilation.[25] A meta-analysis that included 25 peer-reviewed publications determined that TCZ treatment is related to a decreased risk of mortality and the need for mechanical ventilation, as well as a better prognosis in COVID-19 patients, particularly those who are critically ill.[26]

In the unmatched population, patients who received TCZ had greater NIMV, HFNO, mechanical ventilation

Table 4. Comparison of the course of biochemical parameters between stable and clinically worsening groups of patients treated with tocilizumab

Patient group	Baseline	The day before tocilizumab treatment	1st day after tocilizumab treatment	3rd day after tocilizumab treatment	5th day after tocilizumab treatment	7th day after tocilizumab treatment	14h day after tocilizumab treatment	p-value
Lymphocyte [per mm^3]								
All patients	457 (1118)	375 (739)	390 (769)	400 (749)	385 (867)	330 (768)	400 (1035)	0.029 χ^2:14.02
Discharged patients	395 (1034)	420 (769)	399 (799)	415 (825)	558 (998)	530 (971)	580 (1298)	0.004 χ^2: 18.92
Mechanically ventilated patients	490 (1177)	350 (739)	370 (739)	366 (715)	368 (706)	302 (648)	119 (597)	0.787 χ^2: 3.17
Dead patients	503 (1194)	340 (734)	345 (694)	350 (733)	368 (716)	296 (540)	150 (619)	0.684 χ^2: 3.94
Eosinophil [per mm^3]								
All patients	0.006 (0.01)	0.005 (0.02)	0.008 (0.03)	0.015 (0.08)	0.030 (0.12)	0.026 (0.09)	0.039 (0.16)	<0.001 χ^2: 44.09
Discharged patients	0.006 (0.01)	0.005 (0.02)	0.008 (0.03)	0.013 (0.07)	0.031 (0.16)	0.026 (0.09)	0.074 (0.19)	<0.001 χ^2: 31.82
Mechanically ventilated patients	0.004 (0.03)	0.005 (0.01)	0.008 (0.03)	0.033 (0.08)	0.025 (0.06)	0.032 (0.09)	0.014 (0.13)	0.001 χ^2: 23.39
Dead patients	0.005 (0.02)	0.005 (0.02)	0.008 (0.04)	0.034 (0.09)	0.027 (0.08)	0.03 (0.09)	0.01 (0.14)	0.024 χ^2:14.53
Ferritin [ng/mL]								
All patients	596 (883)	1187 (1272)	1029 (1372)	816 (1021)	717 (721)	667 (857)	507 (598)	0.008 χ^2: 40.57
Discharged patients	663 (887)	1194 (1243)	1168 (1198)	775 (909)	731 (705)	657 (756)	516 (495)	<0.001 χ^2: 30.20
Mechanically ventilated patients	463 (832)	1128 (1473)	969 (1845)	919 (1407)	703 (912)	667 (1001)	343 (722)	0.008 χ^2: 17.27
Dead patients	498 (872)	1180 (1445)	969 (1506)	924 (1405)	703 (1135)	667 (1087)	176 (1444)	0.030 χ^2: 13.98
D-dimer [mg/L]								
All patients	0.72 (1.07)	1.33 (3.57)	2.41 (5.24)	2.75 (5.49)	3 (7.93)	3.08 (5.05)	1.37 (1.44)	<0.001 χ^2: 40.34
Discharged patients	0.61 (0.76)	0.91 (2.07)	1.13 (1.98)	1.33 (3.13)	1.31 (4.13)	1.25 (3.90)	1.24 (1.38)	0.001 χ^2: 23.52
Mechanically ventilated patients	0.91 (1.45)	3.22 (5.07)	5.42 (11.26)	6.06 (19.57)	8.05 (14.92)	5.48 (5.41)	1.49 (1.07)	0.003 χ^2: 19.44
Dead patients	0.95 (1.45)	2.97 (5.64)	5.57 (10.75)	6.56 (19.47)	8.82 (15.34)	5.48 (5.41)	1.5 (1.79)	0.003 χ^2: 20.08
CRP [mg/L]								
All patients	92.8 (120)	98.1 (87.9)	55 (76.2)	16 (21.8)	5.9 (10.68)	2.7 (7.95)	2 (31)	<0.001 χ^2: 109.39
Discharged patients	79 (100.1)	80.6 (75.7)	36.6 (63.3)	13.1 (20.0)	3.4 (6.9)	2 (1.45)	2 (0.6)	<0.001 χ^2: 92.42
Mechanically ventilated patients	105.8 (116.4)	116 (106.9)	67.2 (83.0)	18.65 (28.4)	10 (26.9)	9.15 (40.2)	38.4 (99.6)	<0.001 χ^2: 37.25
Dead patients	129.4 (137.1)	116 (102.7)	67.2 (85.8)	18.65 (27.9)	10 (26.9)	9.15 (39.6)	38.4 (106.1)	<0.001 χ^2: 31.77
Procalcitonin [ng/mL]								
All patients	0.09 (0.21)	0.11 (0.25)	0.08 (0.22)	0.06 (0.10)	0.04 (0.12)	0.04 (0.11)	0.02 (0.13)	<0.001 χ^2: 44.87
Discharged patients	0.07 (0.13)	0.07 (0.13)	0.05 (0.10)	0.03 (0.06)	0.02 (0.03)	0.02 (0.04)	0.02 (0.03)	<0.001 χ^2: 44.22
Mechanically ventilated patients	0.11 (0.42)	0.23 (0.68)	0.19 (0.34)	0.12 (0.40)	0.12 (0.40)	0.15 (0.42)	0.20 (1.19)	0.330 χ^2: 6.90
Dead patients	0.18 (0.45)	0.25 (0.60)	0.17 (0.34)	0.12 (0.34)	0.12 (0.40)	0.19 (0.44)	0.47 (3.19)	0.009 χ^2: 17.11

CRP – C-reactive protein. Data are presented as median (interquartile range (IQR)). Overall group comparisons were performed using Friedman's test.

requirements, and mortality. On the contrary, in the propensity score-matched population, less NIMV and mechanical ventilation support were required, and there were fewer deaths in the TCZ-treated patients. In the propensity score-matched population, there was a greater need for HFNO in patients who received TCZ treatment. Stone et al. showed that TCZ was ineffective in preventing intubation or death in moderately ill COVID-19 patients.[27] Another study indicated that treating individuals who have severe COVID-19 pneumonia with TCZ might reduce the risk of needing invasive mechanical ventilation and mortality.[28]

The multivariate adjusted Cox regression model showed that TCZ was associated with an 84% reduction in the risk of in-hospital death. However, the risk of death increased 5.3 times with hypertension and 18.5 times with intubation. The survival probability of TCZ-treated patients was significantly higher than that of untreated patients. In a meta-analysis, the administration of IL-6 antagonists was found to be associated with lower all-cause mortality 28 days after randomization.[29] It has been reported that the relative risk of death is increased two-fold among patients with hypertension compared to patients without hypertension.[30]

Of the 128 TCZ-treated patients, 35 (27.3%) developed a bacterial infection, 4 (3.1%) a fungal infection and 2 (1.6%) a viral infection (cytomegalovirus viremia) while hospitalized. Positive sputum cultures were identified in 25 (19.5%) patients. Keske et al. detected secondary bacterial infections among 9 (41%) of the 22 patients who were admitted to the ICU and treated with TCZ.[14] A meta-analysis of serious adverse events from 23 clinical trials concluded that the risk of secondary infection after 28 days was comparable between patients treated with IL-6 antagonists (750/3428; 21.9%) and those treated with standard care or placebo (330/1787; 17.6%).[29] A single-center investigation found that patients treated with TCZ were more than twice as likely to develop a superinfection as untreated controls (54% compared to 26%), owing principally to a significant increase in ventilator-associated pneumonia (45% compared to 20%).[31]

Limitations

Although these data are retrospective and observational, we used propensity score matching to exclude confounding effects caused by imbalances in TCZ treatment. The limitations of this study include a lack of the evaluation of the secondary infection in patients who did not receive TCZ, and a lack of measurement of the IL-6 levels of the patients. In addition to the administration of TCZ according to the institutional guidelines, it was thought that there might be an indication bias, because the clinician plays an important role in the treatment decision.

Conclusions

This study concluded that TCZ treatment in patients with COVID-19 was associated with better survival, reduced need for mechanical ventilation and reduced hospital-associated mortality.

ORCID IDs

Özge Aydin Güçlü https://orcid.org/0000-0003-1005-3205
Uğur Önal https://orcid.org/0000-0001-6194-3254
Halıs Akalın https://orcid.org/0000-0001-7530-1279
Nilüfer Aylın Acet Öztürk https://orcid.org/0000-0002-6375-1472
Hazel Öztürk Belık https://orcid.org/0000-0002-7415-3339
Ezgı Demırdöğen https://orcid.org/0000-0002-7400-9089
Asli Görek Dılektaşli https://orcid.org/0000-0001-7099-9647
Esra Kazak https://orcid.org/0000-0002-7380-2501
Gökhan Ocakoğlu https://orcid.org/0000-0002-1114-6051
İmran Sağlik https://orcid.org/0000-0003-0864-4989
Funda Coşkun https://orcid.org/0000-0003-3604-8826
Dane Edıger https://orcid.org/0000-0002-2954-4293
Yasemın Heper https://orcid.org/0000-0002-6635-5416
Ahmet Ursavaş https://orcid.org/0000-0003-4482-5904
Emel Yılmaz https://orcid.org/0000-0002-3894-1231
Esra Uzaslan https://orcid.org/0000-0003-3120-6506
Mehmet Karadağ https://orcid.org/0000-0002-9027-1132

References

1. Chen N, Zhou M, Dong X, et al. Epidemiological and clinical characteristics of 99 cases of 2019 novel coronavirus pneumonia in Wuhan, China: A descriptive study. *Lancet*. 2020;395(10223):507–513. doi:10.1016/S0140-6736(20)30211-7
2. Bakanliği, TS. COVID-19 (SARS-CoV2 Enfeksiyonu) Rehberi. https://covid19bilgi.saglik.gov.tr/depo/rehberler/COVID-19_Rehberi.pdf [in Turkish]. Accessed July 16, 2020.
3. Mehta P, McAuley DF, Brown M, Sanchez E, Tattersall RS, Manson JJ. COVID-19: Consider cytokine storm syndromes and immunosuppression. *Lancet*. 2020;395(10229):1033–1034. doi:10.1016/S0140-6736(20)30628-0
4. Mangalmurti N, Hunter CA. Cytokine storms: Understanding COVID-19. *Immunity*. 2020;53(1):19–25. doi:10.1016/j.immuni.2020.06.017
5. Christensen J, Kumar D, Moinuddin I, et al. Coronavirus disease 2019 viremia, serologies, and clinical course in a case series of transplant recipients. *Transplant Proc*. 2020;52(9):2637–2641. doi:10.1016/j.transproceed.2020.08.042
6. Zhu J, Pang J, Ji P, et al. Elevated interleukin-6 is associated with severity of COVID-19: A meta-analysis. *J Med Virol*. 2021;93(1):35–37. doi:10.1002/jmv.26085
7. Tanaka T, Narazaki M, Kishimoto T. Immunotherapeutic implications of IL-6 blockade for cytokine storm. *Immunotherapy*. 2016;8(8):959–970. doi:10.2217/imt-2016-0020
8. Nasonov E, Samsonov M. The role of interleukin 6 inhibitors in therapy of severe COVID-19. *Biomed Pharmacother*. 2020;131:110698. doi:10.1016/j.biopha.2020.110698
9. Liu B, Li M, Zhou Z, Guan X, Xiang Y. Can we use interleukin-6 (IL-6) blockade for coronavirus disease 2019 (COVID-19)-induced cytokine release syndrome (CRS)? *J Autoimmun*. 2020;111:102452. doi:10.1016/j.jaut.2020.102452
10. Antwi-Amoabeng D, Kanji Z, Ford B, Beutler BD, Riddle MS, Siddiqui F. Clinical outcomes in COVID-19 patients treated with tocilizumab: An individual patient data systematic review. *J Med Virol*. 2020;92(11):2516–2522. doi:10.1002/jmv.26038
11. Xu X, Han M, Li T, et al. Effective treatment of severe COVID-19 patients with tocilizumab. *Proc Natl Acad U S A*. 2020;117(20):10970–10975. doi:10.1073/pnas.2005615117
12. Mastroianni A, Greco S, Apuzzo G, et al. Subcutaneous tocilizumab treatment in patients with severe COVID-19-related cytokine release syndrome: An observational cohort study. *EClinicalMedicine*. 2020;24:100410. doi:10.1016/j.eclinm.2020.100410

13. Mert A, Vahaboğlu H, Arslan F, et al. Tocilizumab treatment in severe COVID-19: A multicenter retrospective study with matched controls. *Rheumatol Int*. 2022;42(3):457–467. doi:10.1007/s00296-021-04965-6

14. Keske Ş, Tekin S, Sait B, et al. Appropriate use of tocilizumab in COVID-19 infection. *Int J Infect Dis*. 2020;99:338–343. doi:10.1016/j.ijid.2020.07.036

15. World Health Organization. Coronavirus Disease 2019 (COVID-19). Situation Report – 73. https://www.who.int/docs/default-source/coronaviruse/situation-reports/20200402-sitrep-73-covid-19.pdf?sfvrsn=5ae25bc7_6&download=true. Accessed May 15, 2020.

16. Simpson S, Kay FU, Abbara S, et al. Radiological Society of North America expert consensus document on reporting chest CT findings related to COVID-19: Endorsed by the Society of Thoracic Radiology, the American College of Radiology, and RSNA. *Radiol Cardiothorac Imaging*. 2020;2(2):e200152. doi:10.1148/ryct.2020200152

17. Hosmer DW, Lemeshow S, Sturdivant RX. *Applied Logistic Regression*. 3rd ed. Hoboken, USA: Wiley & Sons; 2013. doi:10.1002/9781118548387

18. Huang C, Wang Y, Li X, et al. Clinical features of patients infected with 2019 novel coronavirus in Wuhan, China. *Lancet*. 2020;395(10223):497–506. doi:10.1016/S0140-6736(20)30183-5

19. Massabeti R, Cipriani MS, Valenti I. Covid-19: A systemic disease treated with a wide-ranging approach. A case report. *J Popul Ther Clin Pharmacol*. 2020;27(S Pt 1):e26–e30. doi:10.15586/jptcp.v27iSP1.691

20. Contoli M, Ito K, Padovani A, et al. Th2 cytokines impair innate immune responses to rhinovirus in respiratory epithelial cells. *Allergy*. 2015;70(8):910–920. doi:10.1111/all.12627

21. Ivan Hariyanto T, Kurniawan A. Tocilizumab administration is associated with the reduction in biomarkers of coronavirus disease 2019 infection. *J Med Virol*. 2021;93(3):1832–1836. doi:10.1002/jmv.26698

22. Toniati P, Piva S, Cattalini M, et al. Tocilizumab for the treatment of severe COVID-19 pneumonia with hyperinflammatory syndrome and acute respiratory failure: A single-center study of 100 patients in Brescia, Italy. *Autoimmun Rev*. 2020;19(7):102568. doi:10.1016/j.autrev.2020.102568

23. Rosas IO, Diaz G, Gottlieb RL, et al. Tocilizumab and remdesivir in hospitalized patients with severe COVID-19 pneumonia: A randomized clinical trial. *Intensive Care Med*. 2021;47(11):1258–1270. doi:10.1007/s00134-021-06507-x

24. Alkofide H, Almohaizeie A, Almuhaini S, Alotaibi B, Alkharfy KM. Tocilizumab and systemic corticosteroids in the management of patients with COVID-19: A systematic review and meta-analysis. *Int J Infect Dis*. 2021;110:320–329. doi:10.1016/j.ijid.2021.07.021

25. Aziz M, Haghbin H, Abu Sitta E, et al. Efficacy of tocilizumab in COVID-19: A systematic review and meta-analysis. *J Med Virol*. 2021;93(3):1620–1630. doi:10.1002/jmv.26509

26. Wei Q, Lin H, Wei RG, et al. Tocilizumab treatment for COVID-19 patients: A systematic review and meta-analysis. *Infect Dis Poverty*. 2021;10(1):71. doi:10.1186/s40249-021-00857-w

27. Stone JH, Frigault MJ, Serling-Boyd NJ, et al. Efficacy of tocilizumab in patients hospitalized with Covid-19. *N Engl J Med*. 2020;383(24):2333–2344. doi:10.1056/NEJMoa2028836

28. Guaraldi G, Meschiari M, Cozzi-Lepri A, et al. Tocilizumab in patients with severe COVID-19: A retrospective cohort study. *Lancet Rheumatol*. 2020;2(8):e474–e484. doi:10.1016/S2665-9913(20)30173-9

29. Gupta S, Wang W, Hayek SS, et al. Association between early treatment with tocilizumab and mortality among critically ill patients with COVID-19. *JAMA Intern Med*. 2021;181(1):41–51. doi:10.1001/jamainternmed.2020.6252

30. Gao C, Cai Y, Zhang K, et al. Association of hypertension and antihypertensive treatment with COVID-19 mortality: A retrospective observational study. *Eur Heart J*. 2020;41(22):2058–2066. doi:10.1093/eurheartj/ehaa433

31. Somers EC, Eschenauer GA, Troost JP, et al. Tocilizumab for treatment of mechanically ventilated patients with COVID-19. *Clin Infect Dis*. 2021;73(2):e445–e454. doi:10.1093/cid/ciaa954

Quality of life in patients with lymphoproliferative neoplasms at diagnosis and after the first-line treatment

Nicola Elżbieta Szeja[A–D], Sebastian Grosicki[E,F]

Department of Hematology and Cancer Prevention, Faculty of Health Sciences in Bytom, Medical University of Silesia in Katowice, Poland

A – research concept and design; B – collection and/or assembly of data; C – data analysis and interpretation;
D – writing the article; E – critical revision of the article; F – final approval of the article

Address for correspondence
Nicola Elżbieta Szeja
E-mail: nszeja@gmail.com

Abstract

Background. The assessment of the quality of life (QoL) in hematology-oncology patients is extremely important. The disease and anti-cancer therapy can cause adverse effects, directly impacting the physical and mental condition of the patient and indirectly influencing their social and professional situation. Therefore, a properly performed QoL assessment should take into account all of these aspects. Moreover, QoL assessment has a prognostic value in regard to treatment success and prognosis; therefore, the improvement in the QoL is often one of the goals of therapy.

Objectives. To identify the changes in QoL during therapy in patients with lymphoproliferative neoplasms.

Materials and methods. Forty-six hematology-oncology patients participated in this prospective single-center study. Their QoL was analyzed at 2 time points (before and after the first-line treatment). For this purpose, the EORTC QLQ-C30 questionnaire was used. All statistical analyses were performed using the STA-TISTICA v. 13 software. A value of $p < 0.05$ was considered statistically significant.

Results. The study included patients with multiple myeloma (MM; 47.8%), non-Hodgkin lymphoma (NHL; 28.3%) and chronic lymphocytic leukemia (CLL; 23.9%). After the first line of treatment, patients perceived their overall QoL as slightly better than before starting the treatment, with an average increase of 1.94. Statistically significant differences were observed in physical and emotional functioning as well as fatigue, pain, dyspnea, appetite, and constipation.

Conclusions. In patients with lymphoproliferative neoplasms, after the first-line treatment, an improvement in an overall QoL and level of functioning, as well as a reduction in the severity of symptoms were observed.

Ke y words: quality of life, chemotherapy, lymphoproliferative neoplasms

Background

Lymphoproliferative neoplasms consist of a diverse group of diseases,[1] in which those with the highest global incidence rate include: non-Hodgkin lymphoma (NHL; 2.8%), leukemia (2.5%) and multiple myeloma (MM; 0.9%). The above diseases accounted for 2.6%, 3.1% and 1.2% of deaths in 2020, respectively.[2]

Non-Hodgkin lymphoma is a heterogeneous group of lymphatic system neoplasms, representing a wide spectrum of diseases with various aggressiveness. These neoplasms can originate from peripheral B lymphocytes (85–90%), T lymphocytes or natural killer cells.[3,4] Clinically, NHL is divided into indolent lymphomas and aggressive lymphomas, according to the proliferation rate of the neoplastic cell and timing of the symptom onset.[5] In highly developed countries, the most common leukemia in adults is chronic lymphocytic leukemia (CLL). This neoplasm is characterized by an increased number of circulating, immunocompetent, small, mature, monoclonal B lymphocytes with typical morphology and immunophenotypes within the peripheral blood.[6,7] In turn, MM is a cytogenetically heterogeneous clonal proliferative disorder of atypical plasma cells, characterized by multifocal bone marrow involvement and specific secondary organ symptoms.[8,9]

Due to the remarkable progress made in the treatment of hematological malignancies (HMs) and significant improvements in the survival rates of patients, it is necessary to adopt a more chronic treatment model for these diseases. Thus, the improvement in the patient's quality of life (QoL) is becoming more and more important.[10] Quality of life is a multidimensional phenomenon covering various domains of human life; therefore, despite many years of analysis, no unambiguous definition of this concept has been achieved.

In medical science, the most commonly used definition of QoL was published in 1995 by the World Health Organization (WHO). According to the WHO, QoL is an individual's perception of their life position in the context of the culture and value systems in which they live, in relation to individual goals, expectations, standards, and fears. This concept includes following elements: physical and emotional health, level of independence, social relationships, personal beliefs, and the relationship of these elements to important environmental characteristics. All aspects must be evaluated in order for a comprehensive, personal QoL assessment to be performed. Moreover, this definition draws the attention to the fact that QoL is a subjective concept that includes both positive and negative aspects of human life.[11]

The concept of health-related quality of life (HRQoL) is equally important, the definition of which is patient-oriented and, above all, functional. Health-related quality of life represents the sum of the daily functional abilities in a patient's life in 4 domains: physical and professional activity, mental functioning, social interactions, and somatic experiences. At the same time, it should be noted that HRQoL is a multifactorial parameter assessed by the patient and can change during the course and treatment of the disease.[12]

Considering the above, the assessment of QoL in hematology-oncology patients in connection with the diagnosis and treatment is extremely important. Both the disease and the anti-cancer therapy can cause adverse effects that directly impact the physical and mental conditions of a patient, and can indirectly influence their social and professional situation. Thus, a properly performed QoL assessment should take into consideration all of these aspects. Moreover, the QoL has a prognostic value with regard to treatment success and prognosis; therefore, the improvement in QoL is often one of the goals of patient therapy.[13]

The QoL analyses can be carried out using various methods, the most common of which are questionnaires. The questionnaires should be characterized by high validity and reliability. Moreover, the questionnaire cannot simply focus on a single domain, as it would not constitute an accurate QoL assessment.[14,15]

The available questionnaires can be divided into:
– general (generic), which are used both in healthy and sick individuals with various clinical diseases;
– detailed (specific), designed to assess a particular disease based on its specific elements – spheres of functioning or factors resulting from the disease;
– mixed, containing the elements of a general questionnaire and those intended for a specific disease.[16]

According to the results of a systematic review of QoL research in medicine and health sciences, the most frequently used general questionnaires were: SF-36, EQ-5D and WHOQOL-BREF. At the same time, among specific questionnaires, the EORTC QLQ-C30 questionnaire is most frequently used.[13] On the other hand, mixed questionnaires are often prepared specifically for a clinical trial and are used solely for this purpose (ad hoc).[16]

The EORTC QLQ-C30 questionnaire (v. 3.0) was developed by the Quality of Life Research Group of the European Organization for Research and Treatment of Cancer (EORTC). Its basic version (core) is a standardized tool intended for oncological patients regardless of the form, type and location of the tumor.[17] However, separate modules for the assessment of QoL related to specific primary tumor sites were also developed.[14] Among HMs, the module for the assessment of QoL in MM patients (QLQ-MY20)[18] is fully validated. On the other hand, the modules for patients with Hodgkin lymphoma (HL; QLQ-HL27), high- or low-grade NHL (HG/LG-NHL; QLQ-NHL-HG29 and QLQ-NHL-LG20, respectively), CLL (QLQ-CLL17),[19] and chronic myeloid leukemia (CML; QLQ-CML24)[20,21] are currently in the final stages of development. The results of previous research suggest that the EORTC QLQ-C30 and its modifications are reliable tools for the assessment of QoL in hematology-oncology patients.[10,22]

Objectives

Individual problems revealed during the QoL assessment may lead to the modification of the treatment or rehabilitation regimen in order to improve the health condition of the patient. Therefore, our study aimed to identify the QoL in patients with lymphoproliferative neoplasms before and after the first line of treatment.

Materials and methods

The presented results are part of a larger research project carried out in the years 2017–2019 at Department of Hematology and Cancer Prevention in Chorzów, Poland. The study protocol was approved by the Bioethical Committee of the Medical University of Silesia in Katowice, Poland, under the resolutions No. KNW/0022/KB1/4/17 and KNW/0022/KBI/4/I/17/19.

Adults with a confirmed diagnosis of CLL, NHL or MM who were receiving an intensive treatment program were eligible for the study. Patients who had previously undergone cancer therapy and those with an active acute or chronic infection, a systemic connective tissue disease, an implanted pacemaker, or a significant clinical burden, were excluded from the study. The inclusion criteria were met by a total of 58 patients, 8 of whom refused to participate and 4 died. The final analysis consisted of 46 people who were monitored twice during their hospitalization:

– after diagnosis, before starting therapy;
– after the first line of treatment, while assessing its effect.

In this study, the standardized EORTC QLQ-C30 questionnaire (v. 3.0) was used to assess the QoL of cancer patients. The questionnaire contains questions regarding the impact of the disease on different areas of a patient's life (physical, role, emotional, cognitive, and social functioning), the occurrence of symptoms (fatigue, nausea and vomiting, pain, dyspnea, insomnia, appetite loss, constipation, and diarrhea), financial difficulties, and an overall assessment of QoL (Table 1).[17]

For each question, the respondent must choose 1 answer. For 28 of the questions, the answers are given on a 4-point Likert-type scale (1 – never, 2 – sometimes, 3 – often, 4 – very often) and assess the intensity of the analyzed parameters. The last 2 questions evaluate the general health of the patient on a 7-point scale (from 1 – very bad to 7 – excellent). Patients completed the questionnaires by themselves. If a question arose, they could ask the researcher for an explanation.

After collecting the responses, a raw score was calculated for each of the abovementioned 15 questionnaire items. Next, a linear transformation was performed to obtain a score in a range from 0 to 100. The conversion of the results to a 100-point scale was made according to the EORTC guidelines.[23] Of note, a higher score on the functional scales means better functioning and a higher response for general health corresponds to a better QoL. The situation is different when interpreting the symptom scales, where a higher score indicates

Table 1. Description of questions included in the EORTC QLQ-C30 questionnaire (own elaboration based on the studies)[19,24]

Scale	Abbreviation	Item numbers	Number of items	Item range*
Functional scales				
Physical functioning	PF	1–5	5	3
Role functioning	RF	6, 7	2	3
Emotional functioning	EF	21–24	4	3
Cognitive functioning	CF	20, 25	2	3
Social functioning	SF	26, 27	2	3
Symptom scales				
Fatigue	FA	10, 12, 18	3	3
Nausea and vomiting	NV	14, 15	2	3
Pain	PA	9, 19	2	3
Symptom items				
Dyspnea	DY	8	1	3
Insomnia	SL	11	1	3
Appetite loss	AP	13	1	3
Constipation	CO	16	1	3
Diarrhea	DI	17	1	3
Financial difficulties	FI	28	1	3
Global health status/QoL	QL	29, 30	2	6

* Item range indicates the difference between the possible maximum and minimum response to individual items. EORTC QLQ-C30 – European Organisation for Research and Treatment of Cancer quality of life questionnaire; QoL – quality of life.

1210

N. Szeja, S. Grosicki. Quality of life of hemato-oncological patients

a higher level of symptom burden.[17,23] Additionally, each patient answered questions concerning sociodemographic data: gender, education, year of birth, place of residence, and a subjective assessment of health.

The normality of the distribution was assessed using the Shapiro–Wilk test. The Pearson's χ^2 test was performed to compare qualitative variables, while quantitative variables before and after treatment were compared using the Wilcoxon signed-rank test. A value of p < 0.05 was considered statistically significant. The analyses were performed using the STATISTICA v. 13 software (TIBCO Software Inc., Palo Alto, USA). The graphic design and supplementary calculations were performed using Microsoft Excel 2016 (Microsoft Corp., Redmond, USA).

The research followed the principles outlined in the Declaration of Helsinki for all human or animal research. In addition, for investigations involving human subjects, informed consent was obtained from the participants involved.

Results

The general characteristics of the study group are presented in Table 2. The youngest patient was 19 years old and the oldest was 81 years old. The median age of the respondents was 62 years, and the mean age was 59.5 (±15.3 years). Men (65.0%) constituted a much greater percentage, with

Table 2. General characteristics of the study group

Parameters	Value
Age [years], mean (±SD)	59.5 (±15.3)
Age [years], median (range)	62 (19–81)
Time duration of treatment [days], mean (±SD)	118 (±48.8)
Gender	
Female, n (%)	16 (35.0)
Male, n (%)	30 (65.0)
Education	
Primary, n (%)	6 (13.0)
Basic vocational, n (%)	14 (30.4)
Secondary, n (%)	16 (34.8)
Higher, n (%)	10 (21.8)
Place of residence	
City, n (%)	42 (91.3)
Village, n (%)	4 (8.7)
Living with the family	
Yes, n (%)	41 (89.1)
No, n (%)	5 (10.9)
Multiple diseases	
Yes, n (%)	28 (60.9)
No, n (%)	18 (39.1)

SD – standard deviation.

a slight majority of patients having secondary education (34.8%). Most of the patients lived in a city (91.3%) with their families (89.1%). The presence of more than 2 comorbidities (including hypertension, type 2 diabetes or prostatic hyperplasia) was reported in 60.9% of patients.

The most common hematology-oncology diagnosis was MM (Fig. 1). All patients enrolled in the study received chemotherapy or chemoimmunotherapy for a mean duration of 118 (±48.8) days. Most of the patients, before starting the treatment (84.8%) and after the first line of treatment (91.3%), described their health as good or very good (Fig. 2). In the case of this parameter, there was no statistically significant difference (χ^2 test; p = 0.3775).

After ending the first line of treatment, patients perceived their overall QoL to be slightly better than before starting the treatment, with an average increase of 1.94. For all functional scales, the results in the 2nd observation period increased, which means a better level of patient functioning. Statistically significant changes were demonstrated in the physical and emotional functioning parameters (Table 3).

In the case of symptom scales, most of the results decreased, which indicates a lower intensity of symptoms. At the same time, respondents indicated the occurrence
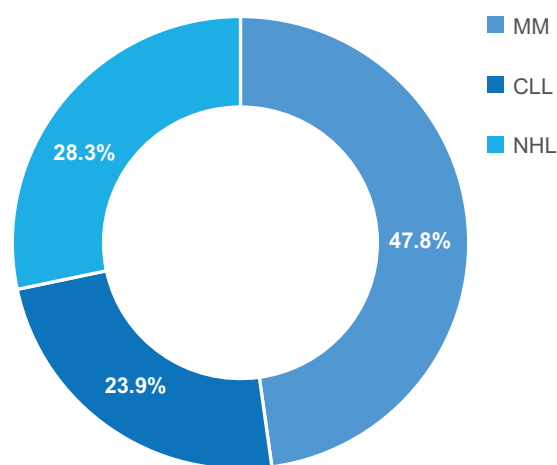

Fig. 1. Incidence of lymphoproliferative neoplasms in the study group

MM – multiple myeloma; CLL – chronic lymphocytic leukemia; NHL – non-Hodgkin lymphoma.
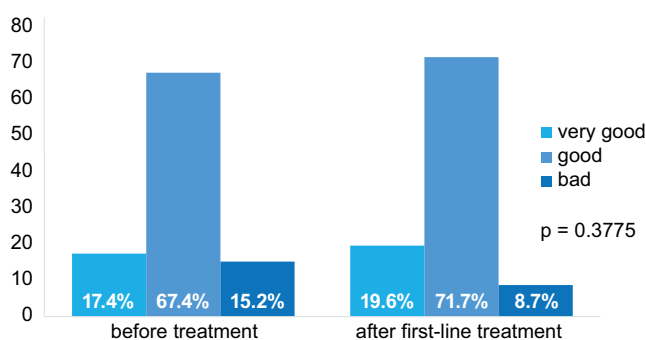

Fig. 2. Self-assessment of patients' health before and after the first-line treatment

Table 3. Parameters of the quality of life and functional scales before and after the first-line treatment

Scale	Before treatment				After first-line treatment				p-value*
	M ±SD	Me	Q1	Q3	M ±SD	Me	Q1	Q3	
QL	60.74 ±15.95	58.33	50.00	75.00	62.68 ±16.73	58.33	58.33	175.00	0.1224
PF	81.59 ±14.14	80.00	80.00	86.67	88.55 ±15.76	93.33	86.67	100.00	0.0004
RF	69.20 ±24.84	66.67	66.67	100.00	72.07 ±22.76	75.00	66.67	100.00	0.1006
EF	71.38 ±12.99	75.00	66.67	83.33	83.88 ±12.47	83.33	83.33	91.67	0.0003
CF	82.97 ±17.39	83.33	66.67	100.00	84.78 ±14.83	83.33	83.33	100.00	0.1219
SF	72.83 ±16.98	66.67	66.67	83.33	74.07 ±18.13	75.00	66.67	100.00	0.1337

* Wilcoxon test; M – mean; SD – standard deviation; Me – median; Q1 – 1st quartile; Q3 – 3rd quartile; QL – global health status/quality of life (QoL); PF – physical functioning; RF – role functioning; EF – emotional functioning; CF – cognitive functioning; SF – social functioning.

Table 4. Parameters of symptom scales and items before and after the first-line treatment

Scale	Before treatment				After first-line treatment				p-value*
	M ±SD	Me	Q1	Q3	M ±SD	Me	Q1	Q3	
FA	21.26 ±18.27	11.11	11.11	22.22	32.13 ±16.27	33.33	22.22	33.33	0.0004
NV	9.42 ±12.98	0.00	0.00	16.67	11.44 ±15.37	0.00	0.00	16.67	0.4445
PA	25.14 ±14.15	22.22	16.67	50.00	10.94 ±13.03	0.00	0.00	33.33	0.0002
DY	18.12 ±26.02	0.00	0.00	33.33	9.42 ±12.95	0.00	0.00	0.00	0.0001
SL	15.94 ±18.24	0.00	0.00	33.33	11.59 ±18.88	0.00	0.00	33.33	0.3612
AP	23.91 ±24.00	33.33	0.00	33.33	12.42 ±15.17	0.00	0.00	33.33	0.0003
CO	18.12 ±16.79	33.33	0.00	33.33	8.70 ±14.80	0.00	0.00	33.33	0.0116
DI	11.59 ±17.52	0.00	0.00	33.33	9.97 ±17.48	0.00	0.00	0.00	0.4567
FI	8.87 ±12.80	0.00	0.00	33.33	11.32 ±14.27	0.00	0.00	33.33	0.1821

* Wilcoxon test; M – mean; SD – standard deviation; Me – median; Q1 – 1st quartile; Q3 – 3rd quartile; FA – fatigue; NV – nausea and vomiting; PA – pain; DY – dyspnea; SL – insomnia; AP – appetite loss; CO – constipation; DI – diarrhea; FI – financial difficulties.

of fatigue and nausea/vomiting more often after the first line of treatment. The average values regarding financial difficulties also increased. Statistically significant differences were observed for fatigue, pain, dyspnea, appetite loss, and constipation (Table 4).

Discussion

The results of a systematic review on QoL in patients with HMs indicate that these diseases negatively affect the overall QoL. The deterioration in quality was found in all domains of life, both in terms of physical and mental health, as well as the social and professional aspects. Fatigue was the most common physical symptom. A decrease in sexual activity and cognitive functions were also noted.[24] At the same time, our research shows that the overall QoL of hematology-oncology patients improved slightly after the end of the first-line treatment. Cancer is a disease that can negatively affect one's perception of QoL through changes in many aspects of life, the lack of acceptance and the need to adapt to a new and not yet fully understood situation. In our patients, the results of the initial follow-up, which was at the time of diagnosis and initiation of anti-cancer treatment, identified additional stress and a sense of danger and uncertainty in their responses.

After completing therapeutic measures, their approach to the disease, and thus also QoL, changed positively. Similar results were obtained by the authors who conducted a longitudinal cohort study in 102 adult oncology patients, performing 3 evaluations (before the administration of the 1st, 2nd and the 3rd/last cycle of chemotherapy), whose QoL was slightly better at the end of treatment.[25] Patients treated with a hematopoietic stem cell transplant showed much better QoL at 3 months after the procedure compared to the baseline period (71.39 ±12.32 compared to 60.00 ±13.20).[26] Also, in patients with acute myeloid leukemia (AML) after induction chemotherapy, the global QoL increased compared to the time of diagnosis (65.5 ±21.0 compared to 49.3 ±26.3).[10] A similar trend was noted in patients with CML, which continued for 2 years from the baseline period.[27] Inverse results were obtained in patients with acute leukemias[28] and MMs.[29] These differences may result from a number of variables, including study size, type and stage of cancer, treatment, adverse effects, and the period of observation.

Interestingly, the improvements in QoL of patients may also be influenced by the favorable changes observed in their diet, as reported in a systematic review by Govindaraju et al. These authors searched 8 databases for publications on the correlation between the use of specific eating patterns and QoL or health status in patients with

an average age ≥60 years old. In the majority of analyzed studies, the use of rational eating patterns (e.g., the Mediterranean diet) was associated with a better self-esteem and QoL in one or more aspects of life.[30]

Based on our analysis, the functional aspects with the greatest changes were seen in the physical and emotional state of the respondents. There was a significant improvement in the physical domain during the observation period (88.55 ±15.76 compared to 81.59 ±14.14). Therefore, it can be concluded that after completing the first-line therapy, everyday activities were less difficult for patients. A slight increase in this parameter was also shown after induction chemotherapy in 255 patients with AML.[10] The same trend was noted after 3, 6, 12, 18, and 24 months in patients with CML.[27] A different result was obtained in patients with newly diagnosed acute leukemias, in whom a significant deterioration of physical functions was observed after the administration of induction chemotherapy. At the same time, when comparing the results for both described groups, it should be noted that patients with AML and acute lymphoblastic leukemia had much lower values in this domain even before the treatment (70.68 ±20.75 compared to 81.59 ±14.14).[28] Patients with MM had an even greater decrease in physical functioning before the treatment (53.9 ±26.3), and it dropped significantly 3 months after chemotherapy (38.9 ±21.3).[29] Conflicting results were obtained in patients with diffuse large B-cell lymphoma, CLL and AML. During the follow-up after the 2nd treatment cycle, the value of physical functioning was 69.67 ±18.16. It slightly decreased (68.89 ±21.81) after the 1st month, and then increased substantially (80.35 ±18.52) 6 months after the end of therapy.[31]

In our study, changes in role and social functioning also slightly improved during the 2nd follow-up period. This means that patients felt slightly less restricted in their work and hobbies, as well as in their family and social life. This is an ambiguous result, which seems to be the outcome of a better organization in this sphere of life, where, despite hospital stays or adverse effects related to the treatment, patients remained professionally and socially active. Similar results were obtained by Salas et al., who showed that patients examined before the last cycle of chemotherapy had better results in terms of role and social functioning.[25] An upward trend in these domains was also shown in patients observed over 3 periods – after the 2nd treatment cycle and at the 1st and 6th month after its completion.[31] Interestingly, in German observations conducted among 109 patients with HMs, the mean values in both spheres were much lower (37.4 ±37.6 for role functioning and 43.9 ±36.8 for social functioning).[32]

It is possible that due to the changes described above, there were significant differences in the emotional domain, assessed in terms of mental tension, worry, irritation, and depression. As shown by the results of a cross-sectional study conducted among 87 patients with HMs,

a disorder in this sphere of life significantly affects one's global QoL.[33] Similar conclusions were reached by other authors who showed that patients with more stress had worse QoL.[32] In our study, patients experienced negative emotions more often during the diagnosis period, likely due to the state of uncertainty about their future and a high level of mental tension. Of course, therapy can also evoke such emotions, but the appropriate support from family, friends and medical staff can reduce their severity. In addition, the treatment aimed at improving a patient's health, which they are aware of, should have a positive effect on the results. Improvements in this parameter were also observed after the completion of induction chemotherapy in patients with AML,[10] CML[27] and MM.[29] The same trend was also shown in patients after the hematopoietic stem cell transplant.[25] Also, comparing the data of hematology-oncology patients after the 2nd treatment cycle and after its completion, the values of emotional functioning significantly increased.[31] However, different results were shown in patients with acute leukemias, in whom the implementation of induction chemotherapy was associated with a significantly negative impact on emotional functioning.[28]

When analyzing cognitive functioning defined by difficulties in focusing attention and remembering, slightly better values were observed in patients during the 2nd period of observation (84.78 ±14.83 compared to 82.97 ±17.39). This may be due to a lower emotional burden which is consistent with the results reported by other authors.[10,31] Interestingly, in a study conducted in patients with AML and acute lymphoblastic leukemia, the baseline results in this sphere of life were higher (91.09 ±15.37) and slightly decreased (88.33 ±21.60) after the treatment. However, these subjects were younger (mean age: 33.03 ±15.4 years).[28] A significant decrease in this domain was observed in patients with MM after induction chemotherapy compared to the period before its implementation (57.3 ±28.1 and 78.0 ±27.1, respectively).[29]

The greatest changes in symptom severity were observed in fatigue, pain, dyspnea, loss of appetite, and constipation. Of these symptoms, only the severity of fatigue, described as the need to rest and feeling of weakness, increased significantly during the 2nd stage of our study (21.26 ±18.27 compared to 32.13 ±16.27). The remaining symptoms decreased significantly in their severity. Among other symptoms, the intensity of nausea and vomiting increased slightly, while insomnia and diarrhea decreased in intensity. This may be largely due to the fact that patients often received medications to alleviate the adverse effects of therapy. Divergent results were obtained in patients with acute leukemia who, after the 1st administration of induction chemotherapy, noticed an increase in all the described symptoms, except for dyspnea.[28] Different results were seen in a study of patients treated for diffuse large B-cell lymphoma, CLL and AML. The severity of fatigue, nausea and vomiting, insomnia, loss of appetite, constipation, and

diarrhea decreased during the period from the 2nd treatment cycle to a month after its completion, while the intensity of pain and dyspnea increased during this time.[31] On the other hand, patients with AML after the completion of induction chemotherapy showed a lower intensity of all these symptoms, except for constipation.[10] Interestingly, the authors of a prospective study of 124 patients with CML reported that the baseline severity of fatigue was an independent predictor of achieving a greater molecular response.[27]

In our study, during the 2nd follow-up, patients more often chose a higher value in the dimension of financial difficulties. This could be related to both the costs of absenteeism at work and the treatment itself. Other authors obtained similar results in this aspect of life.[26,28] However, different results were seen in patients with MM, in which this value decreased significantly 3 months after chemotherapy compared to the period before the treatment (14.7 ±28.9 compared to 41.3 ±41.1).[29]

In summary, assessing the QoL in hematology-oncology patients is extremely important for many clinical reasons. Both the disease itself and the applied anti-cancer therapy may cause adverse effects that directly affect the patient's physical and mental health, indirectly influencing their social and professional situation. At the same time, QoL has a prognostic value in terms of treatment success and prognosis; therefore, the assessment of this parameter should be conducted during early stages of clinical management. Certain types of interventions, such as physical programs and psychotherapy can help in improving the QoL.[24,34]

Limitations

Our study has several limitations. The basic element is the relatively small size of the study group, as well as a wide range of patient ages and their clinical and therapeutic heterogeneity. This also closely correlates with the limitation in the ability to conduct detailed statistical analyses. Moreover, this was a single-center study and the obtained results may not reflect that of the population.

Conclusions

After the 1st line of treatment, patients perceived their overall QoL to be slightly better compared to the diagnostic period.

During the 2nd evaluation period, the results for all functional scales increased, indicating a better level of patient functioning. Additionally, significant changes took place in the physical and emotional spheres.

Most of the values on the symptom scales during the 2nd period of the study significantly decreased, which indicates a lower intensity of symptoms. Additionally, significant differences were seen in pain, dyspnea, appetite loss, and constipation.

After the end of treatment, an increase in the intensity of symptoms was seen in fatigue as well as nausea and vomiting. At this time, patients also experienced financial difficulties more often.

ORCID iDs

Nicola Elżbieta Szeja https://orcid.org/0000-0003-4769-927X
Sebastian Grosicki https://orcid.org/0000-0003-2644-1050

References

1. Swerdlow SH, Campo E, Harris NL, et al., eds. *WHO Classification of Tumours of Haematopoietic and Lymphoid Tissues*. Revised 4th ed. Lyon, France: International Agency for Research on Cancer; 2017.
2. Sung H, Ferlay J, Siegel RL, et al. Global Cancer Statistics 2020: GLOBOCAN estimates of incidence and mortality worldwide for 36 cancers in 185 countries. *CA Cancer J Clin*. 2021;71(3):209–249. doi:10.3322/caac.21660
3. Bowzyk Al-Naeeb A, Ajithkumar T, Behan S, Hodson DJ. Non-Hodgkin lymphoma. *BMJ*. 2018;362:k3204. doi:10.1136/bmj.k3204
4. Armitage JO, Gascoyne RD, Lunning MA, Cavalli F. Non-Hodgkin lymphoma. *Lancet*. 2017;390(10091):298–310. doi:10.1016/S0140-6736(16)32407-2
5. Bispo JAB, Pinheiro PS, Kobetz EK. Epidemiology and etiology of leukemia and lymphoma. *Cold Spring Harb Perspect Med*. 2020;10(6):a034819. doi:10.1101/cshperspect.a034819
6. Campo E, Ghia P, Montserrat E. Chronic lymphocytic leukaemia/small lymphocytic lymphoma. In: Swerdlow SH, Campo E, Harris NL, et al., eds. *WHO Classification of Tumours of Haematopoietic and Lymphoid Tissues*. Revised 4th ed. Lyon, France: International Agency for Research on Cancer; 2017:216–221.
7. Eichhorst B, Robak T, Montserrat E, et al. Chronic lymphocytic leukaemia: ESMO Clinical Practice Guidelines for diagnosis, treatment and follow-up. *Ann Oncol*. 2021;32(1):23–33. doi:10.1016/j.annonc.2020.09.019
8. McKenna R, Kyle R, Kuehl W, Harris N, Coupland R, Fend F. Plasma cell neoplasms. In: Swerdlow SH, Campo E, Harris NL, et al., eds. *WHO Classification of Tumours of Haematopoietic and Lymphoid Tissues*. Revised 4th ed. Lyon, France: International Agency for Research on Cancer; 2017:241–257.
9. Rajkumar SV, Dimopoulos MA, Palumbo A, et al. International Myeloma Working Group updated criteria for the diagnosis of multiple myeloma. *Lancet Oncol*. 2014;15(12):e538–e548. doi:10.1016/S1470-2045(14)70442-5
10. Efficace F, Cottone F, Sommer K, et al. Validation of the European Organisation for Research and Treatment of Cancer Quality of Life Questionnaire Core 30 summary score in patients with hematologic malignancies. *Value Health*. 2019;22(11):1303–1310. doi:10.1016/j.jval.2019.06.004
11. World Health Organization. The World Health Organization Quality of Life Assessment (WHOQOL): Position paper from the World Health Organization. *Soc Sci Med*. 1995;41(10):1403–1409. doi:10.1016/0277-9536(95)00112-K
12. Schipper H. Quality of life: Principles of the clinical paradigm. *J Psychosoc Oncol*. 1990;8(2–3):171–185. doi:10.1300/J077v08n02_09
13. Haraldstad K, Wahl A, Andenæs R, et al. A systematic review of quality of life research in medicine and health sciences. *Qual Life Res*. 2019;28(10):2641–2650. doi:10.1007/s11136-019-02214-9
14. Leppert W, Forycka M, de Walden-Gałuszko K, Majkowicz M, Buss T. Quality of life assessment in cancer patients: Recommendations for the staff of oncology and palliative care units [in Polish]. *Psychoonkologia*. 2014;18(1):17–29. https://www.termedia.pl/Ocena-jakosci-zycia-u-chorych-na-nowotwory-zalecenia-dla-personelu-oddzialow-onkologicznych-i-medycyny-paliatywnej,63,22979,1,0.html. Accessed May 9, 2022.
15. Majkowicz M. Methodological bases of life quality assessment [in Polish]. *Palliat Med Pract*. 2017;11(2):78–83. https://journals.viamedica.pl/palliative_medicine_in_practice/article/view/55505/41810. Accessed May 9, 2022.
16. Cieślik B, Podbielska H. A survey of the quality of life questionnaires [in Polish]. *Acta Bio-Opt Inform Med*. 2015;21(2):102–135. https://yadda.icm.edu.pl/yadda/element/bwmeta1.element.baztech-38b67b03-94f7-417b-af2c-2a4fb15fc9ab/c/Cieslik.pdf. Accessed May 9, 2022.

17. Aaronson NK, Ahmedzai S, Bergman B, et al. The European Organization for Research and Treatment of Cancer QLQ-C30: A quality-of-life instrument for use in International Clinical Trials in Oncology. *J Natl Cancer Inst*. 1993;85(5):365–376. doi:10.1093/jnci/85.5.365

18. Cocks K, Cohen D, Wisløff F, et al. An international field study of the reliability and validity of a disease-specific questionnaire module (the QLQ-MY20) in assessing the quality of life of patients with multiple myeloma. *Eur J Cancer*. 2007;43(11):1670–1678. doi:10.1016/j.ejca.2007.04.022

19. van de Poll-Franse L, Oerlemans S, Bredart A, et al. International development of four EORTC disease-specific quality of life questionnaires for patients with Hodgkin lymphoma, high- and low-grade non-Hodgkin lymphoma and chronic lymphocytic leukaemia. *Qual Life Res*. 2018;27(2):333–345. doi:10.1007/s11136-017-1718-y

20. Efficace F, Baccarani M, Breccia M, et al. International development of an EORTC questionnaire for assessing health-related quality of life in chronic myeloid leukemia patients: The EORTC QLQ-CML24. *Qual Life Res*. 2014;23(3):825–836. doi:10.1007/s11136-013-0523-5

21. Efficace F, Iurlo A, Patriarca A, et al. Validation and reference values of the EORTC QLQ-CML24 questionnaire to assess health-related quality of life in patients with chronic myeloid leukemia. *Leuk Lymphoma*. 2021;62(3):669–678. doi:10.1080/10428194.2020.1838509

22. Sommer K, Cottone F, Aaronson NK, et al. Consistency matters: Measurement invariance of the EORTC QLQ-C30 questionnaire in patients with hematologic malignancies. *Qual Life Res*. 2020;29(3):815–823. doi:10.1007/s11136-019-02369-5

23. Fayers PM, Aaronson N, Bjordal K, Groenvold M, Curran D, Bottomley A. *EORTC QLQ-C30 Scoring Manual*. Brussels, Belgium: European Organisation for Research and Treatment of Cancer; 2001. https://www.eortc.org/app/uploads/sites/2/2018/02/SCmanual.pdf. Accessed September 3, 2021.

24. Allart-Vorelli P, Porro B, Baguet F, Michel A, Cousson-Gélie F. Haematological cancer and quality of life: A systematic literature review. *Blood Cancer J*. 2015;5(4):e305. doi:10.1038/bcj.2015.29

25. Salas S, Mercier S, Moheng B, et al. Nutritional status and quality of life of cancer patients needing exclusive chemotherapy: A longitudinal study. *Health Qual Life Outcomes*. 2017;15(1):85. doi:10.1186/s12955-017-0660-6

26. Elwadhi D, Khandelwal SK, Kumar L, Sharma A. Short-term impact of hematopoietic stem cell transplantation on psychiatric morbidity and quality of life in hematological malignancies in adults. *Indian J Psychol Med*. 2020;42(1):61–68. doi:10.4103/IJPSYM.IJPSYM_70_19

27. Efficace F, Castagnetti F, Martino B, et al. Health-related quality of life in patients with chronic myeloid leukemia receiving first-line therapy with nilotinib: HRQOL and chronic myeloid leukemia. *Cancer*. 2018;124(10):2228–2237. doi:10.1002/cncr.31323

28. Malihi Z, Kandiah M, Chan YM, Hosseinzadeh M, Sohanaki Azad M, Zarif Yeganeh M. Nutritional status and quality of life in patients with acute leukaemia prior to and after induction chemotherapy in three hospitals in Tehran, Iran: A prospective study. *J Hum Nutr Diet*. 2013;26 Suppl 1:123–131. doi:10.1111/jhn.12043

29. Ficko SL, Pejsa V, Zadnik V. Health-related quality of life in Croatian general population and multiple myeloma patients assessed by the EORTC QLQ-C30 and EORTC QLQ-MY20 questionnaires. *Radiol Oncol*. 2019;53(3):337–347. doi:10.2478/raon-2019-0047

30. Govindaraju T, Sahle B, McCaffrey T, McNeil J, Owen A. Dietary patterns and quality of life in older adults: A systematic review. *Nutrients*. 2018;10(8):971. doi:10.3390/nu10080971

31. Olsson C, Sandin-Bojö AK, Bjuresäter K, Larsson M. Changes in sexuality, body image and health related quality of life in patients treated for hematologic malignancies: A longitudinal study. *Sex Disabil*. 2016;34(4):367–388. doi:10.1007/s11195-016-9459-3

32. Senf B, Grabowski K, Spielmann N, Fettel J. Quality of life and distress assessed with self and external assessment screening tools in patients with hematologic malignancies attending treatment in an acute hospital. *Qual Life Res*. 2020;29(12):3375–3385. doi:10.1007/s11136-020-02602-6

33. Papathanasiou IV, Kelepouris K, Valari C, et al. Depression, anxiety and stress among patients with hematological malignancies and the association with quality of life: A cross-sectional study. *Med Pharm Rep*. 2020;93(1):62–68. doi:10.15386/mpr-1502

34. Hathiramani S, Pettengell R, Moir H, Younis A. Relaxation versus exercise for improved quality of life in lymphoma survivors: A randomised controlled trial. *J Cancer Surviv*. 2021;15(3):470–480. doi:10.1007/s11764-020-00941-4

Involvement of endothelial progenitor cells in blood flow recovery through activation of the Wnt/β-catenin signaling pathway and inhibition of high oxidative stress in diabetic hindlimb ischemic rats

Xiongfei Xu[1,2,A–E], Fei Xie[3,B,C,E], Yuping Wang[4,B,C,E], Hong Zeng[1,2,B,C,E], Sen Shi[1,2,B,C,E], Xiaolei Sun[1,2,B,C,E], Huqiang He[1,2,B,C,E], Lei Zhang[1,2,B,C,E], Weiming Wang[1,2,B,C], Tao Xiang[5,B,C], Yanzheng He[1,2,B,C], Yong Liu[1,2,A,C,E,F]

[1] Department of Vascular Surgery, Affiliated Hospital of Southwest Medical University, Luzhou, China

[2] Key Laboratory of Medical Electrophysiology, Ministry of Education, Collaborative Innovation Center of Prevention and Treatment of Cardiovascular Disease of Sichuan Province, Luzhou, China

[3] Department of Thoracic and Cardiovascular Surgery, First People's Hospital of Liangshan Yi Autonomous Prefecture, Xinchang, China

[4] Department of Vascular Surgery, Hospital of Traditional Chinese Medicine, Southwest Medical University, Luzhou, China

[5] Department of Cardiovascular Medicine, Affiliated Hospital of Southwest Medical University, Luzhou, China

A – research concept and design; B – collection and/or assembly of data; C – data analysis and interpretation; D – writing the article; E – critical revision of the article; F – final approval of the article

Abstract

Background. Diabetes mellitus (DM) often causes stenosis and occlusion of hindlimb blood vessels, which are also the main cause for hindlimb ischemia in elderly people.

Objectives. To investigate the therapeutic effect of endothelial progenitor cell (EPC) transplantation on diabetic hindlimb ischemia.

Materials and methods. Endothelial progenitor cells were separated, labeled with PKH-26 and transplanted into rat models (10^7 cells/100 g). Dichlorodihydrofluorescein diacetate (DCFH-DA) was used to detect any oxidative stress. Streptozotocin (STZ) was injected to establish a diabetic rat model and hindlimb ischemia model was established via operation. Western blotting was used to detect total β-catenin (T-β-catenin) and non-phospho-β-catenin (NP-β-catenin) levels. The malondialdehyde (MDA), superoxide dismutase (SOD), Wnt3a, Wnt5a and Wnt7a levels were detected using enzyme-linked immunosorbent assay (ELISA). Oxidative stress was measured using DCFH-DA and dihydroethidium (DHE). The endothelial biomarker CD31 was observed to highlight vessels, and PKH-26 to trace migration/adhesion of EPCs.

Results. Endothelial progenitor cells were successfully isolated and identified, and diabetic hindlimb ischemic rat models were created. Tempol remarkably improved blood flow in diabetic hindlimb ischemic rats compared to DM+EPCs rats at 14 days (p < 0.001) and 28 days post-operation (p < 0.001). High oxidative stress was observed in diabetic hindlimb ischemic rats. Tempol significantly inhibited oxidative stress levels in diabetic hindlimb ischemic rats. Furthermore, Tempol significantly promoted angiogenesis in diabetic hindlimb ischemic rats compared to DM+EPCs rats. The β-catenin inhibitor, XAV (DM+EPCs+Tempol+XAV group), significantly suppressed blood flow recovery and angiogenesis in diabetic hindlimb ischemic rats when compared to the DM+EPCs+Tempol group at 14 days (p = 0.026) and 28 days (p < 0.001). The XAV remarkably reduced T-β-catenin (p < 0.001) and N-β-catenin (p = 0.030) levels in Tempol-treated diabetic hindlimb ischemic rats, as compared to the DM+EPCs+Tempol group. The Wnt5a participated in the pathology of diabetic hindlimb ischemia.

Conclusions. There are high oxidative stress levels in both EPCs in high-glucose environments and diabetic hindlimb ischemia, which can lead to limited blood flow recovery. The high oxidative stress caused the inhibition of Wnt/β-catenin signaling pathway, leading to limited blood flow recovery in diabetic hindlimb ischemia. At the same time, Wnt5a participated in the EPC-mediated blood flow recovery.

Key words: diabetic hindlimb ischemia, EPCs, Wnt/β-catenin signaling pathway, oxidative stress

1216

X. Xu et al. EPCs inhibits diabetic hindlimb ischemia

Background

Diabetes mellitus (DM) often causes stenosis and occlusion of hindlimb blood vessels, ischemia and hypoxia, and is also the main cause of hindlimb ischemia in elderly people.[1,2] Currently, the treatment of diabetic hindlimb ischemia includes drug-conservative treatment, interventional surgery, traditional surgery, stem cell transplantation, physical therapy, and appropriate functional exercise, among others.[3] Due to the prolonged course of diabetic hindlimb ischemia and severity of the disease, the first 3 of the abovementioned treatments cannot completely resolve the problems. In the recent years, stem cell transplantation has become an important strategy for the treatment of severe diabetic hindlimb ischemia, whereas other treatment methods have not produced satisfactory clinical outcomes.[4,5]

The treatment with autologous stem cells can bring the light of recovery for patients with severe diabetic hindlimb ischemia.[6] However, there are many bottlenecks in the application of autologous stem cells for treating diabetic hindlimb ischemia. Firstly, even though they exist in limited amounts, the stem cells in peripheral blood or bone marrow need to be collected. Secondly, the treating effect is not stable and might be affected by time, method and number of transplantations. Finally, autologous stem cells can cause some side effects, including those caused by the collection, local infection, anesthesia, induction of tumor formation, and promotion of tumor growth. Presently, there is no treatment strategy that can completely resolve all of the aforenamed problems. However, the treatment with autologous stem cells an important new strategy for improving the condition of patients and promoting the biological function of stem cells.

The cytological basis for neovascularization is the damage of the endothelial cells and endothelial progenitor cells (EPCs) caused by excessive oxidative stress.[7] Endothelial progenitor cells, as the precursor cells of vascular endothelium, demonstrate the abilities of proliferation and differentiation in adulthood. Also, they are capable of developing into primitive vascular structures. Therefore, EPCs have a strong ability to support angiogenesis.[8] Yet, the number of EPCs in peripheral blood of patients with diabetes was lower than that of nondiabetic people. Many factors can lead to the functional damage of EPCs, including oxidative stress, the induction of endothelial nitric oxide synthase (eNOS)/nitric oxide (NO) cell signaling pathway and inflammatory responses.[9] Among them, oxidative stress can mediate many signaling pathways through reactive oxygen species (ROS), such as Wnt/β-catenin, G protein-coupled receptors, Notch, MAPK, JAK-STAT, and NF-κB.[10] At the same time, the proliferation, migration, adhesion, and angiogenesis of EPCs in vitro decreases significantly after the administration of Wnt inhibitors.[11] Therefore, the excessive oxidative stress may regulate the biological function of EPCs by downregulating Wnt/β-catenin signaling pathway.

The Wnt/β-catenin is one of the most important signaling pathways in cells and has a wide range of regulatory effects.[12] It has been shown that this pathway does not only play an important role in the development of embryonic blood vessels, but also regulates the role of EPCs in retinopathy and tumor angiogenesis.[13] However, there are no studies focusing on oxidative stress and the Wnt/β-catenin signaling pathway, or their function effect on EPCs.

Objectives

Therefore, by establishing diabetic hindlimb ischemic rat model and high-glucose environment in vitro, this study aimed to explore whether Wnt/β-catenin signaling is involved in hindlimb ischemia through modulating oxidative stress in vivo and in vitro. This study provides a novel way to treat hindlimb ischemia in diabetic rats employing stem cell transplantation.

Materials and methods

Animals

Two-month-old Sprague Dawley rats (certificate No. 24101115), weighting from 80–120 g, were purchased from Experimental Animal Center of Southwest Medical University (Chongqing, China). The rats were housed at a temperature of 20–25°C with a humidity of 70–80% and 12 h light/12 h dark light cycle. The rats had access to water and food ad libitum.

Ethical statement

All the experiments were approved by the Ethical Committee of Affiliated Hospital of Southwest Medical University (Lanzhou, China; approval No. 201710133). All animal experiments were conducted in accordance with the Declaration of Helsinki.

Isolation and culture of EPCs

The rats were sacrificed by the intraperitoneal injection of pentobarbital at a dosage of 50 mg/kg. In order to isolate the primary cells, the sacrificed rats were soaked in 75% alcohol for 15 min. Then, the femur and tibia of the rats were dissected for isolating EPCs. The bone marrow cavities collected from tibias and femurs were flushed into 5-mL centrifuge tubes using phosphate-buffered saline (PBS) containing 1% heparin. Then, the bone marrow was transferred into a 15-mL centrifuge tube and isolated using the density gradient centrifugation for 20 min at a speed of 2000 rpm. The middle layer, containing the mononuclear cells (MNCs) was transferred into another centrifuge tube and centrifuged for 5 min at 1500 rpm. The supernatants

were removed, and retained bone marrow was incubated in endothelial cell growth medium (EGM)-2 (Lonza Bioscience, Walkersville, USA), supplemented with 10% fetal bovine serum (FBS; Gibco Grand Island, USA) at 37°C and 5% CO_2. The density of cells was adjusted to 1×10^6/mL and cells were seeded onto 6-well or 12-well plates.

Identification of EPCs

In order to identify EPCs, the uptake for Dil-conjugated acetylated low-density lipoprotein (Dil-Ac-LDL) and the binding of fluorescein isothiocyanate-conjugated ulexeuropaeus agglutinin I (FITC-UEA-I) by cells were analyzed. Briefly, the cells were washed twice in PBS and then incubated using 12 μg/mL of Dil-Ac-LDL for 4 h in the dark. Then, the cells were washed thrice using PBS (5 min per wash) and fixed using 4% paraformaldehyde (ZSGB-BIO, Beijing, China) for 20 min. The cells were washed thrice using PBS (5 min per wash) and then incubated using 10 μg/mL of FITC-UEA-1 for 1 h in the dark. Next, the cells were washed twice using PBS (2 washes 5 min each), captured and analyzed for binding of FITC-UEA-1 and the uptake of Dil-Ac-LDL by means of inverted fluorescence microscopy (DMI 6000 B; Leica, Wetzlar, Germany).

PKH-26 labeling and staining of EPCs

The labeling and staining of EPCs was conducted as previously described,[14] with a few modifications. Briefly, the EPCs were cultured, a single cell suspension was generated and 2×10^7 cells were collected per centrifuge tube. Cells were centrifuged for 5 min at 1500 rpm and the supernatants were discarded. The remaining cells were resuspended and incubated with PKH-26 at 25°C for 3 min, and then the reaction was terminated. Finally, the stained EPCs were centrifuged at 25°C and 1500 rpm for 10 min, the cells were resuspended in 0.9% normal saline and transplanted into the tail vein of rats. The PKH-26-labeled frozen sections of tissues were prepared and observed using fluorescence microscopy.

Diabetic hindlimb ischemic rat model

Sprague Dawley weighing 80–120 g were used to generate the diabetic hindlimb ischemic model, as previously described.[15] Briefly, the diabetes was generated by the intraperitoneal injection of streptozotocin (STZ) at a dosage of 50 mg/kg. At 3, 5, 7, 14, 28, 42, and 56 days post-STZ administration, plasma glucose concentrations were examined. After the treatment of STZ, the rats were fed with high-fat food for 2 months, and then the experiments were carried out. The rats with plasma glucose concentration >16.65 mmol/L over 4 readings were considered diabetic rats. Eight weeks after the diabetes induction, the rats were anaesthetized by the intraperitoneal injection of pentobarbital (50 mg/kg), and the left femoral artery, distal portion and all lateral branches were dissected and

ligated with 7-0 sutures. The treatment for blood vessels in diabetic hindlimb ischemic model was carried out according to a previous report.[16]

Trial grouping

The rats in this study were divided into 2 groups, namely the diabetes group and the control group. The control group consisted of rats injected with normal saline instead of STZ. After laser Doppler monitoring was conducted, the rats were divided into a healthy group (H group, n = 6) and a diabetic hindlimb ischemic rat model group (DM group, n = 6). Some rats were transplanted with EPCs, which were further divided into DM+NS (normal saline) group (n = 6), DM+EPCs group (n = 6), DM+EPCs+Tempol group (n = 6), and DM+EPCs+Tempol+XAV group (n = 6). In the process of EPC transplantation, the EPC single cell suspension was mixed well to avoid cell aggregates and vascular obstruction.

ROS examination

The production of ROS was examined using dichlorodihydrofluorescein diacetate (DCFH-DA) and dihydroethidium (DHE) staining. In brief, the frozen ischemic gastrocnemius muscles of the left hindlimb sections or EPCs were incubated with DCFH-DA (5 μmol/L) or DHE (2 μmol/L) for 30 min at 37°C in dark. Then, the sections were washed 3 times with PBS (5 min per wash). The fluorescent images of DCFH-DA/DHE-stained tissues/cells were observed using fluorescence microscopy (IX53; Olympus Corp., Tokyo, Japan). At least 5 visual fields of 1 section were analyzed regarding the fluorescence intensity using Image-Pro Plus software (v. 6.0; Media Cybernetics, Inc., Bethesda, USA).

Oxidative stress evaluation

In order to evaluate oxidative stress levels, the production of malondialdehyde (MDA) and superoxide dismutase (SOD) in the serum of rats was measured, as previously described.[17] The MDA activity was measured using the MDA assay kit (Cat. No. S0131S; Beyotime, Shanghai, China), following the manufacturer's instructions. The SOD activity was evaluated with the SOD detection kit (Cat. No. S0101M; Beyotime), according to the manufacturer's protocol. The absorbance was captured with the spectrophotometer at the wavelength of 450 nm.

Immunofluorescence and microvascular density evaluation

Briefly, the gastrocnemius muscle of the left hindlimb was fixed with 4% paraformaldehyde at 4°C for 24 h and frozen sections (5 μm) were made. Then, the sections were treated with 0.5% Triton X-100 for 10 min and 0.1% trypsin for 20 min, and blocked with 10% goat serum for 15 min.

1218

X. Xu et al. EPCs inhibits diabetic hindlimb ischemia

The sections were incubated with mouse anti-rat CD31 antibody (1:200) at 4°C overnight. The CD31 is an important cellular immunological biomarker for the vascular endothelial cells.[18] The next day, sections were incubated with FITC-labeled goat anti-mouse immunoglobulin G (IgG) (1:200) for 60 min in dark. In this study, 1 green fluorescence point or cluster was used to represent 1 blood vessel. Five visual fields were selected, green fluorescent spots were photographed (×200 magnification), the microvascular density (MVD) was analyzed, and the mean was generated.

Wnt3a/Wnt5a/Wnt7a levels determined using ELISA

On the 28th day post-operation, the rats were sacrificed to obtain blood. Blood was centrifuged at 2000 rpm for 10 min to obtain serum for the detection of Wnt3a, Wnt5a and Wnt7a. The Wnt3a, Wnt5a and Wnt7a levels were determined using the Wnt3a Detection ELISA kit (Cat. No. 153260; US Biological, Swampscott, USA), Wnt5a Detection ELISA kit (Cat. No. 153265; US Biological) and Wnt7a Detection ELISA kit (Cat. No. ABIN6374423; Rockland Immunochemicals, Inc., Aachen, Germany), respectively, according to the manufacturers' protocols.

Western blotting assay

The total proteins in the gastrocnemius muscles of the left hindlimb tissues were extracted, and the concentration was determined using BCA protein assay kit (Cat. No. P0012S; Beyotime Biotech. Co. Ltd., Wuhan, China). The obtained proteins were separated on a 10% sodium dodecyl-sulfate polyacrylamide gel electrophoresis (SDS-PAGE) and electro-transferred to polyvinylidene fluoride (PVDF) membranes. Then, the membranes were blocked with 5% non-fat milk and incubated with rabbit anti-rat total β-catenin (T-β-catenin) monoclonal antibody (1:1000, Cat. 8480; Cell Signaling Technology, Beverly, USA), rabbit anti-rat non-phospho-β-catenin (NP-β-catenin) polyclonal antibody (1:1000, Cat. No. 19807; Cell Signaling Technology) and rabbit anti-rat GAPDH monoclonal antibody (Cat. No. 5174; Cell Signaling Technology) at 4°C overnight, followed by the incubation with horseradish peroxidase (HRP)-labeled goat anti-rabbit IgG (1:500, Cat. No. A0208; Beyotime) at room temperature for 2 h. Western blotting bands were imaged using an enhanced chemiluminescence (ECL) kit (Amersham Biosciences, Piscataway, USA) and analyzed using Quantity One software (Bio-Rad Laboratories, Inc., Hercules, USA).

Statistical analyses

Data were defined as mean ± standard deviation (SD) and analyzed using IBM SPSS software v. 20.0 (IBM Corp., Armonk, USA). The assumption of the normality and homogeneity of the variances required for the comparison of means were analyzed using the Kolmogorov–Smirnov test and Levene's test, respectively. The differences between the 2 groups were compared using Student's t-test. The data were analyzed using one-way analysis of variance (ANOVA) followed by Tukey's post hoc test for multiple comparisons. When parameters of the same animals were measured over consecutive days, a repeated measures ANOVA was used. A value of $p < 0.05$ was considered statistically significant.

Results

Identification and labeling of EPCs

Endothelial progenitor cells were identified using double staining and labeled with PKH-26. After 3 days of culture, the EPCs were adherent cells, mainly consisting of round and a few oval shapes (Fig. 1A). After 7 days of continuous culture, the amount of cells increased, with obvious oval or spindle-shaped cells, demonstrating the colony-like growth under the microscope (Fig. 1A). After 14 days of culture, the pebble-like cells appeared with vortex-like growth (Fig. 1A). After 7 days of culture, EPCs were stained with Dil-Ac-LDL and FITC-UEA-1 double fluorescence and observed under confocal microscope. The red fluorescence-stained cells were considered Dil-Ac-LDL-positive and yellow fluorescence cells were considered FITC-UEA-1-positive (Fig. 1B). Cells with both red and yellow fluorescence were considered EPCs. The PKH-26-labeled EPCs could also migrate to ischemic sites (Fig. 1C).

Generation of diabetes model and diabetic hindlimb ischemic rat model

After STZ injection, fasting plasma glucose (FPG) was measured on the 3rd, 5th, 7th, 14th, 28th, and 56th day. The average blood glucose level of the experimental group was measured at 16.7 mmol/L, which was significantly higher than in the control group (Fig. 2A; all $p < 0.001$). According to the laser Doppler monitoring, the blood flow of the H group and the DM group were significantly changed before and 0 days after the operation (Fig. 2B). These results showed that the left hindlimb of the 2 groups demonstrated an obvious ischemia (Fig. 2B). According to the repeated measures ANOVA, there were significant differences in L/R blood flow ratio pre-operation, and 0, 7, 14, and 28 days post-treatment, in both the H group (ANOVA, F = 89.011, degrees of freedom (df) = 4, $p < 0.001$) and the DM group (ANOVA, F = 128.794, df = 4, $p < 0.001$). Therefore, the blood flow ratio was changed along with the treatment time. The Tukey's post hoc test showed that the L/R blood flow ratio of the DM group was significantly lower compared to that of the H group 14 days (F = 68.903, df = 10, p = 0.003) and 28 days (F = 6.699, df = 10, $p < 0.001$) after the operation (Fig. 2B).
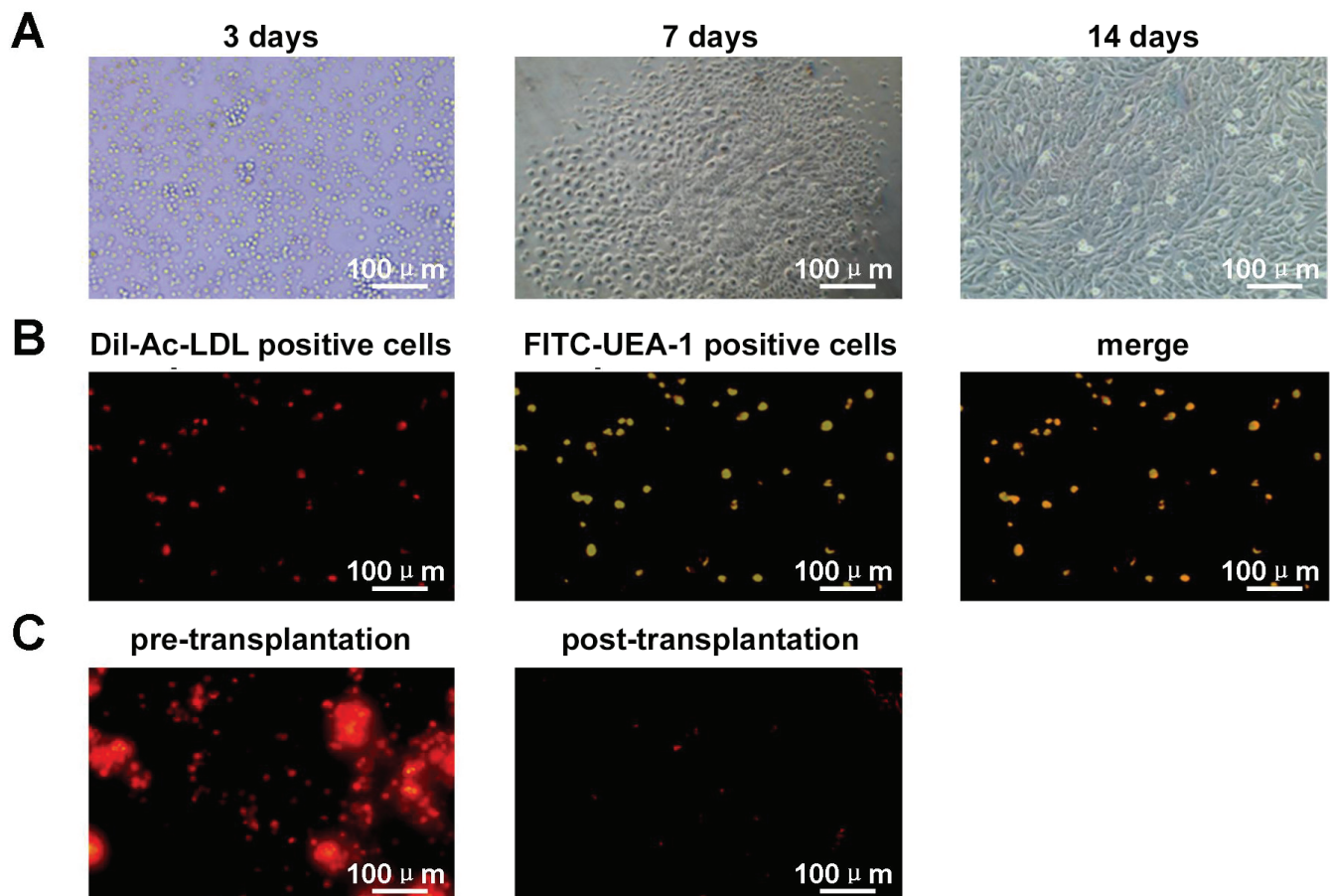
Fig. 1. Identification and label for the endothelial progenitor cells (EPCs). A. EPC morphological changes at 3, 7 and 14 days, ×200 magnification; B. Detection of EPCs by staining with DiI-conjugated acetylated low-density lipoprotein (DiI-Ac-LDL) and fluorescein isothiocyanate-conjugated ulexeuropaeus agglutinin I (FITC-UEA-I). The images of DiI-Ac-LDL-positive cells and FITC-UEA-I-positive cells were merged, ×200 magnification; C. Pre-transplantation and post-transplantation EPCs marked with PKH-26. The post-transplantation EPCs migrated to the gastrocnemius muscle, ×200 magnification

Oxidative stress inhibitor Tempol improved blood flow in hindlimb of diabetic hindlimb ischemic rats

According to the repeated measures ANOVA, there were significant differences for L/R blood flow ratio at the pre-operation time point, in DM+NS (ANOVA, F = 124.482, df = 4, p < 0.001), DM+EPCs (ANOVA, F = 399.254, df = 4, p < 0.001) and DM+EPCs+Tempol (ANOVA, F = 114.956, df = 4, p < 0.001) groups. Thus, the effects of Tempol on L/R blood flow ratio changed with the treatment times. The results showed that there was no significant difference in blood flow of hindlimbs between the DM+NS group and the DM+EPCs group, 0, 7, 14, and 28 days after the operation (Fig. 3A,B; all df = 10, p > 0.05). The results also demonstrated that the recovery of blood flow in diabetic hindlimb ischemic rats was poor after the transplantation of EPCs. However, following Tempol administration, the recovery of blood flow in diabetic hindlimb ischemic rats was significantly improved compared with that of the DM+EPCs group at 14 days (Tukey's post hoc test, F = 69.283, df = 10, p = 0.013) and 28 days (Tukey's post hoc test, F = 106.872, df = 10, p < 0.001) post-operation (Fig. 3A,B).

High oxidative stress observed in hindlimbs of diabetic hindlimb ischemic rats

The MDA levels in the DM group were significantly higher compared to that in the H group, both for pre-operation (Student's t-test, t = −15.123, df = 10, p < 0.001) and post-operation (Student's t-test, t = −9.852, df = 10, p < 0.001) (Fig. 4A). Furthermore, there was a significant difference between the MDA levels among the H group (pre- and post-operation) and DM group (pre- and post-operation) (Fig. 4A; Tukey's post hoc test (ANOVA), F = 81.708, df = 3, p < 0.001). However, there were no significant differences for the MDA levels between the pre-operation group and the post-operation group, for both the H group (p = 0.708) and the DM group (Fig. 4A; p = 0.191). There was a significant difference in the MDA levels among H+NS, DM+NS and DM+EPCs groups (Fig. 4B; Tukey's post hoc test (ANOVA), F = 55.342, df = 2, p < 0.001). However, there were no differences in the MDA levels between the DM+NS group and the DM+EPCs group (Fig. 4B; p = 0.900). Moreover, there were significant differences in SOD levels among H+NS, DM+NS and DM+EPCs groups (Fig. 4C; Tukey's post hoc
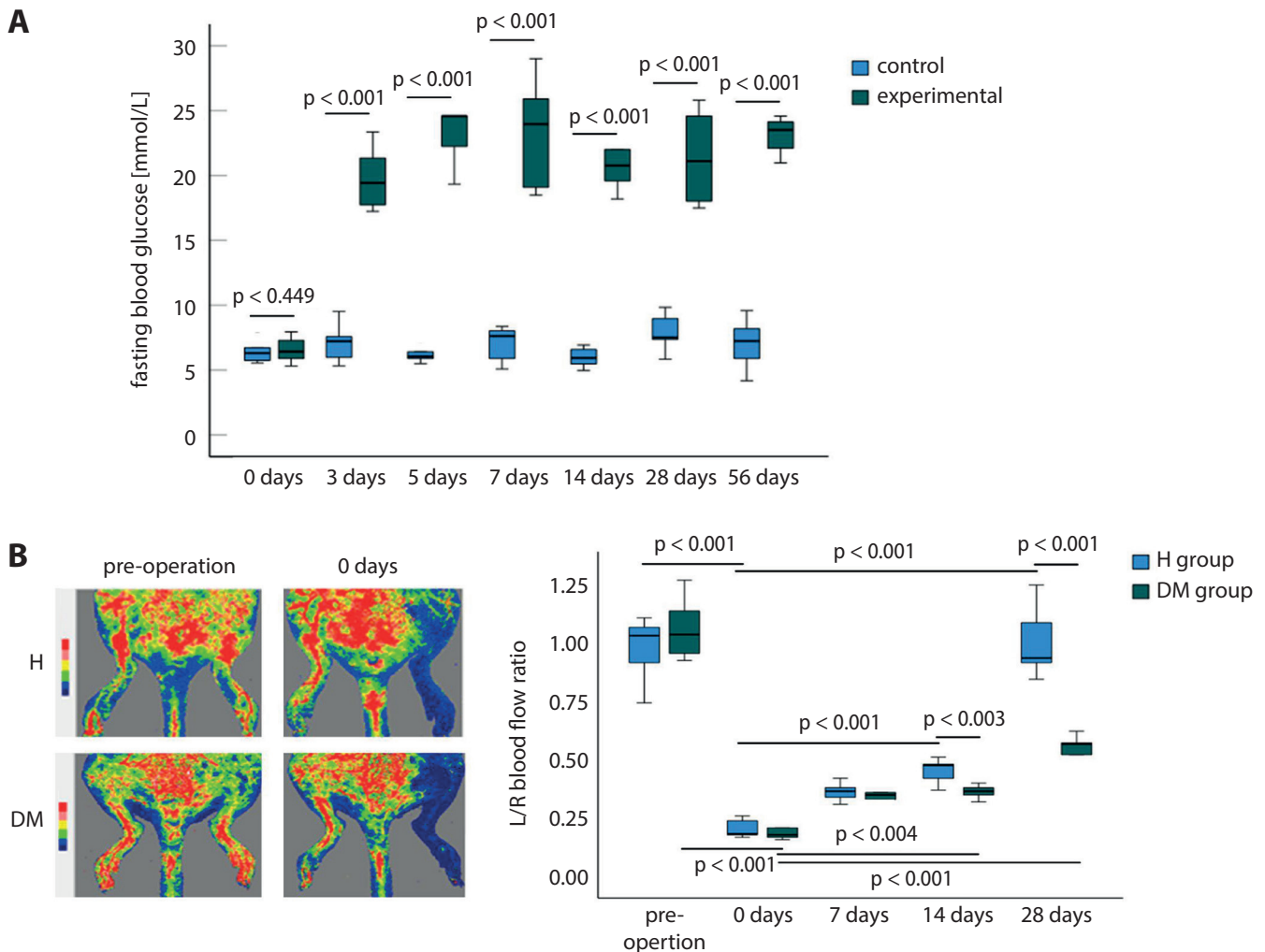
1220

X. Xu et al. EPCs inhibits diabetic hindlimb ischemia

Fig. 2. Establishment of the diabetes rat models and diabetic hindlimb ischemic rat models. A. The fasting blood glucose changes in the rats of the control and experimental group; B. Laser Doppler perfusion imaging (LDPI) in the healthy (H) group and diabetes mellitus (DM) group, preoperative (Pre-) and postoperative (0, 7, 14 and 28 days) showed changes in blood flow (n = 6). The L/R blood flow ratio statistical line chart was drawn. The Tukey's post hoc test (analysis of variance (ANOVA)) and Student's t-test were conducted to analyze the data. The statistical differences (p-values) between the 2 labeled groups (horizontal lines) are depicted

test (ANOVA), F = 22.933, df = 2, p < 0.001). The SOD levels were significantly lower in DM+NS (Fig. 4C; p < 0.001) and DM+EPCs groups (Fig. 4C; p < 0.001) compared to that in the H+NS group. However, there were no differences between the DM+NS and DM+EPCs groups (Fig. 4C; p = 0.903).

Tempol inhibited high oxidative stress in diabetic hindlimb ischemic rats

According to the DCFH-DA staining results, there were plenty of DCFH-DA-positive cells in the gastrocnemius tissues in both DM+NS and DM+EPCs rats, and no DCFH-DA-positive cells in the H+NS rats (Fig. 4D). However, the Tempol administration remarkably reduced the oxidative stress (DCFH-DA staining) compared to both the DM+NS and DM+EPCs groups (Fig. 4D). The DHE staining also indicated that Tempol administration significantly suppressed oxidative stress, compared to both the DM+NS and DM+EPCs groups (Fig. 4D).

Tempol promoted angiogenesis in gastrocnemius of diabetic hindlimb ischemic rats

Compared with the DM+NS group, there was no obvious difference in the number of new microvessels in the DM+EPCs group (Fig. 5A). Furthermore, there were no EPCs in the DM+NS group migrating to the gastrocnemius, indicating that the PKH-26-labeled EPCs (red) demonstrated no false positive value and had a higher specificity in this experiment. Compared with the DM+EPCs group, the oxidative stress was inhibited and new microvessels were generated in the DM+EPCs+Tempol group (Fig. 5A,B; Tukey's post hoc test (ANOVA), F = 183.797, df = 2, p < 0.001). Meanwhile, the number of microvessels migrating to the ischemic gastrocnemius muscle was also increased in diabetic hindlimb ischemic rats.
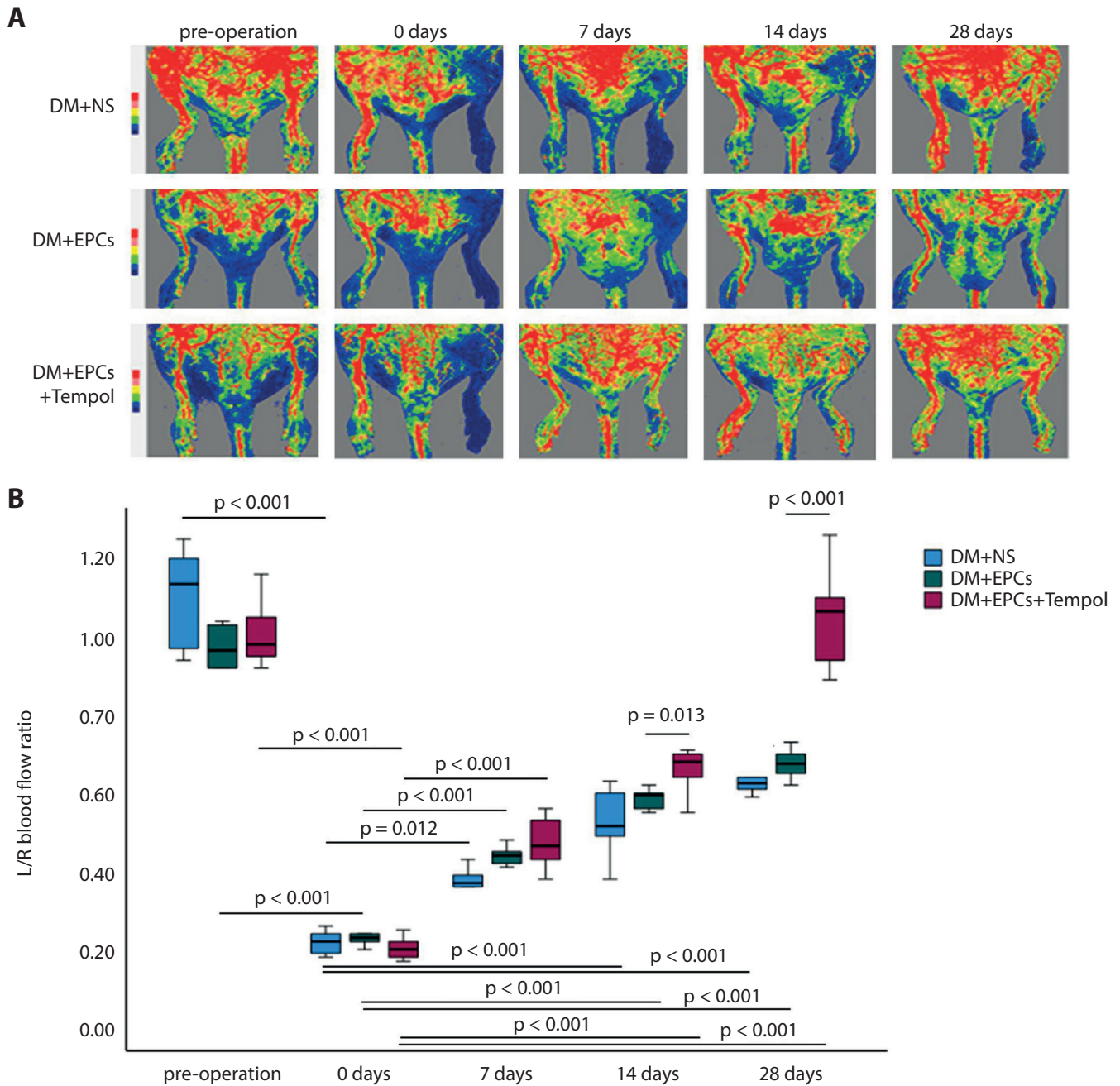
Fig. 3. Effects of oxidative stress inhibitor Tempol on the blood flow in the hindlimbs of diabetic hindlimb ischemic rats. A. Blood flow changes of rats in DM+NS, DM+EPCs and DM+EPCs+Tempol groups at pre-operation and 0, 7, 14, and 28 days post-operation, determined with laser Doppler monitoring; B. The continuous flow ratio statistical analysis for DM+NS, DM+EPCs and DM+EPCs+Tempol groups. The Tukey's post hoc test (analysis of variance (ANOVA)) and Student's t-test were conducted to analyze the data. The statistical differences (p-values) between the 2 labeled groups (horizontal lines) are depicted

DM – diabetes mellitus; NS – normal saline; EPCs – endothelial progenitor cells.

β-catenin inhibitor XAV suppressed blood flow recovery in diabetic hindlimb ischemic rats

The Wnt/β-catenin signaling pathway inhibitor, XAV, significantly decreased the L/R blood flow ratio in the DM+EPCs+Tempol+XAV group compared to that in the DM+EPCs+Tempol group at 14 days (Tukey's post hoc test, F = 83.56, df = 10, p = 0.026) and 28 days post-treatment (Tukey's post hoc test, F = 118.34, df = 10,

p < 0.001) (Fig. 6A,B). In the DM+EPCs+Tempol+XAV group, there were significant differences in L/R blood flow ratio at different time points (pre-operation 0, 7, 14, and 28 days post operation) (Fig. 6A,B; Tukey's post hoc test (ANOVA), F = 47.978, df = 4, p < 0.001). In order to exclude the effect of DMSO on the L/R blood flow ratio, the L/R blood flow ratio was also examined in dimethyl sulfoxide (DMSO)-treated group. However, there was no significant difference between the DM+EPCs+DMSO group and the DM+EPCs group (Fig. 6A,B; all p > 0.05),
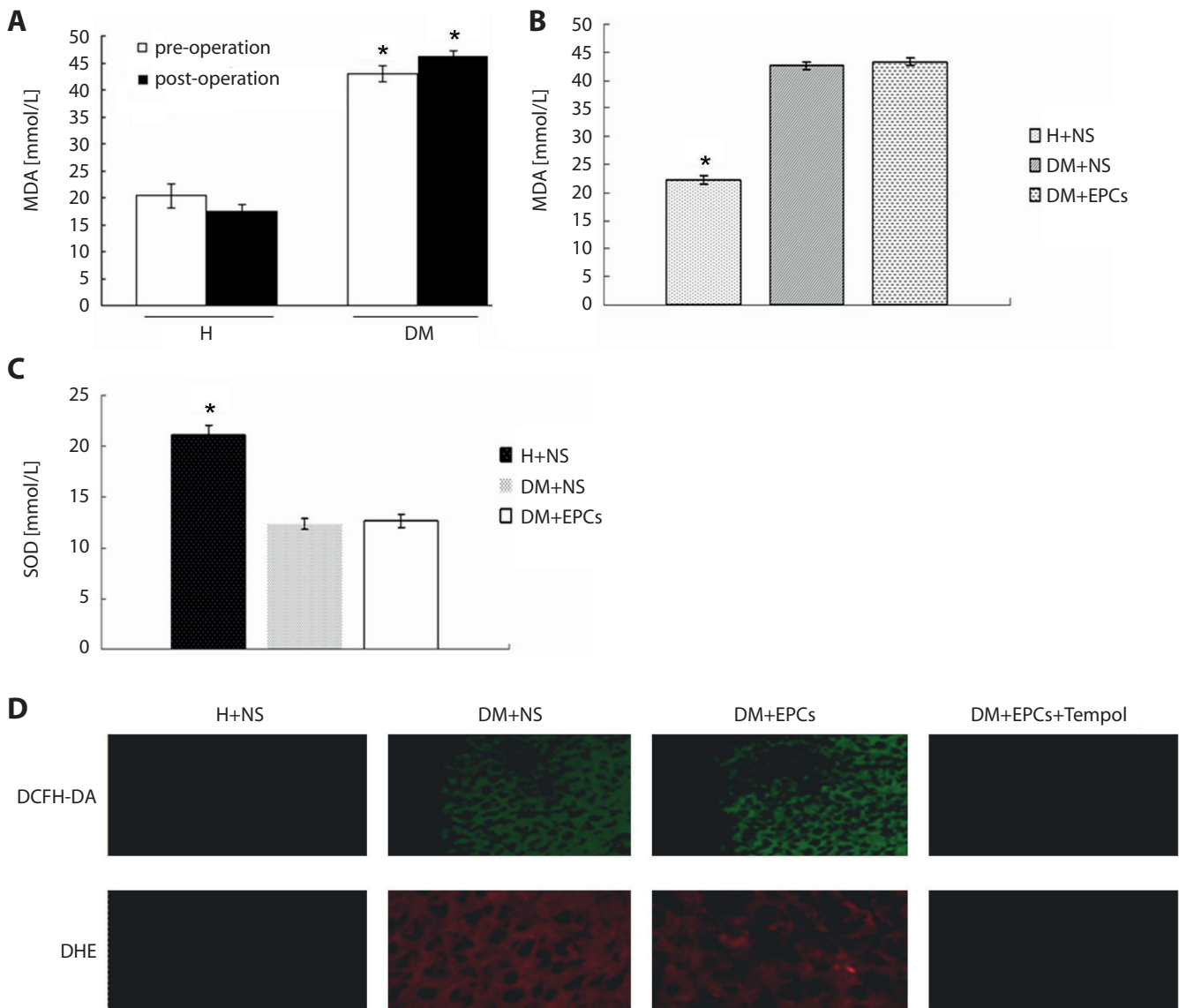
Fig. 4. Determination of high oxidative stress in the hindlimbs of diabetic hindlimb ischemic rats. A. Serum malondialdehyde (MDA) levels in the healthy (H) group and diabetes mellitus (DM) group at pre-operation and post-operation (* $p < 0.05$ for comparison of pre- and post-operation MDA level in the H group); B. Serum MDA levels in the endothelial progenitor cell (EPC)-transplanted diabetic rats (* $p < 0.05$ for comparison of pre- and post-operation MDA level in the DM+EPCs group); C. Effect of the transplantation of EPCs on serum superoxide dismutase (SOD) levels of DM rats (* $p < 0.05$ for comparison of pre- and post-operation MDA level in the DM+EPCs group); D. Determination of the reactive oxygen species (ROS) levels in ischemic gastrocnemius muscle of rats using fluorescent microscope. Green fluorescent dichlorodihydrofluorescein diacetate (DCFH-DA) reflected the ROS levels in gastrocnemius muscle of rats in each group. Red fluorescent dihydroethidium (DHE) reflected the ROS levels in the gastrocnemius muscle of rats in each group (×200 magnification). The Tukey's post hoc test (analysis of variance (ANOVA)) and Student's t-test were conducted to analyze the data. The statistical differences (p-values) between the 2 labeled groups (horizontal lines) have been depicted

NS – normal saline.

which suggests that the XVA buffer DMSO (as a solvent and as a negative control) did not affect blood flow recovery. Moreover, repeated measures ANOVA showed that there were significant differences in the L/R blood flow ratio between different time points (before the operation and 0, 7, 14, and 28 days following the operation) in the DM+EPCs (ANOVA, F = 60.546, df = 4, $p < 0.001$), DM+EPCs+DMSO (ANOVA, F = 67.757, df = 4, $p < 0.001$) and DE+EPCs+Tempol (ANOVA, F = 56.550, df = 4, $p < 0.001$) groups. In summary, L/R blood flow ratio in various groups changed at different treatment time points.

XAV suppressed angiogenesis in gastrocnemius muscle of diabetic hindlimb ischemic rats following Tempol administration

Our results demonstrated that XAV administration suppresses microvessel migration to ischemic gastrocnemius muscle in diabetic hindlimb ischemic rats after the administration of Tempol (Fig. 7A). The ANOVA analysis showed that there were obvious differences for angiogenesis (value of EPCs/MVD) in gastrocnemius muscle among

A

B

Fig. 5. Effects of Tempol on angiogenesis in the gastrocnemius muscle of diabetic hindlimb ischemic rats. A. Counting the numbers of microvessels in frozen section of gastrocnemius muscles of rats by staining with PKH-26. The 4′,6-diamidino-2-phenylindole (DAPI) (blue fluorescence) represents the nuclei. The CD31 (green fluorescence) represents the new microvessels. The PKH-26-labeled red fluorescence or clusters represent the migration of endothelial progenitor cells (EPCs) to the ischemic sites (×200 magnification); B. Statistical analysis for the ratio of number of labeled EPCs migrated to ischemic site to the number of new microvessels. The Tukey's post hoc test (analysis of variance (ANOVA)) was conducted to analyze the data. * p < 0.05 for comparison of DM+NS group or DM+EPCs+Tempol group with the DM+EPCs group.

MVD – microvascular density.

DM+EPCs, DM+EPCs+DMSO, DM+EPCs+Tempol, and DM+EPCs+Tempol+XAV groups (Fig. 7A,B; Tukey's post hoc test (ANOVA), F = 16.921, df = 3, p < 0.001). In a similar manner, Tempol treatment remarkably enhanced angiogenesis in gastrocnemius muscle of Tempol-administered diabetic hindlimb ischemic rats (DM+EPCs+Tempol group) compared to the DM+EPCs group (Fig. 7A,B; p < 0.001). Meanwhile, the angiogenesis in XAV and Tempol-administered diabetic hindlimb ischemic rats (DM+EPCs+Tempol+XAV group) was significantly reduced compared to that in the DM+EPCs+Tempol group (Fig. 7A,B; p < 0.001).

XAV reduced β-catenin expression in Tempol-treated diabetic hindlimb ischemic rats

The T-β-catenin and NP-β-catenin expressions were determined using western blotting assay (Fig. 8A). The results showed that there were significant differences in T-β-catenin expression (Fig. 8B; Tukey's post hoc test (ANOVA), F = 70.149, df = 3, p < 0.001) and NP-β-catenin expression (Fig. 8C; Tukey's post hoc test (ANOVA), F = 9.562, df = 3, p = 0.005) among DM+EPCs, DM+EPCs+DMSO, DM+EPCs+Tempol, and
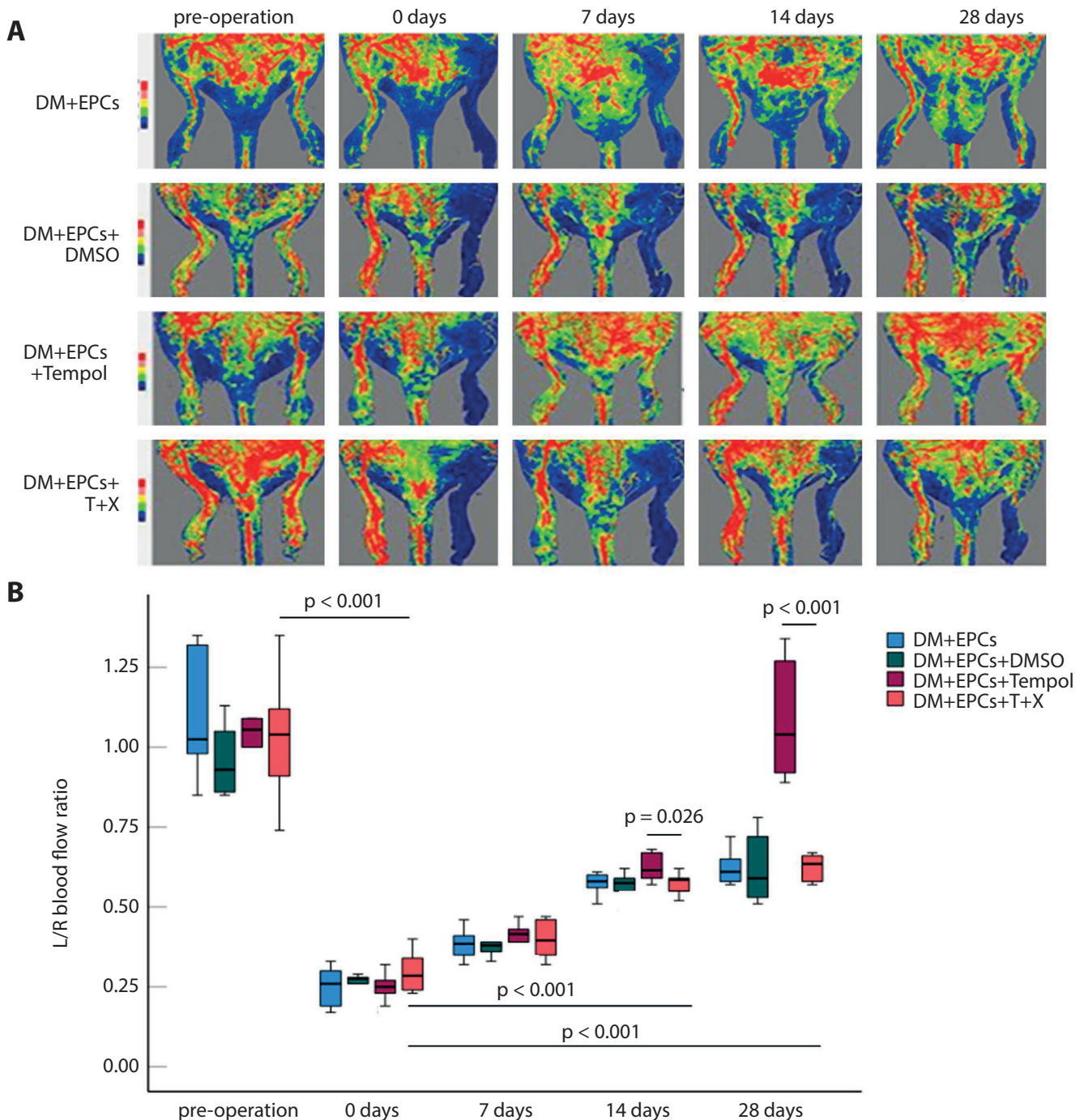
Fig. 6. The effect of inhibition of Wnt/β-catenin signaling pathway on the recovery of blood flow. A. The blood changes for the rats in DM+EPCs, DM+EPCs+DMSO, DM+EPCs+Tempol, and DM+EPCs+Tempol+XAV groups at pre-operation and 0, 7, 14, and 28 days post-operation were determined using laser Doppler monitoring; B. The statistical analysis of the continuous L/R blood flow ratio for each group. The Tukey's post hoc test (analysis of variance (ANOVA)) and Student's t-test were conducted to analyze the data. The statistical differences (p-values) between the 2 labeled groups (horizontal lines) have been depicted

DM – diabetes mellitus; EPCs – endothelial progenitor cells; DMSO – dimethylsulfoxide; T+X – tempol+XAV.

DM+EPCs+Tempol+XAV groups. The Tempol treatment significantly increased T-β-catenin expression (Fig. 8B; p < 0.001) and NP-β-catenin expression (Fig. 8C; p = 0.008) in EPC-transplanted diabetic hindlimb ischemic rats (DM+EPCs+Tempol), compared to those in the DM+EPCs group. However, the XAV administration decreased T-β-catenin expression (Fig. 8B; p < 0.001) and NP-β-catenin expression (Fig. 8C; p = 0.030) in Tempol administered and EPC-transplanted diabetic

hindlimb ischemic rats (DM+EPCs+Tempol+XAV group), compared to those in the DM+EPCs+Tempol group.

Wnt5a participated in the pathology of diabetic hindlimb ischemia

The results showed that the Wnt3a level (Fig. 9A; Tukey's post hoc test (ANOVA), F = 11.210, df = 3, p < 0.001) was
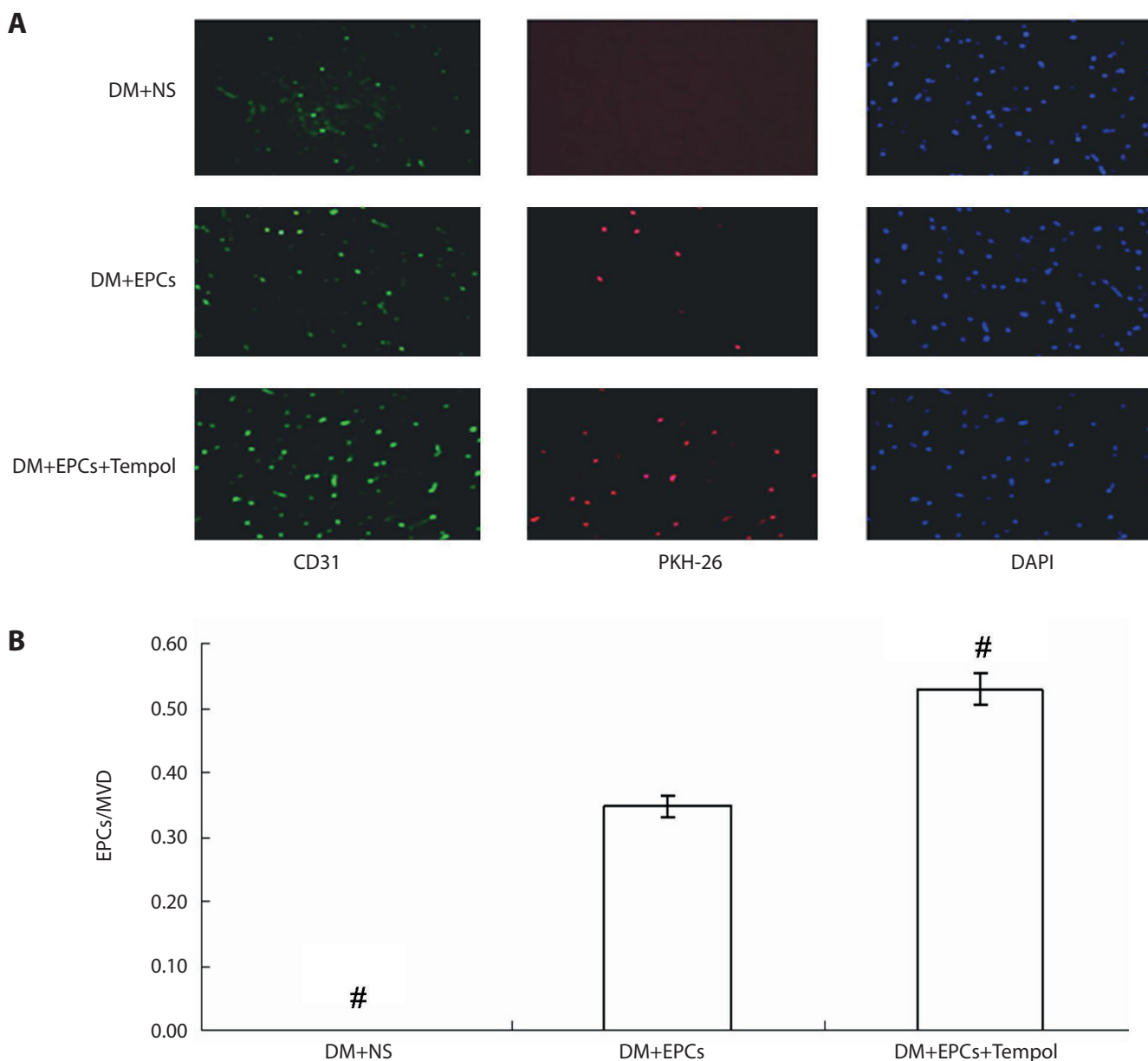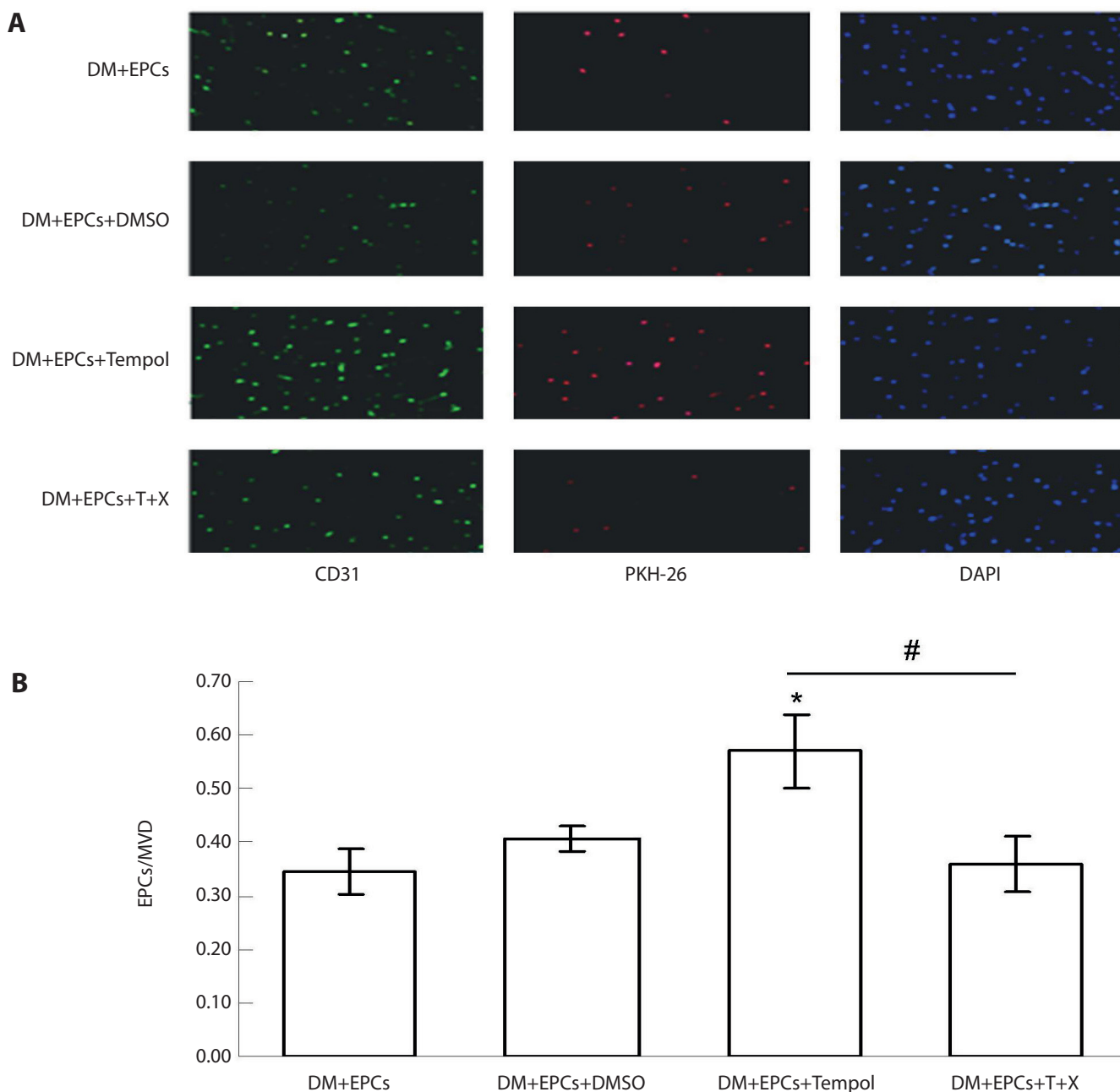
Fig. 7. Effects of Tempol and/or XAV on angiogenesis in gastrocnemius muscles of diabetic hindlimb ischemic rats. A. Counting the numbers of microvessels in the frozen section of gastrocnemius muscles of rat and the numbers of PKH-26-labeled endothelial progenitor cells (EPCs). The 4′,6-diamidino-2-phenylindole (DAPI) (blue fluorescence) represents the nuclei. The CD31 (green fluorescence) represents the new microvessels. The PKH-26-labeled red fluorescence or clusters represent the migration of EPCs to ischemic sites (×200, magnification); B. Statistical analysis for the ratio of number of labeled EPCs migrated to ischemic site to the number of new microvessels. The Tukey's post hoc test (analysis of variance (ANOVA)) was conducted to analyze the data. *p < 0.05 represented EPCs/MVD in DM+PECs+DMSO group compared to the DM+PECs+Tempol group. #p < 0.05 represented EPCs/MVD in DM+PECs+Tempol group compared to the DM+PECs+Tempol+XAV group.

DM – diabetes mellitus; DMSO – dimethylsulfoxide; MVD – microvascular density; T+X – tempol+XAV.

significantly increased, whereas Wnt5a (Fig. 9B; Tukey's post hoc test (ANOVA), F = 18.293, df = 3, p < 0.001) and Wnt7a (Fig. 9C; Tukey's post hoc test (ANOVA), F = 13.149, df = 3, p < 0.001) levels were remarkably decreased in diabetic hindlimb ischemic rats compared to those of healthy rats. Furthermore, the administration of Tempol (DM+EPCs+Tempol group) significantly enhanced Wnt5a levels compared to those in the DM+EPCs group (Fig. 9B; p < 0.001).

Discussion

Diabetic hindlimb ischemia presents with vascular inflammation, lipid deposition and atherosclerosis, which can lead to vascular stenosis and occlusion, followed by ischemia and hypoxia, ulceration, infection, and necrosis of the corresponding blood supply site.[19] In particular, atherosclerosis and acute arterial thrombosis are
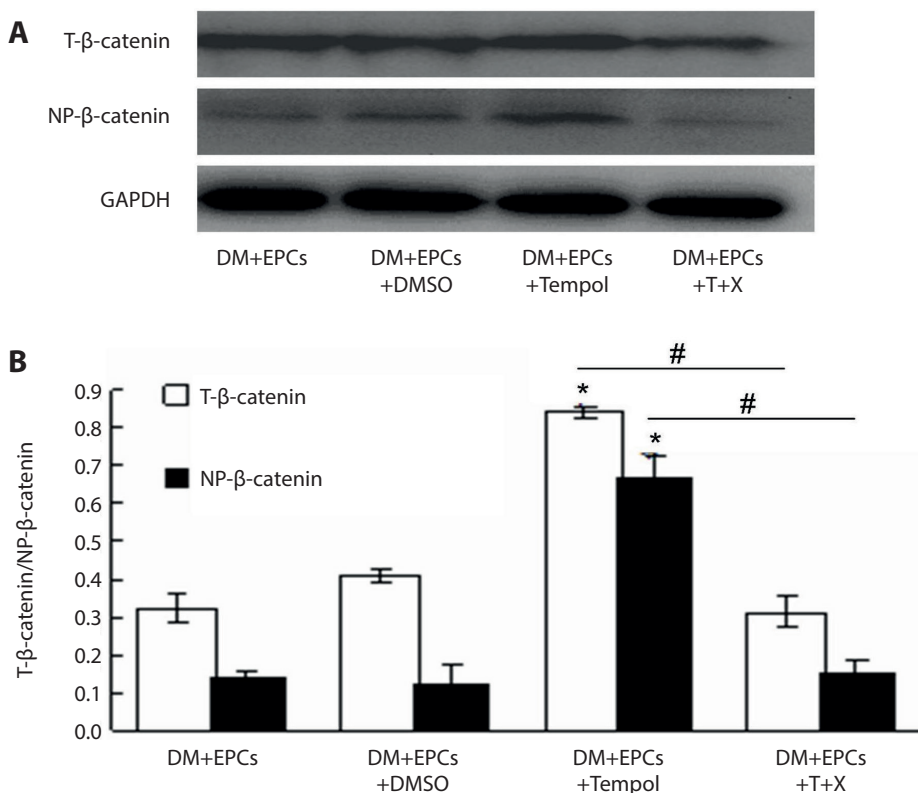
Fig. 8. Effects of Tempol and/or XAV on total β-catenin (T-β-catenin) and non-phospho-β-catenin (NP-β-catenin) expression in gastrocnemius muscles of diabetic hindlimb ischemic rats. A. Western blotting assay for the T-β-catenin and NP-β-catenin expression; B. Statistical analyses for the relative expression of T-β-catenin and β-catenin. Statistical analyses for the relative expression of NP-β-catenin. The Tukey's post hoc test (analysis of variance (ANOVA)) was conducted to analyze the data. * p < 0.05 for DM+EPCs+Tempol group compared to the DM+PECs group, for both T-β-catenin group and NP-β-catenin group. # p < 0.05 for DM+EPCs+Tempol group compared to the DM+PECs+Tempol+XAV group.

GAPDH – glyceraldehyde-3-phosphate dehydrogenase; DM – diabetes mellitus; EPCs – endothelial progenitor cells; DMSO – dimethylsulfoxide; T+X – tempol+XAV for both T-β-catenin and NP-β-catenin.

the primary causes of amputation in the elderly. Diabetic hindlimb ischemia is not only an ischemic disease, but is also often associated with neurotrophic disorders. However, diabetic hindlimb ischemia leads to vascular damage and ischemic disease, accompanied by an impairment of collateral angiogenesis. Diabetic hindlimb ischemia further aggravates ischemia, and any ulcer and necrotic lesions present are more difficult to repair. In this way, a vicious circle will be formed. If timely intervention and treatment are not carried out, the extent and scope of the lesions will be significantly increased.

There are many other factors affecting diabetic hindlimb ischemia, including hypertension, smoking, hyperlipidemia, overweight or obesity, lack of exercise, and poor mental health. In addition, local hemodynamic changes and structural changes of the arterial wall are important factors, creating a complex presentation.[20] Many of the abovementioned factors lead to diabetic limb ischemia and poor blood flow recovery. The same performance can be observed in this experiment. Through the establishment of a diabetic single limb ischemia model, the relative value of blood flow in the left femoral artery and its branches were observed 14 days and 28 days after the operation. The relative blood flow at the same time point in the diabetic group was relatively small, and laser Doppler imaging was found to create better comparisons, indicating that the blood flow recovery effect of diabetic rats after hindlimb ischemia was worse than that of healthy rats. Diabetic angiopathy is a slow and continuous pathological process.[10] After STZ destroys the B cells of islets of Langerhans, hyperglycemia emerges,

indicating that the hindlimb model cannot be established immediately. Therefore, the experiment continued to feed high-fat food for 2 months, and then the follow-up experiment was carried out.

Asahara et al. were the first to isolate EPCs from the bone marrow.[21] The cell surface antigens were CD34+, KDR+, CD133, and VEGFR-2.[22,23] In recent years, it has been found that the mobilization of bone marrow-derived EPCs can repair damaged blood vessels. Therefore, EPCs play an important role in the regeneration of various vascular lesions.[24] Furthermore, EPCs play key roles in generating blood vessels in utero and during post-partum development. Because of the relatively large number of MNCs in the bone marrow of Sprague Dawley rats, simplicity of the method and low costs, bone marrow-derived EPCs were used in this experiment. Cells cultured for 7 days were infused with Dil labeled with acLDL and UEA-1 labeled with FITC. The double-positive cells of UEA-1 and acLDL were considered undifferentiated EPCs.

Diabetic angiopathy is closely related to the decrease of EPCs that can be mobilized and migrate to the ischemic site, as well as the dysfunction of vascular repair, neovascularization, angiogenesis, and arterial angiogenesis caused by this functional impairment. An excessive oxidative stress is an important mechanism of diabetic angiopathy.[10] In recent years, it has been found that the high-glucose environment affects the mitochondrial electron transport chain, continuously producing large amounts of ROS,[25,26] causing oxidative stress damage, and affecting the physiological growth and survival of EPCs. Finally,
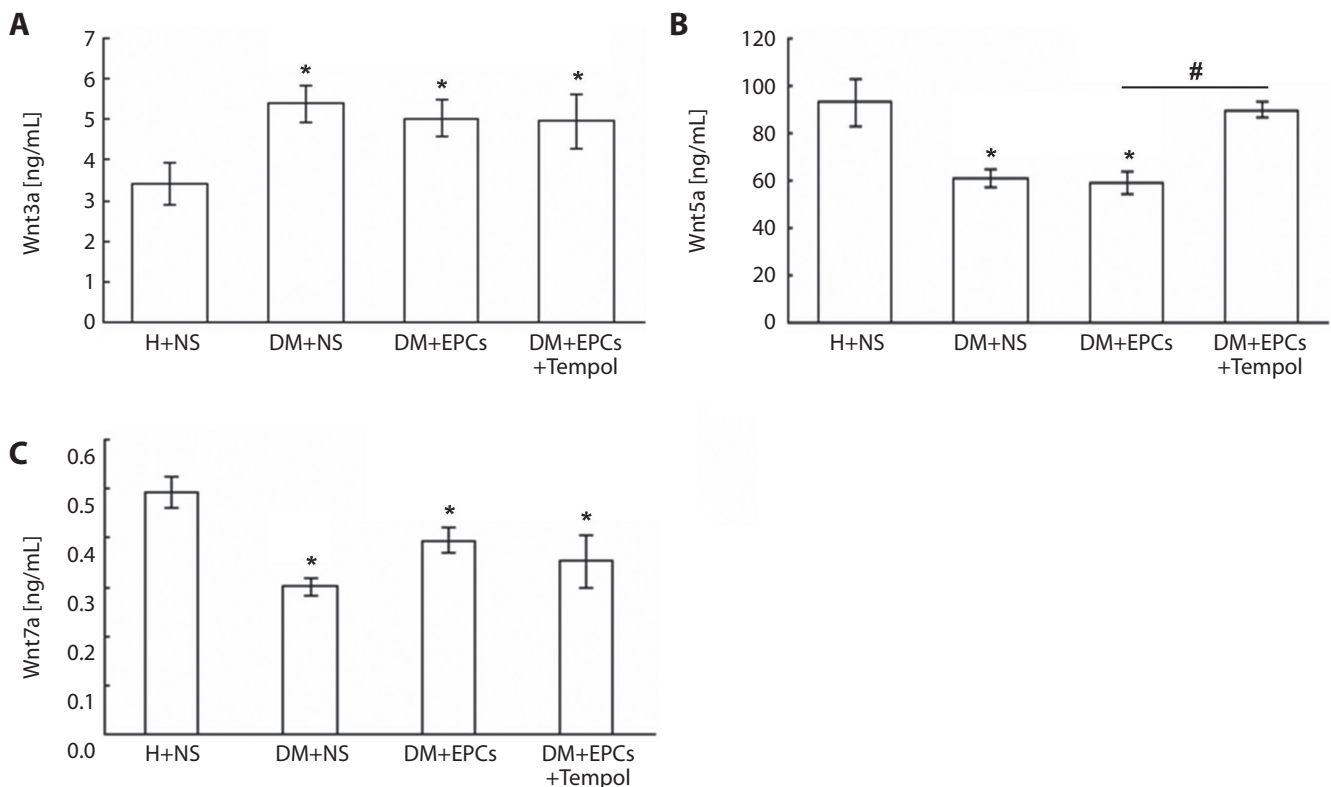
Fig. 9. Serum levels of Wnt3a, Wnt5a and Wnt7a in diabetic hindlimb ischemic rats of the H+NS, DM+NS, DM+EPCs, and DM+EPCs+Tempol groups.
A. Levels of serum Wnt3a; B. Levels of serum Wnt5a; C. Levels of serum Wnt7a. The Tukey's post hoc test (analysis of variance (ANOVA)) was conducted to analyze the data. * $p < 0.05$ for DM+NS, or DM+EPCs, or DM+EPCs+Tempol group compared to the H+NS group. # $p < 0.05$ for DM+EPCs+Tempol group compared to the DM+PECs group.

H – healthy; DM – diabetes mellitus; NS – normal saline; EPCs – endothelial progenitor cells.

this causes abnormal metabolism and function of cells, or even apoptosis. In this study, there was no significant change in the amount of MDA in the diabetic serum before or after the operation, which was 2 times higher than that in the normal group. The serum SOD of healthy rats was significantly higher than that of diabetic rats. There were no significant changes in the MDA serum levels of diabetic and healthy rats before and after the operation. Moreover, there was no significant change in MDA and SOD in the serum of diabetic rats when they were injected with EPCs. Therefore, the effects of the operation and transplantation of EPCs on oxidative stress level in diabetic rats can be excluded. In addition, the rats were divided into 4 groups, including H+NS, DM+NS, DM+EPCs, and DM+EPCs+Tempol. The levels of ROS were measured by DCFH-DA and DHE fluorescence. The results showed that the relative fluorescence value in gastrocnemius muscle of diabetic rats was higher than that of normal rats. The relative fluorescence values of the DM+EPCs+Tempol and DM+EPCs groups were significantly lower than those of the DM+EPCs group. At the same time, EPCs were divided into 3 groups, including the blank group, high-glucose (HG) group and normal glucose (N) concentration group. After 120 h of culture, the level of ROS in EPCs was detected with flow cytometry. The results showed

that ROS was also produced by EPCs under normal glucose concentration, but the amount was significantly lower than in the HG group. The abovementioned in vitro and in vivo experiments showed that high glucose increases the ROS products and the degree of oxidative stress. Compared with the normal rats, the level of oxidative stress in diabetic rats was increased, both locally and systemically, which was not related to cell transplantation and operation.

The level of ROS in vivo affects the number of transplanted cells migrating to the ischemic gastrocnemius muscle, the degree of neovascularization and the recovery of blood flow. In previous studies in vitro, it has been found that oxidative stress induced by high-glucose environment can damage the proliferation and tube-forming ability of EPCs[27] and increase the apoptosis.[28] The ability for migration and adhesion of stem cells transplanted intravenously is of extreme importance. It is possible that the transplantation of stem cells can promote the migration of self-mobilized EPCs to the ischemic site. Therefore, EPCs labeled with PKH-26 can be used to trace the migration of EPCs to the ischemic site. The rats included in our study were divided into 3 groups, namely the DM+NS group, DM+EPCs group and DM+EPCs+Tempol group. This experimental result first confirmed that oxidative

1228

X. Xu et al. EPCs inhibits diabetic hindlimb ischemia

stress is the main factor affecting the therapeutic effect of EPC. In the following experiment, we would further explore Wnt/β-catenin signaling pathway-associated mechanism. The laser Doppler perfusion imaging (LDPI) was used to continuously monitor the blood flow recovery of ischemic hindlimbs, and immunofluorescence was used to detect the neovascularization of the ischemic gastrocnemius muscle and transplanted EPCs. The results showed that the MVD of the DM+EPCs+Tempol rats was higher than that of the DM+EPCs rats, and the relative number of PKH-26-labeled EPCs migrating to ischemic sites was higher, together with the ratio of labeled cells to MVD. The increase in the oxidative stress level in diabetes mellitus leads to the limitation of blood flow recovery in hindlimbs after ischemia. It may be that the oxidative stress level has been increased for a long time, resulting in a decreased number of EPCs adhering to the ischemic site, which in turn decreased the number of new blood vessels. However, this can be reversed by oxidative inhibitors which promote blood flow recovery. However, in this study, the blood flow of the nonsurgical hindlimb (the right hindlimb) was also detected using LDPI and it might have led to the false positive findings, which is a limitation of our study.

The β-catenin is a cytoskeleton protein and a crucial component of the Wnt/β-catenin signaling pathway.[29] The stability of β-catenin and its position in cells is regulated by a series of positive and negative regulatory factors. The abnormal regulation can lead to the inhibition or abnormal activation of Wnt signaling, resulting in a series of abnormalities in gene expression, cell adhesion and development, which are closely related to the cancer occurrence and metastases.[30,31] Our results indicated that Tempol treatment significantly increased T-β-catenin and NP-β-catenin expression in the EPC-transplanted diabetic hindlimb ischemic rats (DM+EPCs+Tempol) compared to those in the DM+EPCs group. However, XAV administration decreased T-β-catenin and NP-β-catenin expression in Tempol administration and in the EPC-transplanted diabetic hindlimb ischemic rats (DM+EPCs+Tempol+XAV) compared to the DM+EPCs+Tempol group. Furthermore, the administration of Tempol (DM+EPCs+Tempol group) significantly enhanced Wnt5a levels compared to those in the DM+EPCs group. All of these results suggest that the limited effect of blood flow recovery in diabetic hindlimb ischemia may be related to the regulation of Wnt/β-catenin signaling pathway.

Limitations

The most obvious limitation of this study is that the sample size for the STZ-induced diabetic rat model and hindlimb ischemia model was small. In future investigations, we aim to involve more animals for clarifying the associated findings.

Conclusions

High oxidative stress levels were noted in both EPCs in high-glucose environment and diabetic hindlimb ischemia, which can lead to limited blood flow recovery post-treatment. The high oxidative stress caused the inhibition of Wnt/β-catenin signaling, leading to limited blood flow recovery in the diabetic hindlimb ischemia. Meanwhile, Wnt5a participated in the EPC-mediated blood flow recovery. The findings of this study would benefit the basic study of a high-glucose environment in animal models of induced diabetic hindlimb ischemia. Moreover, the study might provide insight for the further clinical treatment of diabetic hindlimb ischemia.

ORCID iDs

Xiongfei Xu https://orcid.org/0000-0001-8424-4288
Fei Xie https://orcid.org/0000-0002-0849-5664
Yuping Wang https://orcid.org/0000-0001-6446-9594
Hong Zeng https://orcid.org/0000-0001-5982-4774
Sen Shi https://orcid.org/0000-0002-9812-3230
Xiaolei Sun https://orcid.org/0000-0003-1693-4396
Huqiang He https://orcid.org/0000-0001-8708-9076
Lei Zhang https://orcid.org/0000-0001-6348-3140
Weiming Wang https://orcid.org/0000-0002-3115-4665
Tao Xiang https://orcid.org/0000-0002-6976-811X
Yanzheng He https://orcid.org/0000-0003-4712-6818
Yong Liu https://orcid.org/0000-0001-9969-3078

References

1. Mills JL. Lower limb ischaemia in patients with diabetic foot ulcers and gangrene: Recognition, anatomic patterns and revascularization strategies. *Diabetes Metab Res Rev*. 2016;32:239–245. doi:10.1002/dmrr.2753
2. Chen Y, Niu W, Chao YC, et al. Alagebrium targets the miR-27b/TSP-1 signaling pathway to rescue Nε-carboxymethyl-lysine-induced endothelial dysfunction. *Am J Transl Res*. 2019;11(3):1569–1580. PMID:25669621.
3. Xu YJ, Elimban V, Bhullar SK, Dhalla NS. Effects of CO₂ water-bath treatment on blood flow and angiogenesis in ischemic hind limb of diabetic rat. *Can J Physiol Pharmacol*. 2018;96(10):1017–1021. doi:10.1139/cjpp-2018-0160
4. MacAskill MG, Saif J, Condie A, et al. Robust revascularization in models of limb ischemia using a clinically translatable human stem cell-derived endothelial cell product. *Mol Ther*. 2018;26(7):1669–1684. doi:10.1016/j.ymthe.2018.03.017
5. Svěcený J, Syková E, Tichý M, Laštůvka J. New options for therapeutic revascularization in lower extremity limb ischemia linked to the diabetic foot syndrome by autologous stem cell transplantation [in Czech]. *Cas Lek Cesk*. 2015;154(4):161–167. PMID:26357857.
6. Kim H, Han JW, Lee JY, et al. Diabetic mesenchymal stem cells are ineffective for improving limb ischemia due to their impaired angiogenic capability. *Cell Transplant*. 2015;24(8):1571–1584. doi:10.3727/096368914X682792
7. Nakayoshi T, Sasaki KI, Kajimoto H, et al. FOXO4-knockdown suppresses oxidative stress-induced apoptosis of early pro-angiogenic cells and augments their neovascularization capacities in ischemic limbs. Mohanraj R, ed. *PLoS One*. 2014;9(3):e92626. doi:10.1371/journal.pone.0092626
8. Sheng Z, Li Y, Zheng K, et al. The relationship between number and function of EPCs and concentration of VEGF165 and SDF-1 in coronary artery spasm. *Eur Rev Med Pharmacol Sci*. 2018;22(9):2767–2777. doi:10.26355/eurrev_201805_14974
9. Dai X, Yan X, Zeng J, et al. Elevating CXCR7 improves angiogenic function of EPCs via Akt/GSK-3β/Fyn-mediated Nrf2 activation in diabetic limb ischemia. *Circ Res*. 2017;120(5):e7–e23. doi:10.1161/CIRCRESAHA.117.310619

10. Hamed S, Brenner B, Roguin A. Nitric oxide: A key factor behind the dysfunctionality of endothelial progenitor cells in diabetes mellitus type-2. *Cardiovasc Res*. 2011;91(1):9–15. doi:10.1093/cvr/cvq412

11. Barcelos LS, Duplaa C, Kränkel N, et al. Human CD133+ progenitor cells promote the healing of diabetic ischemic ulcers by paracrine stimulation of angiogenesis and activation of Wnt signaling. *Circ Res*. 2009;104(9):1095–1102. doi:10.1161/CIRCRESAHA.108.192138

12. Yin Z, Peng Z, Wang Z, Meng Q. The oncogenic role of REG γ is exerted by activating the Wnt/β-catenin signaling pathway in osteosarcoma. *Am J Transl Res*. 2020;12(2):563–573. PMID:32194904.

13. Chen Y, Hu Y, Zhou T, et al. Activation of the Wnt pathway plays a pathogenic role in diabetic retinopathy in humans and animal models. *Am J Pathol*. 2009;175(6):2676–2685. doi:10.2353/ajpath.2009.080945

14. Wu YF, He FL, Gu YQ, et al. Evaluation in vivo of autologous cell derived vein grafts based on tissue engineering concept. *Int Angiol*. 2015; 34(5):495–501. PMID:25669621.

15. Hirata K, Li TS, Nishida M, et al. Autologous bone marrow cell implantation as therapeutic angiogenesis for ischemic hindlimb in diabetic rat model. *Am J Physiol Heart Circ Physiol*. 2003;284(1):H66–H70. doi:10.1152/ajpheart.00547.2002

16. Dokun AO, Keum S, Hazarika S, et al. A quantitative trait locus (LSq-1) on mouse chromosome 7 is linked to the absence of tissue loss after surgical hindlimb ischemia. *Circulation*. 2008;117(9):1207–1215. doi:10.1161/CIRCULATIONAHA.107.736447

17. Liao HH, Zhu JX, Feng H, et al. Myricetin possesses potential protective effects on diabetic cardiomyopathy through inhibiting I κ B α/ NF κ B and enhancing Nrf2/HO-1. *Oxid Med Cell Longev*. 2017;2017: 8370593. doi:10.1155/2017/8370593

18. Lertkiatmongkol P, Liao D, Mei H, Hu Y, Newman PJ. Endothelial functions of platelet/endothelial cell adhesion molecule-1 (CD31). *Curr Opin Hematol*. 2016;23(3):253–259. doi:10.1097/MOH.0000000000000239

19. Lu ZY, Li RL, Zhou HS, et al. Therapeutic ultrasound reverses peripheral ischemia in type 2 diabetic mice through PI3K-Akt-eNOS pathway. *Am J Transl Res*. 2016;8(9):3666–3677. PMID:27725849.

20. Smolderen KG, van Zitteren M, Jones PG, et al. Long-term prognostic risk in lower extremity peripheral arterial disease as a function of the number of peripheral arterial lesions. *J Am Heart Assoc*. 2015; 4(10):e001823. doi:10.1161/JAHA.115.001823

21. Asahara T, Murohara T, Sullivan A, et al. Isolation of putative progenitor endothelial cells for angiogenesis. *Science*. 1997;275(5302): 964–967. doi:10.1126/science.275.5302.964

22. Tepper OM, Galiano RD, Capla JM, et al. Human endothelial progenitor cells from type II diabetics exhibit impaired proliferation, adhesion, and incorporation into vascular structures. *Circulation*. 2002;106(22):2781–2786. doi:10.1161/01.CIR.0000039526.42991.93

23. Kim KA, Shin YJ, Kim JH, et al. Dysfunction of endothelial progenitor cells under diabetic conditions and its underlying mechanisms. *Arch Pharm Res*. 2012;35(2):223–234. doi:10.1007/s12272-012-0203-y

24. Ma XL, Sun XL, Wan CY, Ma JX, Tian P. Significance of circulating endothelial progenitor cells in patients with fracture healing process. *J Orthop Res*. 2012;30(11):1860–1866. doi:10.1002/jor.22134

25. Yao EH, Yu Y, Fukuda N. Oxidative stress on progenitor and stem cells in cardiovascular diseases. *Curr Pharm Biotechnol*. 2006;7(2):101–108. doi:10.2174/138920106776597685

26. Loomans CJM, De Koning EJP, Staal FJT, Rabelink TJ, Zonneveld AJV. Endothelial progenitor cell dysfunction in type 1 diabetes: Another consequence of oxidative stress? *Antioxid Redox Signal*. 2005;7(11–12): 1468–1475. doi:10.1089/ars.2005.7.1468

27. Gao J, Wang Y, Li W, et al. Loss of histone deacetylase 2 inhibits oxidative stress induced by high glucose via the HO-1/SIRT1 pathway in endothelial progenitor cells. *Gene*. 2018;678:1–7. doi:10.1016/j.gene. 2018.07.072

28. Liu Y, Xei F, Xu XF, et al. Experimental study on apoptosis of TNFR1 receptor pro-endothelial progenitor cells activated by high glucose induced oxidative stress. *Int J Clin Exp Med*. 2015;8(11):19969–19981. PMID:26884909.

29. Goodwin AM, Sullivan KM, D'Amore PA. Cultured endothelial cells display endogenous activation of the canonical Wnt signaling pathway and express multiple ligands, receptors, and secreted modulators of Wnt signaling. *Dev Dyn*. 2006;235(11):3110–3120. doi:10.1002/ dvdy.20939

30. Boo JH, Song H, Kim JE, Kang DE, Mook-Jung I. Accumulation of phosphorylated β-catenin enhances ROS-induced cell death in presenilin-deficient cells. *PLoS One*. 2009;4(1):e4172. doi:10.1371/journal.pone. 0004172

31. Manolagas SC, Almeida M. Gone with the Wnts: β-catenin, T-cell factor, forkhead box O, and oxidative stress in age-dependent diseases of bone, lipid, and glucose metabolism. *Mol Endocrinol*. 2007;21(11): 2605–2614. doi:10.1210/me.2007-0259

Gene network analysis of the transcriptome impact of methylated microRNAs on oral squamous cell carcinoma

Emilia Gabriela Avram[1,2,B,D], Ioana Alexandra Moatar[1,3,D], Viktorian Miok[4,C], Flavia Baderca[5,C], Corina Samoila[3,6,B], Anda Alexa[3,C], Ioana Nicoleta Andreescu[7,C], Angela Podariu[8,A], Catalin Marian[3,6,E], Ioan Ovidiu Sirbu[3,6,A,D,F]

[1] Doctoral School, Victor Babeş University of Medicine and Pharmacy, Timişoara, Romania

[2] Department of Maxillofacial Surgery, Faculty of Dentistry, "Vasile Goldiş" Western University of Arad, Romania

[3] Department of Biochemistry & Pharmacology, Victor Babeş University of Medicine and Pharmacy, Timişoara, Romania

[4] Department of Informatics & Medical Biostatistics, Victor Babeş University of Medicine and Pharmacy, Timişoara, Romania

[5] Department of Microscopic Morphology, Victor Babeş University of Medicine and Pharmacy, Timişoara, Romania

[6] Center for Complex Network Science, Victor Babeş University of Medicine and Pharmacy, Timişoara, Romania

[7] Department of Microscopic Morphology – Genetics, Center of Genomic Medicine, Victor Babeş University of Medicine and Pharmacy, Timişoara, Romania

[8] Department of Preventive Dentistry, Community and Oral Health, Victor Babeş University of Medicine and Pharmacy, Timişoara, Romania

A – research concept and design; B – collection and/or assembly of data; C – data analysis and interpretation;
D – writing the article; E – critical revision of the article; F – final approval of the article

Abstract

Background. Oral squamous cell carcinoma (OSCC) is one of the most common head and neck squamous cell tumors. MicroRNAs and DNA methylation, as epigenetic mechanisms, regulate the expression of oncogenes and tumor suppressor genes, contributing to the carcinogenic development. However, the current knowledge on the genetic and epigenetic landscape of OSCC is still limited.

Objectives. To assess the transcriptomic impact of microRNAs found to be methylated through Infinium genome-wide methylation profiling of archived OSCC tissues, and to analyze their biological role using gene network analysis.

Materials and methods. We used the Infinium array-based methylation assay to assess the genome-wide methylation status at the single-CpG-site level of DNA purified from archived OSCC tissue samples. After quality control, filtering out poorly performing probes and normalization of data, we identified the differentially methylated microRNA loci. We performed a literature-based analysis of OSCC transcriptomic data to identify the predicted target genes for each microRNA, followed by individual network and pathway enrichment analyses.

Results. The analysis of Infinium methylation array data revealed 1469 differentially hypomethylated loci, 4 of which were of interest, namely hsa-microRNA-124-3, hsa-microRNA-24-1, hsa-microRNA-769, and hsa-microRNA-4500. Network and pathway enrichment analyses revealed multiple pathways modulated through DNA methylation-microRNA expression axes.

Conclusions. We describe the transcriptomic impact of 4 differentially methylated microRNAs in OSCC tissues samples and discuss their role in the pathology of OSCC. These results may contribute to a better understanding of how epigenetic mechanisms such as DNA methylation and microRNAs cooperate to impact the development of OSCC.

Key words: DNA methylation, microRNAs, network analysis, oral squamous cell carcinoma

1232

E.G. Avram et al. Methylated microRNAs in OSCC

Background

Oral squamous cell carcinoma (OSCC) is one of the most common head and neck squamous cell carcinoma (HN-SCC) tumors, with over 350,000 new cases annually.[1] Despite recent therapeutic progress, the cure rate of OSCC is relatively low and closely correlated with the tumor stage at diagnosis. Moreover, in recent years, there has been a change in the incidence of OSCC, with an increased occurrence in young people.[2]

Oral cancer is less studied than other cancers, and there is currently a lack of bona fide diagnostic and prognostic biomarkers. Similarly to other solid cancers,[3–5] OSCC has a multifactorial and multigenic character. Its development is driven by various intricate genetic and epigenetic mechanisms which play important roles in the initiation and development of these tumors.[6]

The DNA methylation and non-coding RNAs are 2 of the most studied epigenetic mechanisms impacting global gene expression.[7] The DNA methylation is essential for several important cellular mechanisms, including regulation of gene expression, differentiation, genome imprinting, and stability.[8] The accumulation of alterations to genome methylation leads to the destabilization of cellular homeostasis. The aberrant DNA hypo- and hypermethylation patterns are critical players in tumorigenesis by promoting the expression of oncogenes and silencing tumor suppressor genes.[9–11]

MicroRNAs are small non-coding RNAs involved in the post-transcriptional regulation of approx. 60% of human genes. Multiple microRNAs have been associated with various aspects of oral cancer biology, including onset, metastasis, recurrence, prognosis, and survival.[12–14] The interest for understanding the regulation of microRNA expression in the context of other epigenetic processes has been growing steadily, and there is a need to understand the global impact of microRNAs on cancer cell transcriptomics.

Network analysis approaches, such as protein–protein interaction networks, have the potential to add biological meaning to large-scale gene datasets such as those obtained from high-throughput RNA sequencing, DNA methylation assays or microRNA target gene analysis.[15] Combining both biological networks and pathway enrichment is meaningful for predicting complex disease mechanisms, disease biomarkers, novel gene interactions, and drug design.[16] An example of this is the integrative analysis of DNA methylation and microRNA expression data that has been conducted for hepatocellular carcinoma.[17] However, a network analysis that integrates these 2 epigenetic mechanisms in the context of OSCC is lacking. Therefore, we investigated the potential interaction between these 2 epigenetic mechanisms, shedding light on unknown mechanisms that might contribute to the development of OSCC.

Objectives

The aim of the current study was to evaluate the impact of differentially methylated microRNAs in the OSCC transcriptome. Therefore, we used Infinium array-based methylation assay to analyze the genome-wide methylation status of microRNA loci in a set of OSCC-archived samples and correlated the results with publicly available microRNA expression data. We retrieved the OSCC transcriptome data from the Gene Expression Omnibus (GEO) database and used miRWalk v. 3.0 prediction algorithms (http://mirwalk.umm.uni-heidelberg.de/) to predict the gene targets of the differentially methylated microRNAs. The commonly predicted gene sets were analyzed further using network clustering coupled to Kyoto Encyclopedia of Genes and Genomes (KEGG) pathway enrichment analysis, in order to predict the biological impact of the differentially methylated microRNAs.

Materials and methods

Sample collection

The present case-control study was reviewed and the analysis of the provided formalin-fixed paraffin-embedded (FFPE) tissue samples was approved by the Ethics Committee of Victor Babeș University of Medicine and Pharmacy, Timișoara, Romania (approval No. SCUM TM 9414/30.05.2018). Due to the retrospective design of the current study and patient anonymity, the ethical review board determined that informed consent was not required. We used 13 FFPE samples from male OSCC patients (demographic characteristics are presented in Table 1); all samples were assessed and graded by 2 independent, trained pathologists. Adjacent tissues, both cancerous and normal, were dissected out of every FFPE block and pooled into 4 tumor (T) and 4 normal (N) samples for downstream methylation analysis.

DNA purification

Genomic DNA was extracted from the FFPE tissue samples using the QIAamp DNA FFPE Tissue Kit (Qiagen, Hilden, Germany), according to the manufacturer's instructions. Paraffin was dissolved in 1 mL of xylene and removed. Afterwards, the samples were lysed using 180 μL of Buffer ATL under denaturing conditions with 20 μL of proteinase K digestion. The samples were then incubated at 90°C to reverse the formalin crosslinking. To obtain RNA-free genomic DNA, 2 μL of RNAse A were added. The genomic DNA was bonded to the membrane using a mixture of Buffer AL and ethanol. In the washing steps, the residual contaminants were washed away using freshly reconstituted Buffer AW1 and AW2, according to the manufacturer's instructions. Finally, the DNA

Table 1. Demographic and clinical characteristics of the patients included in study

Characteristic	Number	Percentage (%)
Patients enrolled	13	100
Mean age (SD) [years]	54.7 (8.03)	15.4
Range	41–67	100
Localization		
Retromolar	1	7.69
Tongue	5	38.46
Alveolar	1	7.69
Floor of the mouth	2	15.38
Oral cavity	3	23.07
Jugal	1	7.69
Pathological TNM		
Early (I–II)	9	69.23
Advanced (III–IV)	4	30.77
Stage		
I	2	15.38
II	3	23.07
IV	8	61.53
Recurrence		
Yes	2	66.67
No	11	64.7
Keratinization status		
Yes	11	84.61
No	2	15.38
Cell differentiation		
G2	12	92.30
G3	1	7.70

SD – standard deviation; TNM – tumor-nodule-metastasis staging.

was eluted in 50 μL of nuclease-free water. The quality and purity of the extracted DNA were measured using a spectrophotometer (NanoDrop™; Thermo Fisher Scientific, Wilmington, USA). The DNA purity of the samples, as measured using the 260/280 ratio, had an average of 1.89 ±0.18.

Genome-wide DNA methylation in the well-differentiated OSCC samples

We used the Infinium 450K array-based methylation assay (Illumina Inc., San Diego, USA) to quantitatively assess the genome-wide methylation status at single-CpG-site level, using the DNA purified from the pooled FFPE samples. The 1-μg genomic DNA samples were incubated in sodium bisulfite buffer (Sigma-Aldrich, St. Louis, USA) in a SimpliAmp Thermal Cycler (Applied Biosystems, Waltham, USA) with alternating cycles of 95°C and 60°C. The resultant DNA was bound again to a membrane, washed, incubated in a desulphonation buffer

(Zymo Research, Orange, USA), and eluted with 20 μL of DNA elution buffer (Zymo Research). The quality and purity of the treated DNA was measured using a spectrophotometer (Nanodrop Technologies, Wilmington, USA). The yields were in the range of 50–100 ng/μL.

After bisulfite conversion, whole-genome methylation patterns were assayed using the Infinium® HumanMethylation450 BeadChip Kit (Illumina Inc.), following the manufacturer's protocol. Briefly, the raw data were obtained in intensity data file format (*.idat) by scanning the processed chips using an iScan reader (Illumina Inc.). Each point of methylation data was presented with fluorescent signals from the methylated (M) and unmethylated (U) alleles. The methylation status of each CpG site was measured based on the ratio of fluorescent signals from one allele relative to the sum of both methylated and unmethylated alleles (β value) using GenomicRatioSet (Illumina Inc.). Probes with a detection p-value cutoff >0.05 were excluded from the subsequent analysis.

To minimize the variation between and within the samples, we applied the preprocess quantile normalization methon, and then performed a PCA analysis and generated multidimensional scaling (MDS) plots to visualize and explore the differences between OSCC and normal tissues.

The differentially methylated microRNA gene loci with an adjusted p-value < 0.05 were selected for further analysis.

Statistical analyses

Illumina methylation *.idat files were imported into R programming language (R Foundation for Statistical Computing, Vienna, Austria) using the minfi function. The quality control of the imported samples was evaluated by calculating the detection p-value for every CpG island in each sample, which is indicative for the quality of the signal. Since the samples from our dataset were all derived from male donors, it was not necessary to filter the sites from X and Y chromosomes. Furthermore, we have removed the probes where common single nucleotide polymorphisms (SNPs) affected the CpG islands. Once the data were normalized and filtered, we visualized the results using MDS plots. In the final step, we calculated the β (percentage of methylation) and M ($\log_2$ ratios of the intensities of methylated compared to unmethylated probes) values.

The differentially methylated microRNAs loci were identified by a two-tailed, heteroscedastic Student's t-test, being ranked according to their Bonferroni adjusted p-values (p = 0.05 as a cutoff).

Cross validation with literature analysis

To determine whether the differentially methylated microRNAs retrieved from our genome-wide DNA methylation analysis had been previously validated through

experimental studies, we chose to perform a literature search in PubMed. In contrast to Web of Science and Google Scholar, PubMed is a human-curated database, that retrieves only peer-reviewed journal articles that fit into the searchable subject matter, with reliable sorting, reproducibility and reportable results.[18] The key words combinations used in the PubMed literature search were: microRNAs AND oral cancer, microRNAs AND oral squamous cell carcinoma. We filtered out reviews, meta-analyses and articles that did not relate to OSCC and microRNAs.

Network analysis

Target predictions (3'UTR, 5'UTR and coding sequence (CDS) region) for hsa-miR-24-1, hsa-miR-124-3, hsa-miR-769, and hsa-miR-4500 were computed with the miRWalk v. 3.0[19] machine learning algorithm (Bonferroni adjusted p-value ≤0.05 as a cutoff), using the following criteria: 1) microRNA binding probability >0.99 and 2) microRNAs concurrently predicted by at least 1 other algorithm (miRDB or TargetScan). The microRNA target prediction datasets were cross-referenced with the differentially expressed genes (DEGs) retrieved after GEO2R analysis (Benjamini–Hochberg adjusted false discovery rate (FDR) <0.05) of the GSE138206 OSCC transcriptome dataset. The common genes of microRNA targets that were differentially expressed in OSCC transcriptomes were then subjected to KEGG pathway enrichment analysis and cluster analysis on the STRING platform[20] using the following criteria: adjusted FDR value of 0.05 as cutoff and high confidence interaction score set at 0.700.

Prediction of CpG islands

MethPrimer platform (http://www.urogene.org/cgi-bin/methprimer/methprimer.cgi) was used for designing the bisulfite sequencing polymerase chain reaction (BSP PCR) primers and for predicting the CpG islands associated with the 4 microRNAs, using the 2-kb DNA sequence upstream of the microRNA loci as input data. For BSP primer selection and CpG island prediction, the general parameters have been set according to the recommendations by Li and Dahiya.[21]

Results

The β values represent the ratio between the methylated probe intensity and the overall intensity. The β-value statistics result in a number between 0 and 1, where 0 indicates that all copies of the CpG islands from analyzed samples are completely unmethylated, and a value of 1 indicates that every copy of CpG sites is methylated.[22] In our case, the β-values results are situated close to 0 and are have higher density for tumor samples in contrast to normal samples. Conversely, the M-values are calculated as the $\log_2$ ratio of methylated compared to unmethylated probes. The M-values close to 0 indicate that CpG sites are approximately half-methylated, negative values mean that there are more unmethylated CpG sites than methylated ones, and positive M-values mean the opposite.[22] In our case, the highest density plot of M-values close to 0 was created for the tumor group in contrast to the normal group. Therefore, the analysis of the Infinium methylation array β-values and M-values indicated that there is a higher degree of hypomethylation globally in the tumor group than in the control group (Fig. 1).

To find the statistically significant genes that encode for microRNAs, we filtered the 440,364 gene loci assayed on the Infinium methylation array based on an adjusted p-value < 0.05. A total of 1469 loci were obtained, of which only 4 proved to encode microRNAs, namely hsa-miR-124-3, hsa-miR-769, hsa-miR-24-1, and hsa-miR-4500. Compared to controls, the microRNA loci from OSCC samples are hypermethylated, with log fold change (logFC) values between 3.21 and 4.99. The genomic locations of all 4 microRNAs are presented in Table 2.

To determine whether our DNA methylation array results are consistent with other published findings, we searched the GEO database the key words "OSCC" and "DNA methylation". We retrieved 9 datasets, of which GSE123781 and
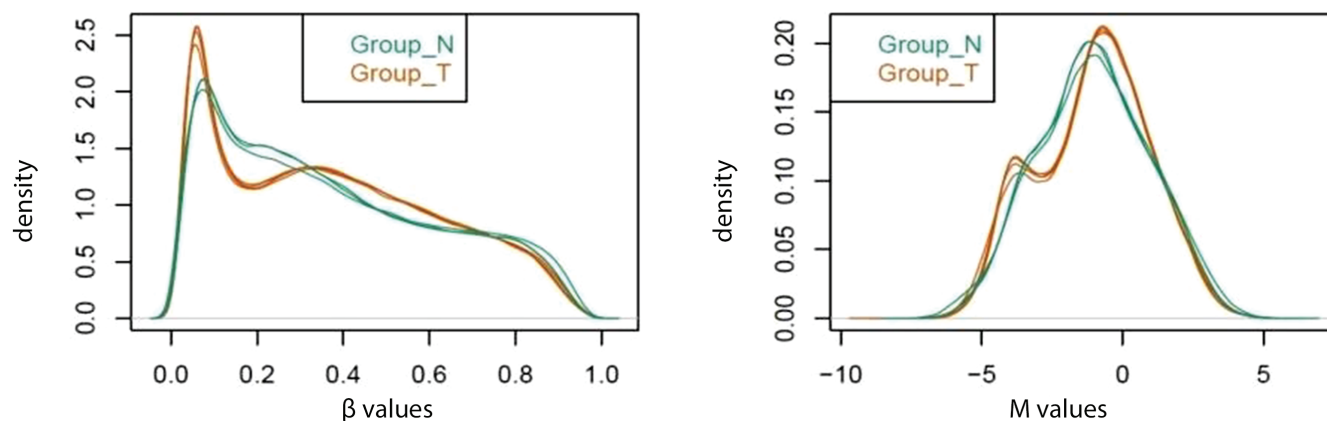
Fig. 1. Distribution of calculated β- and M-values for the oral squamous cell carcinoma (OSCC) tumor and normal groups

Table 2. Differentially methylated microRNAs found in oral squamous cell carcinoma (OSCC) tissues

Chr (strand)	Position	Name	Island name	UCSC ref gene	Gencode name	logFC	adj. p-value
Chr 20(−)	61809724	cg19267861	chr20:61806254-61810867	TSS200	miR124-3; CDH4	4.9	0.0225
Chr 20(−)	61809035	cg02065637	chr20:61806254-61810867	TSS1500	miR124-3; CDH4	3.9	0.0269
Chr 19(+)	46521569	cg08426951	chr19:46518283-46520080	Body; TSS1500	PPP5D15; miR769	3.2	0.0422
Chr 13(+)	88323607	cg26110710	chr13:88323569-88324640	TSS1500	SLITRK5; miR4500	3.9	0.0429
Chr 9(−)	97848222	cg00532885	chr9:97848140-97848525	TSS200; 3'UTR	miR24; C9orf3	3.7	0.0493

TSS – transcription start site; FC – fold change.

Table 3. Common methylated gene loci found in similar Gene Expression Omnibus (GEO) datasets

GSE data	Cases vs. controls	Method	Gene name	adj. p-value	log FC	RangeSTART	RangeEND
GSE 123781	15 vs. 18	Infinium Human Methylation 450K	cg19267861	7.78E-11	0.29	61809724	61809847
			cg26110710	8.13E-03	0.13	88323607	88323730
GSE 87053	11 vs. 10		cg19267861	8.61E-04	0.20	61809724	61809847
			cg02065637	2.37E-02	0.13	61809035	61809158

GSE – list of expression profiles conducted for the experiment (test, controls); FC – fold change.

Table 4. Calculation of CpG island prediction and sequence features for each microRNA

microRNA	Island number	Island size [bp]	Island start	Island end	GC (%)	Obs/Exp ratio
microRNA-124-3	island 1	1855	3	1857	50	0.6
	island 2	175	1862	2036	50	0.6
microRNA-24-1	island 1	186	813	998	50	0.7
	island 2	119	1105	1223	50	0.7
microRNA-4500	island 1	159	55	213	50	0.7
	island 2	146	357	502	50	0.7
	island 3	179	527	705	50	0.7

bp – base pairs; GC – guanine-cytosine; Obs/Exp – observed/expected CpG CG islands ratio.

GSE87053 contained the 4 loci of interest and were further selected for GEO2R analysis. We found that 3 out of the 4 gene loci were significantly hypermethylated, namely cg19267861 (the locus entailing hsa-miR-124-3), cg02065637 (the locus containing hsa-miR-124-3) and cg26110710 (the locus coding for SLITRK5 and hsa-miR-4500) (Table 3).

We used MethPrimer to design BSP PCR primers and predict the presence of CpG islands upstream of genes encoding the 4 microRNAs (Fig. 2, Table 4). The CpG island prediction identified the presence of CpG islands upstream of hsa-miR-124-3 (Fig. 2A) and hsa-miR-769 (Fig. 2B), but not for hsa-miR-4500 and hsa-miR-24-1.

Five sets of BSP primers with their sequences were retrieved for all 4 microRNA molecules, each of them consisting of 2 pairs of forward and reverse primers (Supplementary File 1).

Our PubMed search for microRNAs associated with OSCC led to a total of 189 microRNAs, of which 101 are downregulated, and 88 are upregulated in cancer tissues compared to normal tissues (Supplementary File 2,3). Of note, hsa-miR-24-1 was found to be upregulated,[23] while hsa-miR-769[24] and hsa-miR-124-3[25] were downregulated

in OSCC samples compared to controls. To date, no published data link hsa-miR-4500 to oral cancer.

Next, we used miRWalk v. 3.0 to predict the targets of the 4 microRNAs. By filtering out the genes with a binding probability below 0.99, we retrieved 4147 unique predicted targets for hsa-miR-24-1, 6084 predicted targets for hsa-miR-124-3, 743 targets for hsa-miR-4500, and 7256 targets for hsa-miR-769.

To understand the biological significance of these predicted targets in the specific context of oral cancer, we cross-referenced them with the differentially expressed genes in the GSE138206 OSCC dataset (after GEO2R analysis, adjusted p-value < 0.05). The GEO2R analysis of the GSE138206 dataset retrieved 2289 genes with dysregulated expression, of which 1490 were downregulated (FC < −0.538) and 799 were upregulated (FC > 1.0). Since hsa-miR-24-1 has a documented upregulated expression in OSCC,[23] we chose to compare its predicted target genes with the GSE138206 list of downregulated genes, and found 261 putative common targets. The hsa-miR-769[24] and hsa-miR-124-3[25] have both previously been reported to be downregulated in OSCC. Therefore, we compared their
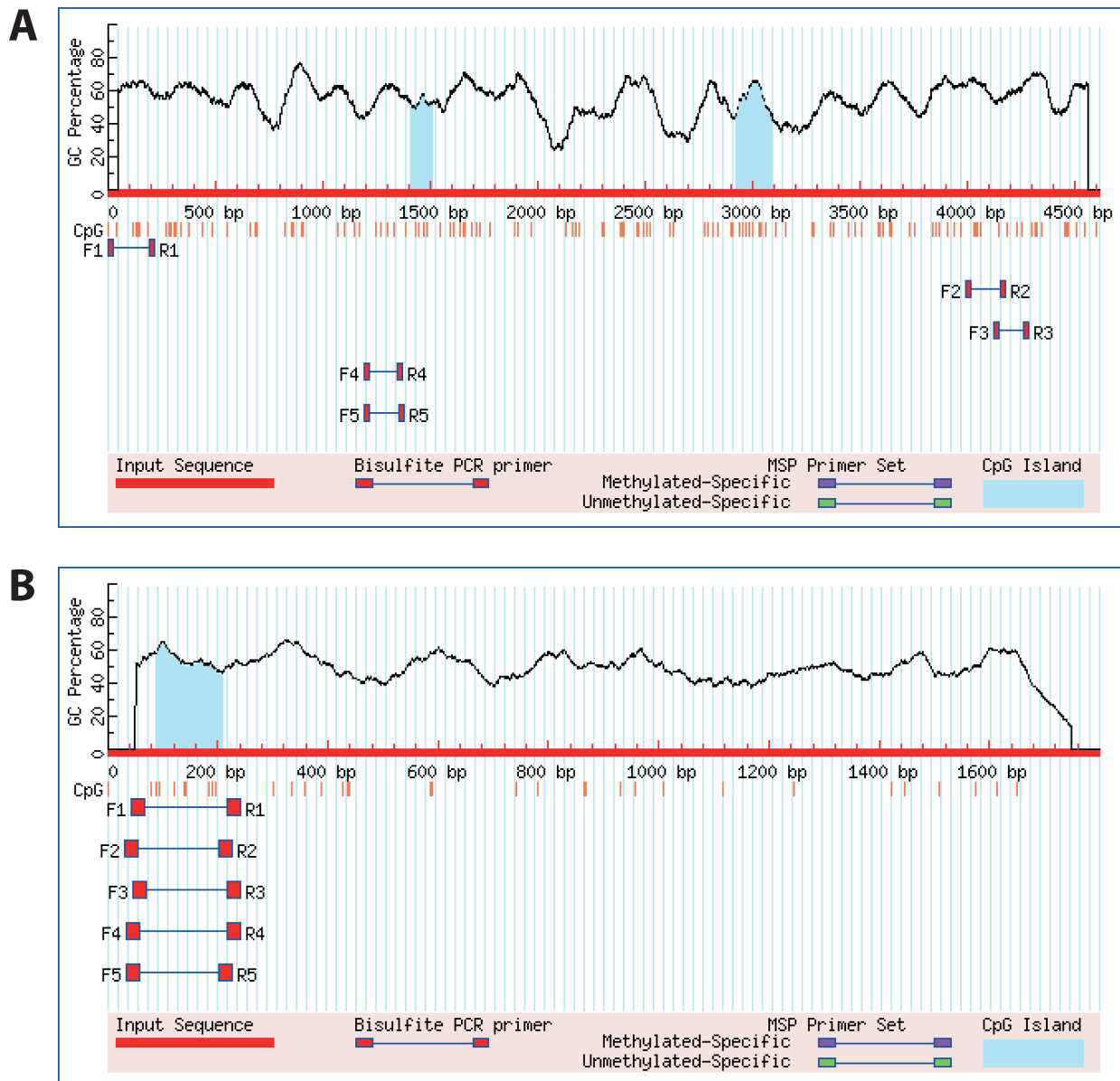
Fig. 2. Visualization of CpG islands predictions results. A. Primers and sequence features such as guanine-cytosine (GC) content percentage, CpG islands (highlighted in light blue) and CpG site for the 2-kb upstream genomic sequence of hsa-microRNA-124-3; B. Primers and sequence features for the 2-kb upstream genomic sequence of hsa-microRNA-769. CpG islands (highlighted in light blue)

predicted targets with the list of upregulated target genes from the GSE138206 dataset and found 274 putative common targets for hsa-miR-124-3 and 298 for hsa-miR-769. To date, there are no published data linking hsa-miR-4500 to OSCC; therefore, we compared its predicted targets with both the upregulated genes (and found 22 common genes) and downregulated genes (and found 51 common genes).

The STRING functional analysis of the hsa-miR-24-1 putative targets led to a protein–protein interaction (PPI) network characterized by 259 nodes, 68 edges and a PPI enrichment p-value of $3.75e^{-12}$, for which no significant signaling pathway could be found after KEGG functional enrichment analysis.

The STRING functional analysis of the hsa-miR-124-3 putative target genes led to a PPI network characterized by 266 nodes, 562 edges and a PPI enrichment p-value below $1.0e^{-16}$. The average local clustering coefficient of the network is 0.359 with an average node degree of 4.23. The cluster analysis using the Markov Cluster Algorithm (MCL) method (inflation parameter of 4) led to the identification of 3 clusters functionally enriched through KEGG pathway analysis (referred to as Cluster 1, 2 and 3) containing 23, 12 and 7 genes, respectively. (Fig. 3, Table 5). Cluster 1 (23 genes) is enriched with genes involved in viral infections, and the local clustering coefficient is high with a value of 0.84 and an average node degree of 10.8. Cluster 2 (local clustering coefficient = 0.769, average node degree = 7.83) includes 12 genes related to protein digestion and absorption, ECM-receptor interaction pathway and focal adhesion.

Cluster 3 contains 7 genes significantly associated with the p53 signaling pathway, with the local clustering coefficient of 0.867 and an average node degree of 2. The high values of the local clustering coefficients suggest that members within these clusters are involved in similar pathways and functions.

The STRING functional analysis of the hsa-miR-769 targets identified a PPI network characterized by 290 nodes, 581 edges, and a PPI enrichment p-value below $1.0e^{-16}$. The average local clustering coefficient of the network was 0.357 and the average node degree was 4.01. The MCL cluster analysis of the network also resulted in 3 clusters functionally enriched in KEGG pathways, containing 25, 13 and 8 genes, respectively (Fig. 4, Table 6). Cluster 1 contains 25 genes that were also enriched in viral infection pathways, with a local clustering coefficient of 0.809 and an average node degree of 10.6. Cluster 2 (local clustering coefficient = 0.79, average node degree = 7.54) includes 13 genes which are most significantly enriched in protein digestion and absorption, ECM receptor interaction and AGE-RAGE signaling pathways. Cluster 3 contains 8 genes significantly enriched in AGE-RAGE signaling pathway, ECM-receptor interaction and cancer-related pathways. The local clustering coefficient for Cluster 3 was 0.893, with an average node degree of 2.5.
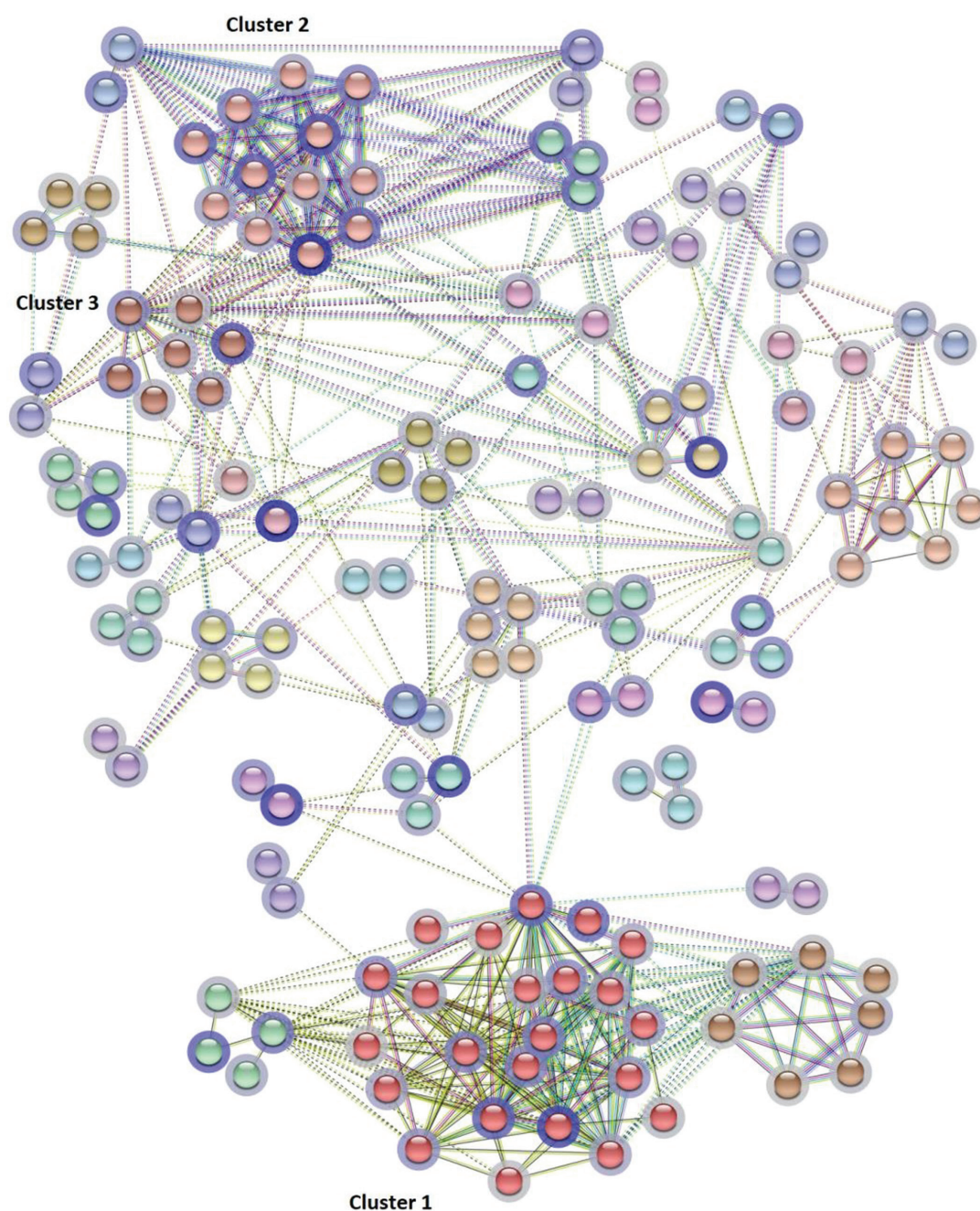
Fig. 3. Cluster analysis (STRING) of the hsa-miR-124-3 target genes in GSE138206 dataset network. The most relevant clusters are the (1) red (Cluster 1), (2) fire brick (Cluster 2) and (3) salmon (Cluster 3). The solid and dotted lines represent connection within the same and different cluster, respectively. Different colors indicate different types of interactions (cyan – databases, pink – experimental, blue – gene co-occurrence, khaki – text mining, black – co-expression, light blue – protein homology). The halo color intensities are based on the fold change values of the submitted genes

1238

E.G. Avram et al. Methylated microRNAs in OSCC

Table 5. Kyoto Encyclopedia of Genes and Genomes (KEGG) pathways potentially impacted by hsa-miR-124-3

Cluster	Term ID	Term description	Count in network	Strength	FDR
Cluster 1	hsa05160	hepatitis C	8 of 156	1.64	3.01E-09
	hsa05164	influenza A	8 of 165	1.62	3.01E-09
	hsa05162	measles	7 of 138	1.63	2.62E-08
	hsa05169	Epstein–Barr virus infection	7 of 193	1.49	1.87E-07
	hsa04621	NOD-like receptor signaling pathway	6 of 174	1.47	3.30E-06
	hsa05168	herpes simplex virus1 infection	7 of 479	1.09	5.39E-05
	hsa05165	human papillomavirus infection	4 of 325	1.02	0.0258
	hsa04217	necroptosis	3 of 149	1.23	0.0304
	hsa05161	hepatitis B	3 of 159	1.21	0.0325
	hsa04630	JAK-STAT signaling pathway	3 of 160	1.2	0.0325
Cluster 2	hsa04974	protein digestion and absorption	9 of 100	2.17	2.67E-16
	hsa04512	ECM-receptor interaction	3 of 88	1.74	0.0035
	hsa04510	focal adhesion	3 of 198	1.39	0.0245
Cluster 3	hsa04115	p53 signaling pathway	3 of 72	2.07	0.00063

FDR – false discovery rate.
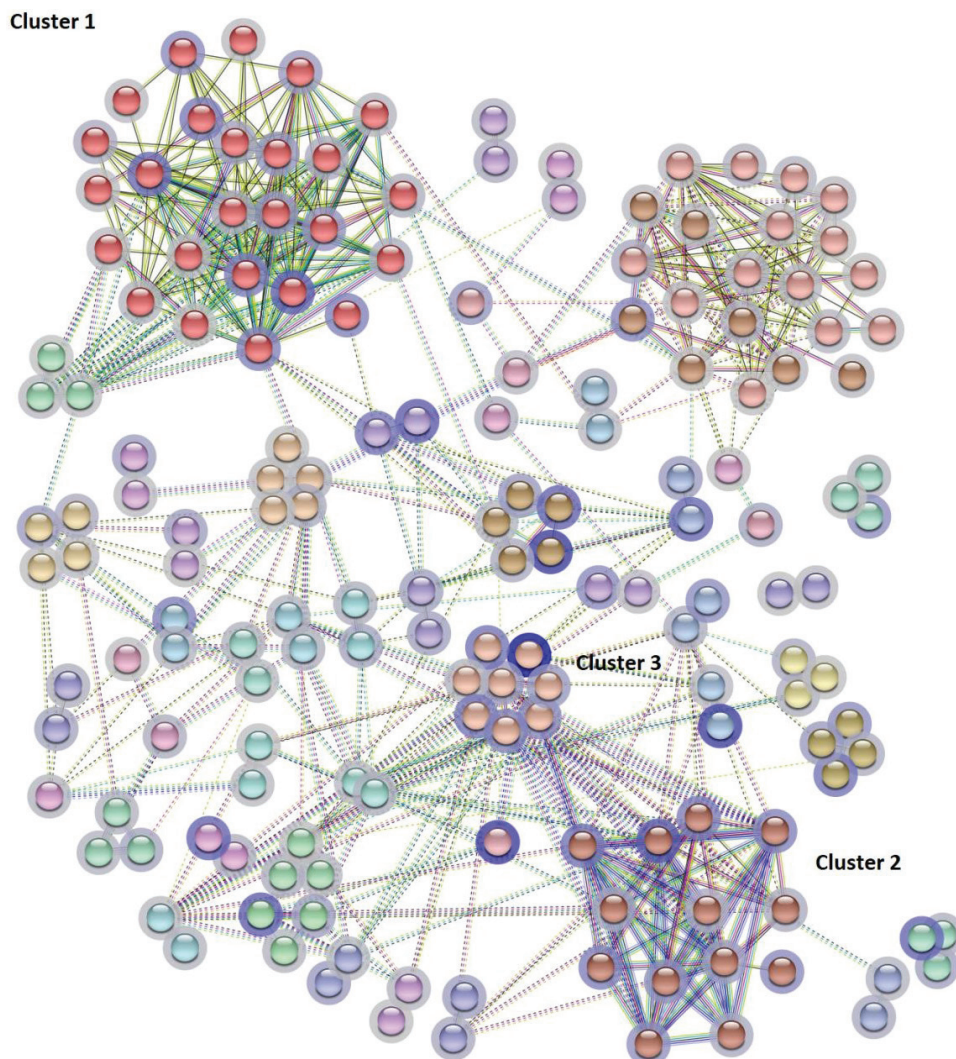
Fig. 4. Cluster analysis (STRING) of the hsa-miR-769 target genes in GSE138206 dataset network. The most relevant clusters are (1) red (Cluster 1), (2) fire brick (Cluster 2) and (3) salmon (Cluster 3). The solid and dotted lines represent connection within the same and different cluster, respectively. Different colors indicate different types of interactions (cyan – databases, pink – experimental, blue – gene co-occurrence, khaki – text mining, black – co-expression, light blue – protein homology)

Table 6. Kyoto Encyclopedia of Genes and Genomes (KEGG) pathways potentially impacted by hsa-microRNA-769

Cluster	Term ID	Term description	Count in network	Strength	FDR
Cluster 1	hsa05169	Epstein–Barr virus infection	8 of 193	1.51	3.34E-08
	hsa05160	hepatitis C	7 of 156	1.55	1.73E-07
	hsa05164	influenza A	7 of 165	1.52	1.73E-07
	hsa05162	Measles	6 of 138	1.53	1.88E-06
	hsa05168	herpes simplex virus 1 infection	8 of 479	1.12	5.40E-04
	hsa04621	NOD-like receptor signaling pathway	5 of 174	1.35	0.00015
	hsa05165	human papillomavirus infection	5 of 325	1.08	0.0025
	hsa05167	Kaposi sarcoma-associated herpes virus infection	4 of 187	1.22	0.0040
	hsa04625	C-type lectin receptor signaling pathway	3 of 102	1.36	0.0118
	hsa04217	necroptosis	3 of 149	1.2	0.0312
	hsa05161	hepatitis B	3 of 159	1.17	0.0341
Cluster 2	hsa04974	protein digestion and absorption	10 of 100	2.18	1.95E-18
	hsa04512	ECM-receptor interaction	3 of 88	1.71	0.0045
	hsa04933	AGE-RAGE signaling pathway in diabetic complications	3 of 98	1.66	0.0045
	hsa05146	amoebiasis	3 of 100	1.65	0.0045
	hsa04611	platelet activation	3 of 122	1.57	0.0047
	hsa04926	relaxin signaling pathway	3 of 128	1.55	0.0047
	hsa04510	focal adhesion	3 of 198	1.36	0.0136
	hsa05165	human papillomavirus infection	3 of 325	1.14	0.0494
Cluster 3	hsa04933	AGE-RAGE signaling pathway in diabetic complications	3 of 98	2.00	1.61E-05
	hsa04512	ECM-receptor interaction	3 of 88	1.92	0.00090
	hsa05222	small cell lung cancer	3 of 92	1.90	0.00090
	hsa05146	amebiasis	3 of 100	1.87	0.00090
	hsa04926	relaxin signaling pathway	3 of 128	1.76	0.0011
	hsa05200	pathways in cancer	4 of 517	1.28	0.0018
	hsa04510	focal adhesion	3 of 198	1.57	0.0028
	hsa05165	human papillomavirus infection	3 of 325	1.35	0.0103
	hsa04151	PI3K-Akt signaling pathway	3 of 350	1.32	0.0114

FDR – false discovery rate.

Due to the limited number of hsa-miR-4500 target genes found in the OSCC transcriptome, the resulting PPI network was very poor and lacked statistical significance. Therefore, this was not pursued further.

Discussion

Oral squamous cell carcinoma (OSCC) is one of the most common types of HNSCC. Therefore, it is critical to gain a better understanding of the epigenetic mechanisms that underlie OSCC initiation, development, evolution, and response to therapy.[26] In patients with OSCC, increased methylation status of microRNA loci has been observed compared to controls, suggesting that this parameter may serve as a predictor for malignant transformations.[27] In the present study, we used archived FFPE samples to explore the OSCC genome-wide methylation profile of microRNA loci.

Our analysis led to the identification of 4 microRNA loci significantly hypermethylated in OSCC tissue compared to normal adjacent tissue, namely hsa-miR-24, hsa-miR-769, hsa-miR-124, and hsa-miR-4500.

The hsa-miR-24 is one of the most heavily studied microRNAs in cancer, being associated with tumor initiation, progression, metastasis, and response to therapy in a wide array of malignant pathologies.[28] In our study, the hsa-miR-24 loci were significantly hypermethylated both at the 3'UTR site and 200 bp upstream of the transcription start site (TSS). There is evidence that if DNA methylation occurs within the 3'UTR region, it can both positively and negatively impact the transcription.[29] Therefore, the hypermethylation status of the hsa-miR-24-1 locus may still correlate with the reported upregulated expression of miR-24-1/-3. Of note, in OSCC, the mature miR-24-1/-3 is overexpressed not only in malignant tissues[23] (where it correlates with the staging of the disease) but also in the patients' saliva, serum and

1240

E.G. Avram et al. Methylated microRNAs in OSCC

plasma, qualifying it as a possible diagnostic and predictive biomarker.[30–32]

We also found that the hsa-miR-124-3 locus is methylated both distally (1500 bp upstream, TSS1500) and in close proximity (200 bp upstream, TSS200) to the TSS, which suggests gene silencing. This is also consistent with reports showing the downregulation of hsa-miR-124-3 in an OSCC cell line[25] and animal models of oral cancer.[33] The KEGG pathway enrichment analysis results for the hsa-miR-124-3 gene targets in OSCC were related to viral infections in the most populated gene cluster. Hepatitis C, Epstein–Barr virus, herpes simplex 1 and human papillomavirus are among the most significant viruses associated with this set of genes. The links between the etiologic causes of OSCC and viruses have long been investigated.[34–36] Hepatitis C virus was demonstrated to be involved in the development of oral lichen planus, a chronic inflammatory condition that increases the risk of OSCC.[37] Epstein–Barr virus,[38] herpes simplex virus 1[39] and human papillomavirus[40] have also been investigated in the promotion of the malignant transformation of cells in OSCC. In Cluster 2, pathways such as protein digestion and absorption, and ECM-receptor interaction pathway proved to be the most relevant ones. The presence of ECM-receptor interaction pathway associated with the Cluster 2 gene set confirms previous literature findings reporting the involvement of hsa-miR-124-3 in the ECM receptor interaction pathway through its direct repression of ITGB1 in OSCC cell lines.[25]

Regarding hsa-miR-769, we found the hypermethylation of both 1500 bp upstream of the TSS and within the miR-locus. Our data are consistent with the documented downregulation of hsa-miR-769 expression in OSCC tissues, since hypermethylation of its TSS may block the transcription.[24] The KEGG pathway enrichment analysis of Cluster 1 identified Epstein–Barr virus infection, hepatitis C and influenza A as the most significant pathways associated with hsa-miR-769 target genes that were differentially expressed in OSCC. In this case, the ECM-receptor interaction was also retrieved from among the significant pathways in Clusters 2 and 3. Interestingly, this pathway has previously been predicted to be associated with OSCC.[41] A new entry for this set of genes is the AGE-RAGE signaling pathway retrieved for Clusters 2 and 3. This pathway was initially reported to be responsible for the initiation of diabetic complications.[42] The receptor for advanced glycation end products (RAGE) molecule, a constituent of this pathway, has been reported to be a key factor that accelerates tumor progression and metastasis in various malignancies.[43–45] Regarding OSCC, there have been several investigations that aimed to evaluate the role and expression of RAGE receptor.[46–48] In a study that evaluated 74 OSCC samples, the RAGE receptor was reported to be a prognostic factor, and was significantly associated with the depth of invasion and local recurrence.[46] Moreover, a particular role of RAGE in OSCC pathogenesis was confirmed in an in vitro study,

where this receptor proved to be activated in a paracrine manner by the extracellular molecule high-mobility group box 1 (HMGB1) that was secreted by the OSCC cells. This activation promotes tumor progression and stimulates bone destruction.[47] Furthermore, RAGE proved to be significantly decreased by evodiamine, a novel anti-tumor drug, inhibiting proliferation, invasion and angiogenesis of OSCC both in vitro and in vivo.[48] Finally, the gene that encodes the RAGE receptor is predicted to be one of the hsa-miR-769-5p targets both in CDS and 5'UTR positions, according to the miRWalk v. 3.0 database.[19]

Finally, for hsa-miR-4500, there is no evidence so far concerning its expression in OSCC. When performing the KEGG pathway functional enrichment analysis for the commonly predicted target genes of this microRNA, there was no significant pathway associated with it due to a limited number of resulting genes.

Limitations

Due to financial limitations, we were not able to validate our methylation results in additional independent cohorts. Caution must be taken given the small sample size and the fact that the findings might not be entirely transferable to a larger population. Further investigations are needed to validate the correlation between the expression and methylation status of hsa-miR-24-1, hsa-miR-124-3 and hsa-miR-769 in OSCC samples through quantitative real-time (qRT)-PCR.

Conclusions

Returning to the study's central question, we suggest that, in stark contrast with the overall genome DNA hypomethylation, microRNA loci could show increased methylation status, which may translate into differential expression of their mature forms. Of note, one of the identified microRNAs has been proposed as an OSCC biomarker, given its presence in multiple biological fluids. Our bioinformatics analysis also suggests that methylation-dependent modulation of microRNA expression could significantly impact the response pathways to viral infections, the ECM-receptor interaction pathway and AGE-RAGE signaling pathway. These may be relevant for the development, progression and pathogenesis of OSCC.

Supplementary data

The supplementary Tables are available at https://doi.org/10.5281/zenodo.6759729.
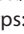
The package contains the following files:
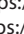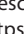
Supplementary File 1. Primer picking results for bisulfite sequencing PCR (BSP);

Supplementary File 2. Downregulated microRNAs curated from literature analysis;

Supplementary File 3. Upregulated microRNAs curated from literature analysis.

The references used for this supplementary data are listed at the end of the files.

ORCID iDs

Emilia Gabriela Avram https://orcid.org/0000-0002-2808-5566
Ioana Alexandra Moatar https://orcid.org/0000-0001-7756-8823
Viktorian Miok https://orcid.org/0000-0003-1018-2111
Flavia Baderca https://orcid.org/0000-0002-5755-179X
Corina Samoila https://orcid.org/0000-0003-2468-6564
Anda Alexa https://orcid.org/0000-0003-4364-0254
Ioana Nicoleta Andreescu https://orcid.org/0000-0002-2647-4234
Angela Podariu https://orcid.org/0000-0003-0505-0018
Catalin Marian https://orcid.org/0000-0002-7749-1384
Ioan Ovidiu Sirbu https://orcid.org/0000-0003-1618-9656

References

1. Pires FR, Ramos AB, de Oliveira JBC, Tavares AS, da Luz PSR, dos Santos TCRB. Oral squamous cell carcinoma: Clinicopathological features from 346 cases from a single Oral Pathology Service during an 8-year period. *J Appl Oral Sci*. 2013;21(5):460–467. doi:10.1590/1679-775720130317

2. Abdulla R, Adyanthaya S, Kini P, Mohanty V, D'Souza N, Subbannayya Y. Clinicopathological analysis of oral squamous cell carcinoma among the younger age group in coastal Karnataka, India: A retrospective study. *J Oral Maxillofac Pathol*. 2018;22(2):180–187. doi:10.4103/jomfp.JOMFP_16_18

3. Garcia-Martinez L, Zhang Y, Nakata Y, Chan HL, Morey L. Epigenetic mechanisms in breast cancer therapy and resistance. *Nat Commun*. 2021;12(1):1786. doi:10.1038/s41467-021-22024-3

4. Isik A, Isik N, Kurnaz E. Complete breast autoamputation: Clinical image. *Breast J*. 2020;26(11):2265–2266. doi:10.1111/tbj.14072

5. Herceg Z, Paliwal A. Epigenetic mechanisms in hepatocellular carcinoma: How environmental factors influence the epigenome. *Mutat Res*. 2011;727(3):55–61. doi:10.1016/j.mrrev.2011.04.001

6. Magic Z, Supic G, Brankovic-Magic M, Jovic N. DNA Methylation in the pathogenesis of head and neck cancer. In: Dricu A, ed. *Methylation: From DNA, RNA and Histones to Diseases and Treatment*. InTech; 2012: 185–216. doi:10.5772/51169

7. Lopez-Serra P, Esteller M. DNA methylation-associated silencing of tumor-suppressor microRNAs in cancer. *Oncogene*. 2012;31(13): 1609–1622. doi:10.1038/onc.2011.354

8. Moore LD, Le T, Fan G. DNA methylation and its basic function. *Neuropsychopharmacology*. 2013;38(1):23–38. doi:10.1038/npp.2012.112

9. Alam H, Kundu ST, Dalal SN, Vaidya MM. Loss of keratins 8 and 18 leads to alterations in α6β4-integrin-mediated signalling and decreased neoplastic progression in an oral-tumour-derived cell line. *J Cell Sci*. 2011;124(Pt 12):2096–2106. doi:10.1242/jcs.073585

10. Zargoun IM, Bingle L, Speight PM. DNA ploidy and cell cycle protein expression in oral squamous cell carcinomas with and without lymph node metastases. *J Oral Pathol Med*. 2017;46(9):738–743. doi:10.1111/jop.12554

11. Kulis M, Esteller M. DNA methylation and cancer. *Adv Genet*. 2010; 70:27–56. doi:10.1016/B978-0-12-380866-0.60002-2

12. Li X, Fan Q, Li J, Song J, Gu Y. miR-124 down-regulation is critical for cancer associated fibroblasts-enhanced tumor growth of oral carcinoma. *Exp Cell Res*. 2017;351(1):100–108. doi:10.1016/j.yexcr.2017.01.001

13. Qiu H, Huang Z, Huang Z, He Z, You S. miR-22 regulates cell invasion, migration and proliferation in vitro through inhibiting CD147 expression in tongue squamous cell carcinoma. *Arch Oral Biol*. 2016;66:92–97. doi:10.1016/j.archoralbio.2016.02.013

14. Hedbäck N, Jensen DH, Specht L, et al. miR-21 expression in the tumor stroma of oral squamous cell carcinoma: An independent biomarker of disease free survival. *PLoS One*. 2014;9(4):e95193. doi:10.1371/journal.pone.0095193

15. Sanchez R, Mackenzie SA. Integrative network analysis of differentially methylated and expressed genes for biomarker identification in leukemia. *Sci Rep*. 2020;10(1):2123. doi:10.1038/s41598-020-58123-2

16. Liu L, Wei J, Ruan J. Pathway enrichment analysis with networks. *Genes (Basel)*. 2017;8(10):246. doi:10.3390/genes8100246

17. Varghese RS, Barefoot ME, Jain S, et al. Integrative analysis of DNA methylation and microRNA expression reveals mechanisms of racial heterogeneity in hepatocellular carcinoma. *Front Genet*. 2021;12:708326. doi:10.3389/fgene.2021.708326

18. Ossom Williamson P, Minter CIJ. Exploring PubMed as a reliable resource for scholarly communications services. *J Med Libr Assoc*. 2019;107(1):16–29. doi:10.5195/jmla.2019.433

19. Sticht C, De La Torre C, Parveen A, Gretz N. miRWalk: An online resource for prediction of microRNA binding sites. *PLoS One*. 2018; 13(10):e0206239. doi:10.1371/journal.pone.0206239

20. Szklarczyk D, Franceschini A, Wyder S, et al. STRING v10: Protein–protein interaction networks, integrated over the tree of life. *Nucleic Acids Res*. 2015;43(Database issue):D447–D452. doi:10.1093/nar/gku1003

21. Li LC, Dahiya R. MethPrimer: Designing primers for methylation PCRs. *Bioinformatics*. 2002;18(11):1427–1431. doi:10.1093/bioinformatics/18.11.1427

22. Du P, Zhang X, Huang CC, et al. Comparison of beta-value and M-value methods for quantifying methylation levels by microarray analysis. *BMC Bioinformatics*. 2010;11:587. doi:10.1186/1471-2105-11-587

23. Lin SC, Liu CJ, Lin JA, Chiang WF, Hung PS, Chang KW. miR-24 up-regulation in oral carcinoma: Positive association from clinical and in vitro analysis. *Oral Oncol*. 2010;46(3):204–208. doi:10.1016/j.oraloncology.2009.12.005

24. Zhou Y, Xu XM, Feng Y. miR-769-5p inhibits cancer progression in oral squamous cell carcinoma by directly targeting JAK1/STAT3 pathway. *Neoplasma*. 2020;67(3):528–536. doi:10.4149/neo_2020_190703N582

25. Hunt S, Jones AV, Hinsley EE, Whawell SA, Lambert DW. MicroRNA-124 suppresses oral squamous cell carcinoma motility by targeting ITGB1. *FEBS Lett*. 2011;585(1):187–192. doi:10.1016/j.febslet.2010.11.038

26. Blatt S, Krüger M, Ziebart T, et al. Biomarkers in diagnosis and therapy of oral squamous cell carcinoma: A review of the literature. *J Craniomaxillofac Surg*. 2017;45(5):722–730. doi:10.1016/j.jcms.2017.01.033

27. Dang J, Bian YQ, Sun JY, et al. MicroRNA-137 promoter methylation in oral lichen planus and oral squamous cell carcinoma. *J Oral Pathol Med*. 2013;42(4):315–321. doi:10.1111/jop.12012

28. Wang H, Chen C, Ding K, Zhang W, Hou J. MiR-24-3p as a prognostic indicator for multiple cancers: From a meta-analysis view. *Biosci Rep*. 2020;40(12):BSR20202938. doi:10.1042/BSR20202938

29. Rauluseviciute I, Drabløs F, Rye MB. DNA hypermethylation associated with upregulated gene expression in prostate cancer demonstrates the diversity of epigenetic regulation. *BMC Med Genomics*. 2020;13(1):6. doi:10.1186/s12920-020-0657-6

30. Zhao J, Hu C, Chi J, et al. miR-24 promotes the proliferation, migration and invasion in human tongue squamous cell carcinoma by targeting FBXW7. *Oncol Rep*. 2016;36(2):1143–1149. doi:10.3892/or.2016.4891

31. He L, Ping F, Fan Z, et al. Salivary exosomal miR-24-3p serves as a potential detective biomarker for oral squamous cell carcinoma screening. *Biomed Pharmacother*. 2020;121:109553. doi:10.1016/j.biopha.2019.109553

32. Karimi A, Bahrami N, Sayedyahossein A, Derakhshan S. Evaluation of circulating serum 3 types of microRNA as biomarkers of oral squamous cell carcinoma: A pilot study. *J Oral Pathol Med*. 2020;49(1):43–48. doi:10.1111/jop.12959

33. Yu T, Wang XY, Gong RG, et al. The expression profile of microRNAs in a model of 7,12-dimethyl-benz[a]anthrance-induced oral carcinogenesis in Syrian hamster. *J Exp Clin Cancer Res*. 2009;28(1):64. doi:10.1186/1756-9966-28-64

34. Sugerman P, Shillitoe E. The high risk human papillomaviruses and oral cancer: Evidence for and against a causal relationship. *Oral Dis*. 2008;3(3):130–147. doi:10.1111/j.1601-0825.1997.tb00025.x

35. Steele C, Shillitoe EJ. Viruses and oral cancer. *Crit Rev Oral Biol Med*. 1991;2(2):153–175. doi:10.1177/10454411910020020201

36. Metgud R, Astekar M, Verma M, Sharma A. Role of viruses in oral squamous cell carcinoma. *Oncol Rev*. 2012;6(2):e21. doi:10.4081/oncol.2012.e21

37. Nagao Y, Sata M, Itoh K, Tanikawa K, Kameyama T. Quantitative analysis of HCV RNA and genotype in patients with chronic hepatitis C accompanied by oral lichen planus. *Eur J Clin Invest*. 1996;26(6):495–498. doi:10.1046/j.1365-2362.1996.167314.x

38. Yen CY, Lu MC, Tzeng CC, et al. Detection of EBV infection and gene expression in oral cancer from patients in Taiwan by microarray analysis. *J Biomed Biotechnol*. 2009;2009:904589. doi:10.1155/2009/904589

1242

E.G. Avram et al. Methylated microRNAs in OSCC

39. Niller HH, Wolf H, Minarovits J. Viral hit and run-oncogenesis: Genetic and epigenetic scenarios. *Cancer Lett*. 2011;305(2):200–217. doi:10.1016/j.canlet.2010.08.007

40. Kingsley K, Johnson D, O'Malley S. Transfection of oral squamous cell carcinoma with human papillomavirus-16 induces proliferative and morphological changes in vitro. *Cancer Cell Int*. 2006;6:14. doi:10.1186/1475-2867-6-14

41. Zhang G, Bi M, Li S, Wang Q, Teng D. Determination of core pathways for oral squamous cell carcinoma via the method of attract. *J Can Res Ther*. 2018;14(Supplement):S1029–S1034. doi:10.4103/0973-1482.206868

42. Kay AM, Simpson CL, Stewart JA. The role of AGE/RAGE signaling in diabetes-mediated vascular calcification. *J Diabetes Res*. 2016;2016: 6809703. doi:10.1155/2016/6809703

43. Wang D, Li T, Ye G, et al. Overexpression of the receptor for advanced glycation endproducts (RAGE) is associated with poor prognosis in gastric cancer. *PLoS One*. 2015;10(4):e0122697. doi:10.1371/journal.pone.0122697

44. Kuniyasu H, Chihara Y, Takahashi T. Co-expression of receptor for advanced glycation end products and the ligand amphoterin associates closely with metastasis of colorectal cancer. *Oncol Rep*. 2003; 10(2):445–448. doi:10.3892/or.10.2.445

45. Ishiguro H, Nakaigawa N, Miyoshi Y, Fujinami K, Kubota Y, Uemura H. Receptor for advanced glycation end products (RAGE) and its ligand, amphoterin are overexpressed and associated with prostate cancer development. *Prostate*. 2005;64(1):92–100. doi:10.1002/pros.20219

46. Sasahira T, Kirita T, Bhawal UK, et al. Receptor for advanced glycation end products (RAGE) is important in the prediction of recurrence in human oral squamous cell carcinoma. *Histopathology*. 2007; 51(2):166–172. doi:10.1111/j.1365-2559.2007.02739.x

47. Sakamoto Y, Okui T, Yoneda T, et al. High-mobility group box 1 induces bone destruction associated with advanced oral squamous cancer via RAGE and TLR4. *Biochem Biophys Res Commun*. 2020;531(3): 422–430. doi:10.1016/j.bbrc.2020.07.120

48. Ren L, Lou Y, Sun M. The anti-tumor effects of evodiamine on oral squamous cell carcinoma (OSCC) through regulating advanced glycation end products (AGE)/receptor for advanced glycation end products (RAGE) pathway. *Bioengineered*. 2021;12(1):5985–5995. doi:10.1080/21655979.2021.1972082

miRNA-323a-3p promoted intracranial, aneurysm-induced inflammation via AMPK/NF-κB signaling pathway by AdipoR1

Bing Sun[1,A–C], Zehao Liu[2,B,C], Zhengquan Yu[1,E,F]

[1] The First Affiliated Hospital of Soochow University, Suzhou, China

[2] Taizhou People's Hospital, China

A – research concept and design; B – collection and/or assembly of data; C – data analysis and interpretation;
D – writing the article; E – critical revision of the article; F – final approval of the article

Address for correspondence
Zhengquan Yu
E-mail: pii33924@163.com

Conflict of interest
None declared

Abstract

Background. An intracranial arterial wall which locally protrudes outward, typically in the capsule and fusiform, is called an intracranial aneurysm (IA). Among these aneurysms, 1–2% might spontaneously rupture before treatment. Anterior and posterior communicating aneurysms are more likely to rupture than other aneurysms, and an anterior communicating aneurysm is more likely to rupture than a posterior communicating aneurysm.

Objectives. To identify the effects of miRNA-323a-3p expression in intracranial aneurysms and its potential regulatory mechanism.

Materials and methods. Patients with IA and healthy volunteers were enrolled, and their serum samples were extracted for the detection of tumor necrosis factor alpha (TNF-α), interleukin 1β (IL-1β), IL-6, IL-18, and miRNA-323a-3p. Then, the regulatory effects of miRNA-323a-3p on the above inflammatory factors and AdipoR1/AMPK/NF-kb signaling were also detected in vitro.

Results. The downregulation of miRNA-323a-3p reduced the expression of inflammatory factors (TNF-α, IL-1β, IL-6, and IL-18) in an in vitro model in comparison with the control group. The overexpression of miRNA-323a-3p suppressed the protein expression of adiponectin receptor R1 (AdipoR1) and p-AMPK, and induced NF-κB-p65 protein expression in an in vitro model.

Conclusions. We showed that AdipoR1 plasmid, AMPK activator 1 or si-NF-κB reduced the pro-inflammatory effects of miRNA-323a-3p in an in vitro model. The miRNA-323a-3p exacerbated the inflammatory reaction in IA through AMPK/NF-κB signaling by AdipoR1. Our findings suggest that miRNA-323a-3p targeting AdipoR1 is promising in further anti-inflammatory treatment of IAs.

Key words: intracranial aneurysm, NF-κB, ADIPOR1, AMPK, miRNA-323a-3p

Background

An intracranial arterial wall which locally protrudes outward is called an intracranial aneurysm (IA).[1] The incidence rate of IAs in the general population is approx. 5%.[2] Aneurysms can occur in intracranial blood vessels, with up to 90% of aneurysms occurring near the circle of Willis.[2] The most lethal complication is rupture, subsequently leading to subarachnoid hemorrhage (SAH)[2]; aneurysm rupture is also the most common cause of SAH.[3] Approximately, 1–2% of aneurysms might spontaneously rupture before treatment. The anterior and posterior communicating aneurysms are more likely to rupture than other aneurysms, and the anterior communicating aneurysm is more likely to rupture than the posterior communicating aneurysm.[3]

In the last decade, the development of genetics and molecular biology has promoted the development of aneurysm-related research.[4] In this paper, we summarize the molecular biological mechanisms of IA rupture and its association with inflammation.[4] Inflammation is closely correlated with aneurysm formation. The pathogenesis may be a damage in the vascular endothelium of intracranial arteries, leading to an inflammatory response, which ultimately endangers the integrity of the vessel wall.[5] During this process, the key characteristics include the loss of the internal elastic layer, endomysial hyperplasia and ectopic distribution of the vascular smooth muscle.[6]

Adiponectin is a cytokine secreted by mature adipocytes and its biological function is facilitated by its receptors, adiponectin receptor R1 (AdipoR1) and AdipoR2.[7] The adiponectin receptors are mainly expressed in insulin target tissues, including liver, skeletal muscle and pancreatic islet.[8] Studies have found the expression of both AdipoR1 and AdipoR2 in islet cells, with AdipoR1 being dominant.[8] The AdipoR1 acts by activating the AMPK pathway.[7] The NF-κB has been revealed to regulate the expression of various genes during the initiation and progression of AMPK. For example, lipids in food – especially free fatty acids – can activate the transcription factor NF-κB and increase the expression of inflammatory cytokines (including tumor necrosis factor alpha (TNF-α), interleukin 6 (IL-6), C-reactive protein (CRP), and others), thereby causing inflammatory damage to liver tissue.[9]

To simplify, the activation of NF-κB is a hallmark of inflammation in IA, which can be detected in the infiltrating macrophages and endothelial cells of IA lesions in mouse models in the early stages, subsequently spreading throughout the arterial wall.[10] A specific inhibition of the activation of NF-κB in macrophages can suppress aneurysm formation, macrophage infiltration and expression of pro-inflammatory factors.[10] Upregulated genes in the intima and media of the aneurysm involve proteases, reactive oxygen species (ROS), growth factors, cytokines, complements, adhesion molecules, and pro-apoptotic proteins.[11]

Downregulated genes play different roles in the vascular smooth muscle cells and endothelial cells.[12] Thus, the occurrence and development of aneurysms is associated with inflammatory responses, changes in extracellular matrices and apoptosis.[12]

Objectives

The purpose of this work is to identify the effects of miRNA-323a-3p in intracranial aneurysms and their potential regulatory mechanism.

Materials and methods

Patients with intracranial aneurysm

The study was approved by the ethics committee of the First Affiliated Hospital of Soochow University, Suzhou, China. Patients with IA and healthy volunteers were enrolled from November to December 2016. The basic information about the patients with IA is presented in Table 1. The following conditions were reasons for exclusion: severe hepatic and renal dysfunction, heart disease, diabetes, known thyrotoxicosis, and a history of hypersensitivity to iodinated contrast agents. Other exclusion criteria included multiple endovascular atheromatous plaques, obviously tortuous neck vessels, and vascular system hypertension (systolic blood pressure (SBP) ≥180 mm Hg or diastolic blood pressure (DBP) ≥110 mm Hg). Detailed inclusion and exclusion criteria are listed in the study protocol.

We chose to restrict the aneurysm size because the largest 2nd-generation hydrogel coil available when the trial started measured 12 mm.

Table 1. Basic information about patients with intracranial aneurysm

Variable	Healthy volunteers	Patients
Number of subjects	12	12
Sex	M: 6/W: 6	M: 6/W: 6
Age [years]	61–69	62–73
WFNS grading		
I	0	1
II–III	0	5
IV–V	0	6

WFNS – World Federation of Neurosurgical Societies.

ELISA experiment

The serum samples were collected and measured using an enzyme-linked immunosorbent assay (ELISA) kit for TNF-α, IL-1β, IL-6, and IL-18 (Thermo Fisher Scientific, Waltham, USA). Cells were also collected at 1000 g and

4°C for 10 min and used to measure TNF-α (H052), IL-1β (H002), IL-6 (H007), and IL-18 (H015) with an ELISA kit. The absorbance was measured at 450 nm using a Multi-skan™ GO spectrophotometer (Thermo Fisher Scientific, Waltham, USA).

qRT-PCR assay

Total RNA was extracted with TRIzol (Sigma-Aldrich, St. Louis, USA), according to the manufacturer's protocol. Then, 1 μg of RNA was reverse-transcribed into cDNA using a reverse reaction kit (Promega, Madison, USA). Quantitative reverse-transcription polymerase chain reaction (qRT-PCR) was performed using SYBR Green (Roche Diagnostics, Basel, Switzerland) and a 7500 real-time PCR system (Applied Biosystems, Mannheim, Germany). The levels of relative expression were calculated and quantified with the $2^{-\Delta\Delta Ct}$ method.

Gene chip profiling

The total RNA was labeled using a miRCURY™ Hy3™/Hy5™ Power labeling kit and hybridized on a miRCURY™ LNA Array (v. 16.0; Exiqon, Vedbæk, Denmark). Scanned images were imported into GenePix Pro v. 6.0 software (Axon Instruments, Foster City, USA) and MEV v. 4.6 software (The Institute for Genomic Research (TIGR), Rockville, USA).

Cell culture and transfection of miR-323a-3p mimics

Human endothelial cells – EA.hy926 (ATCC® CRL-2922™; Fuxiang Biotechnology, Shanghai, China) – were cultured in Dulbecco's modified Eagle's medium (DMEM; Thermo Fisher Scientific) with 10% fetal bovine serum (FBS; Thermo Fisher Scientific), and penicillin (100 U/mL), streptomycin (100 μg/mL) and a 2-mM glutamine mixture at 37°C in a humid, 5% CO_2 atmosphere. The EA.hy926 cells were transfected with miR-323a-3p, anti-miR-323a-3p or negative mimics using Lipofectamine 2000 (Invitrogen, Carlsbad, USA). The EA.hy926 cells were induced with 200 ng of LPS13 into the IA model 48 h after transfection.

Luciferase assay

The 3′UTR of AdipoR1 was cloned into a luciferase reporter vector, pmirGLO (Dual-Luciferase® Reporter Assay System; Promega). The 3′UTR of AdipoR1 and anti-miR-323a-3p mimics were transfected into the cells using Lipofectamine 2000 (Invitrogen). Forty-eight hours after transfection, the luciferase activity in human umbilical vein endothelial cells (HUVECs) was studied with a VIC-TOR analyzer using a Dual-Glo® Luciferase Assay System (Promega).

Western blotting

The cells were collected and the total proteins were extracted using an radioimmunoprecipitation assay (RIPA). Protein concentration was determined using a bicinchoninic acid protein assay. Equal amounts of protein (50 μg) were resolved on 10% sodium dodecyl sulfate-polyacrylamide gel electrophoresis (SDS-PAGE) gels, and then transferred to a polyvinylidene difluoride (PVDF) membrane (Merck Millipore, Bedford, USA). The membrane was blocked with 5% skim milk in Tris-buffered saline with Tween (TBST) and probed with antibodies against AdipoR1, p-AMPK, NF-κB-p65, and GAPDH (Cell Signaling Technology, Danvers, USA) at 4°C overnight. After 3 washes with TBST, the membranes were incubated with horseradish peroxidase (HRP)-conjugated secondary antibodies (Cell Signaling Technology) for 1 h at 37°C. Immunoreactive bands were visualized using an enhanced chemiluminescence (ECL) detection system (Promega) and analyzed using Image-Pro Plus v. 6.0 software (Media Cybernetics, Inc., Rockville, USA).

Immunohistochemistry

The cells were washed with phosphate-buffered saline (PBS) and fixed with 4% paraformaldehyde for 15 min. The cells were blocked with 5% bovine serum albumin (BSA) and 0.25% Triton-x100 in PBS for 1 h. Then, they were incubated with AdipoR1 overnight at 4°C, followed by incubation with fluorescence-labeled secondary antibodies (Alexa Fluor 594; Cell Signaling Technology) for 2 h. The cells were incubated with 4′,6-diamidino-2-phenylindole (DAPI; Cell Signaling Technology) for 15 min and viewed under a confocal fluorescence microscope (model FV1000; Olympus Corp., Tokyo, Japan).

Statistical analyses

The data are presented as median with the range (when n = 3) or the interquartile range (IQR) (when n = 12). The data were analyzed using Kruskal–Wallis test. A value of p < 0.05 was considered statistically significant.

Results

miRNA-323a-3p expression in patients with intracranial aneurysm

To investigate the mechanism of IA, the miRNA expression of patients with IA was measured. There were higher levels of TNF-α (median: 13.08 (IQR: 11.55–14.38) pg/mg of protein compared to median: 113.23 (IQR: 103.7–120.53) pg/mg of protein), IL-1β (median: 8.07 (IQR: 6.33–9.25) pg/mg of protein compared to median: 43.67 (IQR: 42.2–47.45) pg/mg of protein), IL-6 (median:
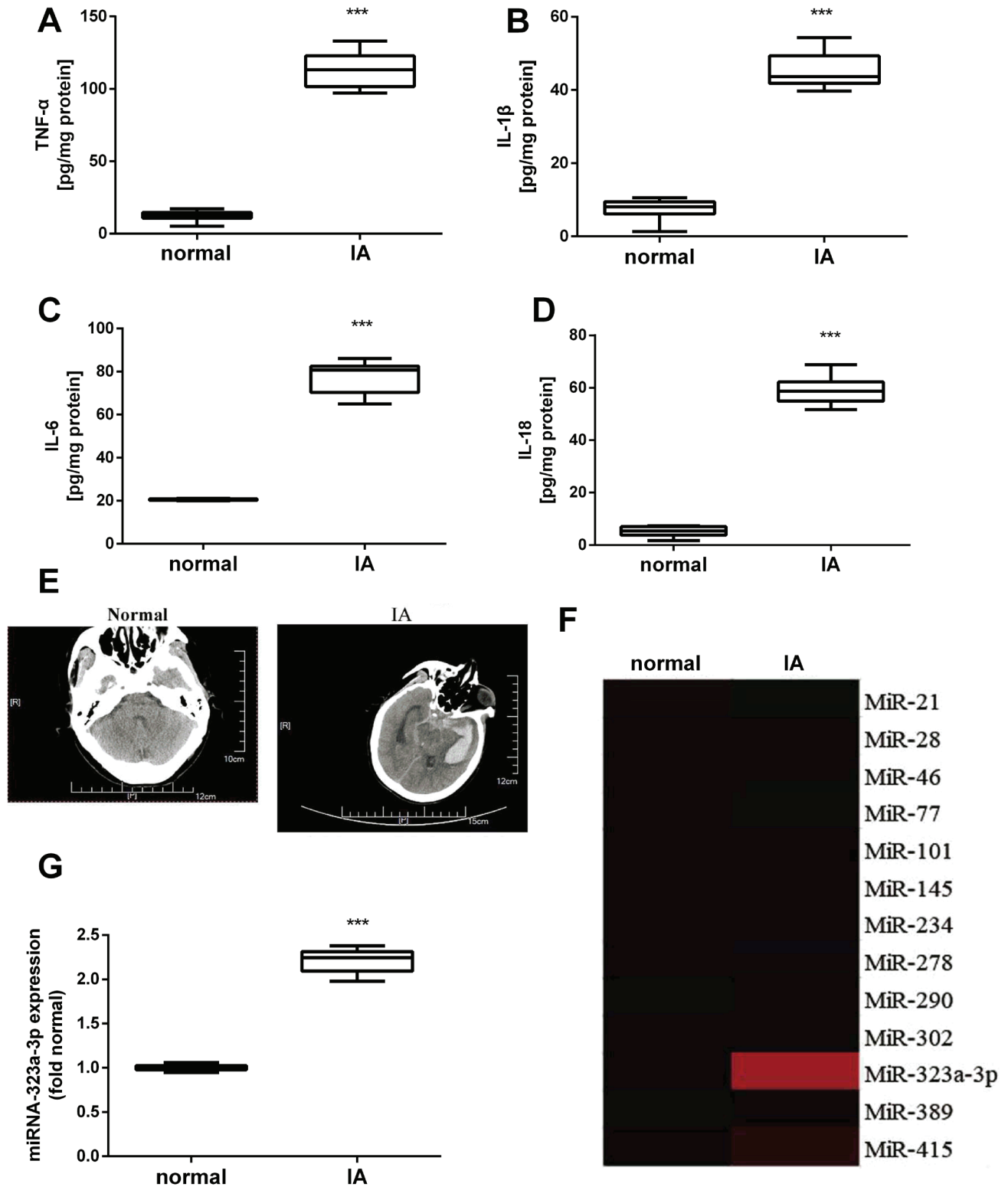
Fig. 1. The miRNA-323a-3p expression in patients with intracranial aneurysm (IA) tumor necrosis factor alpha (TNF-α) (A), interleukin (IL)-1β (B), IL-6 (C), and IL-18 (D) levels; computed tomography (CT) scan of an IA (E); the gene chip (F) and quantitative reverse-transcription polymerase chain reaction (qRT-PCR) (G) for the expression of miRNA-323a-3p in a patient with IA

normal – healthy volunteers; IA – IA patients; ***p < 0.001 compared to the sham control group. The Mann–Whitney tests were used for analysis. A–D,G: U = 0; p < 0.001. Data are presented as median and interquartile range (IQR) (n = 12).

20.6 (IQR: 20.16–20.83) pg/mg of protein compared to median: 80.75 (IQR: 72.75–82.3) pg/mg of protein), and IL-18 (median: 5.41 (IQR: 3.88–6.67) pg/mg of protein compared to median: 58.7 (IQR: 55.64–61.57) pg/mg of protein) in the patients with IA than in the control group (Fig. 1A–D). The results of computed tomography

(CT) showed that IA has appeared in patient with IA, but has not appeared in normal group (Fig. 1E). As shown in Fig. 1F,G, the expression of miRNA-323a-3p (median: 1 (IQR: 0.98–1.02) compared to median: 2.25 (IQR: 2.12–2.30)) was higher in the patients with IA than in the control group.

miRNA-323a-3p regulates inflammation in an in vitro model

The study evaluated the effects of miRNA-323a-3p in an in vitro model of IA. We used miRNA-323a-3p mimics to increase the expression of miRNA-323a-3p (median: 1.00 (range: 0.97–1.03) compared to median: 3.33 (range: 3.07–3.53)) in an in vitro model of IA in comparison with the control group (Fig. 2A). The overexpression of miRNA-323a-3p promoted inflammation factors such as TNF-α (median: 76.07 (range: 74.82–84.40) pg/mg of protein compared to median: 279.29 (range: 270.93–330.06) pg/mg of protein), IL-1β (median: 49.89 (range: 47.88–53.43) pg/mg of protein compared to median: 124.32 (range: 117.77–130.61) pg/mg of protein), IL-6 (median 59.75 (range: 59.04–59.78) pg/mg of protein compared to median 102.47 (range: 98.2–104.48) pg/mg of protein), and IL-18 (median: 20.87 (range: 15.66–29.57) pg/mg of protein compared to median: 117.50 (range: 109.98–129.71) pg/mg of protein) in an in vitro model of IA, in comparison with the control group (Fig. 2B–E). However, anti-miRNA-323a-3p mimics showed reduced miRNA-323a-3p expression (median: 1.00 (range: 0.97–1.03) compared to median: 0.41 (range: 0.38–0.44)) in an in vitro model of IA, in comparison with the control group (Fig. 2F). The downregulation of miRNA-323a-3p reduced the levels of TNF-α (median: 78.10 (range: 74.97–79.22) pg/mg of protein compared to median: 21.03 (range: 19.66–23.59) pg/mg of protein), IL-1β (median: 34.22 (range: 31.69–37.29) pg/mg of protein compared to median: 16.62 (range: 14.66–17.42) pg/mg of protein), IL-6 (median: 41.57 (range: 41.10–41.90) pg/mg of protein compared to median: 12.04 (range: 9.69–13.43) pg/mg of protein), and IL-18 (median: 64.91 (range: 64.56–71.74) pg/mg of protein compared to median: 13.03 (range: 8.78–14.37) pg/mg of protein) in an in vitro model of IA, in comparison with the control group (Fig. 2G–J).

miRNA-323a-3p regulates AdipoR1/AMPK/NF-κB-p65 signaling in an in vitro model

To explore the mechanism of miRNA-323a-3p on signaling in IA, a gene chip was used in an in vitro model of IA. As shown in Fig. 3A, the downregulation of miRNA-323a-3p induced AdipoR1 and NF-κB-p65 protein expression in an in vitro model of IA, in comparison with the control group. The 3'UTR of AdipoR1 was targeted by miRNA-323a-3p, and luciferase activity levels (median: 0.99 (range: 0.97–1.04) compared to median: 1.89

(range: 1.86–2.01)) were increased in the downregulation of the miRNA-323a-3p group (Fig. 3B,C). The downregulation of miRNA-323a-3p induced AdipoR1 protein expression in an in vitro model of IA, in comparison with the control group (Fig. 3D). The overexpression of miRNA-323a-3p suppressed AdipoR1 expression (median: 0.97 (range: 0.94–1.09) compared to median: 0.31 (range: 0.23–0.39)) and p-AMPK (median: 1.00 (range: 0.96–1.04) compared to median: 0.36 (range: 0.33–0.39)) protein expression and induced NF-κB-p65 (median: 1.00 (range: 0.98–1.02) compared to median: 2.41 (range: 2.39–2.52)) protein expression in an in vitro model of IA, in comparison with the control group (Fig. 3E–H). The downregulation of miRNA-323a-3p induced AdipoR1 (median: 1.02 (range: 0.78–1.20) compared to median: 2.95 (range: 2.68–3.07)) and p-AMPK (median: 1.05 (range: 0.81–1.14) compared to median: 2.43 (range: 2.34–2.52)) protein expression and suppressed NF-κB-p65 (median: 0.97 (range: 0.88–1.15) compared to median: 0.31 (range: 0.27–0.44)) protein expression in an in vitro model of IA, in comparison with the control group (Fig. 3I–L).

AdipoR1 reduced the pro-inflammation effects of miRNA-323a-3p in an in vitro model

The role of AdipoR1 in the pro-inflammatory function of miRNA-323a-3p was studied in an in vitro model of IA. The AdipoR1 plasmid induced the expression of AdipoR1 (median: 1.04 (range: 0.92–1.04) compared to median: 0.47 (range: 0.46–0.52) compared to median: 0.73 (range: 0.61–0.78)) and p-AMPK (median: 0.99 (range: 0.94–1.08) compared to median: 0.39 (range: 0.36–0.42) compared to median: 0.83 (range: 0.82–0.84)) and suppressed NF-κB-p65 protein expression (median: 1.02 (range: 0.89–1.08) compared to median: 2.47 (range: 2.46–2.62) compared to median: 1.47 (range: 1.32–1.49)) in an in vitro model of IA following overexpression of miRNA-323a-3p, when compared with the overexpression in the miRNA-323a-3p group (Fig. 4A–D). Compared with the overexpression in the miRNA-323a-3p group, the activation of AdipoR1 reduced the pro-inflammatory function of miRNA-323a-3p on the levels of TNF-α (median: 74.88 (range: 71.03–79.08) pg/mg of protein compared to median: 191.81 (range: 187.82–205.36) pg/mg of protein compared to median: 97.33 (range: 91.38–105.70) pg/mg of protein), IL-1β (median: 42.31 (range: 36.85–45.10) pg/mg of protein compared to median: 161.72 (range: 159.50–169.05) pg/mg of protein compared to median: 74.57 (range: 72.72–84.11) pg/mg of protein), IL-6 (median: 53.50 (range: 53.30–55.20) pg/mg of protein compared to median: 187.84 (range: 184.51–188.66) pg/mg of protein compared to median: 65.43 (range: 63.74–65.84) pg/mg of protein), and IL-18 (median: 31.80 (range: 23.02–36.39) pg/mg of protein compared to median: 125.03 (range: 120.93–129.76) pg/mg of protein compared to median: 52.42 (range: 47.13–60.08) pg/mg of protein)
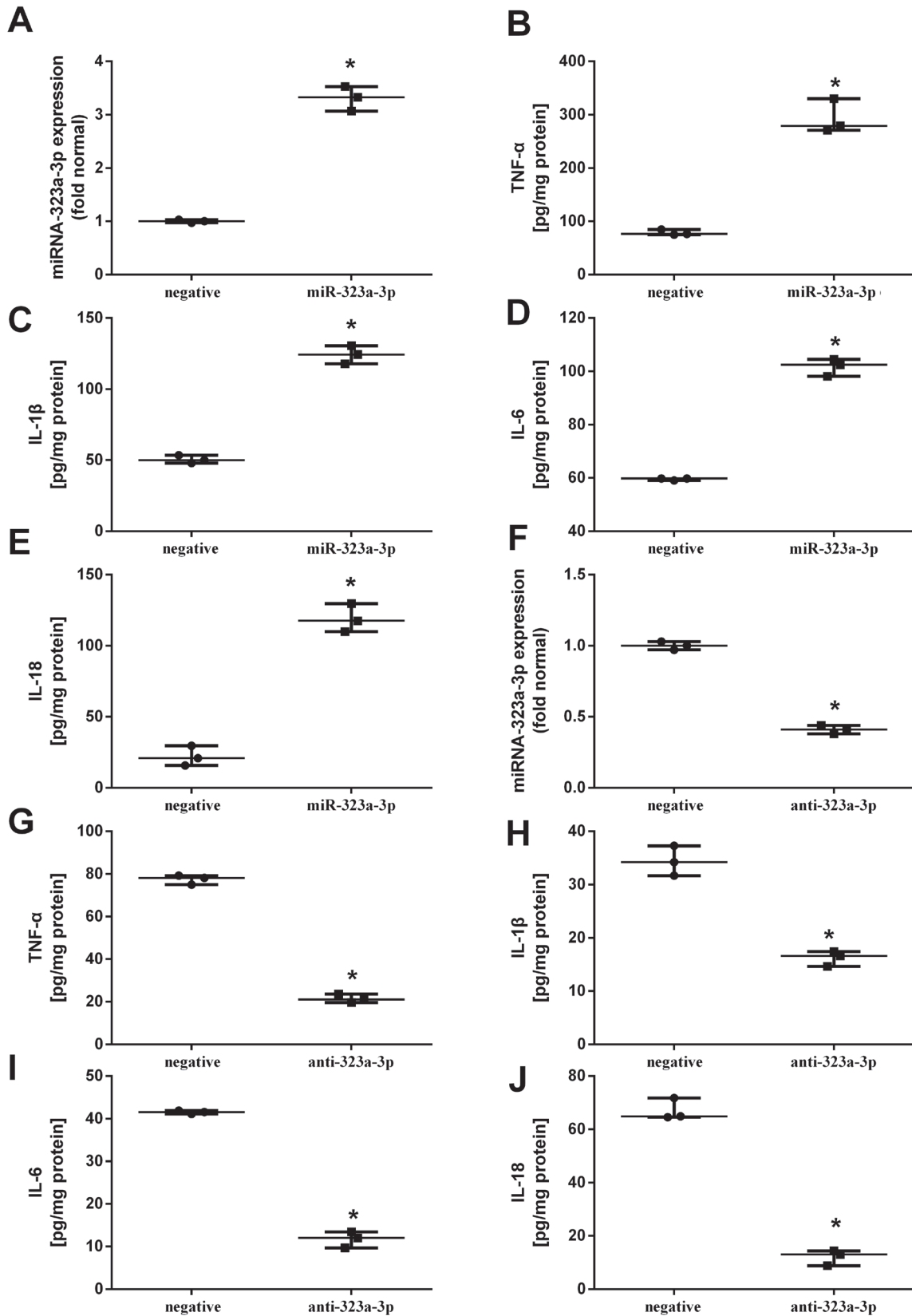
Fig. 2. The miRNA-323a-3p regulates inflammation in an in vitro model. Quantitative reverse-transcription polymerase chain reaction (qRT-PCR) for the expression levels of miRNA-323a-3p (A), tumor necrosis factor alpha (TNF-α) (B), interleukin (IL)-1β (C), IL-6 (D), and IL-18 (E) following the overexpression of miRNA-323a-3p; qRT-PCR for the expression levels of miRNA-323a-3p (F), TNF-α (G), IL-1β (H), IL-6 (I), and IL-18 (J) following the downregulation of miRNA-323a-3p

negative – cells transfected with negative mimics; miR-323a-3p – cells transfected with miR-323a-3p mimics; anti-323a-3p – cells transfected with miR-323a-3p inhibitor; *p < 0.05. The Kruskal–Wallis tests were used for analysis. A–J: χ^2 = 3.86; p = 0.049. Data are presented as median with range (n = 3).
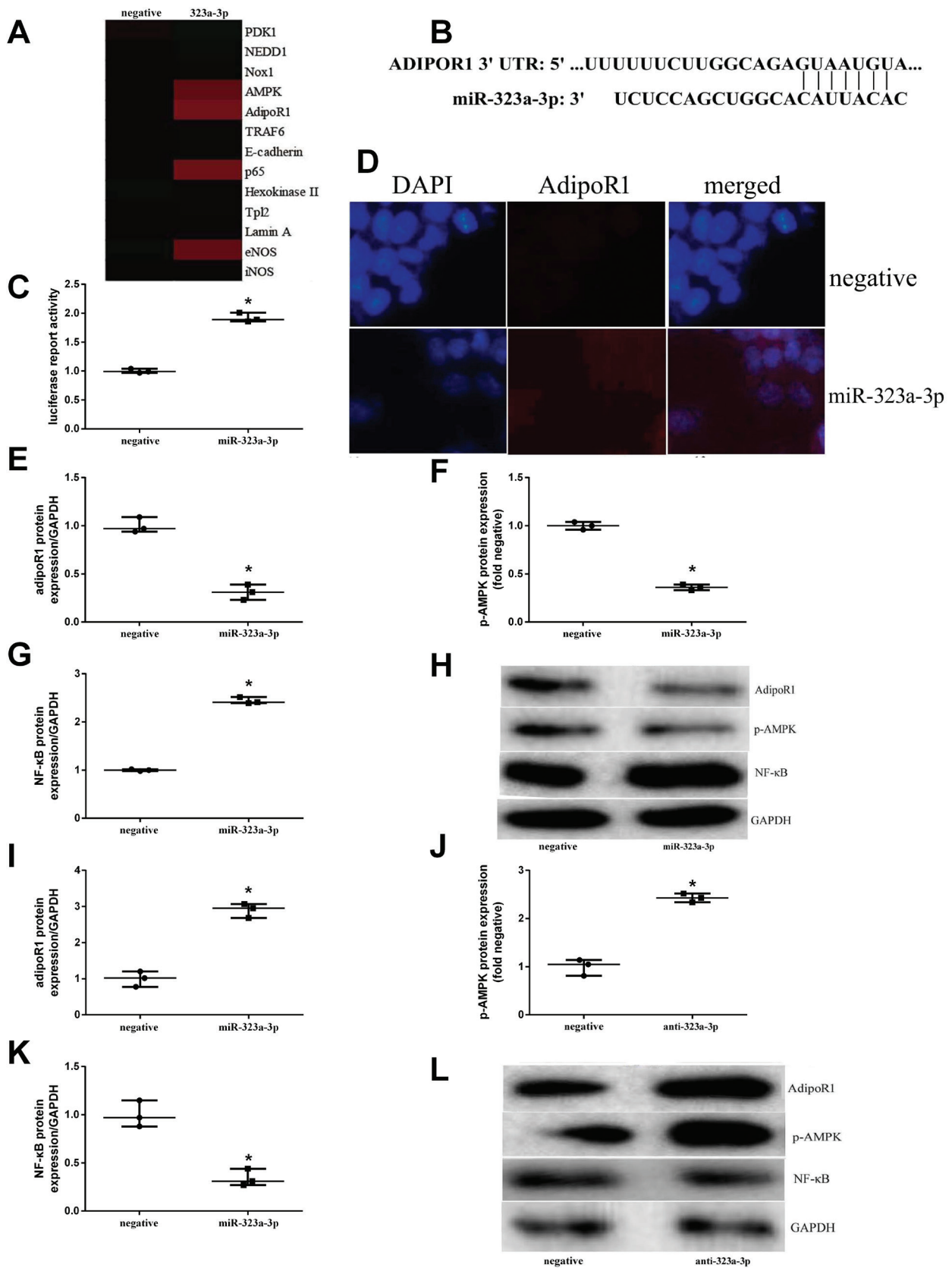
Fig. 3. The miRNA-323a-3p regulates AdipoR1/AMPK/NF-κB-p65 signaling in an in vitro model. A. The gene chip for signaling; B. The 3'UTRs of AdipoR1 was targeted by miRNA-323a-3p; C. Luciferase activity levels; D. Immunohistochemistry for AdipoR1; E–G. AdipoR1, p-AMPK and NF-κB-p65 protein expression using western blot analysis; H. Statistical analysis following the overexpression of miRNA-323a-3p; I–K. AdipoR1, p-AMPK and NF-κB-p65 protein expression using western blot analysis; L. Statistical analysis following the downregulation of miRNA-323a-3p

negative – cells transfected with negative mimics; miR-323a-3p – cells transfected with miR-323a-3p mimics; anti-323a-3p – cells transfected with miR-323a-3p inhibitor. *$p < 0.05$. The Mann–Whitney tests were used for analysis. C, E–G, I–K: U = 0; p = 0.049. Data are presented as median with range (n = 3).
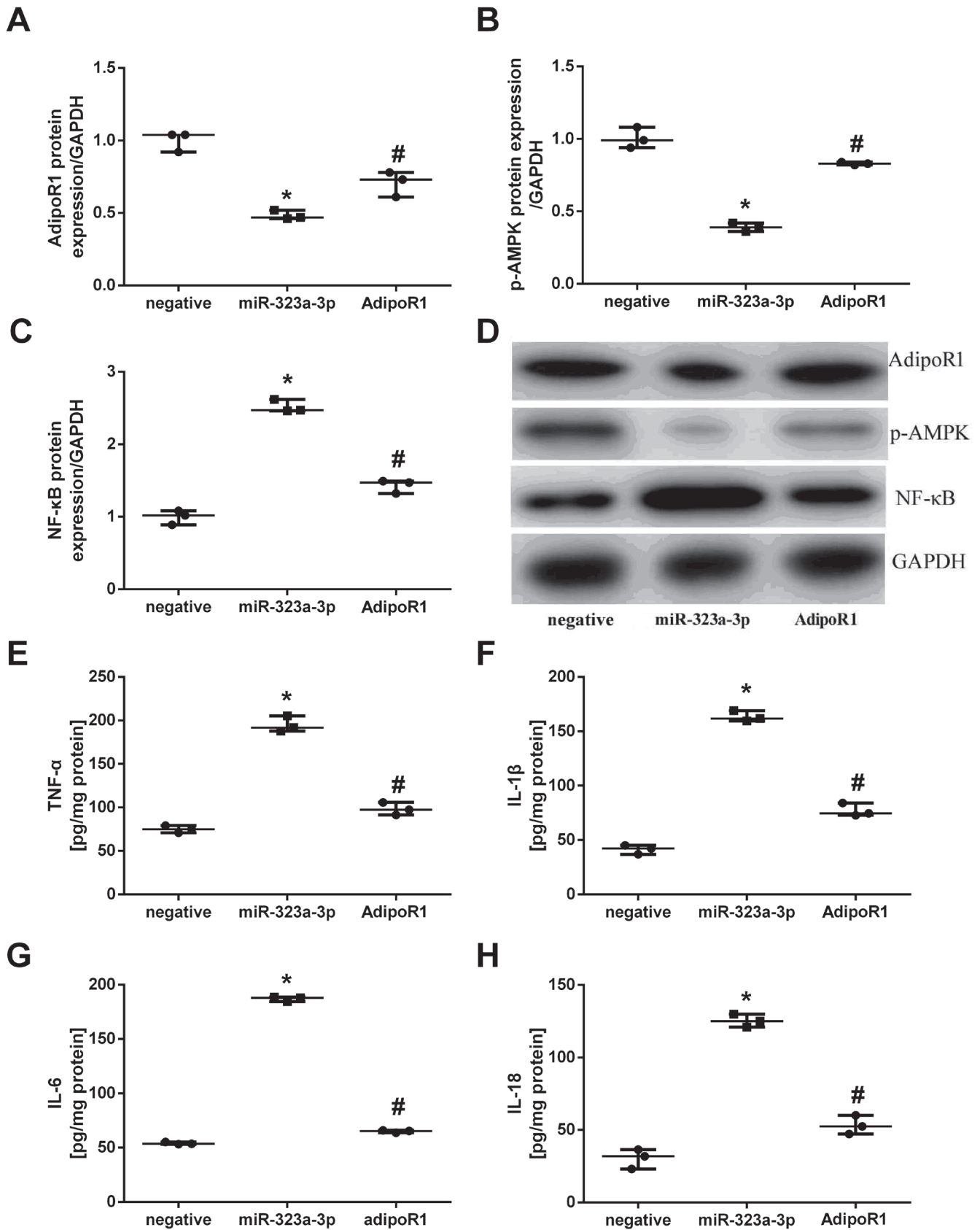
Fig. 4. AdipoR1 reduced the pro-inflammatory effects of miRNA-323a-3p in an in vitro model. AdipoR1, p-AMPK and NF-κB-p65 protein expression using western blot analysis (A, B and C) and statistical analysis (D); tumor necrosis factor alpha (TNF-α) (E), interleukin (IL)-1β (F), IL-6 (G), and IL-18 (H)

negative – cells transfected with negative mimics; miR-323a-3p – cells transfected with miR-323a-3p mimics; AdipoR1 – cells transfected with miR-323a-3p mimics and AdipoR1. The Kruskal–Wallis tests were used for 2 group and multiple group analyses. Multiple group comparisons: A–C, E–H: $\chi^2 = 7.20$; $p = 0.030$. Two group comparisons: *$p < 0.05$; #$p < 0.05$. Data are presented as median with range (n = 3).

in an in vitro model of IA following the overexpression of miRNA-323a-3p, when compared with the overexpression of the miRNA-323a-3p group (Fig. 4E–H).

AMPK reduced the pro-inflammatory effects of miRNA-323a-3p in an in vitro model

The role of AMPK in the pro-inflammatory effects of miRNA-323a-3p was studied in an in vitro model. The AMPK plasmid promoted the protein expression of p-AMPK (median: 1.02 (range: 0.93–1.06) compared to median: 0.21 (range: 0.19–0.24) compared to median: 0.58 (range: 0.44–0.62)), and suppressed NF-κB-p65 expression (median: 0.98 (range: 0.97–1.04) compared to median: 2.95 (range: 2.67– 3.04) compared to median: 1.47 (range: 1.47–1.68)) in an in vitro model of IA following the overexpression of miRNA-323a-3p, when compared with the overexpression of the miRNA-323a-3p group (Fig. 5A–C). The promotion of AMPK reduced the pro-inflammatory effects of miRNA-323a-3p on the levels of TNF-α (median: 74.11 (range: 71.14–82.75) pg/mg of protein compared to median: 193.87 (range: 190.52– 209.61) pg/mg of protein compared to median: 90.87 (range: 83.09–99.47) pg/mg of protein), IL-1β (median: 39.30 (range: 36.89–45.07) pg/mg of protein compared to median: 170.35 (range: 163.51–174.39) pg/mg of protein compared to median: 67.60 (range: 66.48–79.31) pg/mg of protein), IL-6 (median: 28.79 (range: 27.36–38.05) pg/mg of protein compared to median: 137.17 (range: 129.12– 139.43) pg/mg of protein compared to median: 56.52 (range: 47.13–61.98) pg/mg of protein), and IL-18 (median: 56.64 (range: 54.57–56.79) pg/mg compared to median: 190.36 (range: 186.11–190.64) pg/mg of protein compared to median: 69.50 (range: 67.62–69.88) pg/mg of protein) in an in vitro model, in comparison with the overexpression in the miRNA-323a-3p group (Fig. 5D–G).

Si-NF-κB reduced the pro-inflammatory effects of miRNA-323a-3p in an in vitro model

The role of NF-κB in the pro-inflammatory effects of miRNA-323a-3p was explored in an in vitro model. The si-NF-κB suppressed NF-κB-p65 protein expression (median: 1.07 (range: 0.96–1.07) compared to median: 2.11 (range: 2.03–2.20) compared to median: 1.25 (range: 1.13–1.30)) in an in vitro model of IA following the overexpression of miRNA-323a-3p, when compared with the overexpression of the miRNA-323a-3p group (Fig. 6A,B). The inhibition of NF-κB reduced the pro-inflammatory effects of miRNA-323a-3p on the levels of TNF-α (median: 51.13 (range: 44.35–51.53) pg/mg of protein compared to median: 218.88 (range: 204.50– 221.61) pg/mg of protein compared to median: 92.71 (range: 80.86–93.84) pg/mg of protein), IL-1β (median:

31.55 (range: 25.78–33.94) pg/mg of protein compared to median: 200.69 (range: 169.76–209.82) pg/mg of protein compared to median: 77.27 (range: 70.95–83.16) pg/mg of protein), IL-6 (median: 21.57 (range: 19.80–21.63) pg/mg of protein compared to median: 125.91 (range: 124.48– 130.60) pg/mg of protein compared to median: 46.34 (range: 41.45–47.21) pg/mg of protein), and IL-18 (median: 38.98 (range: 38.00–50.23) pg/mg of protein compared to median: 163.27 (range: 162.15–170.30) pg/mg of protein compared to median: 71.35 (range: 61.90– 74.39) pg/mg of protein) in an in vitro model, when compared with the overexpression in the miRNA-323a-3p group (Fig. 6C–F).

Discussion

Intracranial aneurysms are a common cerebrovascular disease, though their pathogenesis is unclear.[2,14] It is currently believed that the mechanisms of IA include endothelial injury, inflammatory response, dysregulation of the phenotype in vascular smooth muscle, extracellular matrix remodeling, apoptosis, and breakdown of the vessel wall.[14] In the current study, we demonstrated that the expression of miRNA-323a-3p was higher in patients with IA. The overexpression of miRNA-323a-3p promoted an increase of TNF-α, IL-1β, IL-6, and IL-18 levels in an in vitro model of IA.

The formation of IA is closely related to immune inflammation, though its origin and mechanism are still not fully understood.[15] The NF-κB is a major regulator of inflammatory cytokines.[16] Relevant studies have shown that NF-κB signaling transduction plays an important role in endothelial cell injury-mediated vascular diseases, and AMPK could regulate NF-κB signaling transduction.[15,16] In this study, we observed that the overexpression of miRNA-323a-3p suppressed the expression of AdipoR1 and p-AMPK and induced NF-κB-p65 protein expression in an in vitro model of IA. The si-NF-κB reduced the pro-inflammatory effects of miRNA-323a-3p in an in vitro model.

The AMPK is a key regulator of energy metabolism in organisms, and can be activated by various factors, including stress, exercise, hormones, and substances which affect cell metabolism.[17] Energy metabolism is also closely associated with immune regulation.[7] In the case of an insufficient supply of nutrients and a lack of energy, the immune function of the body is significantly worsened.[17] As a "cell energy-regulating receptor", when signaling transduction is impaired, AMPK could cause metabolic syndromes such as obesity, diabetes, insulin resistance, etc., which are often accompanied by chronic inflammation (including sepsis, rheumatoid arthritis and cardiovascular disease), seriously endangering human health.[18] In this study, we observed that the activation of AMPK reduced the pro-inflammatory effects of miRNA-323a-3p in an in vitro model.

When AdipoR2 binds to AdipoR2, it activates the downstream AMPK signaling pathway mediated by APPL1 and
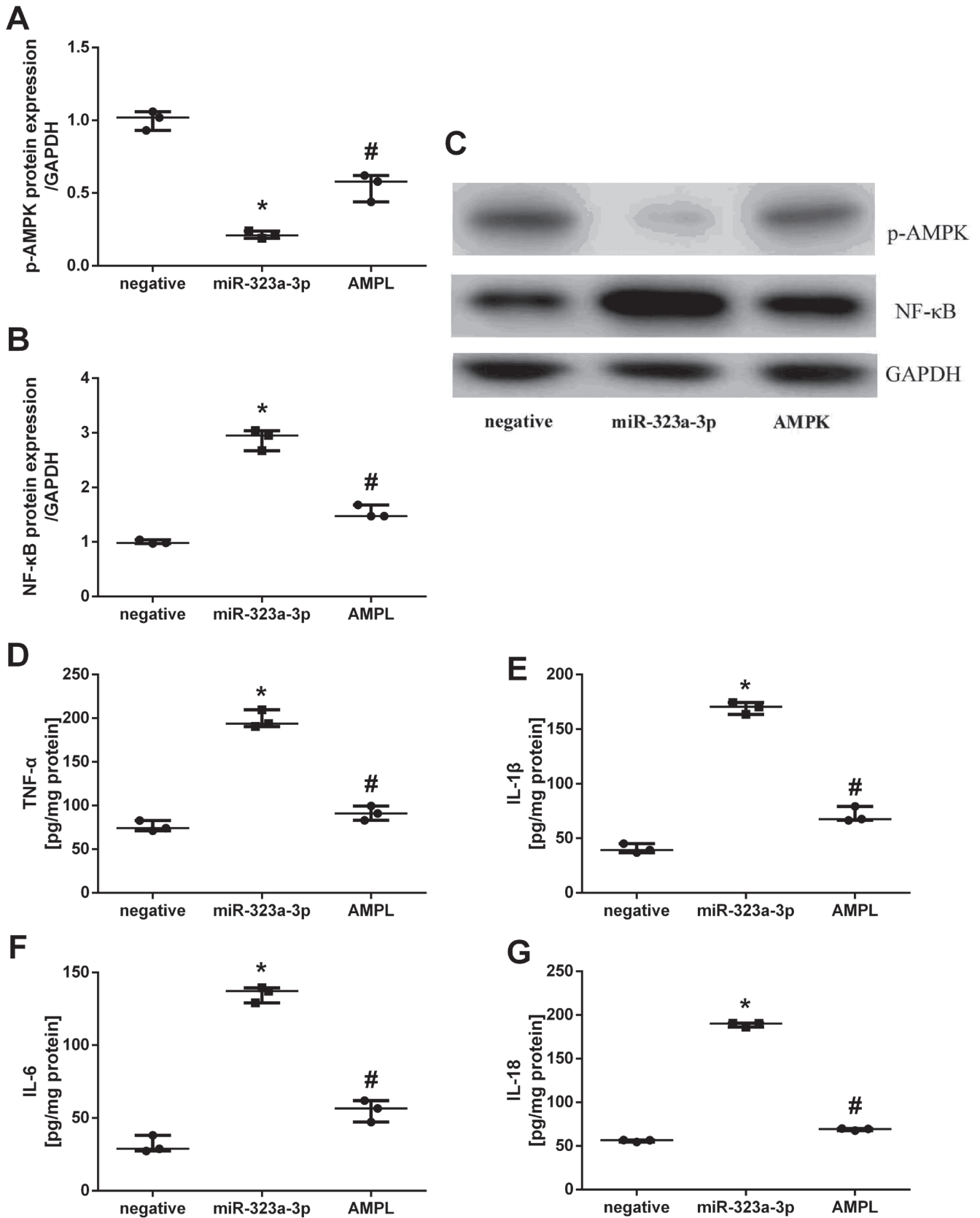
Fig. 5. AMPK reduced the pro-inflammatory effects of miRNA-323a-3p in an in vitro model. The expression of p-AMPK and NF-κB-p65 using western blot analysis (A and B) and statistical analysis (C); tumor necrosis factor alpha (TNF-α) (D), interleukin (IL)-1β (E), IL-6 (F), and IL-18 (G)

negative – cells transfected with negative mimics; miR-323a-3p – cells transfected with miR-323a-3p mimics; AMPK – cells transfected with miRNA-323a-3p mimic and AMPK. The Kruskal–Wallis tests were used for 2 group and multiple group analyses. Multiple group comparisons: A, B, D–G: $\chi^2 = 7.20$; p = 0.030. Two group comparisons: *p < 0.05; #p < 0.05. Data are presented as median with range (n = 3).
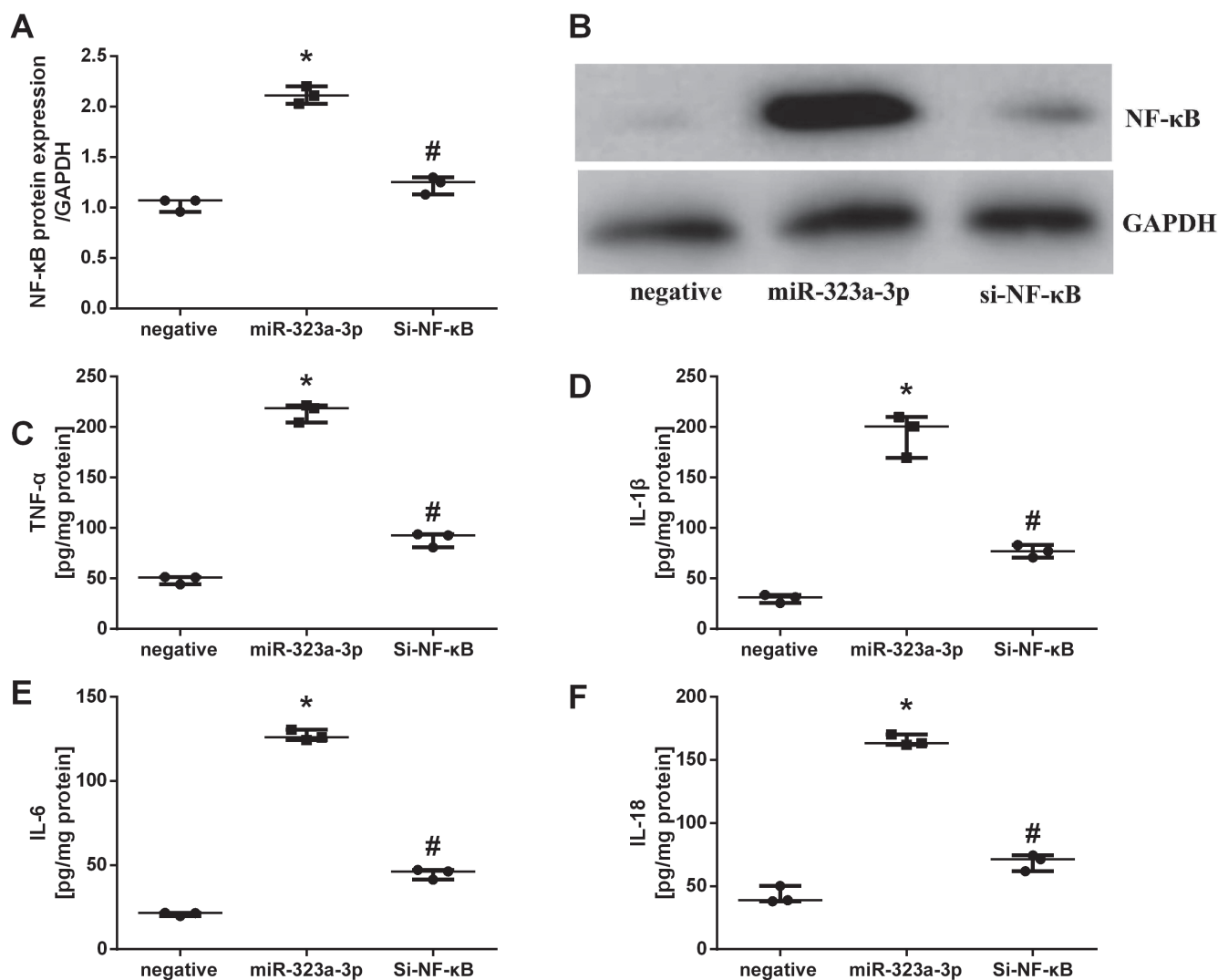
Fig. 6. Si-NF-κB reduced the pro-inflammatory effects of miRNA-323a-3p in an in vitro model. The NF-κB-p65 protein expression using western blot analysis (A) and statistical analysis (B); tumor necrosis factor alpha (TNF-α) (C), interleukin (IL)-1β (D), IL-6 (E), and IL-18 (F)

negative – cells transfected with negative mimics; miR-323a-3p – cells transfected with miR-323a-3p mimics; si-NF-κB – cells transfected with miRNA-323a-3p mimic and NF-κB antagonist. The Kruskal–Wallis tests were used for 2 group and multiple group analyses. Multiple group comparisons: A–H: $\chi^2 = 7.20$; $p = 0.030$. Two group comparisons: *$p < 0.05$; #$p < 0.05$. Data are presented as median with range (n = 3).

participates in glycolipid metabolism; such process can reduce body fat and improve hepatic insulin sensitivity and liver steatosis.[19] Meanwhile, adiponectin decreases the secretion of inflammatory factors such as IL-6 and TNF-α by inhibiting Kupffer cells from activating hepatic stellate cells and mediating the IKK-b/NF-κB pathway by attenuating the nuclear translocation of NF-κB; such action further suppresses the inflammatory response and antagonizes the progression of NAFLD.[20] We found that the activation of AdipoR1 or AMPK reduced the pro-inflammatory effects of miRNA-323a-3p in an in vitro model.

Limitations

This study sill has several limitations. First, due to the small sample size, a stratified analysis of gene expression based on patients' World Federation of Neurosurgical Societies (WFNS) scores was not performed. Second, due to ethical requirements, we were unable to detect the expression of miRNAs and inflammatory factors in tissue samples from aneurysms.
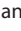
Conclusions

In summary, our study demonstrated that the expression of miRNA-323a-3p was higher in patients with IA. The overexpression of miRNA-323a-3p raised TNF-α, IL-1β, IL-6, and IL-18 levels in an in vitro model of IA via AdipoR1/AMPK/NF-κB. Our findings suggest that miRNA-323a-3p targeting AdipoR1 is promising in further anti-inflammation treatment of IA.

ORCID iDs

Bing Sun   https://orcid.org/0000-0002-8822-5428
Zehao Liu   https://orcid.org/0000-0002-8806-381X
Zhengquan Yu   https://orcid.org/0000-0003-4239-7977

References

1. Rojas HA, da Silva Fernandes KS, Ottone MR, et al. Levels of MMP-9 in patients with intracranial aneurysm: Relation with risk factors, size and clinical presentation. *Clin Biochem*. 2018;55:63–68. doi:10.1016/j.clinbiochem.2018.03.005

2. Shankar JJS, Lum C, Parikh N, dos Santos M. Long-term prospective follow-up of intracranial aneurysms treated with endovascular coiling using contrast-enhanced MR angiography. *AJNR Am J Neuroradiol*. 2010;31(7):1211–1215. doi:10.3174/ajnr.A2064

3. Martínez-Galdámez M, Lamin SM, Lagios KG, et al. Periprocedural outcomes and early safety with the use of the Pipeline Flex Embolization Device with Shield Technology for unruptured intracranial aneurysms: Preliminary results from a prospective clinical study. *J Neurointerv Surg*. 2017;9(8):772–776. doi:10.1136/neurintsurg-2016-012896

4. Pawlowska E, Szczepanska J, Wisniewski K, Tokarz P, Jaskólski DJ, Blasiak J. NF-κB-mediated inflammation in the pathogenesis of intracranial aneurysm and subarachnoid hemorrhage: Does autophagy play a role? *Int J Mol Sci*. 2018;19(4):1245. doi:10.3390/ijms19041245

5. Petridis AK, Filis A, Chasoglou E, et al. Aneurysm wall enhancement in black blood MRI correlates with aneurysm size: Black blood MRI could serve as an objective criterion of aneurysm stability in near future. *Clin Pract*. 2018;8(3):1089. doi:10.4081/cp.2018.1089

6. Gruszka W, Zbroszczyk M, Komenda J, Gruszczynska K, Baron J. The role of inflammation and potential pharmacological therapy in intracranial aneurysms. *Neurol Neurochir Pol*. 2018;52(6):662–669. doi:10.1016/j.pjnns.2018.08.002

7. Yao F, Zhang M, Chen L. 5'-Monophosphate-activated protein kinase (AMPK) improves autophagic activity in diabetes and diabetic complications. *Acta Pharm Sin B*. 2016;6(1):20–25. doi:10.1016/j.apsb.2015.07.009

8. Okada-Iwabu M, Yamauchi T, Iwabu M, et al. A small-molecule AdipoR agonist for type 2 diabetes and short life in obesity. *Nature*. 2013;503(7477):493–499. doi:10.1038/nature12656

9. Wang Y, Liang B, Lau WB, et al. Restoring diabetes-induced autophagic flux arrest in ischemic/reperfused heart by ADIPOR (adiponectin receptor) activation involves both AMPK-dependent and AMPK-independent signaling. *Autophagy*. 2017;13(11):1855–1869. doi:10.1080/15548627.2017.1358848

10. Aoki T, Nishimura M, Matsuoka T, et al. PGE(2)-EP(2) signalling in endothelium is activated by haemodynamic stress and induces cerebral aneurysm through an amplifying loop via NF-κB. *Br J Pharmacol*. 2011;163(6):1237–1249. doi:10.1111/j.1476-5381.2011.01358.x

11. Aoki T, Kataoka H, Ishibashi R, Nozaki K, Morishita R, Hashimoto N. Reduced collagen biosynthesis is the hallmark of cerebral aneurysm: Contribution of interleukin-1beta and nuclear factor-kappaB. *Arterioscler Thromb Vasc Biol*. 2009;29(7):1080–1086. doi:10.1161/ATVBAHA.108.180760

12. Cheng WT, Wang N. Correlation between MMP-2 and NF-κB expression of intracranial aneurysm. *Asian Pac J Trop Med*. 2013;6(7):570–573. doi:10.1016/S1995-7645(13)60098-X

13. Xu L, Gong C, Li G, et al. Ebselen suppresses inflammation induced by *Helicobacter pylori* lipopolysaccharide via the p38 mitogen-activated protein kinase signaling pathway. *Mol Med Rep*. 2018;17(5):6847–6851. doi:10.3892/mmr.2018.8641

14. Urbach H, Dorenbeck U, von Falkenhausen M, et al. Three-dimensional time-of-flight MR angiography at 3 T compared to digital subtraction angiography in the follow-up of ruptured and coiled intracranial aneurysms: A prospective study. *Neuroradiology*. 2008;50(5):383–389. doi:10.1007/s00234-007-0355-5

15. Aoki T, Frösen J, Fukuda M, et al. Prostaglandin E2-EP2-NF-kappaB signaling in macrophages as a potential therapeutic target for intracranial aneurysms. *Sci Signal*. 2017;10(465):eaah6037. doi:10.1126/scisignal.aah6037

16. Liu YF, Zhang Y, Dai D, Xu Z. Expression of NF-κB, MCP-1 and MMP-9 in a cerebral aneurysm rabbit model. *Can J Neurol Sci*. 2014;41(2):200–205. doi:10.1017/s0317167100016589

17. Zhang Y, Tao GJ, Hu L, et al. Lidocaine alleviates morphine tolerance via AMPK-SOCS3-dependent neuroinflammation suppression in the spinal cord. *J Neuroinflammation*. 2017;14(1):211. doi:10.1186/s12974-017-0983-6

18. Kim S, Lee MS, Jung S, et al. Ginger extract ameliorates obesity and inflammation via regulating microRNA-21/132 expression and AMPK activation in white adipose tissue. *Nutrients*. 2018;10(11):1567. doi:10.3390/nu10111567

19. Tang CH, Lu ME. Adiponectin increases motility of human prostate cancer cells via adipoR, p38, AMPK, and NF-kappaB pathways. *Prostate*. 2009;69(16):1781–1789. doi:10.1002/pros.21029

20. Yang Y, Wang Y, Kong Y, et al. Mechanical stress protects against osteoarthritis via regulation of the AMPK/NF-κB signaling pathway. *J Cell Physiol*. 2019;234(6):9156–9167. doi:10.1002/jcp.27592

Cofilin-1 and profilin-1 expression in lung microvascular endothelial cells exposed to titanium dioxide nanoparticles

Min-Hyeok An[A–E], Seon-Muk Choi[B–E], Pureun-Haneul Lee[A–C,E], Shinhee Park[A–C], Ae Rin Baek[A–C], An-Soo Jang[A–F]

Department of Internal Medicine, Soonchunhyang University Bucheon Hospital, South Korea

A – research concept and design; B – collection and/or assembly of data; C – data analysis and interpretation;
D – writing the article; E – critical revision of the article; F – final approval of the article

Abstract

Background. Air pollutants exacerbate chronic airway diseases, such as asthma and chronic obstructive pulmonary disease (COPD). However, the underlying mechanisms are yet to be determined. While a number of studies have reported adverse effects of nanoparticles on humans, little is known about their effects on the respiratory system.

Objectives. To examine the protein expression in human lung microvascular endothelial cells (HMVEC-L) exposed to titanium dioxide (TiO_2) nanoparticles, a common air pollutant.

Materials and methods. A proteomics approach using two-dimensional polyacrylamide gel electrophoresis (2D-PAGE) and matrix-assisted laser desorption/ionization time-of-flight/time-of-flight mass spectrometry (MALDI-TOF/TOF MS) was used to determine the differences in protein expression at 8 h and 24 h, following the treatment of HMVEC-L with 20-µM or 40-µM TiO_2 nanoparticles.

Results. Human lung microvascular endothelial cells treated with 20-µM TiO_2 nanoparticles showed alterations of 7 protein spots, including molecules related to calcium regulation, transport, cytoskeleton, and muscle contraction. The treatment of HMVEC-L with 40-µM TiO_2 nanoparticles resulted in alterations of 4 protein spots, with molecular functions related to the cytoskeleton, myosin regulation, actin modulation, as well as guanosine diphosphate (GDP) and guanosine triphosphate (GTP) regulation. To validate these results, immunohistochemical staining and western blotting analyses were performed on lung tissues collected from mice exposed to TiO_2 nanoparticles. Cofilin-1 and profilin-1 were expressed in the endothelium, epithelium and inflammatory cells, and decreased in lung tissues of TiO_2 nanoparticle-exposed mice compared to sham-treated controls.

Conclusions. These results suggest that some of the differentially expressed proteins may play important roles in airway diseases caused by TiO_2 nanoparticle exposure.

Key words: proteomics, air pollutants, airway disease, nanoparticles

1256

M.N. An et al. Cofilin-1 and profilin-1 expression in lung

Background

Air pollutants encompass also toxic particles and gases emitted in large quantities from many different sources, including vehicles and factories.[1] Major pollutants include particulate matter (PM), ozone, nitrogen dioxide (NO_2), and sulfur dioxide (SO_2). Air pollution negatively impacts human health and increases the burden of disease and demand for healthcare services.[2–4]

The principal component of indoor and outdoor air pollution is PM, which can vary widely in particle size, and includes coarse, fine and ultrafine particles. Furthermore, PM is a complex mixture of materials with a carbonaceous core and associated materials, such as organic compounds, acids and fine metal particles.[5,6]

Inflammation exacerbates pulmonary disease and causes lung dysfunction. The most important issue regarding environmental air pollution is its toxic effect, which can result in inflammatory disease,[7,8] with the lung function of patients with airway disease showing greater deterioration among those living in communities exposed to high levels of air pollution.[9] Toxic titanium dioxide (TiO_2) nanoparticles are produced by human activities, such as driving automobiles and charcoal burning, as well as by natural processes.[10–12] Titanium dioxide nanoparticles have toxic effects that manifest in inflammation and lead to disease.[13–15] Furthermore, the exposure to TiO_2 nanoparticles induces both acute and chronic inflammation, increases inflammatory cell expression and mucosal gland hyperplasia in the airway and alveolar spaces in animal models,[13,16,17] and can cause itching, bronchoconstriction and mucus hypersecretion.[18] The TiO_2 nanoparticles achieve this by penetrating the cell membrane and exerting toxic effects in organs.[19,20] Our previous studies demonstrated that the exposure to TiO_2 nanoparticles induced pulmonary inflammation and activated the inflammasome in mice, causing differential expression of NLRP3, caspase-1, and cytokines IL-1β and IL-18 in the lungs.[5] Moreover, TiO_2 nanoparticles increase the production of reactive oxygen species (ROS) and oxidative products, as well as the depletion of cellular antioxidants.[21,22]

Tight junctions (TJs) are the apical-most constituents of the junctional complex in epithelial cell sheets, also present in vascular endothelial cells and mesothelial cells.[22] Tight junctions act as a semipermeable barrier to the paracellular transport of ions, solutes and water, and function as a barrier between the apical and basolateral domains of plasma membranes.[22] Tight junctions coordinate a variety of signaling and trafficking molecules involved in the regulation of cell differentiation, proliferation and polarity, and thereby serve as multifunctional complexes.[21,23] The disruption of the function of TJs can cause or contribute to a variety of pathological conditions, such as infections, cancers and blood-borne metastasis.[24] Endothelial cells are among the main cellular constituents of blood vessels, and one of their most important functions is the formation of a barrier between blood and underlying tissues. These endothelial junctional proteins play important roles in tissue integrity, vascular permeability, leukocyte extravasation, and angiogenesis.[21]

The actin-severing activity of cofilin is an important factor in the stretch-induced cytoskeletal fluidization and may account for an appreciable part of the bronchodilatory effects of a deep inspiration.[28] Both cigarette smoke-exposed and chronic obstructive pulmonary disease (COPD) patient-derived epithelia display quantitative evidence of cellular plasticity, along with a loss of specialized apical features with distinct cell motion indicative of cellular jamming. These injured/diseased cells have an increased fraction of polymerized actin, due to the loss of the actin-severing protein, cofilin-1.[29] Counteracting cofilin-1 is profilin-1, an actin-binding protein that promotes actin polymerization in vitro,[25,26] endothelial cell migration and proliferation.[27] A requirement for dynamic actin association and dissociation is rendered by reversible Ser^{71} phosphorylation and dephosphorylation. The phosphorylation of Ser^{71} inhibits actin-binding of profilin-1.[30]

The mechanisms by which toxic nanoparticles induce pulmonary disease remain to be elucidated. In this study, we examined whether nanoparticles play a role in lung disease employing two-dimensional polyacrylamide gel electrophoresis (2D-PAGE) and matrix-assisted laser desorption/ionization time-of-flight/time-of-flight mass spectrometry (MALDI-TOF/TOF MS) of endothelial cells, and examined protein expression in the lungs of a mouse model of asthma.

Objectives

This study investigated whether TiO_2 nanoparticle exposure altered protein expression in vitro and in vivo.

Materials and methods

Cell culture and stimulation with TiO_2 nanoparticles

Primary human lung microvascular endothelial cells (HMVEC-L; 5000 cells/cm^2, cat No. CC-2527; Lonza, Basel, Switzerland) were grown in EGM™-2MV Microvascular Endothelial Cell Growth Medium BulletKit™ (Lonza). The medium was replaced every 48 h until cells reached 90% confluence at 37°C in 5% CO_2. The cells were seeded in 6-well plates. Twenty-four hours before the experiment, the medium was changed to EBM-2 supplemented with 0.1% fetal bovine serum (FBS). After 30 min, cells were stimulated with TiO_2 nanoparticles (SRM 1898, 20 or 40 µM; National Institute of Standards & Technology (NIST), Gaithersburg, USA) for 8 h or 24 h. The endotoxin concentration in nanoparticles was <0.064 ng/mL (0.32 EU/mL), based on the limulus amebocyte lysate assay (QCL-1000; BioWhittaker, Walkersville, USA).

Two-dimensional electrophoresis and image analysis

Human lung microvascular endothelial cells were harvested by centrifugation and then disrupted with lysis buffer containing 5 mM Tris-HCl (pH 7.4), 100 mM NaCl, 1% Triton X-100 and 2 mM phenylmethylsulfonyl fluoride (PMSF). Cell lysates were centrifuged at 12,000 rpm for 30 min and the supernatant was collected. The protein concentration was determined using a commercial BCA assay kit (Thermo Fisher Scientific, Rockford, USA) and the samples were stored at −70°C until use. Immobiline DryStrips (Amersham Biosciences, Piscataway, USA) were used for isoelectric focusing (IEF), which was carried out with 1 mg of the protein on an IPGphor system (Amersham Biosciences). The proteins were then separated in the second dimension by sodium dodecyl sulfate (SDS)-PAGE. Staining was performed with Coomassie brilliant blue G250 for the visualization of proteins. The 2-D gels were scanned with an ImageScanner (Amersham Biosciences) in a transmission mode. Spot detection and matching were performed using ImageMaster 2D v. 5.0 (Amersham Biosciences). The 2D spot intensity was calculated by integrating the optical density over the spot area. The data normalization was performed using ImageMaster 2D v. 5.0 (GE Healthcare, Seoul, South Korea) and then the values were exported to SPSS software v. 18.0 (SPSS Inc., Chicago, USA) for statistical analysis.

Protein identification with MALDI-TOF/TOF MS

Mass spectrometry was performed at Yonsei Proteome Research Center (YPRC; Seoul, South Korea). Synovial fluid and serum peptide profiles were analyzed with a MALDI-TOF/TOF mass spectrometer (Micromass, Wilmslow, UK). The following reagents and solutions were used for sample preparation: 70% acetonitrile (ACN), 2% formaldehyde and 2% fluorescent antibody (FA) buffer. Finally, the peptides attached to the resin were eluted in a drop-by-drop manner using an elution buffer.

Database search and protein identification

Peptide matching and protein searches against the Swiss-Prot and NCBI databases were performed using the Mascot software (Matrix Science; http://www.matrixscience.com).

Animal experiment

All experimental protocols were approved by the Animal Care and Use Committee of Soonchunhyang University, Asan, South Korea (approval No. SCHBCA-2015-06).[31] Six-week-old female BALB/c mice (n = 8 per group) were sensitized by intraperitoneal (ip.) injection on days 0 and 14, with grade V chicken egg ovalbumin (OVA, 50 µg; Sigma-Aldrich, St. Louis, USA) emulsified in 10 mg of $Al(OH)_3$ plus Dulbecco's phosphate-buffered saline (D-PBS, 100 µL). On days 21–23, all mice received an intranasal challenge with grade III OVA (150 µg; Sigma-Aldrich) in D-PBS (50 µL). Control mice were sensitized and challenged with saline. In the TiO_2 nanoparticle groups, mice were exposed to TiO_2 nanoparticles by inhalation (200 µg/m³ for 2 h) before OVA challenge, every day for 3 days. The airway hyperresponsiveness was measured on day 23. Bronchoalveolar lavage fluid (BALF) and lung tissues of mice were then collected for further analysis, including measurement of cofilin-1 and profilin-1 in lung protein, as well as BALF.

Determination of airway responsiveness and morphological analysis

Mice were challenged with 0 mg/mL (baseline), 5 mg/mL, 20 mg/mL, or 100 mg/mL methacholine. After challenge, enhanced pause (Penh) was measured using methacholine in a barometric plethysmographic chamber (All Medicus Co., Anyang, South Korea). Mice were anesthetized the next day and BALF was obtained and stored at −20°C until use. Differential cell counts within BALF samples were determined with Diff-Quick staining of cytospin slides (500 cells per animal). A portion of the lung was fixed in 4% buffered paraformaldehyde and embedded in paraffin. The tissue was cut into 4-µm-thick sections for histological analysis. The images were captured using an ECLIPSE Ci-L microscope (Nikon Corp., Tokyo, Japan) equipped with a DS-Ri2 digital camera (Nikon Corp.).

Western blotting analysis

The extracted lung tissue was homogenized in protein lysis solution containing 50 mM Tris-HCl (pH 7.4), 50 mM NaCl, 0.1% SDS, 1% Triton X-100, 0.5 mM ethylenediaminetetraacetic acid (EDTA), and 100 mM PMSF in distilled water, and centrifuged at 14,000 rpm for 30 min at 4°C. Then, the soluble fraction was collected. Mouse lung proteins were separated with SDS-PAGE and transferred onto polyvinylidene difluoride (PVDF) membranes, which were then blocked with 5% bovine serum albumin (BSA) plus 0.1% Tween 20 in Tris-buffered saline (TBS) for 2 h at room temperature. The membranes were incubated with rabbit anti-cofilin-1 (1:5000; Abcam, Cambridge, UK), mouse anti-profilin-1 (1:100; Santa Cruz Biotechnology, Santa Cruz, USA) or rabbit anti-profilin-1 (1:1000; ECM Biosciences, Versailles, USA) antibody overnight at 4°C. The next day, the membranes were incubated with horseradish peroxidase (HRP)-conjugated secondary antibodies. The detection was performed using EzWestLumi plus western blot detection reagent (ATTO Corporation, Tokyo, Japan). The relative abundances of the proteins were determined using quantitative densitometry with normalization relative to β-actin (Sigma-Aldrich).

Immunohistochemistry

Mouse lung sections were deparaffinized and rehydrated by passage through a series of increasing concentrations of ethanol. The sections were treated with 1.4% H_2O_2 in methanol for 30 min to block endogenous peroxidase activity, and nonspecific binding was then blocked with 1.5% normal horse serum. Next, the samples were incubated with rabbit anti-cofilin-1 (1:2000; Abcam) or mouse anti-profilin-1 (1:50; Santa Cruz Biotechnology) antibody. The next day, the sections were incubated using an ABC kit (Vector Laboratories, Burlingame, USA), and the color reaction was developed by staining with a DAB substrate kit (Golden Bridge International Inc., Mukilteo, USA). After immunohistochemical staining, the slides were counterstained with Harris hematoxylin for 1 min. Staining was quantified using ImageJ software (National Institutes of Health (NIH), Bethesda, USA).

Statistical analyses

The researchers hypothesized that the TiO_2 affects asthma pathogenesis through regulating cofilin-1 and profilin-1. Alternatively, a null hypothesis was proposed by the researchers, which advocated that there was no statistically significant difference between the groups. The data were expressed as median and interquartile range (IQR). All data were analyzed using IBM SPSS v. 22.0 software (IBM Corp., Armonk, USA). The differences between groups were determined using the nonparametric Kruskal–Wallis test, followed by Dunn's post hoc test. A value of $p < 0.05$ was considered statistically significant.

Results

2D-PAGE of HMVEC-L exposed to TiO_2 nanoparticles

A proteomics approach was used to determine the differential expression of proteins 8 h and 24 h after treating HMVEC-L with 20- or 40-μM TiO_2 nanoparticles (Fig. 1). A total of 11 spots were detected on each gel, all identified spots were localized in the 3–10 pH range, and the molecular mass ranged from 10 kDa to 150 kDa.

Protein spots selected on 2D-PAGE

Following the treatment for 8 h or 24 h with TiO_2 nanoparticles, 7 and 4 spots were found to have a differential, greater than two-fold expression on 2D-PAGE gel extracts (concentrations of 20 μM and 40 μM, respectively). These spots were excised from the gel and incubated with trypsin to digest the proteins in the gel, and then analyzed using MALDI-TOF/TOF MS (Table 1).

Identification of protein in each spot

Moesin, calreticulin precursor, eukaryotic initiation factor 4A-I isoform 1, heat shock protein β-1, profilin-1, myosin light polypeptide 6, and chain A were identified in the spots showing a differential expression. The differential expression (up or down) was shown in the Table 1 (average at 8 h and 24 h) on exposure to TiO_2 nanoparticles at a concentration of 20 μM. Furthermore, changes
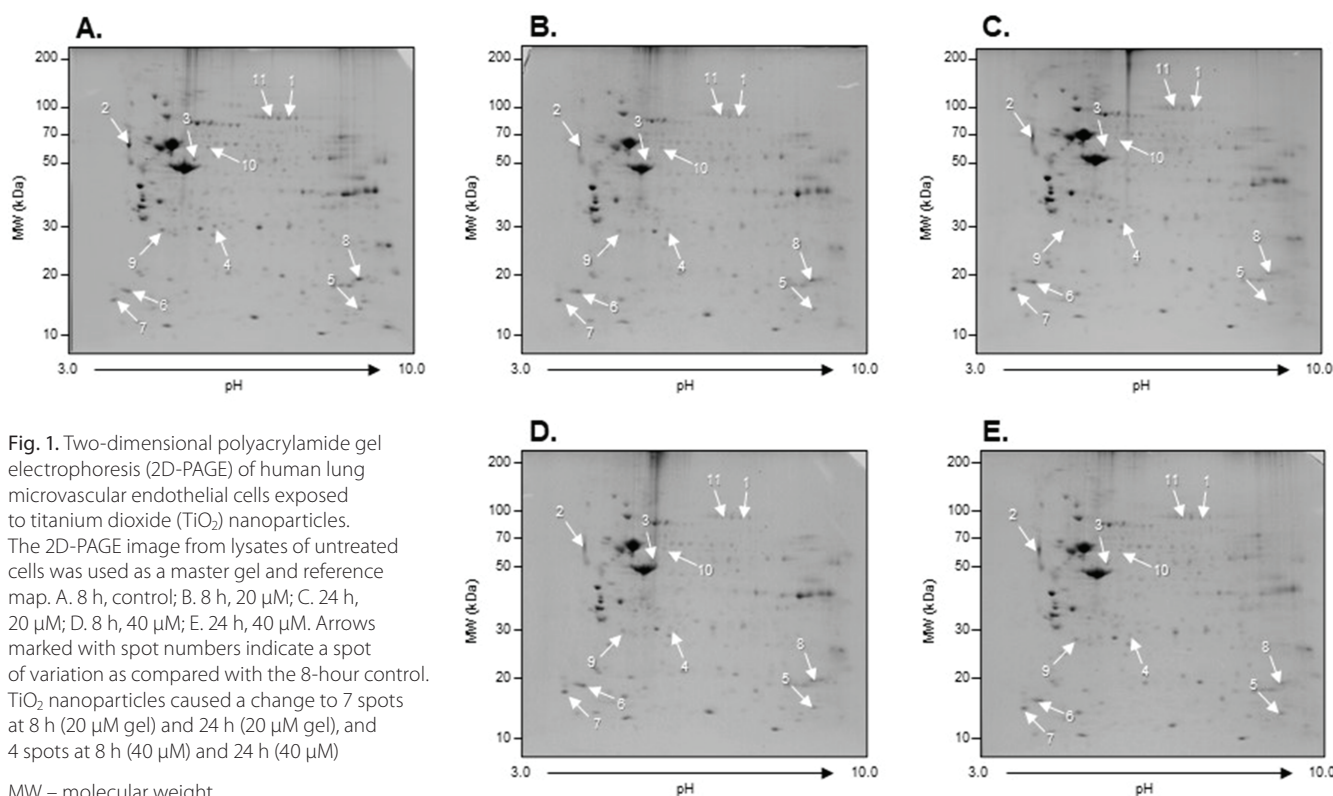
Fig. 1. Two-dimensional polyacrylamide gel electrophoresis (2D-PAGE) of human lung microvascular endothelial cells exposed to titanium dioxide (TiO_2) nanoparticles. The 2D-PAGE image from lysates of untreated cells was used as a master gel and reference map. A. 8 h, control; B. 8 h, 20 μM; C. 24 h, 20 μM; D. 8 h, 40 μM; E. 24 h, 40 μM. Arrows marked with spot numbers indicate a spot of variation as compared with the 8-hour control. TiO_2 nanoparticles caused a change to 7 spots at 8 h (20 μM gel) and 24 h (20 μM gel), and 4 spots at 8 h (40 μM) and 24 h (40 μM)

MW – molecular weight.

Table 1. List of proteins identified using matrix-assisted laser desorption/ionization time-of-flight/time-of-flight mass spectrometry (MALDI-TOF/TOF MS)

No.	TiO$_2$ NPs	Protein	Functional categorization	Accession number	Amino acid sequence	pI/molecular mass [Da]	Sequence coverage [%]	Average ratio (8 h)	Average ratio (24 h)
1.	concentration: 20 µM	moesin	cytoskeleton	4505257	K.VTAQDVR.K	6.08/67892	34	−2.59	−2.12
2.		calreticulin precursor	Ca^{2+} regulation	45757900	K.NVLINK.D	4.29/48283	17	−2.27	−1.72
3.		eukaryotic initiation factor 4A-I isoform 1	initiation factor	4503529	R.ENYIHR.I	5.32/46353	31	−3.37	−2.58
4.		heat shock protein β-1	cytoskeleton	4504517	R.VPFSLLR.G	5.98/22826	28	−1.83	2.54
5.		Profilin-1	transport	4826898	K.TLVLLMGK.E	8.44/15216	26	−3.21	2.89
6.		myosin light polypeptide 6 isoform	muscle contraction	17986258	K.SDEMNVK.V	4.56/17090	38	−1.34	1.85
7.		chain A target enzyme recognition by calmodulin	Ca^{2+} regulation	640285	K.ELGTVMR.S	4.04/16568	6	1.96	2.68
8.	concentration: 40 µM	cofilin-1	actin modulation	5031635	K.VFNDMK.V	8.22/18719	34	−3.04	2.5
9.		rho GDP-dissociation inhibitor 1 isoform A	regulation GDP/GTP	4757768	K.EGVEYR.I	5.02/23250	16	−2.32	2.83
10.		cytokeratin 7	cytoskeleton	67782365	R.LEAELR.S	5.40/51411	36	−1.8	2.31
11.		glycyl-tRNA synthetase	protein coding	578814645	R.AEFLNK.S	6.18/62596	11	−2.41	2.19

NPs – nanoparticles; GDP/GTP – guanosine diphosphate/guanosine triphosphate; pI – isoelectric point.

in the expression of cofilin-1, rho GDP-dissociation inhibitor 1 isoform A, cytokeratin 7, and glycyl-tRNA synthetase were detected in cells exposed to 40-µM TiO$_2$ nanoparticles. The identified spots had biological functions related to the cytoskeleton, calcium regulation, initiation factors, transport, muscle contraction, actin modulation, guanosine diphosphate/guanosine triphosphate (GDP/GTP) regulation, and protein coding.

Airway hyperresponsiveness and inflammatory changes on exposure to OVA and OVA plus TiO$_2$ nanoparticles

Airway hyperresponsiveness and inflammatory cells were increased in mice exposed to OVA and TiO$_2$ nanoparticles, compared to sham-treated control mice. Moreover, the increase was more pronounced with OVA+TiO$_2$ nanoparticles compared to OVA alone (Fig. 2, Table 2,3).

Protein validation with western blotting and immunohistochemical analyses

Western blotting analysis revealed decreases in cofilin-1 and profilin-1 expressions in HMVEC-L exposed to TiO$_2$ nanoparticles for 24 h, but not in cells exposed for 8 h (Fig. 3A, Table 4,5). Furthermore, there were no

changes in protein expression after 8 h or 24 h of starving the cells. The expression of profilin-1 was increased by exposure to TiO$_2$ nanoparticles in a time-dependent manner (Fig. 3A, Table 4,5). The expression levels of cofilin-1 and profilin-1 were increased in lung tissue of asthmatic mice compared to control mice and were decreased in the OVA+TiO$_2$ nanoparticles group compared to the OVA group (Fig. 3B, Table 2,3). The level of profilin-1 was significantly decreased in the sham-treated group, but it was increased in both the OVA group and the TiO$_2$ groups (Fig. 3B, Table 2,3). The immunohistochemical analysis indicated that cofilin-1 and profilin-1 levels in lung tissue were increased in the OVA group compared to the control group, but the increase was less pronounced in the OVA+TiO$_2$ nanoparticles group (Fig. 4, Table 2,3).

Discussion

This study revealed changes in protein expression in endothelial cells exposed to TiO$_2$ nanoparticles using a proteomics approach. Cofilin-1 and profilin-1 were shown to contribute to airway inflammation in the lungs of mice exposed to these potent air pollutants.

Ambient pollution has both a particulate component and a gaseous component, with the major fractions relevant

1260

M.N. An et al. Cofilin-1 and profilin-1 expression in lung
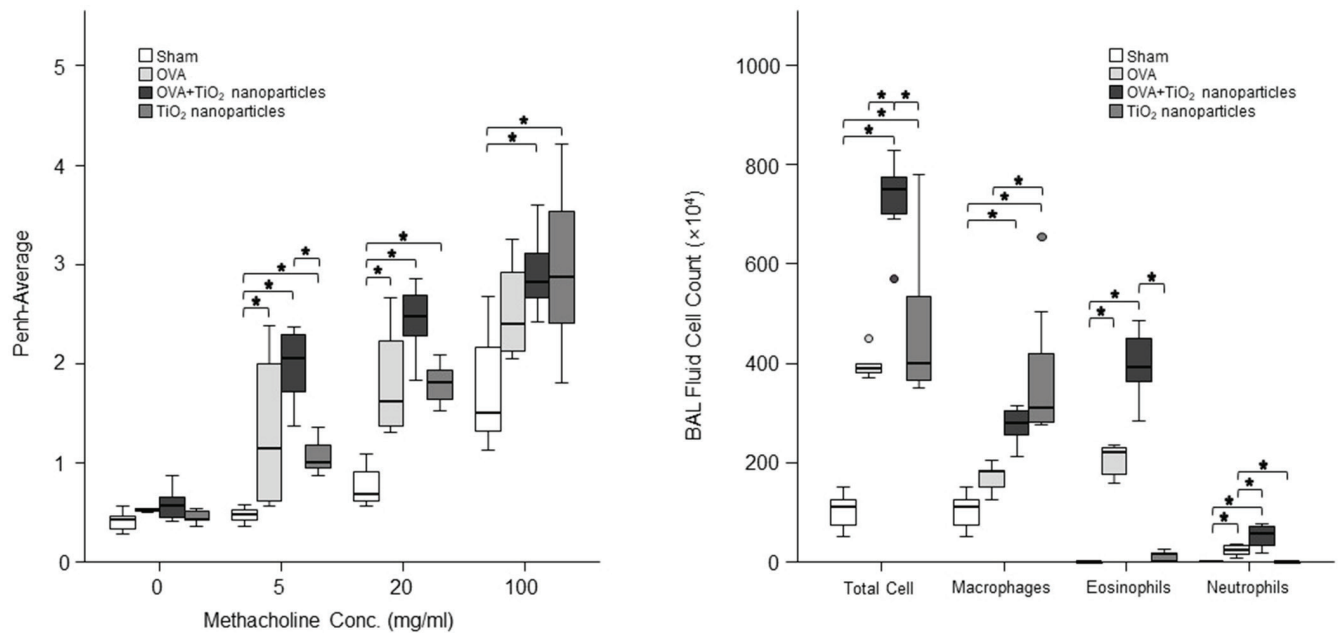
Fig. 2. Airway hyperresponsiveness and airway inflammation changes in a mouse ovalbumin (OVA)/titanium dioxide (TiO$_2$) nanoparticle-treated model. A. Airway hyperresponsiveness in OVA/TiO$_2$ nanoparticle-treated mice; B. Differential inflammatory cell counts in the bronchoalveolar lavage fluid (BALF) of OVA/TiO$_2$ nanoparticle-treated mice. The data are presented as median (interquartile range (IQR)) of 8 mice per group (* p < 0.05 compared with the sham group)

Table 2. Comparison of the analyzed variables in titanium dioxide (TiO$_2$) nanoparticle-exposed mice model profile using Kruskal–Wallis test (median, interquartile range (IQR))

Variable	Groups				Kruskal–Wallis test	
	group A (sham)	group B (OVA)	group C (OVA+TiO$_2$)	group D (TiO$_2$)	χ^2	p-value
AHR						
Mch 0 mg/mL	0.42 (0.33–0.47)	0.53 (0.51–0.56)	0.57 (0.43–0.67)	0.43 (0.41–0.52)	9.273	0.095
Mch 5 mg/mL	0.48 (0.43–0.53)	0.67 (0.59-2.00)	2.05 (1.59–2.32)	1.00 (0.91–1.24)	20.125	<0.001*
Mch 20 mg/mL	0.68 (0.62–0.97)	1.79 (1.37–2.33)	2.48 (2.23–2.77)	1.74 (1.55–1.97)	20.494	<0.001*
Mch 100 mg/mL	1.51 (1.32–2.29)	2.58 (2.13–3.09)	2.82 (2.63–3.16)	2.79 (1.88–3.63)	12.755	0.005*
Diff (×10^4)						
Total cells	110 (60–130)	390 (375–425)	750 (695–777.5)	400 (357.5–592.5)	19.131	<0.001*
Macrophages	109.78 (59.64–129.48)	181.74 (138.16–194.56)	278.81 (255.63–307.575)	309.57 (278.58–461.76)	16.661	0.001*
Eosinophils	0.36 (0–0.52)	220.5 (167.56–233.23)	390.03 (360.405–451.9)	15.38 (2.355–18.345)	24.042	<0.001*
Neutrophils	0 (0–0)	23.4 (11.67–34.23)	55.9 (31–73.005)	0 (0–0.82)	23.531	<0.001*
Lymphocytes	0 (0–0)	0.9 (0.38–1.94)	0 (0–0)	0 (0–0)	20.547	<0.001*
WB (intensity) (protein:b-actin ratio)						
Cofilin	0.659 (0.385–1.036)	1.166 (0.851–1.692)	0.663 (0.335–0.942)	0.332 (0.184–0.793)	9.353	0.025*
Profilin	0.7 (0.629–0.889)	1.055 (0.97–1.252)	0.859 (0.625–1.111)	0.577 (0.317–0.727)	10.393	0.016*
Profilin-1	0.588 (0.424–0.761)	0.357 (0.333–0.407)	0.49 (0.384–0.55)	1.592 (1.464–1.669)	17.42	0.001*
IHC (intensity [%])						
Cofilin	8.22 (7.625–10.546)	21.374 (18.246–24.895)	13.888 (11.559–16.773)	5.822 (4.063–7.805)	13.5	0.004*
Profilin	9.205 (8.204–11.887)	26.578 (15.872–30.421)	15.129 (12.401–18.199)	8.022 (6.378–10.439)	11.713	0.008*

AHR – airway hyperresponsiveness; Mch – methacholine; Diff – different cell count; WB – western blot; IHC – immunohistochemistry; OVA – ovalbumin; p > 0.05: non-significant, * p < 0.05: significant.

to health designated as PM$_{10}$ (10 μm), PM$_{2.5}$ (2.5 μm) and ultrafine PM.[32] Moreover, air pollution causes and exacerbates asthma, as demonstrated in a meta-analysis that revealed the associations between the exposure to traffic-related pollutants (black carbon, NO), PM$_{2.5}$ and PM$_{10}$, and the development of asthma in children.[32] Meta-analyses of the associations between air pollution and asthma exacerbations requiring emergency healthcare

Table 3. The p-values of Dunn's post hoc test comparisons for variables between the titanium dioxide (TiO$_2$) nanoparticle-exposed mice groups

	Groups					
Variable	A vs B	A vs C	A vs D	B vs C	B vs D	C vs D
AHR						
Mch 0 mg/mL	–	–	–	–	–	–
Mch 5 mg/mL	0.017*	<0.001*	0.022*	0.217	0.651	0.045*
Mch 20 mg/mL	0.04*	<0.001*	0.011*	0.105	0.92	0.073
Mch 100 mg/mL	0.123	0.002*	0.003*	0.304	0.336	0.958
Diff (×10^4)						
Total cells	0.074	<0.001*	0.029*	0.034*	0.879	0.024*
Macrophages	0.27	0.002*	<0.001*	0.082	0.03*	0.627
Eosinophils	0.006*	<0.001*	0.166	0.165	0.122	0.001*
Neutrophils	0.007*	<0.001*	0.491	0.279	0.031*	<0.001*
Lymphocytes	<0.001	1	1	<0.001	<0.001	1
WB (intensity) (protein:b-actin ratio)						
Cofilin	0.111	0.744	0.153	0.003*	0.055	0.27
Profilin	0.041*	0.488	0.27	0.178	0.002*	0.072
Profilin-1	0.037*	0.462	0.045*	0.178	<0.001*	0.006*
IHC (intensity [%])						
Cofilin	0.012*	0.181	0.373	0.235	0.001*	0.026*
Profilin	0.017*	0.119	0.504	0.414	0.002*	0.026*

AHR – airway hyperresponsiveness; Mch – methacholine; Diff – different cell count; WB – western blot; IHC – immunohistochemistry; OVA – ovalbumin; p > 0.05: non-significant, p < 0.05: significant*. Groups (A: sham, B: OVA, C: OVA+TiO$_2$, D: TiO$_2$). The Kruskal–Wallis test and the Dunn's post hoc test were used.
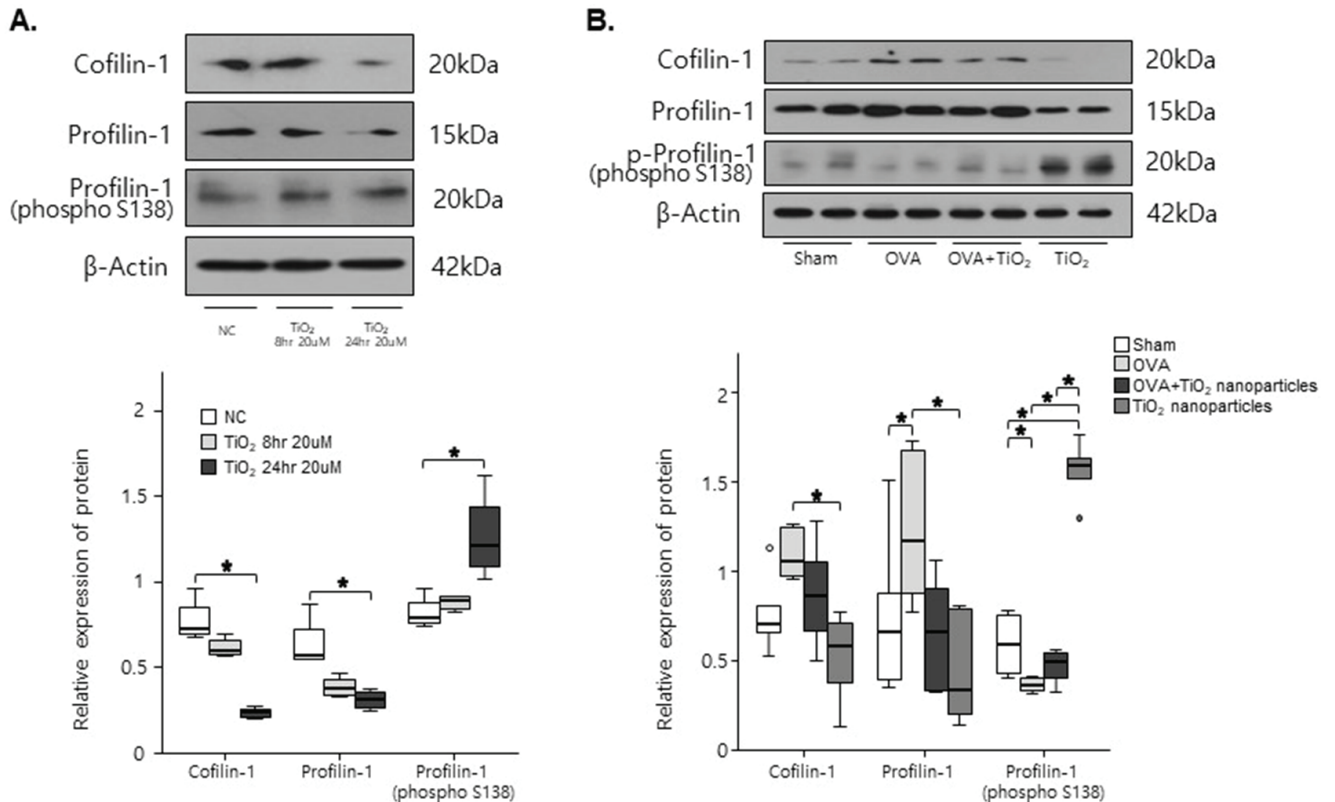
Fig. 3. The expression levels of cofilin-1 and profilin-1 proteins dected with western blotting. A. Cofilin-1 and profilin-1 levels in human lung microvascular endothelial cells (HMVEC-L) exposed to 20-μM TiO$_2$ nanoparticles for 8 h or 24 h (* p < 0.05 compared to normal controls (NC)); B. Cofilin-1 and profilin-1 levels determined with western blotting in ovalbumin (OVA)/titanium dioxide (TiO$_2$) nanoparticle-treated mice. The band intensities of cofilin-1 and profilin-1 were compared to that of β-actin. The data presented as the median (interquartile range (IQR)) of 8 mice per group (* p < 0.05 compared with the sham group)
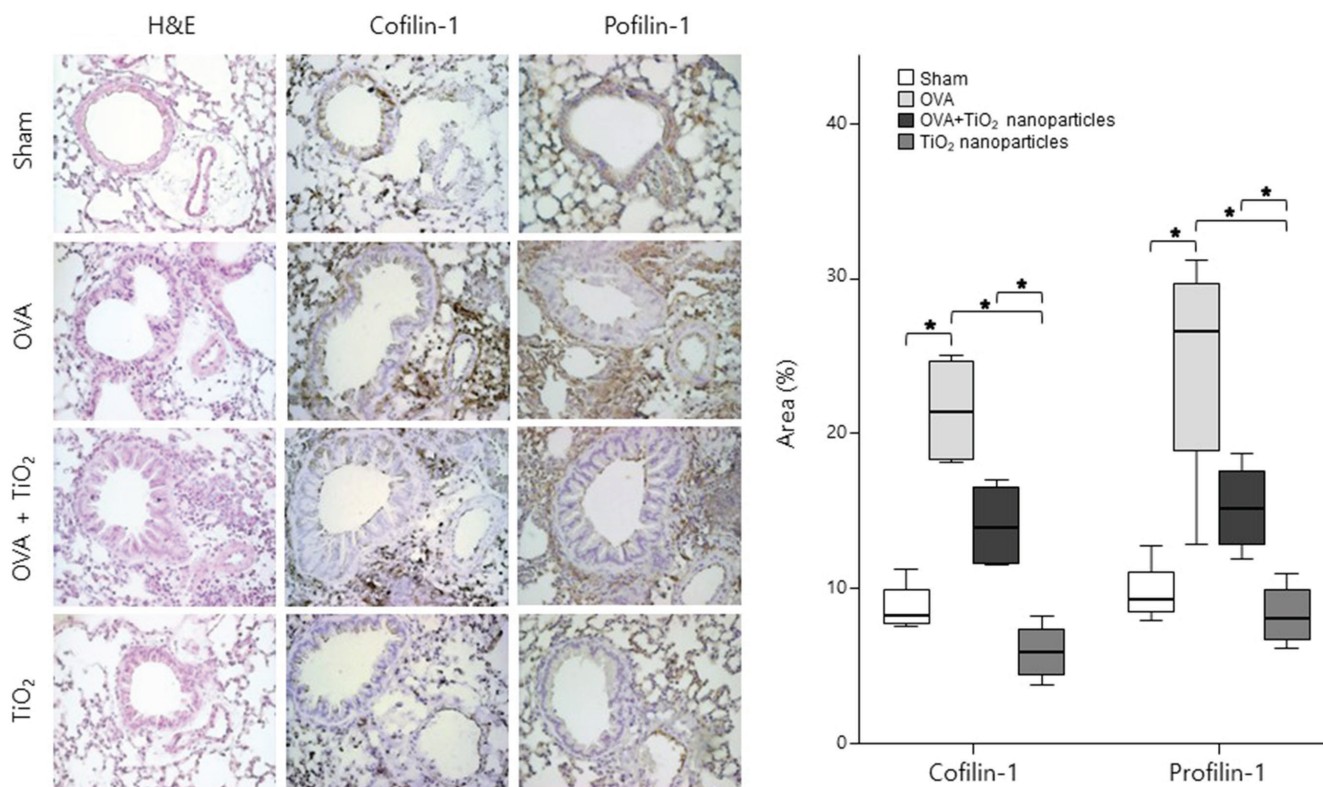
Fig. 4. Lung tissue cofilin-1 and profilin-1 protein expression visualized using hematoxylin and eosin (H&E) and immunohistochemical stain in ovalbumin (OVA)/titanium dioxide (TiO$_2$) nanoparticle-treated and sham mice

* p < 0.05 compared with the sham group.

Table 4. Comparison of the analyzed variables in 20-μM titanium dioxide (TiO$_2$) nanoparticle-exposed human lung microvascular endothelial cells (HMVEC-L) profile using Kruskal–Wallis test (median, interquartile range (IQR))

Variable	Groups			Kruskal–Wallis test	
	group A (NC)	group B (8 h)	group C (24 h)	X^2	p-value
WB (intensity) (protein:b-actin ratio)					
Cofilin	0.727 (0.689–0.904)	0.596 (0.572–0.676)	0.236 (0.206–0.267)	9.269	0.01*
Profilin	0.566 (0.55–0.795)	0.374 (0.336–0.448)	0.309 (0.257–0.369)	8.346	0.015*
Profilin-1	0.791 (0.75–0.922)	0.886 (0.836–0.916)	1.209 (1.054–1.53)	8	0.018*

WB – western blot; p > 0.05: non-significant, p < 0.05: significant*; NC – normal controls.

Table 5. The p-values of Dunn's post hoc test comparisons for variables between the 20-μM titanium dioxide (TiO$_2$) nanoparticle-exposed human lung microvascular endothelial cells (HMVEC-L) groups

Variable	Groups		
	A vs B	A vs C	B vs C
WB (intensity) (protein:b-actin ratio)			
Cofilin	0.17	0.002*	0.096
Profilin	0.062	0.004*	0.327
Profilin-1	0.433	0.006*	0.05

WB – western blot; p > 0.05: non-significant, p < 0.05: significant*. Groups (A: NC – normal controls. B: TiO$_2$ exposed 8 h, C: TiO$_2$ exposed 24 h).
The Kruskal–Wallis test and the Dunn's post hoc test were used.

utilization in children and/or adults also showed significant associations for NO$_2$, PM$_{2.5}$, CO, and O$_3$.[33,34]

Particulate matter with a diameter smaller than 100 nm is defined as ultrafine particles or nanoparticles. Nanoparticles are mainly found in urban air as single and aggregated particles, and can be divided into 2 major categories based on their source. Typically, nanoparticles are generated incidentally, often as byproducts of fossil fuel combustion and condensation

of semi-volatile substances or industrial emissions, although they can also be produced through engineering processes.[19,35] The exposure to PM induces oxidative stress and inflammation, stimulating both the innate and acquired immune responses in laboratory animals and humans. Oxidant-mediated cellular damage, including the production of ROS and oxidative stress, and innate and adaptive immunity, can lead to PM-mediated adverse health effects.[19]

Our previous studies showed that air pollutants promote lung disease through various mechanisms, including innate immunity (e.g., via macrophage migration inhibitory factor and inflammasomes) and neuroinflammation.[8,31,36] Nanoparticles also alter lung structure, reflected in goblet cell hyperplasia and airway remodeling.[13,37]

In this study, proteomic analyses showed that the treatment of HMVEC-L with 20-µM TiO_2 nanoparticles altered the expression of 7 proteins, including moesin, calreticulin precursor, eukaryotic factor 4A-isoform 1, heat shock protein β-1, profilin-1, myosin light polypeptide 6, and chain A, while the treatment with 40-µM TiO_2 nanoparticles altered the expression of 4 proteins, including cofilin-1, rho GDP-dissociation inhibitor 1 isoform A, cytokeratin 7, and glycyl-tRNA synthetase, that have roles in calcium regulation, transport, cytoskeleton, muscle contraction, myosin regulation, actin modulation, and GDP and GTP regulation.[38,39] Further studies are needed to clarify the role of this variety of expressed proteins in air pollutant-induced lung diseases.

Cofilin is a widely distributed intracellular actin-modulating protein that binds and depolymerizes filamentous (F)-actin and inhibits the polymerization of monomeric globular (G)-actin in a pH-dependent manner. It is involved in the translocation of actin-cofilin complex from the cytoplasm to the nucleus.[39] Cofilin modulates actin transport and function in the nucleus as well as actin organization associated with mitochondrial fission and mitophagy. Cofilin-saturated F-actin fragments under stress conditions can undergo oxidative cross-linking and bundle together to form cofilin-actin rods.[41] Cofilin-1 is a part of a novel mechanism linking mechano-transduction and transcription.[42] Profilin-1 is a 140-amino acid protein that regulates the growth of F-actin by binding to monomeric G-actin.[38] In the present study, cofilin-1 and profilin-1 protein expression levels were changed in endothelial cells and lungs exposed to TiO_2 nanoparticles, suggesting that these proteins may be useful markers of nanoparticle exposure in the lung. These results can be partly explained by recent experiments.[40–42] Injured epithelial cells exposed to cigarette smoke in COPD have an increased fraction of polymerized actin, due to loss of the actin-severing protein cofilin-1.[40] Further studies are needed to clarify the underlying signaling pathways and implications of these findings for airway diseases.

The respiratory epithelia function as a selective barrier between the outside environment and underlying tissue. Tight junctions are considered to function as a barrier between the apical and basolateral domains of plasma membranes.[21,43] In this study, TiO_2 nanoparticles altered the lung structure and disrupted the function of TJs in epithelial cells and endothelial cells, suggesting that nanoparticles can penetrate cell barriers and promote airway inflammation and hyperresponsiveness, thus contributing to airway remodeling.

Limitations

Future studies are needed for the multi-omics approaches which would lead to a more comprehensive overview, as compared to single-omics layer with slight advantages for combinations that complement each other directly, e.g., proteome and metabolome.[44–47]

Conclusions

In conclusion, nanoparticles are involved in airway inflammation and responsiveness (mediated by cofilin-1 and profilin-1), and in the change of cell membranes. Further studies are necessary to determine the mechanisms underlying these effects.

ORCID iDs

Min-Hyeok An https://orcid.org/0000-0002-7058-1870
Seon-Muk Choi https://orcid.org/0000-0003-4831-049X
Pureun-Haneul Lee https://orcid.org/0000-0002-1431-2393
Shinhee Park https://orcid.org/0000-0002-5783-6795
Ae Rin Baek https://orcid.org/0000-0003-1350-610X
An-Soo Jang https://orcid.org/0000-0001-5343-023X

References

1. McCormack MC, Breysse PN, Hansel NN, et al. Common household activities are associated with elevated particulate matter concentrations in bedrooms of inner-city Baltimore pre-school children. *Environ Res.* 2008;106(2):148–155. doi:10.1016/j.envres.2007.08.012
2. Murray CJL, Aravkin AY, Zheng P, et al. Global burden of 87 risk factors in 204 countries and territories, 1990–2019: A systematic analysis for the Global Burden of Disease Study 2019. *Lancet.* 2020;396(10258): 1223–1249. doi:10.1016/S0140-6736(20)30752-2
3. Lee PH, Park S, Lee YG, Choi SM, An MH, Jang AS. The impact of environmental pollutants on barrier dysfunction in respiratory disease. *Allergy Asthma Immunol Res.* 2021;13(6):850–862. doi:10.4168/aair. 2021.13.6.850
4. Leikauf GD, Kim SH, Jang AS. Mechanisms of ultrafine particle-induced respiratory health effects. *Exp Mol Med.* 2020;52(3):329–337. doi:10.1038/s12276-020-0394-0
5. Chipps BE, Murphy KR, Oppenheimer J. 2020 NAEPP Guidelines Update and GINA 2021: Asthma care differences, overlap, and challenges. *J Allergy Clin Immunol Pract.* 2022;10(1):S19–S30. doi:10.1016/j. jaip.2021.10.032
6. Stojanovic N, Glisovic J, Abdullah OI, Belhocine A, Grujic I. Particle formation due to brake wear, influence on the people health and measures for their reduction: A review. *Environ Sci Pollut Res.* 2022; 29(7):9606–9625. doi:10.1007/s11356-021-17907-3
7. Müzes G, Sipos F. Inflammasome, inflammation and cancer: An interrelated pathobiological triad. *Curr Drug Targets.* 2015;16(3):249–257. doi:10.2174/1389450115666141229154157
8. Kim BG, Lee PH, Lee SH, Park MK, Jang AS. Effect of TiO_2 nanoparticles on inflammasome-mediated airway inflammation and responsiveness. *Allergy Asthma Immunol Res.* 2017;9(3):257–264. doi:10.4168/ aair.2017.9.3.257

1264

M.N. An et al. Cofilin-1 and profilin-1 expression in lung

9. Decrue F, Gorlanova O, Salem Y, et al. Increased impact of air pollution on lung function in preterm versus term infants: The BILD study. *Am J Respir Crit Care Med*. 2022;205(1):99–107. doi:10.1164/rccm.202102-0272OC

10. Guo C, Yu T, Bo Y, et al. Long-term exposure to fine particulate matter and mortality: A longitudinal cohort study of 400,459 adults. *Epidemiology*. 2022;33(3):309–317. doi:10.1097/EDE.0000000000001464

11. Grande F, Tucci P. Titanium dioxide nanoparticles: A risk for human health? *Mini Rev Med Chem*. 2016;16(9):762–769. doi:10.2174/1389557516666160321114341

12. Iswarya V, Palanivel A, Chandrasekaran N, Mukherjee A. Toxic effect of different types of titanium dioxide nanoparticles on *Ceriodaphnia dubia* in a freshwater system. *Environ Sci Pollut Res*. 2019;26(12):11998–12013. doi:10.1007/s11356-019-04652-x

13. Meldrum K, Guo C, Marczylo EL, Gant TW, Smith R, Leonard MO. Mechanistic insight into the impact of nanomaterials on asthma and allergic airway disease. *Part Fibre Toxicol*. 2017;14(1):45. doi:10.1186/s12989-017-0228-y

14. Meyer TJ, Scherzad A, Moratin H, et al. The radiosensitizing effect of zinc oxide nanoparticles in sub-cytotoxic dosing is associated with oxidative stress in vitro. *Materials (Basel)*. 2019;12(24):4062. doi:10.3390/ma12244062

15. Feltis BN, Elbaz A, Wright PFA, Mackay GA, Turney TW, Lopata AL. Characterizing the inhibitory action of zinc oxide nanoparticles on allergic-type mast cell activation. *Mol Immunol*. 2015;66(2):139–146. doi:10.1016/j.molimm.2015.02.021

16. Korábková E, Kašpárková V, Jasenská D, et al. Behaviour of titanium dioxide particles in artificial body fluids and human blood plasma. *Int J Mol Sci*. 2021;22(19):10614. doi:10.3390/ijms221910614

17. Kang CM, Jang AS, Ahn MH, et al. Interleukin-25 and interleukin-13 production by alveolar macrophages in response to particles. *Am J Respir Cell Mol Biol*. 2005;33(3):290–296. doi:10.1165/rcmb.2005-0003OC

18. Sarasola M de la P, Táquez Delgado MA, Nicoud MB, Medina VA. Histamine in cancer immunology and immunotherapy: Current status and new perspectives. *Pharmacol Res Perspect*. 2021;9(5):e00778. doi:10.1002/prp2.778

19. Leikauf GD, Kim SH, Jang AS. Mechanisms of ultrafine particle-induced respiratory health effects. *Exp Mol Med*. 2020;52(3):329–337. doi:10.1038/s12276-020-0394-0

20. Lee YG, Lee PH, Choi SM, An MH, Jang AS. Effects of air pollutants on airway diseases. *Int J Environ Res Public Health*. 2021;18(18):9905. doi:10.3390/ijerph18189905

21. Lee PH, Park S, Lee YG, Choi SM, An MH, Jang AS. The impact of environmental pollutants on barrier dysfunction in respiratory disease. *Allergy Asthma Immunol Res*. 2021;13(6):850–862. doi:10.4168/aair.2021.13.6.850

22. Wang Y, Rezey AC, Wang R, Tang DD. Role and regulation of Abelson tyrosine kinase in Crk-associated substrate/profilin-1 interaction and airway smooth muscle contraction. *Respir Res*. 2018;19(1):4. doi:10.1186/s12931-017-0709-4

23. Sugimoto K, Chiba H. The claudin–transcription factor signaling pathway. *Tissue Barriers*. 2021;9(3):1908109. doi:10.1080/21688370.2021.1908109

24. Nur Husna SM, Tan HTT, Md Shukri N, Mohd Ashari NS, Wong KK. Nasal epithelial barrier integrity and tight junctions disruption in allergic rhinitis: Overview and pathogenic insights. *Front Immunol*. 2021;12:663626. doi:10.3389/fimmu.2021.663626

25. Yang C, Huang M, DeBiasio J, et al. Profilin enhances Cdc42-induced nucleation of actin polymerization. *J Cell Biol*. 2000;150(5):1001–1012. doi:10.1083/jcb.150.5.1001

26. Porta JC, Borgstahl GEO. Structural basis for profilin-mediated actin nucleotide exchange. *J Mol Biol*. 2012;418(1–2):103–116. doi:10.1016/j.jmb.2012.02.012

27. Ding Z, Lambrechts A, Parepally M, Roy P. Silencing profilin-1 inhibits endothelial cell proliferation, migration and cord morphogenesis. *J Cell Sci*. 2006;119(Pt 19):4127–4137. doi:10.1242/jcs.03178

28. Lan B, Krishnan R, Park CY, et al. Transient stretch induces cytoskeletal fluidization through the severing action of cofilin. *Am J Physiol Lung Cell Mol Physiol*. 2018;314(5):L799–L807. doi:10.1152/ajplung.00326.2017

29. Ghosh B, Nishida K, Chandrala L, et al. Epithelial plasticity in COPD results in cellular unjamming due to an increase in polymerized actin. *J Cell Sci*. 2022;135(4):jcs258513. doi:10.1242/jcs.258513

30. Wang F, Zhu C, Cai S, et al. Ser71 phosphorylation inhibits actin-binding of profilin-1 and its apoptosis-sensitizing activity. *Front Cell Dev Biol*. 2021;9:692269. doi:10.3389/fcell.2021.692269

31. Kim BG, Park MK, Lee PH, et al. Effects of nanoparticles on neuroinflammation in a mouse model of asthma. *Respir Physiol Neurobiol*. 2020;271:103292. doi:10.1016/j.resp.2019.103292

32. Kelly FJ, Fussell JC. Air pollution and public health: Emerging hazards and improved understanding of risk. *Environ Geochem Health*. 2015;37(4):631–649. doi:10.1007/s10653-015-9720-1

33. Khreis H, Kelly C, Tate J, Parslow R, Lucas K, Nieuwenhuijsen M. Exposure to traffic-related air pollution and risk of development of childhood asthma: A systematic review and meta-analysis. *Environ Int*. 2017;100:1–31. doi:10.1016/j.envint.2016.11.012

34. Orellano P, Quaranta N, Reynoso J, Balbi B, Vasquez J. Effect of outdoor air pollution on asthma exacerbations in children and adults: Systematic review and multilevel meta-analysis. *PLoS One*. 2017;12(3):e0174050. doi:10.1371/journal.pone.0174050

35. Orach J, Rider CF, Carlsten C. Concentration-dependent health effects of air pollution in controlled human exposures. *Environ Int*. 2021;150:106424. doi:10.1016/j.envint.2021.106424

36. Cha MH, Rhim T, Kim KH, Jang AS, Paik YK, Park CS. Proteomic identification of macrophage migration-inhibitory factor upon exposure to TiO_2 particles. *Mol Cell Proteomics*. 2007;6(1):56–63. doi:10.1074/mcp.M600234-MCP200

37. Kim BG, Lee PH, Lee SH, et al. Long-term effects of diesel exhaust particles on airway inflammation and remodeling in a mouse model. *Allergy Asthma Immunol Res*. 2016;8(3):246–256. doi:10.4168/aair.2016.8.3.246

38. Pandey DK, Chaudhary B. Evolutionary expansion and structural functionalism of the ancient family of profilin proteins. *Gene*. 2017;626:70–86. doi:10.1016/j.gene.2017.05.024

39. Chang CY, Leu JD, Lee YJ. The actin depolymerizing factor (ADF)/cofilin signaling pathway and DNA damage responses in cancer. *Int J Mol Sci*. 2015;16(2):4095–4120. doi:10.3390/ijms16024095

40. Ghosh B, Nishida K, Chandrala L, et al. Epithelial plasticity in COPD results in cellular unjamming due to an increase in polymerized actin. *J Cell Sci*. 2022;135(4):jcs258513. doi:10.1242/jcs.258513

41. Bamburg JR, Minamide LS, Wiggan O, Tahtamouni LH, Kuhn TB. Cofilin and actin dynamics: Multiple modes of regulation and their impacts in neuronal development and degeneration. *Cells*. 2021;10(10):2726. doi:10.3390/cells10102726

42. Domingues C, Geraldo AM, Anjo SI, et al. Cofilin-1 is a mechanosensitive regulator of transcription. *Front Cell Dev Biol*. 2020;8:678. doi:10.3389/fcell.2020.00678

43. Zihni C, Mills C, Matter K, Balda MS. Tight junctions: From simple barriers to multifunctional molecular gates. *Nat Rev Mol Cell Biol*. 2016;17(9):564–580. doi:10.1038/nrm.2016.80

44. Karkossa I, Raps S, von Bergen M, Schubert K. Systematic review of multi-omics approaches to investigate toxicological effects in macrophages. *Int J Mol Sci*. 2020;21(24):9371. doi:10.3390/ijms21249371

45. Bannuscher A, Karkossa I, Buhs S, et al. A multi-omics approach reveals mechanisms of nanomaterial toxicity and structure–activity relationships in alveolar macrophages. *Nanotoxicology*. 2020;14(2):181–195. doi:10.1080/17435390.2019.1684592

46. Bannuscher A, Hellack B, Bahl A, et al. Metabolomics profiling to investigate nanomaterial toxicity in vitro and in vivo. *Nanotoxicology*. 2020;14(6):807–826. doi:10.1080/17435390.2020.1764123

47. Karkossa I, Bannuscher A, Hellack B, et al. An in-depth multi-omics analysis in RLE-6TN rat alveolar epithelial cells allows for nanomaterial categorization. *Part Fibre Toxicol*. 2019;16(1):38. doi:10.1186/s12989-019-0321-5

GLP-1 receptor agonists, polycystic ovary syndrome and reproductive dysfunction: Current research and future horizons

Georgios S. Papaetis[1,2,A,D–F], Angelos Kyriacou[3,4,D–F]

[1] Internal Medicine and Diabetes Clinic, Paphos, Cyprus

[2] CDA College, Paphos, Cyprus

[3] CEDM Centre of Endocrinology, Diabetes & Metabolism, Limassol, Cyprus

[4] Department of Diabetes, Endocrinology & Obesity Medicine, Salford Royal NHS Foundation Trust, United Kingdom

A – research concept and design; B – collection and/or assembly of data; C – data analysis and interpretation;
D – writing the article; E – critical revision of the article; F – final approval of the article

Address for correspondence
Georgios S. Papaetis
E-mail: gpapaetis@yahoo.gr

Abstract

Polycystic ovary syndrome (PCOS) is a disorder that involves several organ systems and cellular pathways. It is strongly influenced by environmental and epigenetic factors. The principal goal of all therapeutic approaches to individuals with reproductive abnormalities is the treatment of subfertility or the regulation of menstruation when pregnancy is not desired. Obesity is closely related to insulin resistance (IR) and subsequent hyperinsulinemia, which aggravate hyperandrogenism and impair early follicle development. Weight loss is of vital importance for overweight/obese individuals with anovulatory infertility. The GLP-1R agonists have achieved remarkable weight reduction and abdominal fat loss in patients with type 2 diabetes (T2D), as well as in overweight/obese individuals and individuals with prediabetes. They have also been shown to promote lower fasting insulin levels and insulin resistance markers. These beneficial effects have been suggested to be particularly helpful in women with PCOS, while their possible role in the hypothalamic–pituitary–gonadal axis is under intense research. This review analyzes the current evidence for GLP-1R agonists, focusing on their effects on ovarian morphology, menstrual dysfunction and fertility outcomes. It also discusses their future role in achieving targeted therapeutic approaches.

Key words: polycystic ovary syndrome, fertility, incretins, weight loss, GLP-1R agonists

Introduction

Polycystic ovary syndrome (PCOS) is a disorder that involves several organ systems and cellular pathways. It is strongly influenced by environmental and epigenetic factors.[1] About 5–20% of women all over the world are affected during their fertility years; its prevalence depends on ethnicity, phenotype and classification system applied. The principal goal of all therapeutic approaches to women with reproductive problems is an improvement of subfertility or management of menstrual frequency in those who do not want to become pregnant.[2] Dysregulated negative feedback control of luteinizing hormone (LH), combined with insulin resistance (IR) with subsequent hyperinsulinemia, can affect ovarian hormone production and promote decreased ovulation. Hence, all treatment strategies aim to shift the balance of intraovarian steroid synthesis away from LH-insulin-driven stimulated androgen synthesis toward a follicle-stimulating hormone-driven final evolution of a dominant follicle.[1,2]

Mounting evidence has demonstrated that IR is present both in lean and obese individuals with PCOS.[3,4] Obesity, particularly the abdominal/visceral phenotype, is observed in approx. 80% of affected women.[3] It is closely related to IR and increased insulin levels, which aggravate hyperandrogenism (mainly by the stimulation of androgen synthesis from the ovarian theca cells) and impair early follicle development.[5,6] Hyperinsulinemia also stimulates androgen secretion from the adrenal glands and modulates LH release.[3,5] Furthermore, hyperandrogenemia can increase the deposition of visceral adipose tissue (VAT) and subsequently promote the resistance to insulin effects, causing a vicious cycle of feed-forward activation.[5,7] Treatment approaches that target weight loss and abdominal fat reduction do not only benefit the cardiometabolic status of these women but can also suppress this vicious cycle.

Weight loss is of vital importance in overweight/obese women with PCOS and subfertility.[1,2] The suppression of hyperinsulinemia and hyperandrogenism after weight reduction were shown to promote an improve regularity of menses and fertility potential.[1,3,5] Significant metabolic and reproductive benefits, as well as a complete resolution of this syndrome were observed in a significant percentage of obese women affected with PCOS who had undergone bariatric surgery and experienced a substantial weight loss.[8,9] Interestingly, in the latest international evidence-based practice guidelines for PCOS management, it was stated that weight loss therapies combined with lifestyle changes could be useful options for overweight/obese women after lifestyle modification alone has failed.[10]

Objectives

To explore the possible role of glucagon-like peptide-1 receptor (GLP-1R) agonists in improving menstrual dysfunction in women with PCOS.

Materials and methods

A literature search was performed systematically through PubMed, Scopus, Embase, Google, and Google Scholar until April 2022. It identified relevant preclinical and clinical peer-reviewed studies to be included in this review. Case reports and case series, as well as studies in languages other than English were not included in the study. The following Medical Subject Headings (MeSH) terms and relevant terms were used in the search process: PCOS, GLP-1, GLP-1R agonists, Liraglutide (LIRA), Exenatide (EXE), Semaglutide (SEMA), Dulaglutide (DULA), infertility/subfertility, IR, and obesity (Fig. 1).

GLP-1 and PCOS

The GLP-1 and glucose-dependent insulinotropic polypeptide (GIP) are the 2 main incretins described; they make up approx. 90% of the incretin activity.[11] The GLP-1 is a peptide that originates from proglucagon, which is synthesized and secreted from enteroendocrine L-cells after meals. It promotes weight loss and has an appetite suppressant activity due to its direct effect on the arcuate nucleus (ARC). Specifically, GLP-1 was shown to stimulate the electrical status of the hypothalamic proopiomelanocortin neurons of the ARC by enhancing the production of protein kinase A and promoting L-type calcium channel expression.[12] However, multiple regions within the central nervous system (CNS) appear to transduce pharmacological signals that connect GLP-1R activation with reduced food consumption and weight loss.[13] The GLP-1 also delays gastric secretion and intestinal motility due to its effect on the regulation of autonomous CNS function; it can also increase thermogenesis.[11–13] Dipeptidyl peptidase-4 (DPP-4) quickly breaks down native GLP-1, having 1–2 min of half-life; then, it undergoes a rapid renal clearance.[11,13]

The hypothalamic–pituitary–gonadal axis expresses GLP-1Rs, while GLP-1 has been suggested to regulate the hypothalamic neurons in order to release gonadotropin-releasing hormone (GnRH). The GLP-1 was also reported to have anti-inflammatory and anti-fibrotic activity in both the ovaries and endometrium.14 The GLP-1R knockout mice experienced disturbed estrous cycles, impaired fertility and delayed puberty compared to normal control mice.[15] The altered secretion and incretin activity were also shown in several small trials on affected women. However, the results are inconsistent and inconclusive, possibly because different protocols were utilized in metabolically heterogeneous PCOS populations.[16–22] The secretion of GLP-1 was not related to insulin levels and markers of IR per se in most of these studies.

GLP-1R agonists

The GLP-1R agonists activate GLP-1Rs and are resistant to the effect of DPP-4; reduced glycated hemoglobulin (A1C) levels and significant weight loss were observed after
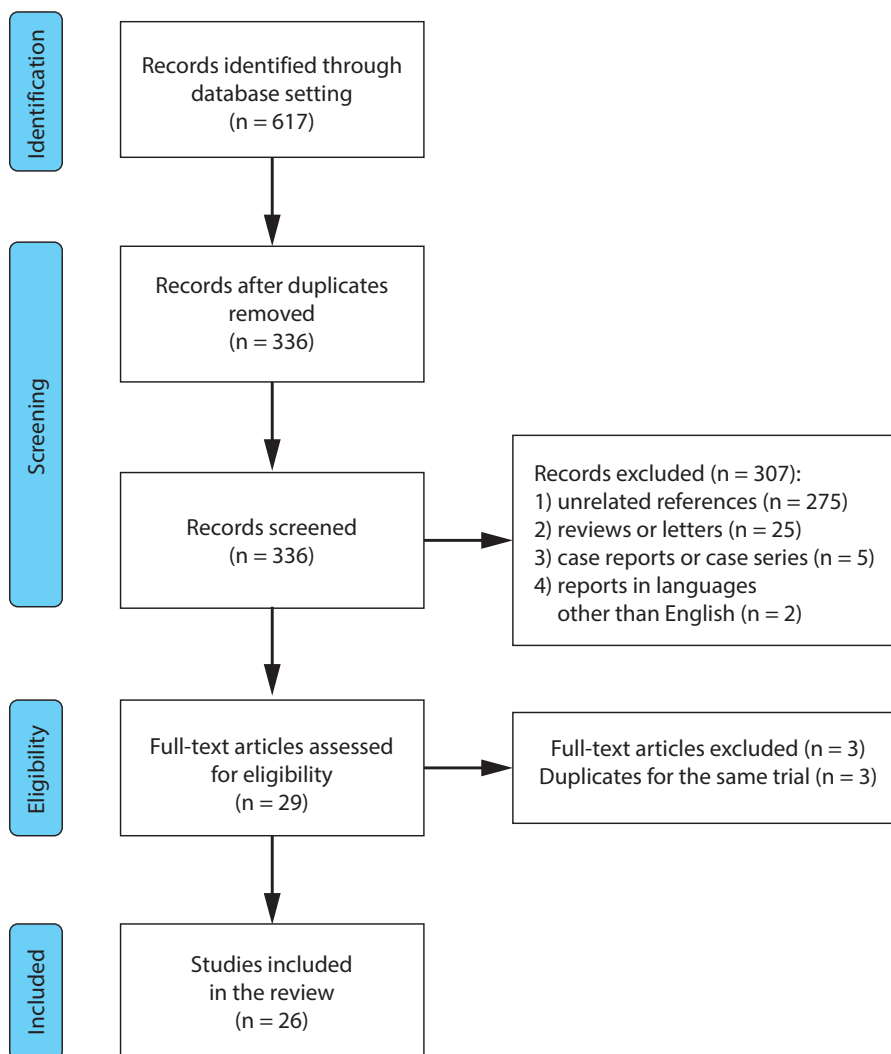
they had been administered to patients with type 2 diabetes (T2D).[23] Abdominal fat reduction, as well as improvements in IR indices and insulin levels during fasting were also described in T2D individuals, overweight/obese individuals and/or prediabetic individuals after the administration of GLP-1R agonists.[23–26] Additionally, GLP-1R agonists were shown to reduce urinary albumin excretion and mortality (cardiovascular and from any cause) in T2D patients.[27]

Liraglutide and SEMA were approved for weight reduction by both the United States Food and Drug Administration (FDA) and the European Medicines Agency (EMA) for individuals with established obesity or overweight people with a body mass index (BMI) ≥27 kg/m^2 and at least 1 weight-related condition (e.g., hypertension, prediabetes, abnormal lipid levels, and obstructive sleep apnea) combined with lifestyle modifications.[25,28] Semaglutide was recently suggested to be the most effective of its class in terms of weight loss; it can penetrate regions of CNS, which is essential for the control of appetite and hunger, and is not impeded by the blood–brain barrier.[13,28] These beneficial effects of GLP-1R agonists were suggested to be particularly helpful in women with PCOS. Hence, their possible role has become a field of intense research in this population.[29,30]

Liraglutide

Preclinical evidence

When LIRA was administered in preclinical PCOS models, it promoted significant reductions in body weight, abdominal fat deposition and IR markers.[31–33] Liraglutide may also suppress the overexpressed Notch signaling pathway, which causes neuroinflammation and can promote cognitive dysfunction.[34] Moreover, in ovariectomized mice, LIRA was found to modulate Kisspeptin 1 neuronal populations in the ARC, which control the secretion of GnRH in a pulsatile fashion.[35,36] However, this effect was insufficient to exert LH maintenance during fasting conditions.[35]

The possible effects of LIRA administration on reproductive dysfunction were investigated in 2 studies.[31,33] In the first study, female Sprague Dawley (SD) rats (4 weeks of age) were treated with a dihydrotestosterone (DHT) pellet (DHT-induced PCOS group, n = 31), or they received sham surgery without any pellet implant (control group, n = 13).[31] In the DHT arm, a subgroup of 15 rats aged 12 weeks received LIRA, while other 16 rats received saline injections twice a day for a total of 4 weeks. Menstrual

cyclicity did not improve. However, it is unknown whether longer LIRA treatment could improve the menstrual status. In the second study, which was conducted in dehydroepiandrosterone (DHEA)-induced PCOS mice, LIRA was administered in 2 doses intraperitoneally for 2 weeks (100 μg/kg and 200 μg/kg).[33] Mice with PCOS that were given the lower dose of LIRA experienced an acyclic condition, followed by a normal menstrual cycle. Those that were given the higher dose of LIRA had 1 short acyclic period, followed by 2 normal menstrual cycles. The LIRA therapy also promoted enhanced staining in the granulosa cells, theca cells and the stroma of the ovaries.

Clinical studies

Significant reductions in BMI, abdominal circumference and body weight were reported when LIRA was administered, both as a monotherapy and together with metformin (MET), in overweight or obese women with PCOS.[37–45] Sex hormone-binding globulin (SHBG) levels were significantly increased and free testosterone (T) levels were significantly reduced in several of these studies.[38,41,43,44] A preprint version of the SAXAPCOS study (NCT03480022),

in which 82 women with PCOS were randomly assigned to LIRA group (3 mg, n = 55) or placebo group (n = 27) for 32 weeks, stated that LIRA decreased the free androgen index (FAI), while it increased SHBG levels compared to placebo (p < 0.049 and p < 0.006, respectively). The frequency of menses after LIRA therapy significantly increased, as compared to the placebo group.[46] The results concerning menstrual dysfunction were reported in 5 published studies (Table 1).[37,39,40,42,44] Significant effects of LIRA were observed in 2 studies.[42,44] In the first study, the combination of 1.2 mg of LIRA every day with 1000 mg of MET twice a day or MET monotherapy were administered in obese women with PCOS and infertility.[42] Their effects on in vitro fertilization (IVF) rates, pregnancy rates (PRs) and cumulative PRs (spontaneous pregnancies and IVF pregnancies) were explored. None of the included women had experienced weight loss in the past despite changes in their daily habits. They were resistant to first-line reproductive therapeutic approaches with aromatase inhibitors or clomiphene. Twenty-eight individuals were initially enrolled, and 27 ultimately finished the medical protocol; their data were analyzed for 12 weeks (14 were treated with MET only, and 13 received the combination therapy). All participants

Table 1. Clinical studies of liraglutide in women with polycystic ovary syndrome (PCOS), in which results on menstrual dysfunction were reported

Reference	Study population	Study design	Main results
Jensterle Sever et al.[37]	36 obese women with PCOS (mean BMI: 37.1 ±4.6 kg/m²). They were pretreated with MET for 6 months and have lost less than 5% of BW.	12-week prospective open-label trial. The individuals were randomized to receive 1.2 mg of LIRA daily (n = 11), 1000 mg of MET twice daily (n = 14) or combined 1000 mg of MET twice daily and 1.2 mg of LIRA daily (n = 11).	Combination therapy achieved a significant reduction of androstenedione levels (2.2 ±3.7 nmol/L), while LIRA and MET monotherapy promoted a significant increase of androstenedione (1.9 ±4.2 and 0.8 ±1.70 nmol/L, respectively). Menstrual frequency was not significantly changed.
Jensterle et al.[39]	32 obese women recently diagnosed with PCOS (mean BMI: 39.5 ±6.2 kg/m²).	12-week prospective open-label study. Participants were randomized to receive 1000 mg of MET twice daily (n = 15) or 1.2 mg of LIRA daily (n = 17). A total of 28 participants completed the study (14 women in each arm) and their data were eventually analyzed.	LIRA promoted a significant increase in LH levels and no essential change in total T levels. MET caused significant LH reduction, as well as significant decrease in total T levels. No significant menstrual frequency changes were found in either group.
Jensterle et al.[40]	41 obese drug-naïve women with PCOS (mean BMI 38.6 ±6.0 kg/m²).	12-week prospective open-label study. Participants were randomized to receive 1.2 mg of LIRA daily (n = 14), 1000 mg of MET twice daily (n = 13) or 500 mg of ROF daily (n = 14).	Menstrual frequency increased in all treatment arms and was slightly greater in patients treated with ROF.
Salamun et al.[42]	28 obese women with PCOS (mean BMI: 36.7 ±3.5 kg/m²).	12-week prospective open-label study. Data from 27 women were finally analyzed: 13 received the combination of 1000 mg of MET twice daily and 1.2 mg of LIRA daily, while 14 were treated with MET monotherapy. The IVF protocol was offered to all women who completed the medical treatment protocol after 4 weeks of washout period.	After 1 year of follow-up, pregnancy was achieved in 69.2% of women in the combination arm and in 35.4% of women in the monotherapy arm. The PR per ET was significantly higher (85.7%) in the participants in the combination arm compared to 28.6% in the other group (p = 0.03).
Nylander et al.[44]	72 overweight or obese women with PCOS.	Prospective, double blind, placebo-controlled study. Duration of 26 weeks. All women enrolled were randomized to receive either 1.8 mg of LIRA (mean BMI (SD): 33.3 (5.1) kg/m²) daily or placebo (mean BMI (SD): 33.3 (4.6) kg/m²) in a 2:1 ratio. Finally, 65 participants (44 in the LIRA arm and 21 in the placebo) completed the trial.	The SHBG levels increased by 19% (p = 0.03) and free T levels decreased by 19% (p = 0.054) in the LIRA arm. When multiple regression analysis was performed with a change in bleeding ratio as dependent variable, LIRA had a significant impact on increase in menstrual frequency (p < 0.05). There was also a trend towards a lower stromal and ovarian volume in the drug therapy arm.

LIRA – liraglutide; MET – metformin; ROF – roflumilast; BW – body weight; BMI – body mass index; T – testosterone; LH – luteinizing hormone; SHBG – sex hormone-binding globulin; PR – pregnancy rate; ET – embryo transfer; IVF – in vitro fertilization.

who eventually completed the medical therapy were included in the IVF protocol. A 4-week washout period was an important prerequisite. Eventually, cumulative PRs were found in 69.2% of the participants in the combination group after 12 months, as compared to 35.4% in the monotherapy group. Significantly increased PRs per embryo transfer (ET) were found in the women who received LIRA/MET (85.7%), compared to those in the MET-only arm (28.6%; p = 0.03). Since the IVF PR per ET in women who experience PCOS and receive MET is approx. 30%, the possible effect of LIRA on the quality and receptivity of the endometrium was suggested.[47] Interestingly, comparable VAT reduction and body weight loss were demonstrated in both arms, suggesting that pathophysiological mechanisms other than the suppression of IR could underlie this effect. This is the first trial to show that LIRA/MET given for a short-term preconception period increased PRs per ET and cumulative PRs in this population, compared to monotherapy with MET.

In the other 26-week randomized trial, LIRA was administered to 72 women with PCOS in a daily dose of 1.8 mg (mean age: 31.4 (24.6–35.6) years; mean BMI: 33.3 (5.1) kg/m^2) compared to the placebo group (mean age: 26.2 (24.8–31.5) years; mean BMI: 33.3 (4.6) kg/m^2).[44] Sixty-five women (21 in the placebo group and 44 in the LIRA group) eventually finished the trial. The multiple regression analysis (change in the bleeding ratio was a dependent variable) suggested that the bleeding ratio at baseline (p < 0.0001) and LIRA (p < 0.05) achieved significant increases in the frequency of menses. A trend for reduced ovarian and stromal volume, which decreased by 1.6 mL after LIRA administration, was observed. Visceral adipose tissue was reduced by 18%, the proportion of fat in the liver by 44%, and the prevalence of non-alcoholic fatty liver disease by 33% in the LIRA group, as compared to the placebo group (all p < 0.01).[48]

Exenatide

Preclinical evidence

Significant reductions in body weight, abdominal fat deposition, fasting insulin levels, fasting glucose levels, and IR markers were observed when EXE was administered in preclinical PCOS models.[49–51] The upregulation of the molecular pathway of the AMP-activated protein kinase α-SIRT1 was also demonstrated after EXE therapy; the downregulation of this molecular pathway was associated with higher IR during a PCOS state.[49]

The possible activity of EXE on reproductive dysfunction and ovarian morphology was investigated in 2 studies.[50,51] In the first study, 45 female SD rats were randomly divided into 2 arms: the DHEA arm (n = 35) and the control arm (n = 10).[50] The DHEA group was then subdivided into 3 groups: the EXE arm (n = 10), the MET arm (n = 10) and the DHEA arm (n = 15), in which the rats were treated

with saline for a total of 4 weeks. In the DHEA-treated arm, the ovarian morphology revealed several histological PCOS findings, such as increased numbers of atretic/cystic follicles and reduced corpus luteum. Both the MET-treated and EXE-treated arms had fewer cystic follicles and several other follicles, such as antral or preantral, as well as more layers of granular cells. In the second randomized study, 24 female SD rats were separated into the PCOS with IR arm group (n = 18) and the control group (n = 6).[51] The SD rats in the PCOS with IR model were randomized into 3 arms: MET (n = 6), EXE (n = 6) and PCOS with IR (n = 6) that were treated with letrozole for 3 weeks. Interestingly, 83.3% of the rats in the EXE arm and 67.7% of the rats in the MET arm recovered their regular estrous cycles, while the PCOS with IR rats experienced irregular estrous cycles.

Clinical studies

Significant improvements in BMI, body weight, abdominal circumference, and IR markers occurred when EXE was administered either alone or together with MET in women who experienced PCOS and were overweight or obese. Significant improvements in glucolipid metabolism, amino acid metabolic disorders and markers of endothelial function were also demonstrated.[52–59] Notably, the combination of EXE with dapagliflozin (DAPA) achieved the highest reductions of weight loss and total body fat compared to either drug alone (EXE or DAPA) or a combination of DAPA/MET.[57] In a recent study in which 150 women with prediabetes and PCOS received MET, EXE or a combination of both for 12 weeks (n = 50 in each group), remission rates for prediabetes were 64% in the combination arm and 56% in the EXE group. Both remission rates were significantly higher than those found in the MET arm (32%).[59] Significant reductions of LH levels, compared to baseline values, occurred in the MET and combination arms but not in the EXE arm. Androstenedione and total T levels were significantly reduced, while SHBG was significantly increased compared to the initial concentrations in all 3 treatment arms.

Any possible effects of EXE on reproductive dysfunction were investigated in 2 studies.[52,58] In the first randomized study, 60 overweight/obese oligo-ovulatory women who experienced PCOS (70% finished the study protocol) received 1000 mg of MET twice daily, 10 μg of EXE twice daily, or a combination of both for a total of 24 weeks.[52] Free testosterone levels and FAI decreased significantly in all treatment arms. Significantly lower FAI concentrations were shown in women who received EXE/MET compared to those who received MET treatment only. Increased adiponectin levels were also found in all treatment groups and were strongly associated with decreased FAI levels. More regular menses were observed in the women randomized to the EXE/MET group compared to those in the MET group; they regular menses also strongly associated with weight loss (p = 0.018). The ovulation rate

1270

G.S. Papaetis, A. Kyriacou. GLP-1R agonists and reproductive dysfunction

was higher in the women randomized to the combination arm (86%) compared with the EXE arm (50%) and the MET group (29%) (p < 0.01). This is the first published study to demonstrate that a combination of EXE and MET for 24 weeks was superior to single-agent EXE or MET in improving menstrual cyclicity and ovulation rates in women who experienced PCOS and were overweight or obese.

In the second 12-week randomized trial, 176 individuals who experienced PCOS and were overweight or obese received either 1000 mg of MET twice a day (n = 88) or 10 µg of EXE twice a day (n = 88); all participants were treated with MET monotherapy for another 12 weeks, after the end of the first 12 weeks of the randomized study.[58] All participants were advised to adopt the same diet and physical exercise routines. Ultimately, 158 women (89.8%; 78 on EXE therapy and 80 on MET therapy) completed the study protocol. The women who were treated with EXE experienced on average a 4.29 ±1.29 kg weight loss compared to 2.28 ±0.55 kg of weight loss in those randomized to the MET group (p < 0.001). In addition, the women who received EXE experienced a significantly lower android and total fat mass percentage compared to those who received MET (p < 0.001). Free androgen index was significantly reduced and SHBG concentrations were significantly increased in both treatment arms, with no significant difference between them (all p < 0.001). The menstrual frequency ratio (MFR) was 0.90 ±0.13 in the EXE arm compared to 0.68 ±0.03 in the MET arm (p < 0.001); this significant increase in MFR was associated with weight reduction. The PR was 43.6% in the EXE arm compared

to 18.7% in the MET group (p < 0.05). This is the first trial to report that EXE therapy for a short time increased natural PRs more than MET therapy. The clinical and preclinical data regarding EXE administration on ovarian morphology, menstrual dysfunction and/or fertility outcomes are shown in Table 2.

Dulaglutide

The escalation of DULA given once every week in a dose of 3 mg or 4.5 mg achieved further incremental reductions in body weight, regardless of baseline A1C or BMI, compared to 1.5 mg once weekly in patients with T2D.[60] In a recent study, which was conducted in a DHEA-induced PCOS female rat model, 3 different doses of DULA were administered subcutaneously for 3 weeks in the treatment arm.[61] Fifty SD rats were randomized into either the DHEA-induced PCOS arm (n = 40) or the control arm (n = 10). Forty SD rats in the DHEA-induced PCOS model were then randomly divided into 4 arms (n = 10 in every arm): PCOS arm (model) that received normal saline; PCOS+DULA in a dose of 50 µg/kg (D-50 group); PCOS+DULA in a dose of 150 µg/kg (D-150 group); and PCOS+DULA in a dose of 450 µg/kg (D-450 group).

Insulin concentrations in the ovaries of the PCOS arm were significantly higher than those in the control arm. After DULA therapy, insulin concentrations in the ovaries in all 3 DULA groups were lower than those in the PCOS arm. The rats in all 3 DULA-treated arms experienced statistically significant reductions in serum T levels

Table 2. Preclinical and clinical studies of exenatide in polycystic ovary syndrome (PCOS), in which results on ovarian morphology and/or menstrual dysfunction were reported

Reference	Study design	Main results
Sun et al.[50]	45 SD rats were randomly divided into 2 arm groups: the DHEA arm group (n = 35) and the control arm group (n = 10). The DHEA arm group was then divided into 3 other groups: EXE group (n = 10), MET group (n = 10) and DHEA group, in which rats were treated with saline for a total of 4 weeks.	Both the MET-treated and EXE-treated arms showed decreased numbers of cystic follicles and various other follicles (such as antral and preantral follicles). Increased numbers of granular cell layers were found.
Xing et al.[51]	24 SD female rats were randomly divided into PCOS with IR group (n = 18) and the control group (n = 6). The SD rats in the PCOS with IR model were randomly divided into 3 arm groups: MET (n = 6), EXE (n = 6), and PCOS with IR (n = 6) that were treated with letrozole for a total of 3 weeks.	83.3% of the rats in the EXE arm group and 67.7% in the MET arm group recovered their regular estrous cycle, while PCOS with IR SD rats experienced irregular estrous cycles.
Elkind-Hirsch et al.[52]	60 overweight/obese oligo-ovulatory women with PCOS were randomized to receive 1000 mg of MET twice daily, 10 µg of EXE twice daily, or the combination of both medications for a total of 24 weeks.	Higher menses frequency and ovulation rates were shown in all groups after treatment. The improvement of bleeding frequency was strongly associated with weight loss. However, more regular menses were demonstrated in the combination arm compared to the MET arm. Moreover, the ovulation rate in the combination arm was significantly higher (86%) compared to the EXE group (50%) and the MET group (29%).
Liu et al.[58]	176 overweight/obese women with PCOS were randomized to receive either 1000 mg of MET twice daily (n = 88) or 10 µg of EXE twice daily (n = 88) for the first 12 weeks; all participants were treated with MET monotherapy during the next 12 weeks.	FAI was significantly reduced (p < 0.001) and SHBG levels significantly increased (p < 0.001) in both treatment arms, with no significant difference between them. The MFR was 0.90 ±0.13 in the EXE arm compared to 0.68 ±0.03 in the MET arm (p < 0.001); the significant increase of MFR was associated with weight reduction. The PR was 43.6% in the EXE arm compared to 18.7% in the MET group (p < 0.05).

EXE – exenatide; MET – metformin; DHEA – dehydroepiandrosterone; SHBG – sex hormone-binding globulin; FAI – free androgen index; PR – pregnancy rate; IR – insulin resistance; SD – Sprague Dawley; MFR – menstrual frequency ratio.

and statistically higher serum SHBG levels compared to those in the PCOS arm. There were fewer cystic follicles in the D-150 and D-450 arms, while the total population of the corpus luteum was significantly higher than in the PCOS arm. Moreover, the population of preantral follicles in all 3 DULA arms was significantly suppressed compared to the PCOS arm. Steroid hormone production-related genes, namely *3β-HSD*, *CYP19α1* and *StAR*, were significantly downregulated in the ovaries of the rats randomized to the 3 treatment groups; *StAR*- and *CYP19α1*-induced protein synthesis was significantly decreased in the ovaries after DULA therapy compared to the control arm.

Semaglutide

When administered to overweight/obese individuals, SEMA achieved remarkable reductions in body weight and significant improvements in cardiovascular and metabolic health risk factors.[62] Semaglutide decreased tongue fat tissue and fat proportion (a possible early marker of body fat deposition) compared to placebo, when given in a weekly dose of 1 mg during 16 weeks, in 25 obese women with PCOS.[63] The Treating PCOS With Semaglutide vs Active Lifestyle Intervention (TEAL) trial is active and is recruiting individuals with PCOS and obesity.[64] Participants in this study will be randomized to receive either oral SEMA (3 mg or 7 mg once daily) for 4 months or dietary modification.

Limitations

The limitations of this review are the factors that limit the quality and generability of the results of current literature, namely the short period of research, the small number of women investigated, the absence of a control arm (in some studies), and the lack of large, well-organized, double-blind, placebo-controlled studies over longer periods of time.

Conclusions

Preclinical studies on the administration of GLP-1R agonists in PCOS have shown promising results, both metabolic and reproductive. The majority of clinical studies concerning monotherapy with LIRA or EXE and their administration together with MET have demonstrated statistically significant improvements in BMI, abdominal circumference, total weight, markers of IR, and beneficial effects on glucolipid metabolism. Significant improvements in physical, psychological and social health were also reported.[65] Interindividual variations of body weight reduction could be the result of several genetic polymorphisms that contribute to GLP-1R genotype variability.[66] Most of their important effects were also illustrated in several recent meta-analyses; monotherapy with GLP-1R agonists or their combination with MET were superior to MET monotherapy in terms of reduction of waist circumference, body weight and BMI.[67–73] In order to enhance the cardiometabolic and hormonal defects associated with this syndrome, the potential combination of GLP-1R agonists/sodium-glucose co-transporter 2 (SGLT2) inhibitors is also being studied.[57,74]

Decreased free T levels and FAI have been shown both after LIRA and EXE administration. Significantly increased SHBG concentrations were also reported in numerous studies of LIRA and EXE administration.[38,41,44,52,58,59] However, the short period of research, the small number of women investigated and the absence of a control arm (in some studies) were major limitations. Whether the effect of GLP-1R agonists on increased androgen levels is the consequence of weight loss and the suppression of IR rather than an activity directly related to ovarian function per se, has not been clearly addressed. Furthermore, the rate of rebound weight gain following the cessation of this drug class is another issue that needs to be considered in future studies.

Both EXE and LIRA achieved significant increases in menstrual frequency and ovulation rates (Table 1 and Table 2). The improvement in bleeding frequency was significantly associated with weight loss in some studies. Notably, more regular menses were demonstrated after their combination with MET compared to MET monotherapy.[42,52] It should be stated that both EXE and LIRA failed to reduce LH levels.[39,59] On the contrary, MET promoted significant reductions of LH levels and meaningful reductions of total T concentrations, highlighting its key role in the regulation of LH secretion and the steroidogenesis coming from the ovaries.[75] In addition, important reductions of androstenedione concentrations were found after LIRA/MET combination therapy compared to monotherapy with LIRA, indicating the significance of their combination in this setting.[30,37] Metformin could also exhibit synergistic effects with GLP-1R agonists through the stimulation of GLP-1R expression/biosynthesis.[76] In this way, combining GLP-1R agonists with MET can be more effective compared to monotherapy of each drug class, in order to achieve significant hormonal and metabolic effects in women with PCOS, after lifestyle changes fail with or without MET.[30]

The GLP-1R agonists are classified as pregnancy class C medications and are contraindicated during pregnancy.[10,14,30] However, the higher rate of natural PRs after EXE therapy and IVF PR per ET/cumulative PRs after LIRA/MET combination suggests their promising role in the treatment of subfertility when they are administered during the preconception period.[42,58] Safety problems were unremarkable after the administration of EXE or LIRA in this setting; thus, their clinical use seems to have an acceptable profile. Close monitoring and a reasonable washout period are essential prerequisites. Interestingly, in the SEMA approval package inserts, it is stated that SEMA should be discontinued for at least 2 months before

a planned pregnancy due to its long half-life.[30] The clinical relevance of GLP-1R agonists on the hypothalamic–pituitary–gonadal axis, as well as on the quality and receptivity of the endometrium, merit future investigation.[14,30,77]

The recent dual GIP/GLP-1 receptor agonist tirzepatide promoted greater body weight loss compared to SEMA (at a dose of 1 mg) in patients with T2D. In addition, both dual GLP-1/glucagon receptor agonists and triple GLP-1/GIP/glucagon receptor agonists are under intense investigation; their possible effects on women with PCOS who are overweight or obese should be explored in future studies.[78–80]

The major adverse effects of GLP-1R agonists were nausea and vomiting, mainly during the up-titration phase; these effects were short-term and not associated with any significant termination of therapy.[25,30,66,67] In such cases, nausea and vomiting can be minimized by introducing certain treatment approaches, such as: prolonging the escalation period and titrating the LIRA dose in increments of 0.3 mg (5 click steps) rather than in increments of 0.6 mg (10 click steps), and/or dividing the dose twice a day.[25,30,81] Consistent with other interventions that cause substantial weight loss, cholelithiasis has also been reported and must be taken into consideration during the therapy and follow-up periods.[25,30] Another issue with GLP-1R agonist therapy is the high cost. The early cessation of the administration of GLP-1R agonists in individuals unlikely to experience any beneficial metabolic effects can help medical specialists reduce any probable adverse effects in the future, enhance the risk/benefit ratio and decrease the entire financial cost.[82]

Longer, larger, well-organized, multicenter, double-blind, placebo-controlled studies with thorough design and prolonged post-interventional follow-up are recommended in order to investigate the safety and activity of this drug class in women with PCOS who are overweight or obese. Convincing data with sufficient power to detect the risk/benefit profile of their use remain to be obtained. Hormonal, metabolic and fertility outcomes must be thoroughly explored. This will provide clinicians with valuable information helpful in clarifying their future role and adapting targeted therapeutic approaches in order to be successful in obtaining beneficial long-term outcomes.

ORCID iDs

Georgios S. Papaetis   https://orcid.org/0000-0002-8143-7145
Angelos Kyriacou   https://orcid.org/0000-0003-2282-0192

References

1. Escobar-Morreale HF. Polycystic ovary syndrome: Definition, aetiology, diagnosis and treatment. *Nat Rev Endocrinol*. 2018;14(5):270–284. doi:10.1038/nrendo.2018.24
2. Tanbo T, Mellembakken J, Bjercke S, Ring E, Åbyholm T, Fedorcsak P. Ovulation induction in polycystic ovary syndrome. *Acta Obstet Gynecol Scand*. 2018;97(10):1162–1167. doi:10.1111/aogs.13395
3. Diamanti-Kandarakis E. Insulin resistance in PCOS. *Endocrine*. 2006; 30(1):13–17. doi:10.1385/ENDO:30:1:13
4. Dunaif A, Segal KR, Futterweit W, Dobrjansky A. Profound peripheral insulin resistance, independent of obesity, in polycystic ovary syndrome. *Diabetes*. 1989;38(9):1165–1174. doi:10.2337/diab.38.9.1165
5. Lim SS, Davies MJ, Norman RJ, Moran LJ. Overweight, obesity and central obesity in women with polycystic ovary syndrome: A systematic review and meta-analysis. *Hum Reprod Update*. 2012;18(6):618–637. doi:10.1093/humupd/dms030
6. Papaetis GS, Papakyriakou P, Panagiotou TN. Central obesity, type 2 diabetes and insulin: Exploring a pathway full of thorns. *Arch Med Sci*. 2015;11(3):463–482. doi:10.5114/aoms.2015.52350
7. Lovejoy JC, Bray GA, Bourgeois MO, et al. Exogenous androgens influence body composition and regional body fat distribution in obese postmenopausal women: A clinical research center study. *J Clin Endocrinol Metab*. 1996;81(6):2198–2203. doi:10.1210/jcem.81.6.8964851
8. Escobar-Morreale HF, Botella-Carretero JI, Álvarez-Blasco F, Sancho J, San Millán JL. The polycystic ovary syndrome associated with morbid obesity may resolve after weight loss induced by bariatric surgery. *J Clin Endocrinol Metab*. 2005;90(12):6364–6369. doi:10.1210/jc.2005-1490
9. Kyriacou A, Hunter AL, Tolofari S, Syed AA. Gastric bypass surgery in women with or without polycystic ovary syndrome: A comparative observational cohort analysis. *Eur J Intern Med*. 2014;25(2):e23–e24. doi:10.1016/j.ejim.2013.09.012
10. Teede HJ, Misso ML, Costello MF, et al. Recommendations from the international evidence-based guideline for the assessment and management of polycystic ovary syndrome. *Hum Reprod*. 2018;33(9): 1602–1618. doi:10.1093/humrep/dey256
11. Papaetis GS. Incretin-based therapies in prediabetes: Current evidence and future perspectives. *World J Diabetes*. 2014;5(6):817–834. doi:10.4239/wjd.v5.i6.817
12. Grill HJ. A role for GLP-1 in treating hyperphagia and obesity. *Endocrinology*. 2020;161(8):bqaa093. doi:10.1210/endocr/bqaa093
13. Drucker DJ. GLP-1 physiology informs the pharmacotherapy of obesity. *Mol Metab*. 2022;57:101351. doi:10.1016/j.molmet.2021.101351
14. Jensterle M, Janez A, Fliers E, DeVries JH, Vrtacnik-Bokal E, Siegelaar SE. The role of glucagon-like peptide-1 in reproduction: From physiology to therapeutic perspective. *Hum Reprod Update*. 2019;25(4):504–517. doi:10.1093/humupd/dmz019
15. MacLusky NJ, Cook S, Scrocchi L, et al. Neuroendocrine function and response to stress in mice with complete disruption of glucagon-like peptide-1 receptor signaling. *Endocrinology*. 2000;141(2):752–762. doi:10.1210/endo.141.2.7326
16. Vrbikova J, Hill M, Bendlova B, et al. Incretin levels in polycystic ovary syndrome. *Eur J Endocrinol*. 2008;159(2):121–127. doi:10.1530/EJE-08-0097
17. Aydin K, Arusoglu G, Koksal G, Cinar N, Yazgan Aksoy D, Yildiz BO. Fasting and post-prandial glucagon like peptide 1 and oral contraception in polycystic ovary syndrome. *Clin Endocrinol*. 2014;81(4):588–592. doi:10.1111/cen.12468
18. Lin T, Li S, Xu H, et al. Gastrointestinal hormone secretion in women with polycystic ovary syndrome: An observational study. *Hum Reprod*. 2015;30(11):2639–2644. doi:10.1093/humrep/dev231
19. Gama R, Norris F, Wright J, et al. The entero-insular axis in polycystic ovarian syndrome. *Ann Clin Biochem*. 1996;33(3):190–195. doi:10.1177/000456329603300303
20. Pontikis C, Yavropoulou MP, Toulis KA, et al. The incretin effect and secretion in obese and lean women with polycystic ovary syndrome: A pilot study. *J Womens Health (Larchmt)*. 2011;20(6):971–976. doi:10.1089/jwh.2010.2272
21. Svendsen PF, Nilas L, Madsbad S, Holst JJ. Incretin hormone secretion in women with polycystic ovary syndrome: Roles of obesity, insulin sensitivity, and treatment with metformin. *Metabolism*. 2009; 58(5):586–593. doi:10.1016/j.metabol.2008.11.009
22. Cassar S, Teede HJ, Harrison CL, Joham AE, Moran LJ, Stepto NK. Biomarkers and insulin sensitivity in women with polycystic ovary syndrome: Characteristics and predictive capacity. *Clin Endocrinol (Oxf)*. 2015;83(1):50–58. doi:10.1111/cen.12619
23. Meier JJ. GLP-1 receptor agonists for individualized treatment of type 2 diabetes mellitus. *Nat Rev Endocrinol*. 2012;8(12):728–742. doi:10.1038/nrendo.2012.140
24. Davies MJ, Bergenstal R, Bode B, et al. Efficacy of liraglutide for weight loss among patients with type 2 diabetes: The SCALE diabetes randomized clinical trial. *JAMA*. 2015;314(7):687–699. doi:10.1001/jama.2015.9676
25. Papaetis GS. Liraglutide therapy in a prediabetic state: Rethinking the evidence. *Curr Diabetes Rev*. 2020;16(7):699–715. doi:10.2174/1573399816666191230113446

26. Lundkvist P, Pereira MJ, Katsogiannos P, Sjöström CD, Johnsson E, Eriksson JW. Dapagliflozin once daily plus exenatide once weekly in obese adults without diabetes: Sustained reductions in body weight, glycaemia and blood pressure over 1 year. *Diabetes Obes Metab*. 2017;19(9):1276–1288. doi:10.1111/dom.12954

27. Kristensen SL, Rørth R, Jhund PS, et al. Cardiovascular, mortality, and kidney outcomes with GLP-1 receptor agonists in patients with type 2 diabetes: A systematic review and meta-analysis of cardiovascular outcome trials. *Lancet Diabetes Endocrinol*. 2019;7(10):776–785. doi:10.1016/S2213-8587(19)30249-9

28. Shi Q, Wang Y, Hao Q, et al. Pharmacotherapy for adults with overweight and obesity: A systematic review and network meta-analysis of randomised controlled trials. *Lancet*. 2022;399(10321):P259–P269. doi:10.1016/S0140-6736(21)01640-8

29. Legro RS. Obesity and PCOS: Implications for diagnosis and treatment. *Semin Reprod Med*. 2012;30(6):496–506. doi:10.1055/s-0032-1328878

30. Papaetis GS, Filippou PK, Constantinidou KG, Stylianou CS. Liraglutide: New perspectives for the treatment of polycystic ovary syndrome. *Clin Drug Investig*. 2020;40(8):695–713. doi:10.1007/s40261-020-00942-2

31. Hoang V, Bi J, Mohankumar SM, Vyas AK. Liraglutide improves hypertension and metabolic perturbation in a rat model of polycystic ovarian syndrome. *PLoS One*. 2015;10(5):e0126119. doi:10.1371/journal.pone.0126119

32. Torres Fernandez ED, Huffman AM, Syed M, Romero DG, Yanes Cardozo LL. Effect of GLP-1 receptor agonists in the cardiometabolic complications in a rat model of postmenopausal PCOS. *Endocrinology*. 2019;160(12):2787–2799. doi:10.1210/en.2019-00450

33. Singh A, Fernandes JRD, Chhabra G, Krishna A, Banerjee A. Liraglutide modulates adipokine expression during adipogenesis, ameliorating obesity, and polycystic ovary syndrome in mice. *Endocrine*. 2019;64(2):349–366. doi:10.1007/s12020-019-01891-3

34. Saad MA, Eltarzy MA, Abdel Salam RM, Ahmed MAE. Liraglutide mends cognitive impairment by averting Notch signaling pathway overexpression in a rat model of polycystic ovary syndrome. *Life Sci*. 2021;265:118731. doi:10.1016/j.lfs.2020.118731

35. Heppner KM, Baquero AF, Bennett CM, et al. GLP-1R signaling directly activates arcuate nucleus kisspeptin action in brain slices but does not rescue luteinizing hormone inhibition in ovariectomized mice during negative energy balance. *eNeuro*. 2017;4(1):ENEURO.0198-16.2016. doi:10.1523/ENEURO.0198-16.2016

36. Szeliga A, Rudnicka E, Maciejewska-Jeske M, et al. Neuroendocrine determinants of polycystic ovary syndrome. *Int J Environ Res Public Health*. 2022;19(5):3089. doi:10.3390/ijerph19053089

37. Jensterle Sever M, Kocjan T, Pfeifer M, Kravos NA, Janez A. Short-term combined treatment with liraglutide and metformin leads to significant weight loss in obese women with polycystic ovary syndrome and previous poor response to metformin. *Eur J Endocrinol*. 2014;170(3):451–459. doi:10.1530/EJE-13-0797

38. Jensterle M, Goricar K, Janez A. Metformin as an initial adjunct to low-dose liraglutide enhances the weight-decreasing potential of liraglutide in obese polycystic ovary syndrome: Randomized control study. *Exp Ther Med*. 2016;11(4):1194–1200. doi:10.3892/etm.2016.3081

39. Jensterle M, Kravos NA, Pfeifer M, Kocjan T, Janez A. A 12-week treatment with the long-acting glucagon-like peptide 1 receptor agonist liraglutide leads to significant weight loss in a subset of obese women with newly diagnosed polycystic ovary syndrome. *Hormones (Athens)*. 2015;14(1):81–90. doi:10.1007/BF03401383

40. Jensterle M, Salamun V, Kocjan T, Vrtacnik Bokal E, Janez A. Short term monotherapy with GLP-1 receptor agonist liraglutide or PDE 4 inhibitor roflumilast is superior to metformin in weight loss in obese PCOS women: A pilot randomized study. *J Ovarian Res*. 2015;8:32. doi:10.1186/s13048-015-0161-3

41. Jensterle M, Kravos NA, Goričar K, Janez A. Short-term effectiveness of low dose liraglutide in combination with metformin versus high dose liraglutide alone in treatment of obese PCOS: Randomized trial. *BMC Endocr Disord*. 2017;17(1):5. doi:10.1186/s12902-017-0155-9

42. Salamun V, Jensterle M, Janez A, Vrtacnik Bokal E. Liraglutide increases IVF pregnancy rates in obese PCOS women with poor response to first-line reproductive treatments: A pilot randomized study. *Eur J Endocrinol*. 2018;179(1):1–11. doi:10.1530/EJE-18-0175

43. Kahal H, Aburima A, Ungvari T, et al. The effects of treatment with liraglutide on atherothrombotic risk in obese young women with polycystic ovary syndrome and controls. *BMC Endocr Disord*. 2015;15:14. doi:10.1186/s12902-015-0005-6

44. Nylander M, Frøssing S, Clausen HV, Kistorp C, Faber J, Skouby SO. Effects of liraglutide on ovarian dysfunction in polycystic ovary syndrome: A randomized clinical trial. *Reprod Biomed Online*. 2017;35(1):121–127. doi:10.1016/j.rbmo.2017.03.023

45. Rasmussen CB, Lindenberg S. The effect of liraglutide on weight loss in women with polycystic ovary syndrome: An observational study. *Front Endocrinol (Lausanne)*. 2014;5:140. doi:10.3389/fendo.2014.00140

46. Elkind-Hirsch K, Chappell N, Shaler D, Storment J, Bellanger D. A randomized, double-blind, placebo-controlled study of liraglutide 3 mg [LIRA 3mg] on weight, body composition, hormonal and metabolic parameters in women with obesity and polycystic ovary syndrome (PCOS) [published online ahead of print August 24, 2021]. 2021. doi:10.21203/rs.3.rs-799341/v1

47. Tso LO, Costello MF, Albuquerque LET, Andriolo RB, Macedo CR. Metformin treatment before and during IVF/ICSI in women with polycystic ovarian syndrome. *Cochrane Database Syst Rev*. 2006;12(12):CD006105. doi:10.1002/14651858.CD006105.pub4

48. Frøssing S, Nylander M, Chabanova E, et al. Effect of liraglutide on ectopic fat in polycystic ovary syndrome: A randomized clinical trial. *Diabetes Obes Metab*. 2018;20(1):215–218. doi:10.1111/dom.13053

49. Tao X, Cai L, Chen L, Ge S, Deng X. Effects of metformin and Exenatide on insulin resistance and AMPKα-SIRT1 molecular pathway in PCOS rats. *J Ovarian Res*. 2019;12(1):86. doi:10.1186/s13048-019-0555-8

50. Sun L, Ji C, Jin L, et al. Effects of Exenatide on metabolic changes, sexual hormones, inflammatory cytokines, adipokines, and weight change in a DHEA-treated rat model. *Reprod Sci*. 2016;23(9):1242–1249. doi:10.1177/1933719116635278

51. Xing C, Lv B, Zhao H, Wang D, Li X, He B. Metformin and exenatide upregulate hepatocyte nuclear factor-4α, sex hormone binding globulin levels and improve hepatic triglyceride deposition in polycystic ovary syndrome with insulin resistance rats. *J Steroid Biochem Mol Biol*. 2021;214:105992. doi:10.1016/j.jsbmb.2021.105992

52. Elkind-Hirsch K, Marrioneaux O, Bhushan M, Vernor D, Bhushan R. Comparison of single and combined treatment with exenatide and metformin on menstrual cyclicity in overweight women with polycystic ovary syndrome. *J Clin Endocrinol Metab*. 2008;93(7):2670–2678. doi:10.1210/jc.2008-0115

53. Dawson AJ, Sathyapalan T, Vince R, et al. The effect of Exenatide on cardiovascular risk markers in women with polycystic ovary syndrome. *Front Endocrinol (Lausanne)*. 2019;10:189. doi:10.3389/fendo.2019.00189

54. Zheng S, Liu E, Zhang Y, et al. Circulating zinc-α2-glycoprotein is reduced in women with polycystic ovary syndrome, but can be increased by exenatide or metformin treatment. *Endocr J*. 2019;66(6):555–562. doi:10.1507/endocrj.EJ18-0153

55. Ma RL, Deng Y, Wang YF, Zhu SY, Ding XS, Sun AJ. Short-term combined treatment with exenatide and metformin for overweight/obese women with polycystic ovary syndrome. *Chin Med J (Engl)*. 2021;134(23):2882–2889. doi:10.1097/CM9.0000000000001712

56. Tang L, Yuan L, Yang G, et al. Changes in whole metabolites after exenatide treatment in overweight/obese polycystic ovary syndrome patients. *Clin Endocrinol (Oxf)*. 2019;91(4):508–516. doi:10.1111/cen.14056

57. Elkind-Hirsch KE, Chappell N, Seidemann E, Storment J, Bellanger D. Exenatide, Dapagliflozin, or Phentermine/Topiramate differentially affect metabolic profiles in polycystic ovary syndrome. *J Clin Endocrinol Metab*. 2021;106(10):3019–3033. doi:10.1210/clinem/dgab408

58. Liu X, Zhang Y, Zheng SY, et al. Efficacy of exenatide on weight loss, metabolic parameters and pregnancy in overweight/obese polycystic ovary syndrome. *Clin Endocrinol (Oxf)*. 2017;87(6):767–774. doi:10.1111/cen.13454

59. Tao T, Zhang Y, Zhu YC, et al. Exenatide, metformin, or both for prediabetes in PCOS: A randomized, open-label, parallel-group controlled study. *J Clin Endocrinol Metab*. 2021;106(3):e1420–e1432. doi:10.1210/clinem/dgaa692

60. Bonora E, Frias JP, Tinahones FJ, et al. Effect of dulaglutide 3.0 and 4.5 mg on weight in patients with type 2 diabetes: Exploratory analyses of AWARD-11. *Diabetes Obes Metabol*. 2021;23(10):2242–2250. doi:10.1111/dom.14465

61. Wu LM, Wang YX, Zhan Y, et al. Dulaglutide, a long-acting GLP-1 receptor agonist, can improve hyperandrogenemia and ovarian function in DHEA-induced PCOS rats. *Peptides*. 2021;145:170624. doi:10.1016/j.peptides.2021.170624

62. Wilding JPH, Batterham RL, Calanna S, et al. Once-weekly semaglutide in adults with overweight or obesity. *N Engl J Med*. 2021;384(11):989–1002. doi:10.1056/NEJMoa2032183

63. Jensterle M, Ferjan S, Vovk A, Battelino T, Rizzo M, Janež A. Semaglutide reduces fat accumulation in the tongue: A randomized single-blind, pilot study. *Diabetes Res Clin Pract*. 2021;178:108935. doi:10.1016/j.diabres.2021.108935

64. ClinicalTrials. Treating PCOS With Semaglutide vs Active Lifestyle Intervention (TEAL). https://www.clinicaltrials.gov/ct2/show/NCT03919929?term=semaglutide&cond=pcos&draw=2&rank=1. Accessed May 27, 2021.

65. Kahal H, Kilpatrick E, Rigby A, Coady A, Atkin S. The effects of treatment with liraglutide on quality of life and depression in young obese women with PCOS and controls. *Gynecol Endocrinol*. 2019;35(2):142–145. doi:10.1080/09513590.2018.1505848

66. Jensterle M, Pirš B, Goričar K, Dolžan V, Janež A. Genetic variability in GLP-1 receptor is associated with inter-individual differences in weight lowering potential of liraglutide in obese women with PCOS: A pilot study. *Eur J Clin Pharmacol*. 2015;71(7):817–824. doi:10.1007/s00228-015-1868-1

67. Han Y, Li Y, He B. GLP-1 receptor agonists versus metformin in PCOS: A systematic review and meta-analysis. *Reprod Biomed Online*. 2019;39(2):332–342. doi:10.1016/j.rbmo.2019.04.017

68. Wang FF, Wu Y, Zhu YH, et al. Pharmacologic therapy to induce weight loss in women who have obesity/overweight with polycystic ovary syndrome: A systematic review and network meta-analysis: Pharmacologic therapy for weight management in PCOS. *Obes Rev*. 2018;19(10):1424–1445. doi:10.1111/obr.12720

69. Abdalla MA, Shah N, Deshmukh H, et al. Impact of pharmacological interventions on insulin resistance in women with polycystic ovary syndrome: A systematic review and meta-analysis of randomized controlled trials. *Clin Endocrinol (Oxf)*. 2022;96(3):371–394. doi:10.1111/cen.14623

70. Ma R, Ding X, Wang Y, Deng Y, Sun A. The therapeutic effects of glucagon-like peptide-1 receptor agonists and metformin on polycystic ovary syndrome: A protocol for systematic review and meta-analysis. *Medicine (Baltimore)*. 2021;100(23):e26295. doi:10.1097/MD.0000000000026295

71. Lyu X, Lyu T, Wang X, et al. The antiobesity effect of GLP-1 receptor agonists alone or in combination with metformin in overweight/obese women with polycystic ovary syndrome: A systematic review and meta-analysis. *Int J Endocrinol*. 2021;2021:6616693. doi:10.1155/2021/6616693

72. Tian D, Chen W, Xu Q, Li X, Lv Q. Liraglutide monotherapy and add on therapy on obese women with polycystic ovarian syndromes: A systematic review and meta-analysis. *Minerva Med*. 2021. doi:10.23736/S0026-4806.21.07085-3

73. Ge JJ, Wang DJ, Song W, Shen SM, Ge WH. The effectiveness and safety of liraglutide in treating overweight/obese patients with polycystic ovary syndrome: A meta-analysis. *J Endocrinol Invest*. 2022;45(2):261–273. doi:10.1007/s40618-021-01666-6

74. Papaetis GS. Empagliflozin therapy and insulin resistance-associated disorders: Effects and promises beyond a diabetic state. *Arch Med Sci Atheroscler Dis*. 2021;6:e57–e78. doi:10.5114/amsad.2021.105314

75. Kurzthaler D, Hadziomerovic-Pekic D, Wildt L, Seeber BE. Metformin induces a prompt decrease in LH-stimulated testosterone response in women with PCOS independent of its insulin-sensitizing effects. *Reprod Biol Endocrinol*. 2014;12:98. doi:10.1186/1477-7827-12-98

76. Maida A, Lamont BJ, Cao X, Drucker DJ. Metformin regulates the incretin receptor axis via a pathway dependent on peroxisome proliferator-activated receptor-α in mice. *Diabetologia*. 2011;54(2):339–349. doi:10.1007/s00125-010-1937-z

77. Moffett RC, Naughton V. Emerging role of GIP and related gut hormones in fertility and PCOS. *Peptides*. 2020;125:170233. doi:10.1016/j.peptides.2019.170233

78. Frías JP, Davies MJ, Rosenstock J, et al. Tirzepatide versus semaglutide once weekly in patients with type 2 diabetes. *N Engl J Med*. 2021;385(6):503–515. doi:10.1056/NEJMoa2107519

79. Spezani R, Mandarim-de-Lacerda CA. The current significance and prospects for the use of dual receptor agonism GLP-1/glucagon. *Life Sci*. 2022;288:120188. doi:10.1016/j.lfs.2021.120188

80. Bednarz K, Kowalczyk K, Cwynar M, et al. The role of Glp-1 receptor agonists in insulin resistance with concomitant obesity treatment in polycystic ovary syndrome. *Int J Mol Sci*. 2022;23(8):4334. doi:10.3390/ijms23084334

81. Reid TS. Practical use of glucagon-like peptide-1 receptor agonist therapy in primary care. *Clinical Diabetes*. 2013;31(4):148–157. doi:10.2337/diaclin.31.4.148

82. Fujioka K, O'Neil PM, Davies M, et al. Early weight loss with Liraglutide 3.0 mg predicts 1-year weight loss and is associated with improvements in clinical markers. *Obesity (Silver Spring)*. 2016;24(11):2278–2288. doi:10.1002/oby.21629

Pharmacotherapeutic pain management in patients undergoing laparoscopic cholecystectomy: A review

Baofang Jiang[1,A,B,D], Song Ye[2,C,E,F]

[1] Operating Room, Tianchang City People's Hospital, China

[2] Department of Anesthesiology, Tianchang City People's Hospital, China

A – research concept and design; B – collection and/or assembly of data; C – data analysis and interpretation;
D – writing the article; E – critical revision of the article; F – final approval of the article

Address for correspondence
Song Ye
E-mail: songye1965@outlook.com

Abstract

Laparoscopic cholecystectomy is widely performed because it results in a relatively easier pain management and shorter hospital stay. Although postoperative pain following laparoscopic cholecystectomy tends to be less intense compared to that following open cholecystectomy, early discomfort from operation after laparoscopy can be similar or even more intense than after open surgery. Consequently, it remains a source of apparent pain and surgical stress. Thus, proactive pain control is a priority for both patients and doctors. A considerable amount of new research about pain and pain management has been documented in the literature over the last 2 decades. In addition, novel medications and technologies for acute pain control after laparoscopic cholecystectomy have been investigated for patient care. Nevertheless, a significant proportion of patients still have excessively high pain levels after laparoscopic surgery. Acute pain after laparoscopic cholecystectomy is complicated in nature and has multiple causes; therefore, a single treatment modality is rarely sufficient. A combined approach to pain management is often the best option. In this review, the wide range of pharmacotherapeutic agents that have been used to control pain after laparoscopic surgery are critically assessed. The article also focuses on new techniques and medications that have been investigated in recent years to manage pain after laparoscopic surgery as quickly and safely as possible.

Key words: surgery, pain management, gallbladder, laparoscopic cholecystectomy, pharmacotherapeutics

Introduction

The gallbladder is a small organ located in the upper right abdomen. Bile, which aids in food digestion, is stored in the gallbladder. Gallstones are solid pieces of bile that form as a result of alterations in bile composition and concentration induced by hormones, dietary changes, drugs, and rapid weight loss or gain. Gallstones can sometimes migrate out of the gallbladder, obstructing the normal flow of bile and causing gallbladder inflammation and infection. Continuous sharp abdominal discomfort, fever, nausea, and vomiting are all possible symptoms.[1] The gallbladder can be removed in a minimally invasive manner using laparoscopic cholecystectomy. The most common reasons for laparoscopic cholecystectomy are choledocholithiasis (gallstones in the bile duct), cholelithiasis (cholesterol stones) and acute cholecystitis (inflammation of the gallbladder wall).[2] Gallstones are divided into 2 types based on their composition: cholesterol stones and pigmented stones. Cholesterol stones are the more common type; they form when the amounts of cholesterol and bile salts in the gallbladder are out of equilibrium. Cholesterol can precipitate out of the bile salt-lecithin-cholesterol micelles when the concentration of bile salts drops, resulting in cholesterol stones.[3] There are 2 categories of pigmented stones: black pigment stones and brown pigment stones. Patients with high levels of unconjugated bilirubin, which are most often caused by hemolytic blood dyscrasias, and patients with bile stasis caused by gallbladder hypoactivity, which is common in patients on complete parenteral nutrition, can develop black pigment stones.[4,5] Brown pigment stones usually develop from infected bile, which causes high calcium concentrations in the bile to precipitate, resulting in stone formation. Brown stones are more likely to occur in the intrahepatic or extrahepatic ducts than in the gallbladder.[6] During a meal, the gallbladder releases bile into the small intestine to facilitate fat digestion. Gallstones can become caught in the thin conduit (cystic duct) that links the gallbladder to the main bile duct (common bile duct) during this process. Pain, nausea and vomiting can occur as the gallbladder contracts to force the bile past the blockage. This causes persistent sharp pain that primarily affects the upper abdomen, back and right shoulder. If the stone becomes entirely trapped and cannot be moved into the small intestine, it can cause cholecystitis, bile duct obstruction and pancreatic inflammation (gallstone pancreatitis).[7]

Gallstones are a common ailment in developed countries, but they are less common in developing communities that still eat traditional diets.[8] Intestinal hypomotility has recently been identified as a major contributor to cholesterol lithogenesis. Fiber may help prevent gallstone development by accelerating intestinal transit and decreasing the production of secondary bile acids, such as deoxycholate, which has been linked to a higher bile cholesterol saturation.[9–11] Gallbladder diseases can be affected by various factors, such as drugs,[12–14] diet (i.e., fried foods, fatty red meat, highly processed foods),[15] obesity,[16,17] physical activity,[18,19] gender and oral contraceptives,[20] rapid weight loss,[21,22] diabetes,[23,24] genetics,[25,26] and age,[27–29] which are presented in Fig. 1.

In this review, a wide range of pharmacotherapeutic agents that have been used to control pain after laparoscopic surgery are critically assessed. The article also focuses on new techniques and medications that have been investigated in recent years to manage pain after laparoscopic surgery as quickly and safely as possible.

Materials and methods

Sources for this review article were collected from electronic scientific databases, including ScienceDirect, PubMed, Scopus, and Google Scholar, as well as books and other reports. Various recent research and review papers were also studied to gain insight into pharmacotherapeutic treatments aimed at alleviating pain after laparoscopic surgery. Following an extensive literature survey, we collected relevant information on pain management after laparoscopic surgery. All of the collected information was classified into different sections according to the objective of the paper. To obtain the relevant articles, various keywords, namely "laparoscopic cholecystectomy", "gallbladder", "pain management", and "surgery", were used for the search. Among the 139 studies identified, 102 articles were shortlisted, and 37 articles were excluded due to insufficient data or not being suitable for the purposes of this review article. Of the 102 articles, 38 primarily focused on the introduction and factors influencing gallbladder diseases, 32 highlighted pharmacotherapeutic pain management in laparoscopic cholecystectomy using local anesthetics, 11 presented opioids used for pain management, and 21 investigated the role of non-opioids in pain management (Fig. 2).

Laparoscopic and open cholecystectomy

The gold standard for the treatment of benign gallbladder problems is laparoscopic cholecystectomy.[30] This approach can be used in 90% of elective cholecystectomies and 70% of emergency cholecystectomies.[31] Acute cholecystitis, particularly if it is thick, can alter the aforementioned paradigm, requiring conversion to open surgery or a technique adjustment. A difficult cholecystectomy is defined by the following criteria: need for conversion from laparoscopic to open surgery, length of the process greater than 180 min, blood loss greater than 300 mL, and urgent need for an experienced surgeon.[32] The gallbladder can be removed using one of two methods: open cholecystectomy or laparoscopic cholecystectomy. During an open cholecystectomy, a 10–15-cm long incision
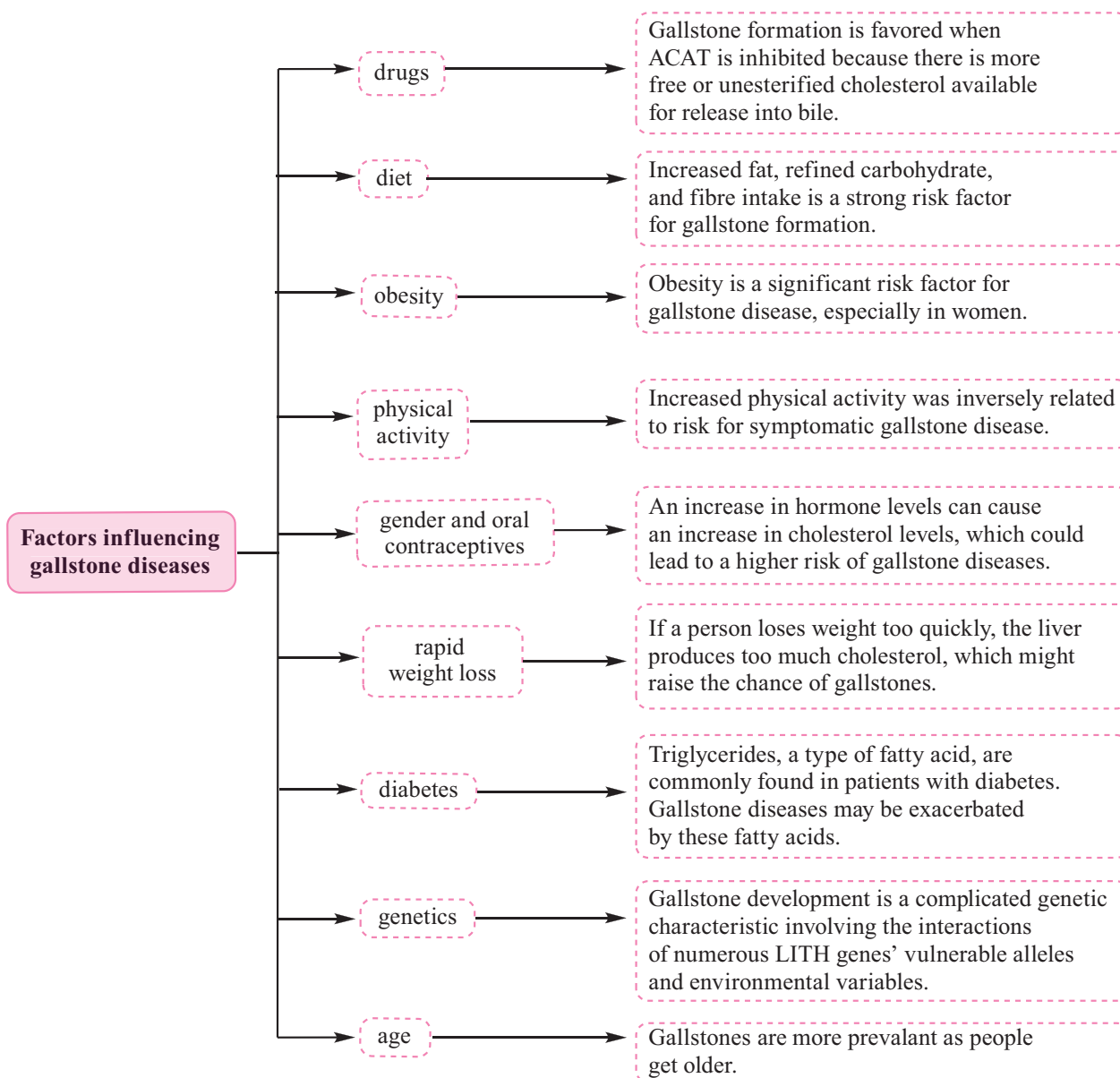
Fig. 1. Factors influencing gallstone diseases

is made in the right upper quadrant of the abdomen. The surgeon locates and removes the gallbladder through the incision. Conversely, in the laparoscopic cholecystectomy procedure, 3–4 very small incisions are performed. This technique employs a long, thin tube known as a laparoscope. A tiny video camera and surgical equipment are included in the tube. The tube, camera and instruments are inserted through the incisions. The surgeon can visualize the instruments and anatomy on video display monitors in real time. One of the incisions is used to remove the gallbladder (Fig. 3). A laparoscopic cholecystectomy is less invasive than a traditional open cholecystectomy because 3–4 tiny incisions are made in the abdomen rather than 1 large incision. There is less bleeding and, in most cases, the recovery time is shorter than following open operations. In some circumstances, the laparoscope may reveal that the gallbladder is severely diseased or unveil

additional technical issues. The surgeon may then have to convert to open surgery to safely and securely remove the gallbladder. Because laparoscopic cholecystectomy has largely replaced open cholecystectomy for benign gallbladder disease, many gallbladder cancers are discovered incidentally during or after laparoscopic cholecystectomy.[33] The need for open cholecystectomies has diminished since the introduction of laparoscopic cholecystectomy. The most common reason for an open cholecystectomy (2–10% of the cases) is a conversion from a laparoscopic to an open procedure. This modification is elected for a number of reasons. Surgeons may switch to the open method if there is a concern about the anatomy of the gallbladder. Inflammation, adhesions, anatomical differences, bile duct injury, retained bile duct stones, and uncontrollable bleeding are all indications that the operation should be converted to open surgery.[34]
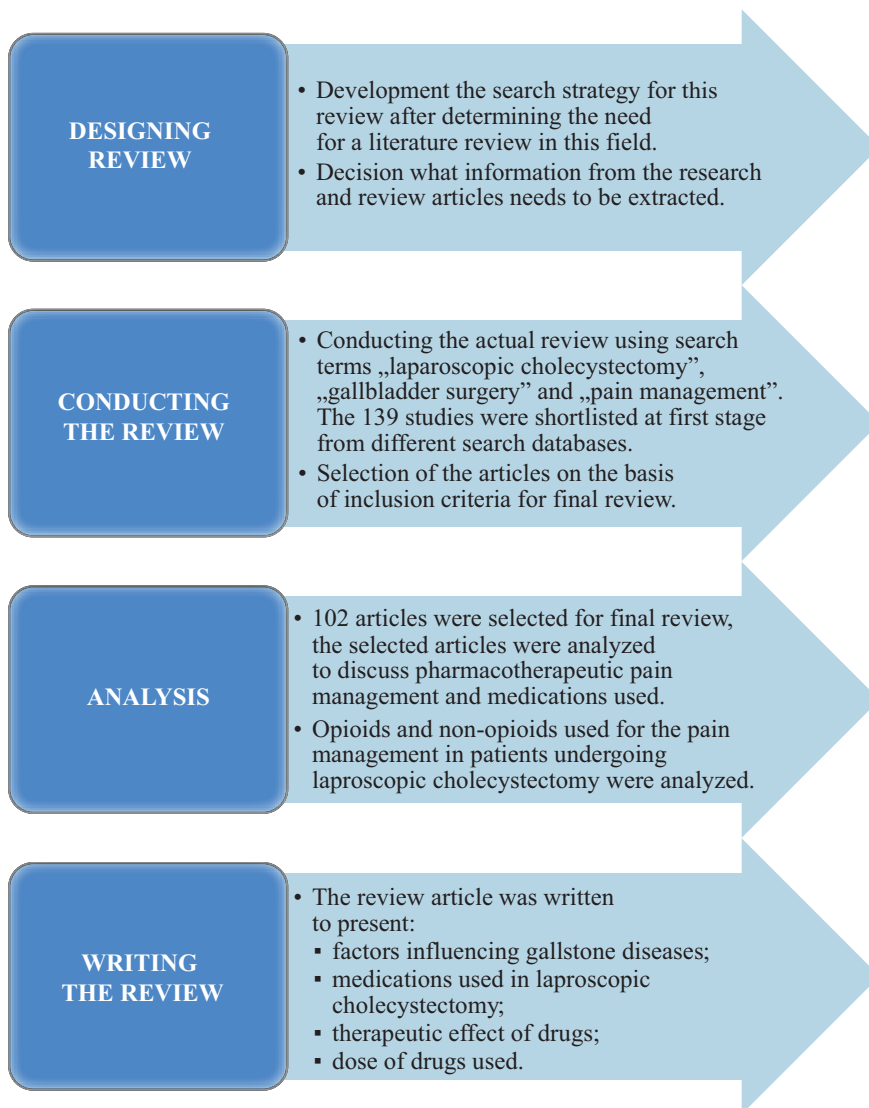
Fig. 2. The 4-step methodology adopted for conducting the literature review

DESIGNING REVIEW
- Development the search strategy for this review after determining the need for a literature review in this field.
- Decision what information from the research and review articles needs to be extracted.

CONDUCTING THE REVIEW
- Conducting the actual review using search terms „laparoscopic cholecystectomy", „gallbladder surgery" and „pain management". The 139 studies were shortlisted at first stage from different search databases.
- Selection of the articles on the basis of inclusion criteria for final review.

ANALYSIS
- 102 articles were selected for final review, the selected articles were analyzed to discuss pharmacotherapeutic pain management and medications used.
- Opioids and non-opioids used for the pain management in patients undergoing laproscopic cholecystectomy were analyzed.

WRITING THE REVIEW
- The review article was written to present:
  - factors influencing gallstone diseases;
  - medications used in laproscopic cholecystectomy;
  - therapeutic effect of drugs;
  - dose of drugs used.

Methods for removal of gallbladder

Open cholecystectomy

Laproscopic cholecystectomy

A 10–15-cm long incision is made in upper right hand of abdomen. Gallbladder is removed through incision by surgeon.

3–4 small incisons are made through which camera, tube and tools are inserted. Surgery is performed by the surgeon using a video monitor to visualize the operating field.

Fig. 3. Methods for gallbladder removal (open and laparoscopic cholecystectomy)

Inappropriate patient selection, surgical inexperience and technological limitations inherent in the less invasive procedure can all contribute to serious complications of laparoscopic cholecystectomy, including bile duct injury, bile leakage, hemorrhage, and intestine injury.[35,36] Diathermy burns are a common cause of ductal injuries that may go initially unreported; they mainly affect the right or common hepatic ducts. These considerations, as well as the inherent complications of biliary tract illnesses, such as inflammation and scarring, have led to the development of "stop rules" for surgeons performing this procedure. Specifically, when a safe dissection cannot be achieved laparoscopically, an early open approach should be considered the best option.[37,38]

Pharmacotherapeutic pain management during laparoscopic cholecystectomy

Laparoscopic surgery has several advantages over open surgery, including less postoperative pain, smaller incisions, shorter postoperative ileus, less blood loss, shorter hospital stay, faster recovery, and earlier return to preoperative activities and work.[39–41] Reduced postoperative pain is one of the most significant advantages of laparoscopy when compared to open surgery. However, a discomfort from the operation cannot be completely prevented, so several pharmacotherapeutic options are available.[42] Pain following laparoscopic cholecystectomy has been shown to increase morbidity and is the major cause of extended hospitalization.[43] Incisional pain may still be present at the laparoscopic port insertion sites. Abdominal discomfort can vary in intensity and is linked to the extent of surgery and manipulation.[44]

Patients commonly complain of upper abdominal, back and right shoulder pain, as well as discomfort from the port incision sites. Shoulder and subdiaphragmatic discomfort affect between 12% and 60% of patients. The level of discomfort peaks within the first few hours after surgery and usually decreases after 2 or 3 days.[45–47] Pain following laparoscopic cholecystectomy has a complex origin. Peritoneal insufflation with CO_2 and phrenic nerve irritation in the peritoneal cavity are 2 possible causes of discomfort after laparoscopy.[48–50] In fact, in laparoscopic cholecystectomy, the acidic environment formed by CO_2 gas dissolution can cause peritoneal irritation and phrenic nerve injury. Effective pain relief is of the utmost importance for anyone treating patients undergoing surgery.

One of the most important aspects of enhanced recovery after surgery (ERAS) programs, and indeed all anesthetic care, is effective analgesia. It is important for minimizing postoperative stress, encouraging a return to regular functions like breathing, eating and sleeping, and supporting early mobilization. It may also help reduce organ dysfunction and expedite hospital discharge.[51] Various medications are used to relieve pain during and after laparoscopic cholecystectomy.

Local anesthetics

Lidocaine

Lidocaine 1 (Fig. 4) is an amino-amide local anesthetic that reduces neuronal transmission by inhibiting sodium channels. It provides analgesia, reduces the need for opioids, and alleviates nausea and vomiting symptoms. It also reduces the risk of ileus when administered as a systemic infusion.[52] Local anesthetics block nociceptive input into the central nervous system, have anti-inflammatory

properties and are often very helpful in neuropathic pain. Furthermore, selective sympathetic blockade can be particularly beneficial for visceral pain at lower local anesthetic dosages. Unfortunately, the therapeutic ratio of local anesthetics for pain management after laparoscopy is low. Intravenous local anesthetics are linked to neurological and tissue toxicity at higher tissue and systemic doses, and high plasma concentrations can have substantial negative central nervous system and cardiovascular consequences. Furthermore, interindividual variability in local anesthetic tolerance exists.[53] Intravenous lidocaine infusion (lidocaine is given at steady rate at low doses) is a good alternative for postoperative pain relief for these reasons.[54] Different doses have been used; typically, a bolus of 1–1.5 mg/kg is administered, followed by a 2–3 mg/kg/h infusion that lasts until the completion of surgery or for the first 24 h afterwards.[55] Neurological changes, such as lightheadedness, dizziness and visual disturbances, as well as cardiac dysrhythmias are extremely rare side effects of perioperative lidocaine infusion.[56]

Intraperitoneal instillation and nebulization

Intraperitoneal instillation of local anesthetics has been used in laparoscopic cholecystectomy to lessen postoperative pain and the need for postoperative analgesics.[57] After laparoscopic cholecystectomy, intraperitoneal instillation of bupivacaine 2 (Fig. 4) 100 mg with adrenaline was as efficacious as a similar volume (80 mL) of normal saline.[58] Surgical maneuvers, disturbance of the peritoneum and dissection of the viscera cause peritoneal nerve irritation, resulting in visceral and shoulder pain during and after laparoscopic cholecystectomy. Sedation, nausea, delayed stomach emptying, and respiratory depression are all adverse effects of using opioids to manage this pain. Therefore, according to various studies, instillation and nebulization of local anesthetics into the peritoneal cavity can be used to reduce discomfort following laparoscopic surgery as an alternative to opioids. Sandhya et al. investigated and employed ropivacaine 3 (Fig. 4) for intraperitoneal nebulization because it has lower toxicity and is as effective as bupivacaine.[59] Dose-finding research discovered that 50 mg of nebulized ropivacaine provided acceptable analgesia in individuals undergoing laparoscopic cholecystectomy. An increase in the ropivacaine dose did not result in any additional benefits. Pain alleviation was adequate for patients administered a smaller dose of 30 mg of ropivacaine.[59] (Fig. 4).

Central neuraxial blocks

Studies have found that epidural analgesia using bupivacaine 2 or chloroprocaine 4 (Fig. 4) was superior to intravenous opioid analgesia for pain control after laparoscopic surgery.[60] The use of epidural analgesia appears to be safe and
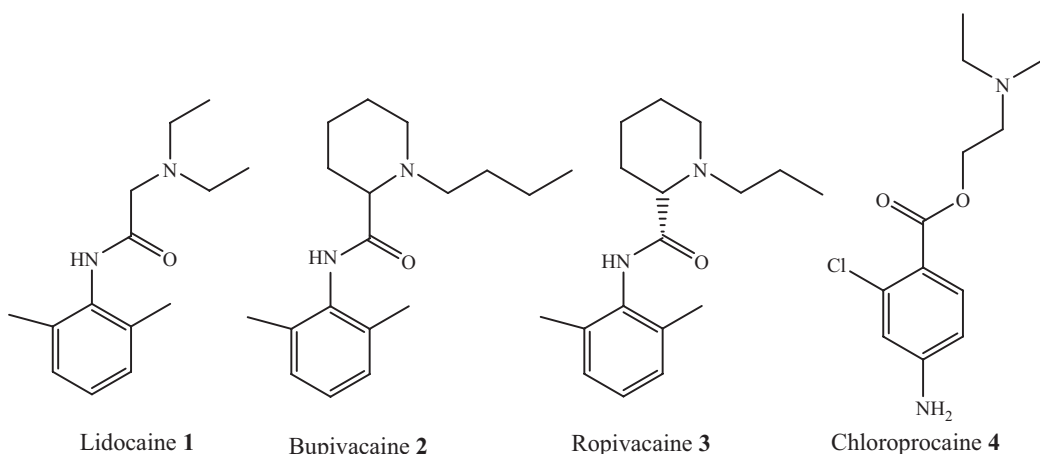
Fig. 4. Local anesthetics for pain management during laparoscopic cholecystectomy

Lidocaine **1**   Bupivacaine **2**   Ropivacaine **3**   Chloroprocaine **4**

effective after major abdominal laparoscopic surgery. However, it is associated with longer hospital stays and higher rates of urinary tract infections; these are the consequences of urinary catheters, which often accompany this treatment method.[61] Anticoagulants and other drugs that impair hemostatic function are becoming more widely used, which may limit the use of epidural analgesia during laparoscopic surgery, despite its effectiveness in pain control. Intrathecal indwelling catheters are also linked to an increased risk of infectious problems, which is concerning given the multidrug-resistant bacterial outbreaks that have become common over the last 2 decades. As a result, following careful analysis of the risks and benefits, the decision to use epidural analgesia should be made on an individual basis.[62]

Transversus abdominis plane block

A transversus abdominis plane (TAP) block is a peripheral nerve block that achieves abdominal wall anesthesia. The procedure can be performed using a surface landmark-based technique, laparoscopically or with ultrasound guidance. Proponents believe that TAP blocks have a lower risk of complications and are more acceptable to patients than epidural analgesia. Research has examined the effects of TAP rectus sheath blocks on pain relief following abdominal surgery, but there is not enough information on the method of localization, timing, dosages, and volumes of local anesthetic. Transversus abdominis plane blocks are obviously influenced by operator skill and can be unpredictable.[63] Use of TAP blocks in colorectal surgery has been the subject of recent research. Transversus abdominis plane blocks plus intravenous acetaminophen in laparoscopic colorectal surgery resulted in earlier resumption of eating and discharge from hospital in an accelerated recovery regimen compared to patient-controlled analgesia (PCA) with morphine.[64] In an open right hemicolectomy study from 2012, TAP+PCA was compared with subcutaneous local infiltration+PCA.[65] In the TAP arm, there was less PCA morphine use and less sedation after 24 h. Similarly, Conaghan et al. found that TAP+PCA reduced intravenous opioid use in laparoscopic colorectal

resections compared to PCA alone. Although there are data showing that TAP blocks improve pain scores and reduce opioid consumption following abdominal surgery, more research is needed to compare TAP blocks with other pain management methods, such as epidural anesthesia.[66]

Ultrasound-guided TAP nerve blocks have become a common analgesic method after abdominal wall surgery. Because TAP blocks are confined to somatic anesthesia of the abdominal wall and are heavily reliant on interfascial dissemination, a number of innovative approaches have been developed to improve analgesia, either in conjunction with TAP nerve blocks or as standalone modalities.[67]

Several trials have determined that ultrasound-guided TAP blocks, as a part of a multimodal analgesic approach to postoperative analgesia, increase patient satisfaction and reduce opioid use. Given that the greatest amount of pain during the 24 h after laparoscopic cholecystectomy occurs at the trocar sites, it is critical to determine the best time to perform TAP blocks (before or after surgery) to maximize block effectiveness. Rahimzadeh et al. found that ultrasound-guided TAP blocks reduced the use of pethidine in the postoperative group compared to the preemptive group, thus lowering opioid analgesic side effects, including nausea, vomiting, pruritus, and dizziness. A transversus abdominis plane block is an affordable, straightforward and easy-to-perform treatment that can be used as part of a multimodal analgesic strategy.[68]

Incisional infiltration of local anesthetic

Local anesthetics are widely used in numerous medical and surgical specialties, including anesthesia, ophthalmology, otorhinolaryngology, dentistry, urology, and aesthetic surgery. They cause superficial loss of pain sensation after direct injection. Their delivery and effectiveness can be enhanced by using free bases, increasing the drug concentration, lowering the melting point, employing physical and chemical permeation enhancers, and using lipid delivery vesicles. Several studies have found that local anesthesia reduces postoperative pain after laparoscopic procedures, but there are few data on the effect of local

anesthesia on nausea in the postoperative period.[69] Inan et al. examined the effects and timing of local anesthesia during laparoscopic surgery on postoperative pain, nausea, and opioid and antiemetic requirements. Their prospective study included 142 individuals who underwent laparoscopic cholecystectomy. Fifty-three individuals did not receive any local anesthetics during surgery (group A). In group B, 46 patients had their skin, subcutis, fascia and parietal peritoneum infiltrated with 0.5% bupivacaine hydrochloride at the trocar sites prior to insertion. At the conclusion of surgery, local anesthetic was administered in similar doses and in the same manner to the remaining 43 patients (group C). When compared to patients in groups B and C, group A had a statistically significantly higher requirement for analgesics. The mean analgesic doses were substantially higher in group B than in group C after surgery. In group A, the period between the first antiemetics was much shorter than in group C. Using trocar sites to administer local anesthetic to the skin, subcutis, fascia, and parietal peritoneum lowered the need for postoperative analgesics as well as pain severity.[70]

Opioids

Opioids are the most commonly recommended drugs for the treatment of acute and chronic postoperative pain. The greatest challenges to successful opioid analgesia are underestimation of pain, prolonged duration of action and fear of addiction. Opioid receptors in the cell membranes of the presynaptic nerve terminals in the central nervous system mediate the bulk of the pharmacological actions of opioids.[71] Opioids have long been considered an important aspect of postoperative pain management, but they have many negative effects, including urinary retention, ileus, nausea, vomiting, pruritus, respiratory depression, and central nervous system depression. In surgical patients, these side effects are linked to higher mortality, longer duration of stay, greater risk of readmission, and higher healthcare expenses. Therefore, constant monitoring of breathing and oxygen saturation in patients using opioids after surgery is critical.[72] Despite years of progress in pain management, opioids remain the basis of postoperative pain management in many situations. Numerous opioids used for postoperative pain management in laparoscopic cholecystectomy are discussed below (Fig. 5).

Morphine

Morphine 5 (Fig. 5) is the most common opiate. At one time, it was the gold standard for postoperative pain. It has a quick onset of action, with a peak effect of 1–2 h. Fentanyl and hydromorphone are synthetic derivatives of morphine that are more potent, have faster onsets of action and shorter half-lives. Only a few pain studies have compared morphine to other opioids following
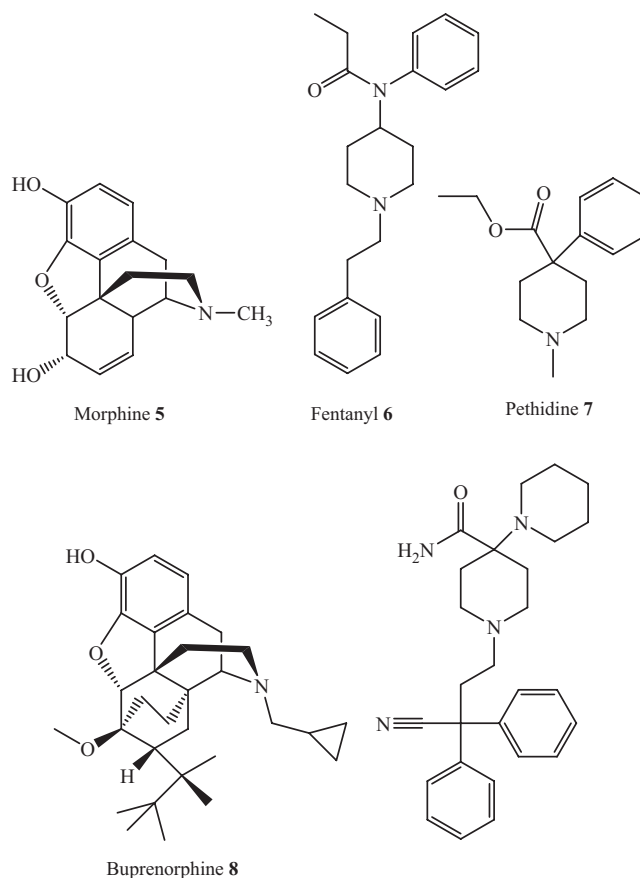
Fig. 5. Opioid drugs used in pain management during laparoscopic cholecystectomy

laparoscopy. Naguib et al. found that morphine is superior to tramadol in terms of perioperative pain control for patients undergoing laparoscopic cholecystectomy. In a small study of people who underwent laparoscopic colorectal surgery, epidural ropivacaine 2 mg/mL was contrasted with intravenous morphine for postoperative pain relief. Although epidural ropivacaine had significant opioid-sparing efficacy and sooner recovery of bowel movement, 20% of patients experienced motor block.[73] In addition, a low dose of intrathecal morphine appears to be particularly beneficial in controlling pain following laparoscopy. Patients undergoing laparoscopic colorectal surgery received a 15 mg bupivacaine spinal injection with or without 0.2 mg morphine. At this low dose, morphine was extremely effective. Throughout the first 24 postoperative hours, both rescue intravenous morphine use (10 mg compared to 30 mg) and dynamic pain levels were markedly lower in the bupivacaine and morphine group compared to the intrathecal bupivacaine only group.[74]

Fentanyl

Fentanyl 6 (Fig. 5) is an artificial opioid agonist that has a potency of 100 times that of morphine and 75 times that of oxycodone. Fentanyl is a lipophilic drug that quickly enters the central nervous system. Intravenous fentanyl

is commonly used for anesthesia and analgesia during surgery.[75] Fentanyl is mainly metabolized in the liver and intestinal mucosa, so it is not administered orally. Fentanyl, like oxycodone, is rapidly absorbed by mucosal membranes after intraoral and intranasal administration. Transmucosal fentanyl may be a viable approach to acute pain management. However, transmucosal delivery is only used to treat cancer pain that has become unbearable. The most important concern with the use of fentanyl for acute pain management is its low utility function, which means that the dosage required for effective pain relief is higher than the dose that can cause respiratory depression.[76]

Pethidine (meperidine)

Pethidine has been used for many years to relieve pain caused by laparoscopic surgery. However, because it contains an active metabolite (norpethidine) that is toxic to the central nervous system, it is not the ideal opioid. Norpethidine has a 14–21-hour elimination half-life, which can extend to 35 h in cases of renal failure. When pethidine 7 (Fig. 5) is administered in high doses, the level of norpethidine rises, putting vulnerable patients at risk of side effects.[77] Intraperitoneal pethidine with or without local anesthetic instillation was compared by Fogach et al. to intramuscular pethidine and intraperitoneal local anesthetic instillation. In addition to the toxicity of the metabolite norpethidine on the central nervous system, the parent chemical pethidine causes local discomfort.[78]

Buprenorphine

Buprenorphine 8 (Fig. 5) can operate as both an opioid agonist and antagonist. This chemical is a viable option for pain management in laparoscopy because both injectable and sublingual versions are available. It has 30 times the analgesic effectiveness of morphine in opioid-naïve patients. Buprenorphine has high transmucosal absorption, and the analgesia lasts substantially longer (6–8 h) than when morphine is used. No dose adjustments are required for elderly patients and patients with diminished renal function. Buprenorphine has a generally favorable safety profile; it rarely causes clinically significant respiratory depression, euphoria or sedation. Buprenorphine has a positive utility function.[79]

Piritramide

Piritramide 9 (Fig. 5), a 4-amino piperidine derivative, is used in several European countries and is structurally similar to pethidine. Piritramide has a wide volume of distribution (4.7 L/kg) and a long terminal half-life (7–8 h). It is almost entirely processed by the liver, with only approx. 1% being removed by the kidneys.[80] The analgesic potency of piritramide is comparable to that of morphine; a dose of 15–20 mg administered intramuscularly provides analgesia similar to 10–15 mg of morphine administered intramuscularly, and the analgesic ratio with oxycodone ranges between 1.6 and 2.2 (piritramide:oxycodone).[81]

Non-opioids

Opioid receptor agonist medications are being increasingly used for the treatment of a wide range of chronic pain problems. Tolerance and opioid-induced hyperalgesia can develop as a result of opioid use, which can contribute to long-term postsurgical pain. Furthermore, opioid use in the postoperative setting has been associated with a higher risk of persistent opioid addiction, which is particularly concerning considering the current national opioid abuse epidemic.[82] As a result, enhanced recovery pathways (ERPs) normally use opioid drugs sparingly, only when other therapies have failed, and only in conjunction with non-opioid analgesic treatments (Table 1).[83] Patients with chronic pain who are taking opioids before surgery are more likely to encounter significant postoperative pain, poor postoperative pain control, and opioid-related adverse effects. Hence, non-opioid analgesic modalities are especially important for this patient population. Several non-opioid medications used in pain management in patients undergoing laparoscopic cholecystectomy are discussed below (Fig. 6).

Nonsteroidal anti-inflammatory drugs

Ibuprofen, ketorolac and celecoxib are examples of nonsteroidal anti-inflammatory drugs (NSAIDs) that cause analgesia by blocking the cyclooxygenase enzyme and interrupting prostaglandin synthesis.[84–86] Nonsteroidal anti-inflammatory drugs are significant adjuncts in a multimodal analgesia regimen for the management of postoperative pain and are effective therapies for postoperative pain.[87] When NSAIDs and acetaminophen are used together, they have an additive or potentially synergistic analgesic effect. Furthermore, NSAID use has been linked to a reduced likelihood of opioid-related side effects, such as nausea, vomiting and drowsiness. Nonsteroidal anti-inflammatory drugs are associated with an increased risk of gastrointestinal ulcers, bleeding and renal impairment despite the fact that they are generally well tolerated. Celecoxib, an NSAID that selectively inhibits the cyclooxygenase-2 (COX-2) enzyme, may lessen the risk of gastrointestinal disturbances and bleeding. It should be noted, however, that COX-2 inhibitors are usually avoided following cardiac surgery because they increase the risk of negative cardiovascular consequences.[88] The inhibition of the enzyme cyclooxygenase is the principal mechanism of action of NSAIDs. Arachidonic acid is converted into thromboxane, prostaglandins and prostacyclin by the enzyme cyclooxygenase. The absence of these eicosanoids is thought to be responsible for the therapeutic effects of NSAIDs.[89]
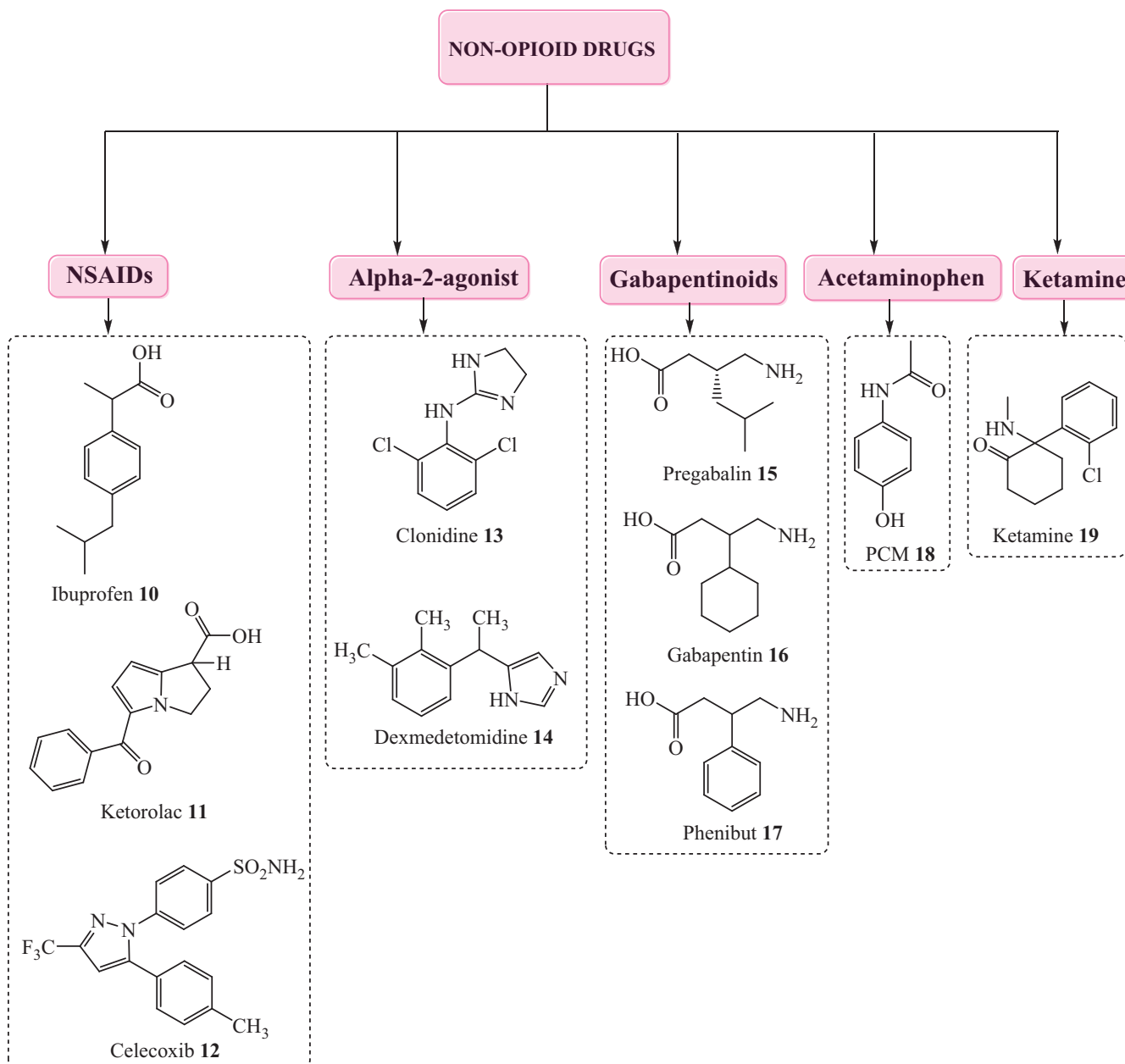
Fig. 6. Structures of non-opioid drugs used in pain management during laparoscopic cholecystectomy

Alpha-2 agonists

Analgesia can be produced by alpha-2 agonists, such as clonidine and dexmedetomidine, which stimulate alpha-2 receptors in the dorsal horn of the spinal cord and reduce nociceptive signal transmission. While these medications can be administered in a variety of ways, clonidine is usually administered intravenously or orally for postoperative pain relief, while dexmedetomidine is usually administered intravenously. Despite the lack of data to support these claims, clonidine and dexmedetomidine can be administered as adjuvants in epidurals and peripheral nerve plugs to potentially improve and prolong analgesia.[90] A study conducted by Rabie and Abdelfattah demonstrated that in patients undergoing laparoscopic cholecystectomy,

an intravenous infusion of 0.6 g/kg/h dexmedetomidine before induction can minimize hemodynamic stress, incidence of cough, postoperative nausea and vomiting, as well as reduce postoperative analgesic requirements, without significantly prolonging the spontaneous respiratory recovery period.[91] Alpha-2 agonists work by stimulating presynaptic alpha-2 receptors, which activate inhibitory neurons in the central nervous system, resulting in a decrease in sympathetic output via a signaling pathway.[92]

Gabapentinoids

Gabapentinoids, such as gabapentin and pregabalin, are antiepileptic drugs that work by inhibiting voltage-gated calcium channels to generate analgesia. Traditionally, these

Table 1. Nonopioid drugs used in pain management in laparoscopic cholecystectomy

Nonopioid drugs	Description	Advantages	Disadvantages
NSAIDs	NSAIDs such as ibuprofen,[10] ketorolac[11] and celecoxib[12] produce analgesia by inhibiting prostaglandin synthesis through inhibiting the cyclooxygenase enzyme.	Better pain control, synergistic analgesic effect when paired with acetaminophen, reduced opioid consumption.	Gastrointestinal ulcers, bleeding, renal dysfunction, and cardiovascular problems are all possible side effects. After colorectal surgery, it may be associated with anastomotic leak.
Alpha-2 agonists	Analgesia is produced by alpha-2 agonists such as clonidine[13] and dexmedetomidine,[14] which stimulate alpha-2 receptors in the dorsal horn of the spinal cord and reduce nociceptive signal transmission.	Better pain control, reduced opioid usage; used as a supplement to regional anesthetic techniques.	Sedation, hypotension and bradycardia are all possible side effects. There is little evidence to support its usage in the postoperative situation.
Gabapentinoids	Gabapentinoids, such as pregabalin,[15] gabapentin[16] and phenibut,[17] are antiepileptic drugs that work by inhibiting voltage-gated calcium channels to generate analgesia.	Reduced reliance on opioids, improved pain control.	Sedation risk, vision impairment and respiratory depression. Cautious use required in patients with renal insufficiency. Available only in oral forms. Optimal dose regimen uncertain.
Acetaminophen	In ERPs, acetaminophen (PCM)[18] is a key component of multimodal postoperative pain management. Though the exact etiology is uncertain, its analgesic effect is thought to be mediated mostly by cyclooxygenase pathway inhibition.	When used with nonsteroidal anti-inflammatory medicines, it has a synergistic analgesic effect. Generally well-tolerated, better pain management, opioid needs are reduced.	Hepatotoxicity at larger doses should be avoided in persons with liver disease.
Ketamine	Ketamine[19] is a dissociative anesthetic that blocks the transmission of pain signals by antagonizing NMDA receptors in the brain and spinal cord.	Lower risk of opioid-induced hyperalgesia and tolerance, reduced opioid usage, better pain control.	Optimal dose regimen unknown in individuals with cardiovascular illness, hepatic impairment, high intracranial and intraocular pressure, active psychosis, and pregnancy. Neuropsychiatric symptoms are a possibility.

NSAIDs – nonsteroidal anti-inflammatory drugs; ERP – Enhanced Recovery Pathway; NMDA – N-methyl-D-aspartate.

medications have been used to treat chronic neuropathic pain. There is research suggesting that gabapentinoids may lower initial postoperative pain, opiate requirements, and postoperative nausea and vomiting when used perioperatively.[93] Gabapentinoids, however, have been linked to drowsiness, visual abnormalities and dizziness, all of which can impair early postoperative mobilization and delay recovery. Furthermore, perioperative gabapentin use has been linked to an increased risk of respiratory depression, particularly in older patients and those taking large opioid doses.[94] Gabapentinoids are commonly prescribed for neuropathic pain, restless legs syndrome and focal seizures. Their effectiveness in these conditions is due to their ability to inhibit the actions of the $\alpha2\delta$ subunits of presynaptic voltage-gated calcium channels and thereby lower neurotransmitter release.[95]

Acetaminophen

Acetaminophen is a key component of multimodal postoperative pain management in ERPs. Although its exact mechanism of action is unknown, its analgesic impact is considered to be mediated mostly through suppression of the cyclooxygenase pathway. In nearly half of patients with mild to severe acute postoperative pain, a single dose of acetaminophen has been shown to offer 50% pain reduction for 4 h. When acetaminophen is used with NSAIDs, the analgesic effect can be additive or even synergistic. Furthermore, acetaminophen use has been linked to a lower need for opioids throughout the postoperative period.[96] Thus, oral acetaminophen is recommended in people who can tolerate it, while intravenous acetaminophen is effective in patients who cannot tolerate oral consumption or have reduced gastrointestinal tract function.[97] Acetaminophen works by inhibiting cyclooxygenases (COX-1, COX-2 and COX-3) as well as interfering with the endocannabinoid system and serotonergic pathways.[98] According to the study conducted by Mulita et al., the combinations of pethidine/acetaminophen and parecoxib/acetaminophen exhibited equivalent analgesic effectiveness and proved better than acetaminophen monotherapy for the management of postoperative pain following laparoscopic cholecystectomy. Reducing opioid doses by using postoperative non-opioid analgesics is a vital strategy to limit drowsiness, reduced pulmonary function and constipation in postsurgical patients.[99]

Ketamine

Ketamine is a dissociative anesthetic that blocks the transmission of pain signals by antagonizing N-methyl-D-aspartate (NMDA) receptors in the brain and spinal cord. Subanesthetic intravenous ketamine infusions have been found to minimize opiate usage and enhance pain control without creating significant side effects.[100] Ketamine is a glutamate and NMDA receptor antagonist that is noncompetitive. It works by blocking HCN1 receptors. The specific dissociative action and partial agonism of opiate μ-receptors allow for persistent sedation and patient

comfort throughout painful procedures.[101] Ketamine has also been proven to minimize the incidence of postoperative nausea and vomiting when combined with an opioid regimen. Ketamine could potentially assist in preventing opioid-induced hyperalgesia and tolerance from developing. However, it is uncertain if ketamine use during surgery lessens the likelihood of persistent postsurgical discomfort. Neuropsychiatric symptoms, such as hallucinations and nightmares, are the most common negative consequences linked to the use of subanesthetic dosages of ketamine in the postoperative environment.[102]

Limitations of the study

Despite the extensive research conducted in this review article on pain management in patients undergoing laparoscopic cholecystectomy, there are some limitations. The mechanisms of action of some treatments are not fully described. In addition, the article focuses solely on the medications used in pain management of laparoscopic cholecystectomy, as well as the doses used. However, the pharmacokinetics and side effects of these drugs are not explained in detail. There is no diagrammatic representation of the laparoscopic cholecystectomy procedure. Some articles were excluded because they did not meet our requirements.

Conclusions

Gallstones are solid pieces of bile that form as a result of changes in bile concentration and composition. They can cause sharp, constant abdominal pain, fever, nausea, and vomiting. Gallstones are divided into 2 types based on their composition: cholesterol stones and pigmented stones. Gallstones are a common ailment in developed countries but less common in developing communities that still eat traditional diets. Gallbladder diseases can be influenced by many factors, including age, genetics, diabetes, physical activity, drugs, obesity, rapid weight loss, gender, and oral contraceptives. Sedentary lifestyle is linked to an increased risk of cholecystectomy. Increased estrogen levels in the bile as a result of pregnancy or hormone therapy may cause gallstone formation. Gallbladder contraction is reduced during fasting associated with severely fat-restricted diets. The gallbladder can be removed using one of the two methods: open cholecystectomy or laparoscopic cholecystectomy. A laparoscope is a long, thin tube with a video camera and surgical equipment inserted into it. Three to four tiny incisions are made in the abdomen to introduce the surgical instruments. The need for an open cholecystectomy has diminished since the introduction of laparoscopic surgery, but the surgeon may convert to the open method if there is a concern about anatomy or other challenges.

Pain following laparoscopic cholecystectomy has a complex origin. Numerous medications are used to relieve pain during and after surgery. Local anesthetics block nociceptive input into the central nervous system, have anti-inflammatory properties, and are often very helpful in neuropathic pain. Morphine is superior to tramadol in terms of perioperative pain control. Fentanyl is a very powerful lipophilic opiate that quickly enters the central nervous system. The use of epidural ropivacaine resulted in considerable opioid sparing and faster bowel movement recovery. Pethidine is inadequate for pain reduction at a dose of 50 mg. Buprenorphine has 30 times the analgesic effectiveness of morphine in opioid-naïve patients. Piritramide resembles pethidine structurally. Tolerance and opioid-induced hyperalgesia can develop as a result of opioid use. Nonsteroidal anti-inflammatory drugs are significant supplements to a multimodal analgesic regimen for the management of postoperative pain. The COX-2 inhibitors are normally avoided following cardiac surgery. Gabapentinoids are antiepileptic medications that work by inhibiting voltage-gated calcium channels to generate analgesia. Acetaminophen is a key component of multimodal postoperative pain management. Ketamine has been proven to minimize the incidence of postoperative nausea and vomiting.

ORCID iDs

Baofang Jiang https://orcid.org/0000-0002-8937-8143
Song Ye https://orcid.org/0000-0001-8589-1524

References

1. Kim SS, Donahue TR. Laparoscopic cholecystectomy. *JAMA*. 2018; 319(17):1834. doi:10.1001/jama.2018.3438
2. Sartin J. Alterations in function of the gallbladder and exocrine pancreas. In: Copstead LE, Banasik JL, eds. *Study Guide for Pathophysiology*. 5th ed. London, UK: Elsevier Health Sciences; 2013:741–752. http://public.ebookcentral.proquest.com/choice/publicfullrecord.aspx?p=2074388. Accessed July 14, 2022.
3. Carey MC. Pathogenesis of gallstones. *Am J Surg*. 1993;165(4):410–419. doi:10.1016/S0002-9610(05)80932-8
4. Tazuma S. Gallstone disease: Epidemiology, pathogenesis, and classification of biliary stones (common bile duct and intrahepatic). *Best Pract Res Clin Gastroenterol*. 2006;20(6):1075–1083. doi:10.1016/j.bpg.2006.05.009
5. Trotman BW. Pigment gallstone disease. *Gastroenterol Clin North Am*. 1991;20(1):111–126. PMID:2022417.
6. Lammert F, Gurusamy K, Ko CW, et al. Gallstones. *Nat Rev Dis Primers*. 2016;2(1):16024. doi:10.1038/nrdp.2016.24
7. Baiu I, Hawn MT. Gallstones and biliary colic. *JAMA*. 2018;320(15):1612. doi:10.1001/jama.2018.11868
8. Schwesinger WH, Kurtin WE, Page CP, Stewart RM, Johnson R. Soluble dietary fiber protects against cholesterol gallstone formation. *Am J Surg*. 1999;177(4):307–310. doi:10.1016/S0002-9610(99)00047-1
9. LaMont JT, Smith BF, Moore JRL. Role of gallbladder mucin in pathophysiology of gallstones. *Hepatology*. 1984;4(5 Suppl):51S–56S. doi:10.1002/hep.1840040809
10. Marcus SN, Heaton KW. Effects of a new, concentrated wheat fibre preparation on intestinal transit, deoxycholic acid metabolism and the composition of bile. *Gut*. 1986;27(8):893–900. doi:10.1136/gut.27.8.893
11. Njeze GE. Gallstones. *Niger J Surg*. 2013;19(2):49–55. doi:10.4103/1117-6806.119236
12. Kurtin WE, Schwesinger WH, Diehl AK. Age-related changes in the chemical composition of gallstones. *Int J Surg Investig*. 2000; 2(4):299–307. PMID:12678532.
13. Diehl AK, Sugarek NJ, Todd KH. Clinical evaluation for gallstone disease: Usefulness of symptoms and signs in diagnosis. *Am J Med*. 1990; 89(1):29–33. doi:10.1016/0002-9343(90)90094-T

14. Liddle RA, Goldstein RB, Saxton J. Gallstone formation during weight-reduction dieting. *Arch Intern Med*. 1989;149(8):1750–1753. PMID:2669662.

15. Raghu T. Dietary factors influencing the pathogenesis of gallstone disease in Kerala, India. *IJARS*. 2021;10(2):SO01–SO04. https://www.ijars.net/article_fulltext.asp?issn=0973-709x&year=2021&month=April&volume=10&issue=2&page=SO01-SO04&id=2615. Accessed May 29, 2022.

16. Bonfrate L, Wang DQH, Garruti G, Portincasa P. Obesity and the risk and prognosis of gallstone disease and pancreatitis. *Best Pract Res Clin Gastroenterol*. 2014;28(4):623–635. doi:10.1016/j.bpg.2014.07.013

17. Trotman BW, Petrella EJ, Soloway RD, Sanchez HM, Morris TA, Miller WT. Evaluation of radiographic lucency or opaqueness of gallstones as a means of identifying cholesterol or pigment stones: Correlation of lucency or opaqueness with calcium and mineral. *Gastroenterology*. 1975;68(6):1563–1566. PMID:1093922.

18. Donovan JM, Carey MC. Physical-chemical basis of gallstone formation. *Gastroenterol Clin North Am*. 1991;20(1):47–66. PMID:2022425.

19. Aune D, Leitzmann M, Vatten LJ. Physical activity and the risk of gallbladder disease: A systematic review and meta-analysis of cohort studies. *J Phys Act Health*. 2016;13(7):788–795. doi:10.1123/jpah.2015-0456

20. Valdivieso V, Covarrubias C, Siegel F, Cruz F. Pregnancy and cholelithiasis: Pathogenesis and natural course of gallstones diagnosed in early puerperium. *Hepatology*. 1993;17(1):1–4. PMID:8423030.

21. Gebhard RL, Prigge WF, Ansel HJ, et al. The role of gallbladder emptying in gallstone formation during diet-induced rapid weight loss. *Hepatology*. 1996;24(3):544–548. doi:10.1002/hep.510240313

22. Capron JP, Delamarre J, Herve MA, Dupas JL, Poulain P, Descombes P. Meal frequency and duration of overnight fast: A role in gall-stone formation? *Br Med J (Clin Res Ed)*. 1981;283(6304):1435. doi:10.1136/bmj.283.6304.1435

23. Aune D, Vatten LJ. Diabetes mellitus and the risk of gallbladder disease: A systematic review and meta-analysis of prospective studies. *J Diabetes Complications*. 2016;30(2):368–373. doi:10.1016/j.jdiacomp.2015.11.012

24. Koppisetti S, Jenigiri B, Terron MP, et al. Reactive oxygen species and the hypomotility of the gall bladder as targets for the treatment of gallstones with melatonin: A review. *Dig Dis Sci*. 2008;53(10):2592–2603. doi:10.1007/s10620-007-0195-5

25. Nakeeb A, Comuzzie AG, Martin L, et al. Gallstones: Genetics versus environment. *Ann Surg*. 2002;235(6):842–849. doi:10.1097/00000658-200206000-00012

26. Chuang SC, Hsi E, Lee KT. Genetics of gallstone disease. *Adv Clin Chem*. 2013;60:143–185. doi:10.1016/b978-0-12-407681-5.00005-2

27. Lopushinsky SR, Urbach DR. Gallstone disease in the elderly: Diagnosis and management. *Aging Health*. 2005;1(3):441–447. doi:10.2217/1745509X.1.3.441

28. Paumgartner G, Gerok W, Bertolotti M, Bortolotti S, Menozzi D. Ageing and bile acid metabolism: Studies on 7α hydroxylation of cholesterol in humans. In: Paumgartner G, Stiehl A, Gerok W, eds. *Trends in Bile Acid Research*. Proceedings of the 52nd Falk Symposium held in Freiburg, Federal Republic of Germany, June 9–11, 1988. Dordrecht, the Netherlands: Kluwer Academic Publishers; 1989:75–78. ISBN:0746201125.

29. Einarsson K, Nilsell K, Leijd B, Angelin B. Influence of age on secretion of cholesterol and synthesis of bile acids by the liver. *N Engl J Med*. 1985;313(5):277–282. doi:10.1056/NEJM198508013130501

30. Purzner RH, Ho KB, Al-Sukhni E, Jayaraman S. Safe laparoscopic subtotal cholecystectomy in the face of severe inflammation in the cystohepatic triangle: A retrospective review and proposed management strategy for the difficult gallbladder. *Can J Surg*. 2019;62(6):402–411. doi:10.1503/cjs.014617

31. Taki-Eldin A, Badawy AE. Outcome of laparoscopic cholecystectomy in patients with gallstone disease at a secondary level care hospital. *Arq Bras Cir Dig*. 2018;31(1):e1347. doi:10.1590/0102-672020180001e1347

32. Maehira H, Kawasaki M, Itoh A, et al. Prediction of difficult laparoscopic cholecystectomy for acute cholecystitis. *J Surg Res*. 2017;216:143–148. doi:10.1016/j.jss.2017.05.008

33. Zhao X, Li X, Ji W. Laparoscopic versus open treatment of gallbladder cancer: A systematic review and meta-analysis. *J Min Access Surg*. 2018;14(3):185–191. doi:10.4103/jmas.JMAS_223_16

34. Jones MW, Guay E, Deppen JG. Open cholecystectomy. In: *StatPearls*. Treasure Island, USA: StatPearls Publishing; 2022. http://www.ncbi.nlm.nih.gov/books/NBK448176/. Accessed July 14, 2022.

35. Khan MH, Howard TJ, Fogel EL, et al. Frequency of biliary complications after laparoscopic cholecystectomy detected by ERCP: Experience at a large tertiary referral center. *Gastrointest Endosc*. 2007;65(2):247–252. doi:10.1016/j.gie.2005.12.037

36. Binenbaum SJ, Goldfarb MA. Inadvertent enterotomy in minimally invasive abdominal surgery. *JSLS*. 2006;10(3):336–340. PMID:17212891.

37. Strasberg SM. Biliary injury in laparoscopic surgery. Part 1. Processes used in determination of standard of care in misidentification injuries. *J Am Coll Surg*. 2005;201(4):598–603. doi:10.1016/j.jamcollsurg.2005.05.009

38. Strasberg SM. Biliary injury in laparoscopic surgery. Part 2. Changing the culture of cholecystectomy. *J Am Coll Surg*. 2005;201(4):604–611. doi:10.1016/j.jamcollsurg.2005.04.032

39. Buanes T, Mjåland O. Complications in laparoscopic and open cholecystectomy: A prospective comparative trial. *Surg Laparosc Endosc*. 1996;6(4):266–272. PMID:8840447.

40. Mendoza-Sagaon M, Hanly EJ, Talamini MA, et al. Comparison of the stress response after laparoscopic and open cholecystectomy. *Surg Endosc*. 2000;14(12):1136–1141. doi:10.1007/s004640020035

41. Jatzko GR, Lisborg PH, Pertl AM, Stettner HM. Multivariate comparison of complications after laparoscopic cholecystectomy and open cholecystectomy. *Ann Surg*. 1995;221(4):381–386. doi:10.1097/00000658-199504000-00008

42. Boddy AP, Mehta S, Rhodes M. The effect of intraperitoneal local anesthesia in laparoscopic cholecystectomy: A systematic review and meta-analysis. *Anesth Analg*. 2006;103(3):682–688. doi:10.1213/01.ane.0000226268.06279.5a

43. Bisgaard T, Kehlet H, Rosenberg J. Pain and convalescence after laparoscopic cholecystectomy. *Eur J Surg*. 2001;167(2):84–96. doi:10.1080/110241501750070510

44. Sen S, Morrison B, O'Rourke K, Jones C. Analgesia for enhanced recovery after surgery in laparoscopic surgery. *Dig Med Res*. 2019;2:25. doi:10.21037/dmr.2019.08.09

45. Morsy K, Mohamad Abdalla E. Postoperative pain relief after laparoscopic cholecystectomy: Intraperitoneal lidocaine versus nalbuphine. *Ain Shams J Anaesthesiol*. 2014;7(1):40–44. doi:10.4103/1687-7934.128402

46. Alkhamesi NA, Peck DH, Lomax D, Darzi AW. Intraperitoneal aerosolization of bupivacaine reduces postoperative pain in laparoscopic surgery: A randomized prospective controlled double-blinded clinical trial. *Surg Endosc*. 2007;21(4):602–606. doi:10.1007/s00464-006-9087-6

47. Dey A, Malik VK. Shoulder tip pain following laparoscopic cholecystectomy: A randomized control study to determine the cause. *Indian J Surg*. 2015;77(Suppl 2):381–384. doi:10.1007/s12262-013-0849-9

48. Jackson SA, Laurence AS, Hill JC. Does post-laparoscopy pain relate to residual carbon dioxide? *Anaesthesia*. 1996;51(5):485–487. doi:10.1111/j.1365-2044.1996.tb07798.x

49. Tsimoyiannis EC, Siakas P, Tassis A, Lekkas ET, Tzourou H, Kambili M. Intraperitoneal normal saline infusion for postoperative pain after laparoscopic cholecystectomy. *World J Surg*. 1998;22(8):824–828. doi:10.1007/s002689900477

50. Wills VL, Hunt DR. Pain after laparoscopic cholecystectomy. *Br J Surg*. 2002;87(3):273–284. doi:10.1046/j.1365-2168.2000.01374.x

51. Saadati K, Razavi MR, Nazemi Salman D, Izadi S. Postoperative pain relief after laparoscopic cholecystectomy: Intraperitoneal sodium bicarbonate versus normal saline. *Gastroenterol Hepatol Bed Bench*. 2016;9(3):189–196. PMID:27458511.

52. Kranke P, Jokinen J, Pace NL, et al. Continuous intravenous perioperative lidocaine infusion for postoperative pain and recovery. *Cochrane Database Syst Rev*. 2015;(7):CD009642. doi:10.1002/14651858.CD009642.pub2

53. Bardsley H, Gristwood R, Baker H, Watson N, Nimmo W. A comparison of the cardiovascular effects of levobupivacaine and rac-bupivacaine following intravenous administration to healthy volunteers. *Br J Clin Pharmacol*. 1998;46(3):245–249. doi:10.1046/j.1365-2125.1998.00775.x

54. McCarthy GC, Megalla SA, Habib AS. Impact of intravenous lidocaine infusion on postoperative analgesia and recovery from surgery: A systematic review of randomized controlled trials. *Drugs*. 2010;70(9):1149–1163. doi:10.2165/10898560-000000000-00000

55. Yang SY, Kang H, Choi GJ, et al. Efficacy of intraperitoneal and intravenous lidocaine on pain relief after laparoscopic cholecystectomy. *J Int Med Res*. 2014;42(2):307–319. doi:10.1177/0300060513505493

56. Beaussier M, Delbos A, Maurice-Szamburski A, Ecoffey C, Mercadal L. Perioperative use of intravenous lidocaine. *Drugs*. 2018;78(12): 1229–1246. doi:10.1007/s40265-018-0955-x

57. Sharan R, Singh M, Kataria A, Jyoti K, Jarewal V, Kadian R. Intraperitoneal instillation of bupivacaine and ropivacaine for postoperative analgesia in laparoscopic cholecystectomy. *Anesth Essays Res*. 2018;12(2):377–380. doi:10.4103/aer.AER_6_18

58. Joris J, Thiry E, Paris P, Weerts J, Lamy M. Pain after laparoscopic cholecystectomy: Characteristics and effect of intraperitoneal bupivacaine. *Anesth Analg*. 1995;81(2):379–384. doi:10.1097/00000539-199508000-00029

59. Sandhya S, Puthenveettil N, Vinodan K. Intraperitoneal nebulization of ropivacaine for control of pain after laparoscopic cholecystectomy: A randomized control trial. *J Anaesthesiol Clin Pharmacol*. 2021;37(3):443–448. doi:10.4103/joacp.JOACP_358_19

60. Liu H, Hu X, Duan X, Wu J. Thoracic epidural analgesia (TEA) vs. patient controlled analgesia (PCA) in laparoscopic colectomy: A meta-analysis. *Hepatogastroenterology*. 2014;61(133):1213–1219. PMID:25436285.

61. Halabi WJ, Kang CY, Nguyen VQ, et al. Epidural analgesia in laparoscopic colorectal surgery: A nationwide analysis of use and outcomes. *JAMA Surg*. 2014;149(2):130–136. doi:10.1001/jamasurg.2013.3186

62. Christie IW, McCabe S. Major complications of epidural analgesia after surgery. Results of a six-year survey: Epidural complications. *Anaesthesia*. 2007;62(4):335–341. doi:10.1111/j.1365-2044.2007.04992.x

63. Charlton S, Cyna AM, Middleton P, Griffiths JD. Perioperative transversus abdominis plane (TAP) blocks for analgesia after abdominal surgery. *Cochrane Database Syst Rev*. 2010;(12):CD007705. doi:10.1002/14651858.CD007705.pub2

64. Zafar N, Davies R, Greenslade GL, Dixon AR. The evolution of analgesia in an 'accelerated' recovery programme for resectional laparoscopic colorectal surgery with anastomosis. *Colorectal Dis*. 2010; 12(2):119–124. doi:10.1111/j.1463-1318.2009.01768.x

65. Brady R, Ventham N, Roberts D, Graham C, Daniel T. Open transversus abdominis plane block and analgesic requirements in patients following right hemicolectomy. *Ann R Coll Surg Engl*. 2012;94(5): 327–330. doi:10.1308/003588412X13171221589856

66. Conaghan P, Maxwell-Armstrong C, Bedforth N, et al. Efficacy of transversus abdominis plane blocks in laparoscopic colorectal resections. *Surg Endosc*. 2010;24(10):2480–2484. doi:10.1007/s00464-010-0989-y

67. Elsharkawy H, Bendtsen TF. Ultrasound-Guided Transversus Abdominis Plane and Quadratus Lumborum Nerve Blocks. New York, USA: The New York School of Regional Anesthesia. https://www.nysora.com/topics/regional-anesthesia-for-specific-surgical-procedures/abdomen/ultrasound-guided-transversus-abdominis-plane-quadratus-lumborum-blocks/. Accessed May 29, 2022.

68. Rahimzadeh P, Faiz SHR, Latifi-Naibin K, Alimian M. A comparison of effect of preemptive versus postoperative use of ultrasound-guided bilateral transversus abdominis plane (TAP) block on pain relief after laparoscopic cholecystectomy. *Sci Rep*. 2022;12(1):623. doi:10.1038/s41598-021-04552-6

69. Lee IO, Kim SH, Kong MH, et al. Pain after laparoscopic cholecystectomy: The effect and timing of incisional and intraperitoneal bupivacaine. *Can J Anaesth*. 2001;48(6):545–550. doi:10.1007/BF03016830

70. Inan A, Sen M, Dener C. Local anesthesia use for laparoscopic cholecystectomy. *World J Surg*. 2004;28(8):741–744. doi:10.1007/s00268-004-7350-3

71. Heinke B, Gingl E, Sandkuhler J. Multiple targets of μ-opioid receptor-mediated presynaptic inhibition at primary afferent Aδ- and C-fibers. *J Neurosci*. 2011;31(4):1313–1322. doi:10.1523/JNEUROSCI.4060-10.2011

72. Shafi S, Collinsworth AW, Copeland LA, et al. Association of opioid-related adverse drug events with clinical and cost outcomes among surgical patients in a large integrated health care delivery system. *JAMA Surg*. 2018;153(8):757–763. doi:10.1001/jamasurg.2018.1039

73. Naguib M, Seraj M, Attia M, Samarkandi AH, Seet M, Jaroudi R. Perioperative antinociceptive effects of tramadol: A prospective, randomized, double-blind comparison with morphine. *Can J Anaesth*. 1998;45(12):1168–1175. doi:10.1007/BF03012458

74. Kong SK, Onsiong SMK, Chiu WKY, Li MKW. Use of intrathecal morphine for postoperative pain relief after elective laparoscopic colorectal surgery: Postoperative pain relief after laparoscopic colorectal surgery. *Anaesthesia*. 2002;57(12):1168–1173. doi:10.1046/j.1365-2044.2002.02873.x

75. Sjövall S, Kokki M, Kokki H. Laparoscopic surgery: A narrative review of pharmacotherapy in pain management. *Drugs*. 2015;75(16): 1867–1889. doi:10.1007/s40265-015-0482-y

76. Boom M, Olofsen E, Neukirchen M, et al. Fentanyl utility function: A risk-benefit composite of pain relief and breathing responses. *Anesthesiology*. 2013;119(3):663–674. doi:10.1097/ALN.0b013e31829ce4cb

77. Latta KS, Ginsberg B, Barkin RL. Meperidine: A critical review. *Am J Ther*. 2002;9(1):53–68. doi:10.1097/00045391-200201000-00010

78. Forgach L, Ong BY. Failure of meperidine wound infiltration to reduce pain after laparoscopic tubal ligation. *Can J Anaesth*. 1995;42(12): 1085–1089. doi:10.1007/BF03015093

79. Heel RC, Brogden RN, Speight TM, Avery GS. Buprenorphine: A review of its pharmacological properties and therapeutic efficacy. *Drugs*. 1979; 17(2):81–110. doi:10.2165/00003495-197917020-00001

80. Kumar N, Rowbotham DJ. Piritramide. *Br J Anesth*. 1999;82(1):3–5. doi:10.1093/bja/82.1.3

81. Stamer UM, Zhang L, Book M, Lehmann LE, Stuber F, Musshoff F. *CYP2D6* genotype dependent oxycodone metabolism in postoperative patients. *PLoS One*. 2013;8(3):e60239. doi:10.1371/journal.pone.0060239

82. Benyamin R, Trescot AM, Datta S, et al. Opioid complications and side effects. *Pain Physician*. 2008;11(2 Suppl):S105–S120. PMID:18443635.

83. Cheung CK, Adeola JO, Beutler SS, Urman RD. Postoperative pain management in enhanced recovery pathways. *J Pain Res*. 2022;15: 123–135. doi:10.2147/JPR.S231774

84. Sehajpal S, Prasad DN, Singh RK. Prodrugs of non-steroidal anti-inflammatory drugs (NSAIDs): A long march towards synthesis of safer NSAIDs. *Mini Rev Med Chem*. 2018;18(14):1199–1219. doi:10.2174/1389557518666180330112416

85. Sehajpal S, Prasad DN, Singh RK. Novel ketoprofen–antioxidants mutual codrugs as safer nonsteroidal anti-inflammatory drugs: Synthesis, kinetic and pharmacological evaluation. *Arch Pharm (Weinheim)*. 2019;352(7):e1800339. doi:10.1002/ardp.201800339

86. Sehajpal S, Prasad DN, Singh RK. Synthesis and evaluation of prodrugs of ketoprofen with antioxidants as gastroprotective NSAIDs. *Asian J Chem*. 2018;30(9):2145–2150. doi:10.14233/ajchem.2018.21495

87. Gupta A, Bah M. NSAIDs in the treatment of postoperative pain. *Curr Pain Headache Rep*. 2016;20(11):62. doi:10.1007/s11916-016-0591-7

88. Benarroch EE. What is the mechanism of therapeutic and adverse effects of gabapentinoids? *Neurology*. 2021;96(7):318–321. doi:10.1212/WNL.0000000000011424

89. Przybyła GW, Szychowski KA, Gmiński J. Paracetamol: An old drug with new mechanisms of action. *Clin Exp Pharmacol Physiol*. 2021; 48(1):3–19. doi:10.1111/1440-1681.13392

90. Rosenbaum SB, Gupta V, Palacios JL. Ketamine. In: *StatPearls*. Treasure Island, USA: StatPearls Publishing; 2022. http://www.ncbi.nlm.nih.gov/books/NBK470357/. Accessed July 15, 2022.

91. Edwards DA, Hedrick TL, Jayaram J, et al. American Society for Enhanced Recovery and Perioperative Quality Initiative joint consensus statement on perioperative management of patients on preoperative opioid therapy. *Anesth Analg*. 2019;129(2):553–566. doi:10.1213/ANE.0000000000004018

92. McNicol ED, Ferguson MC, Schumann R. Single-dose intravenous ketorolac for acute postoperative pain in adults. *Cochrane Database Syst Rev*. 2021;5(5):CD013263. doi:10.1002/14651858.CD013263.pub2

93. Bell S, Rennie T, Marwick CA, Davey P. Effects of peri-operative non-steroidal anti-inflammatory drugs on post-operative kidney function for adults with normal kidney function. *Cochrane Database Syst Rev*. 2018;11(11):CD011274. doi:10.1002/14651858.CD011274.pub2

94. Schnabel A, Reichl SU, Weibel S, et al. Efficacy and safety of dexmedetomidine in peripheral nerve blocks: A meta-analysis and trial sequential analysis. *Eur J Anaesthesiol*. 2018;35(10):745–758. doi:10.1097/EJA.0000000000000870

95. Rabie A, Abdelfattah M. Outcome of intraoperative dexmedetomidine infusion in laparoscopic cholecystectomy. *Egypt J Anesth*. 2022; 38(1):16–22. doi:10.1080/11101849.2021.2004501

96. Verret M, Lauzier F, Zarychanski R, et al. Perioperative use of gabapentinoids for the management of postoperative acute pain. *Anesthesiology*. 2020;133(2):265–279. doi:10.1097/ALN.0000000000003428

97. Cavalcante AN, Sprung J, Schroeder DR, Weingarten TN. Multimodal analgesic therapy with gabapentin and its association with postoperative respiratory depression. *Anesth Analg*. 2017;125(1):141–146. doi:10.1213/ANE.0000000000001719

98. McNicol ED, Ferguson MC, Haroutounian S, Carr DB, Schumann R. Single dose intravenous paracetamol or intravenous propacetamol for postoperative pain. *Cochrane Database Syst Rev*. 2016;2016(5): CD007126. doi:10.1002/14651858.CD007126.pub3

99. Jibril F, Sharaby S, Mohamed A, Wilby KJ. Intravenous versus oral acetaminophen for pain: Systematic review of current evidence to support clinical decision-making. *Can J Hosp Pharm*. 2015;68(3): 238–247. doi:10.4212/cjhp.v68i3.1458

100. Mulita F, Karpetas G, Liolis E, Vailas M, Tchabashvili L, Maroulis I. Comparison of analgesic efficacy of acetaminophen monotherapy versus acetaminophen combinations with either pethidine or parecoxib in patients undergoing laparoscopic cholecystectomy: A randomized prospective study. *Med Glas (Zenica)*. 2021;18(1): 27–32. doi:10.17392/1245-21

101. Pendi A, Field R, Farhan SD, Eichler M, Bederman SS. Perioperative ketamine for analgesia in spine surgery: A meta-analysis of randomized controlled trials. *Spine (Phila Pa 1976)*. 2018;43(5): E299–E307. doi:10.1097/BRS.0000000000002318

102. Ding X, Jin S, Niu X, et al. Morphine with adjuvant ketamine versus higher dose of morphine alone for acute pain: A meta-analysis. *Int J Clin Exp Med*. 2014;7(9):2504–2510. PMID:25356103.

CREB-associated glycosylation and function in human disease

Ning Zhang[1,B–D], Liu Shi[1,B], Yuli Wang[2,E,F]

[1] Division of Gastroenterology, The Affiliated Ganzhou Hospital of Nanchang University, China
[2] Division of Oncology, The Affiliated Ganzhou Hospital of Nanchang University, China

A – research concept and design; B – collection and/or assembly of data; C – data analysis and interpretation;
D – writing the article; E – critical revision of the article; F – final approval of the article

Address for correspondence
Yuli Wang
E-mail: wyl_918@126.com

Abstract

The shortcomings of mRNA sequencing in explaining biological functions have resulted in proteomics gradually becoming a hotspot for research. However, the function of proteins becomes complicated as a result of post-translational modifications (PTMs) such as phosphorylation, glycosylation, acetylation, etc. Post-translational modifications do not change the physicochemical properties such as charge and solubility of the proteins, but they can have significant consequences on disease initiation in living organisms. The cyclic adenosine monophosphate (cAMP) response element-binding protein (CREB) is an important transcription regulator in eukaryotic cells. It is involved in the development of neurodegenerative diseases, diabetic complications, tumorigenesis, and neurogenesis. Previously, researchers have paid much more attention to the phosphorylation modification of CREB. However, it seems that the functional regulation-mediated glycosylation modification of CREB was just beginning to be understood. In this review, the current studies and most updated insights on how the glycosylation modification of CREB affects targeted gene expression and disease development will be comprehensively discussed. We hope to further evaluate the role of CREB glycosylation on the regulation of gene function.

Key words: CREB, function, glycosylation modification

Introduction

In the field of genomics, a great achievement have been made, including the complete genetic sequencing of many species. With the further development of genome sequencing, more research has focused on organ complexity in higher organisms and the encoding of rare genes. However, gene sequencing is still unable to elucidate the biological function of genes. Although genome sequencing has contributed greatly to scientific research, there is no strict linear relationship between proteins and genes. Therefore, proteomics, which is the study of protein characteristics, including protein expression levels, protein–protein interactions and post-translational modifications (PTMs), has gradually become a hotspot for research. Proteomics research provides a comprehensive understanding of disease occurrence and cellular metabolism at the protein level; these issues could provide solutions for disease prevention and treatment.

Previous studies have shown that O-GlcNAc glycosylation may regulate transcription factors and other proteins in the nucleus.[1,2] For example, the O-GlcNAc glycosylation of RNA polymerase II regulates the structure of the enzyme[3] and inhibits transcriptional elongation by preventing phosphorylation of the C-terminal domain.[3] The O-GlcNAc glycosyltransferase (OGT) catalyzes the covalent bonding of O-GlcNAc to substrate in vivo, and has been shown to promote gene silencing by binding to mSin3A, a transcription inhibitor.[4] However, the understanding of the extent of O-GlcNAc glycosylation and its effects on gene regulation is still under research.

Cyclic adenosine monophosphate (cAMP) response element-binding protein (CREB) is an important transcriptional regulator in eukaryotic cells that exists in all mammalian cells. It can bind to the cAMP response element (CRE) sequence TGACGTCA, or the conserved half CRE TGACG. The CREB family members include CREB-1, CREB-2, CREB-3, CREB-5, CREB3L1, CREB3L2, CREB3L3 (CREBH), and CREB3L4. The CREB is also a DNA-binding protein member belonging to a leucine zipper family that includes the activating transcription factor (ATF). The cAMP-responsive transcription factors within the CREB/ATF family include CREB, ATF-1 and cAMP response element modulator (CREM) τ. The structure of CREB contains a signal-responsive kinase-inducible domain (KID), glutamine-rich (Q1 and Q2) constitutive activation domain(s) and a basic leucine zipper (bZIP) domain (Fig. 1A).

The differences in the molecular structures of CREBs are caused by different factors such as splicing, protein translation initiation sites, RNA molecular stability, and PTMs. The CREB plays an important regulatory role in the fields involved in, i.a., regulating gene transcription, physiological rhythm, cell development and survival, addiction, learning, and memory.[5–7] Post-translational modifications play a vital role in the dynamic regulation and complexity of biological processes including the cell cycle, transcription and programmed cell death.[8–11] Most importantly, CREB is regulated by PTMs and is subject to post-transcriptional regulation by phosphorylation, ubiquitination, SUMOylation, and miRNA regulation (Fig. 1B). In living organisms, alterations of proteins are dynamic and several methods of PTMs, such as phosphorylation, glycosylation, acetylation, lipoylation, ubiquitination, and methylation, exist. The phosphorylation of Ser133 site is the central link of CREB activation.[12] After the Ser133 site of CREB is phosphorylated, it can be recognized by the CREB-binding protein (CBP) and bind to it. This acetylates the CRE in the CREB promoter sequence and initiates the gene transcription process. In contrast, other modifications regulate the transcriptional activity of CREB by affecting the Ser133 site. In addition, the CREB

A. **CREB structure**

B.

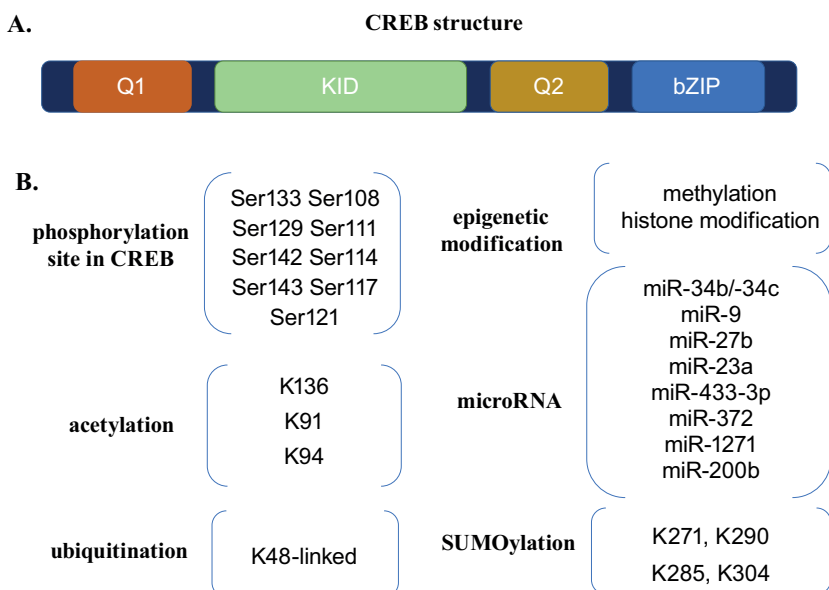| phosphorylation site in CREB	Ser133 Ser108 Ser129 Ser111 Ser142 Ser114 Ser143 Ser117 Ser121	epigenetic modification	methylation histone modification
acetylation	K136 K91 K94	microRNA	miR-34b/-34c miR-9 miR-27b miR-23a miR-433-3p miR-372 miR-1271 miR-200b
ubiquitination	K48-linked	SUMOylation	K271, K290 K285, K304

Fig. 1. A. Structure of cyclic adenosine monophosphate (cAMP) response element-binding protein (CREB); B. Post-translational modifications and post-transcriptional regulation of CREB and related amino acid residues in CREB

KID – kinase-inducible domain; bZIP – basic leucine zipper; Q1 – glutamine (Q) domain 1; Q2 – glutamine (Q) domain 2.

molecule is the phosphorylation substrate of other protein kinases such as protein kinase A (PKA), mitogen-activated protein kinase (MAPK) and protein kinase C (PKC). Therefore, CREB acquires diverse biological functions through orderly PTMs that can be affected by different signaling pathways and various regulatory factors to induce CREB activation.

In our review, we summarized studies published between January 1, 2000 and December 31, 2021, relevant to glycosylation-mediated CREB regulation, that promoted a comprehensive understanding of glycosylation-mediated CREB transcriptional activation and the effect of other factors on glycosylation modification. These findings will further elucidate the role of CREB glycosylation in the regulation of gene function.

Objectives

In this review, we aimed to summarize studies involving the regulating model of CREB-associated glycosylation and develop a comprehensive insight into its functional regulation pathway.

Methodology

Literature search strategy

In our review, we followed the Preferred Reporting Items for Systematic Reviews and Meta-Analyses (PRISMA) guidelines. Seven databases were systematically searched including PubMed, Scopus, ScienceDirect, ProQuest, EBSCO, Wiley Online, and Taylor & Francis Online from January 1, 2000 to December 31, 2021.

Study selection criteria

Researchers examined the titles for relevance to our study. Additionally, based on the abstracts, we evaluated the eligibility for inclusion. If the abstract was ambiguous, the researchers examined the full text in order to determine whether the report met the inclusion criteria. All references were imported into an Endnote X9 library (Clarivate Analytics, Philadelphia, USA) and duplicates were removed. All citations were included if they met the following criteria: 1) the study pertained to the glycosylation of CREB; 2) the study concerned the glycosylation of CREB cofactors; 3) the study referred to the biological function of CREB or to the CREB-related diseases; and 4) the full text of the study was published in English. Reports were excluded if: 1) they did not describe original research; or 2) the abstract screening demonstrated that the research did not concern CREB-associated glycosylation.

Types of CREB glycosylation modifications

O-GlcNAc glycosylation of CREB

Protein O-GlcNAc glycosylation refers to the dynamic PTM occurring in the cytoplasm and nucleus where only one N-acetylglucosamine (G1cNAc) is connected to serine or threonine (Ser/Thr) hydroxyl groups through O-glycosidic bonds. This protein modification is abundant in eukaryotic cells. Its distribution in nuclear pore complexes and chromatin is the highest, followed by a large number of proteins distributed in the cytoplasm, mitochondria and membrane.[12] As a critical eukaryotic transcription factor, CREB is also subject to the O-GlcNAc glycosylation, which is the main form of CREB protein glycosylation.

The O-GlcNAc glycosylation of CREB is similar to that of most proteins, mainly because O-linked GlcNAc transferase includes OGT and O-GlcNAcase (OGA). Namely, OGT is responsible for adding the glycosyl group and OGA is responsible for removing it.[13]

N-glycosylation of CREB

N-glycosylation refers to the glycosylation of an asparagine (Asn) amide group. The N-terminal α-amino or arginine ω-amino groups are the connecting points for N-linked glycosylation and are the most common forms in eukaryotes. N-glycosylation is generally carried out in the endoplasmic reticulum (ER) and catalyzed by oligosaccharyltransferase (OST). The N-glycosylation modification site has the conserved amino acid sequence, Asn-X-Ser/Thr, in which X is an amino acid other than proline and the oligosaccharide chain is relatively conserved. Finally, the core sugar chain is transferred to Asn of the target protein.[14]

The ATF6β, a subtype of the ER transmembrane glycoprotein ATF6 within the ATF/CREB family, undergoes N-glycosylation and participates in the regulation of the subtype, ATFα, and downstream genes.[15] Additionally, CBP can interact with BRCA2 and affect the N-linked post-translational glycosylation of BRCA2.[16] N-linked glycosylation is required for the optimal proteolytic activation of the membrane-bound transcription factor CREBH.[17] In general, N-glycosylation plays a pivotal role in protein folding, stabilization and degradation processes (Table 1).

Table 1. Glycosylation modification effect on cyclic adenosine monophosphate (cAMP) response element-binding protein (CREB) cofactors and binding protein

CREB cofactors	Modification way	Mechanism
CRTC	O-GlcNAc	Glycosylation represses CREB-dependent transcription by impairing its association with CREB-regulated transcription coactivator.
CBP	N-glycosylation	The binding of CBP to the N-terminal region of BRCA2 is necessary for N-glycosylation of residue 272 on BRCA2.
CBP	O-linked N-acetylglucosamine	Ser147 and Ser236 sites of CREB-binding protein are O-glycosylated.

CREB – cyclic adenosine monophosphate (cAMP) response element binding protein; CRTC – CREB transcription coactivator; CBP – CREB-binding protein.

Glycosylation of CREB and its cofactors

Glycosylation affects CREB and its family members

The CREB is a key regulator in a variety of neuronal processes, such as brain development, circadian rhythm and long-term memory. Multiple studies have suggested that CREB-1 can be glycosylated by O-O-GlcNAc in the Q2 domain, of which the main glycosylation sites are Ser260, Thr256, Thr259, and Thr261. After analyzing the relationship between glycosylation levels and the nuclear extracts of glycosylated CREB-1, it was demonstrated that glycosylated CREB-1 transcriptional activity is 41.5% higher than that of nonglycosylated CREB-1. An in vitro assay validated that glycosylation affects the interaction between CREB-1 and TAFI130 by inhibiting the transcriptional activity of CREB-1.[18] These studies indicate that O-glycosylation is involved in gene regulation and provides a link between O-GlcNAc and information storage processes occurring in the brain.

Rexach et al. explored the functional role the glycosylation of CREB plays in neurons using chemical enzyme quantification.[12] They demonstrated that CREB is dynamically modified with an O-linked β-N-acetyl-D-glucosamine sugar in response to neuronal activity and that glycosylation represses CREB-dependent transcription by impairing its association with CREB-regulated transcription coactivator (CRTC). In another study, it was demonstrated that by blocking the glycosylation of CREB, the function and behavior of cells changed and the growth of neuronal axons and dendrites was enhanced, improving long-term memory.[19] This finding suggested a novel role of O-glycosylation of CREB in memory formation.

In diabetes, researchers used a high-glucose microenvironment in order to induce proinflammatory cytokine signaling, and demonstrated that high glucose levels increased the recruitment of the interleukin-1β (IL-1β) promoter to CBP. This promoted chromatin remodeling and transcription. Phenolic acid treatment interfered with chromatin remodeling and monocyte transcription, weakening protein glycosylation. High glucose levels stimulated the inflammatory response by acting as an anti-glycosylation agent and signaling pathway modifier.[20]

The CREBH is a member of the CREB3 transcription factor subfamily with a bZIP domain, and is a transmembrane transcription factor anchored to the ER. It is cleaved by dictyosome protease when adapting to ER stress and then transferred to the nucleus. It was found that only 3 out of 4 N-glycosylation sites in the ER lumen region of CREBH located at the CREBH C-terminus were conserved in humans and mice, namely Thr413, Thr420 and Thr427. The CREBH undergoes glycosylation in response to ER stress and then induces proteasome hydrolyzation. Next, it is transferred to the nucleus to play a role in transcriptional regulation. However, using site-directed mutations, the conserved Thr residue can be converted to isoleucine, which weakens or destroys the N-linked glycosylation of CREBH. The CREBH remains inactive in the ER and exhibits a significantly reduced ability to drive the unfolded protein response (UPR)/cAMP receptor protein promoter. Collectively, N-glycosylation modifications are necessary for proteolysis-dependent activation of CREBH.[21] The CREBH can also undergo deglycosylation and degradation via ER-related degradation pathways, enhancing the clearance of CREBH and nuclear transport of N-terminal truncated products.[22] In addition, Zhong et al. reported that the inhibition of protein glycosylation by hexosamine D-mannosamine (ManN) is a novel pro-angiogenic strategy that acts via activation of stress pathways in endothelial cells.[23] Although ManN activated extracellular signal-regulated kinase (ERK), AKT (also known as protein kinase B), the mammalian target of rapamycin (mTOR), and CREB at 40 μM, they hypothesized that a unique mechanism may be implicated in the endothelial cell mitogenic effects of ManN. Several studies have shown that the glycosylation process corresponds to protein degradation and proteolysis, the extent of which depends on the level of cellular stress and dynamic environmental changes.

Activated transcription factor 6 (ATF6) is a member of the transcription factor ATF/CREB family and a heterodimer of CREBH. The ATF6β contains 5 conserved N-linked glycosylation sites and is a key transcriptional inhibitor of ATF6α, which assists in regulating the intensity and duration of the ATF6-dependent ER stress response. Nonglycosylated ATF6β has been shown

to directly elevate levels of *ERSR* gene expression through the loss of its inhibitory function on ATF6α.[15,24] However, low levels of glycosylation of ATF6 allow it to act as a balancing receptor in the ER and induce the activation of ATF6. Because of this, when the ER stress response is absent, nonglycosylated ATF6 is transferred to the dictyosome complex more rapidly and is cleaved by S1P and S2P proteases, leading to the constitutive nuclear localization and transcriptional activation.[25] In contrast, nonglycosylated CREBH inhibits the activation of proteolysis and reduces transcriptional activation,[21] revealing the reverse effect of N-glycosylation on CREBH and ATF6.

The *Tisp40* is a spermatid gene expressed during spermiogenesis in mice. It encodes a CREB family transcription factor and contains 2 isoforms including Tisp40α and Tisp40β. The C-terminus of Tisp40α/β is glycosylated.[26] The functions of Tisp40 are changed by the binding of unfolded protein response elements (UPREs) and are activated via the RIP pathway.

Effect of glycosylation on CREB cofactors and binding protein

CREB transcription coactivator (CRTC) was first discovered by genome high-throughput screening technology in 2003. It is a protein family that can regulate the activity of transcription factors.[27] As a coactivator of CREB, 3 members of the CRTC family have been identified, namely CRTC1, CRTC2 and CRTC3. Their C-terminals

were found to bind to transcription activators and enhance the transcriptional activity of CREB.[28]

The synthesis of O-GlcNAc mainly occurs through the hexosamine biosynthetic pathway (HBP), which utilizes glucose, acetyl-CoA, glutamine, and uridine triphosphate (UTP) to produce uridine dipho-sphate N-acetylglucosamine (UDP-GlcNAc). Approximately 2–3% of fructose 6-phosphate enters the HBP, and HBP reflects the nutritional status of the cells and plays an important role in biological regulation. Due to its reversible regulation of target protein activities, it is also called the hexosamine cycle or hexosamine (O-GlcNAc) signaling. The CRTC2 is modified by O-glycosylation in the cytoplasm through a phosphorylation-dependent mechanism. The glycosylated form activates hepatic gluconeogenesis, whereas the deglycosylated O-glycosyltransferase inhibits gluconeogenesis, revealing a novel mechanism of chronic hyperglycemia, and connects the interaction between HBP and CREB O-GlcNAc (Fig. 2).[29]

The CREB-binding protein is a transcription coactivator with highly conserved sequence, considered to be an important factor in the regulation of mammalian gene transcription.[30] The CREB-binding protein was found to specifically bind phosphorylated CREB to promote its transcriptional activation.[31] In addition, CBP regulates CREB-dependent gene transcription through CRTC.[32] Some studies have identified O-linked GlcNAc-modified sites of CBP on osteoblasts by means of electron-transfer dissociation tandem mass spectrometry (ETD-MS). This shows that the Ser147 and Ser236 sites of CBP, as well
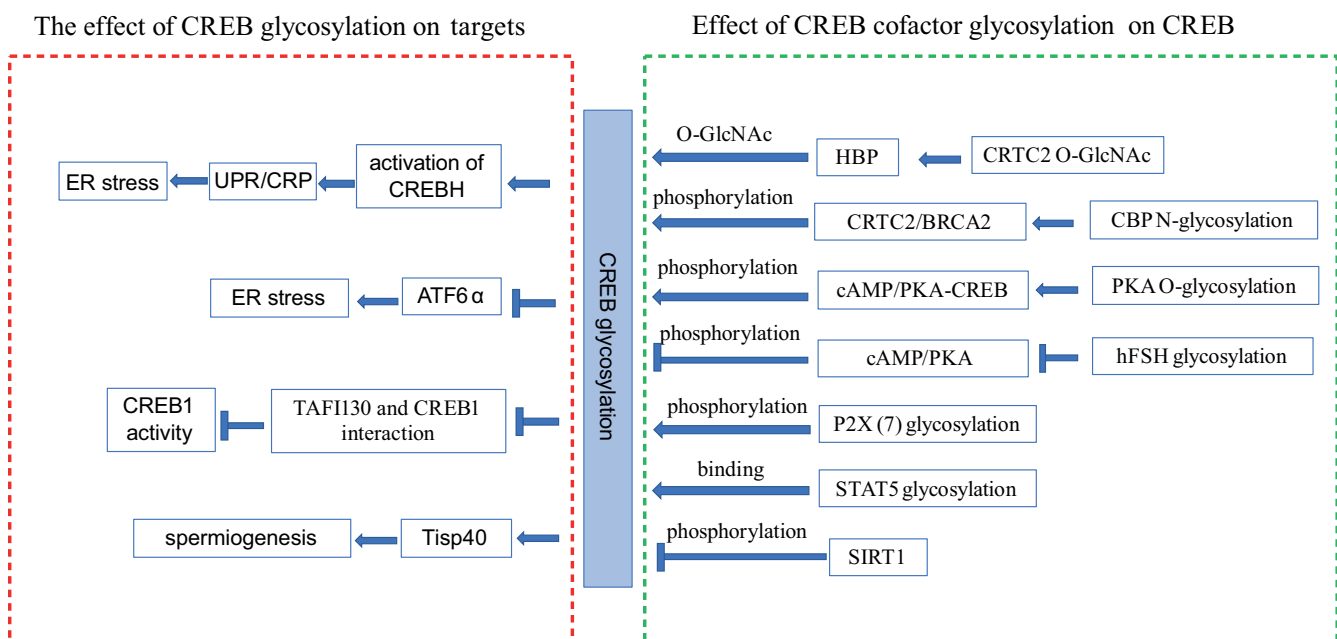
Fig. 2. The regulating network between the glycosylation of cyclic adenosine monophosphate (cAMP) response element-binding protein (CREB) and cofactors. The left panel in the red frame represents the effect of CREB glycosylation on targeted genes. The right panel in the green frame represents the effect of glycosylation on CREB cofactors and CREB post-translational modifications (PTMs)

ER – endoplasmic reticulum; ATF – activating transcription factor; HBP – hexosamine biosynthetic pathway; CRTC – CREB transcription coactivator; CBP – CREB-binding protein; cAMP – cyclic adenosine monophosphate; PKA – protein kinase A; hFSH – human follicle-stimulating hormone; SIRT1 – Sirtuin 1.

as the phosphorylation sites of CREB could be O-glycosylated. Thus, the O-glycosylation of CREB is crucial for bone formation, remodeling and fracture healing, and the effects of glycosylation on protein function and regulation warrant further study.[33] The CREB-binding protein is a transcription cofactor that has been validated to interact with BRCA2 and facilitate the N-linked glycosyl-mediated regulation of BRCA2. The binding of CBP to the N-terminal region of BRCA2 is required for the N-glycosylation of residue 272 on BRCA2 (Table 1). Studies have shown that this CBP-mediated N-glycosylation changes the structure of CBP-related proteins, resulting in the regulation of targeted gene expression, cell growth and differentiation (Fig. 2).[16]

Glycosylation of other factors regulating CREB and its cofactors

The CREB and its cofactors are also regulated by the glycosylation of other factors including kinases, transcription factors, cytokines, and enzymes. Phosphorylation and O-glycosylation are often reciprocal and may affect the subsequent activation and biological function of CREB. Here, we summarize the recent research on this topic (Fig. 2).

PKA signaling pathway

This pathway is also called the cAMP/PKA-CREB signaling pathway and is associated with the activation of CREB. When PKA is activated by cAMP, it immediately enters the nucleus inducing the inactivation of CREB phosphorylation and thus, its biological activity and regulation of target gene transcription.[34] In particular, the Ser residue at position 133 of CREB plays an important role in the regulation of transcriptional activity. The phosphorylation at the site 133 by PKA increases CREB transcriptional activity 10–20 times.[35] Recent studies have shown that high levels of the PKA O-glycosylation enhance the phosphorylation of CREB, but CRBH inhibits this process; such phenomenon suggests that the O-glycosylation of PKA affects the PKAc-CREB signaling pathway by regulating CREB phosphorylation.[36]

With regard to learning and memory, glucose uptake and the levels of O-glycosylation are decreased in brains of individuals with Alzheimer's disease (AD).[37] It has been found that the catalytic subunit of PKA can be modified by O-linked GIcNAc. Afterwards, the subcellular localization of PKAcα and PKAcβ was shown to change and their kinase activity enhanced. This study suggests that in addition to cAMP and phosphorylation, glycosylation is a novel regulating mechanism in PKA-CREB signal transduction.[38]

Human follicle-stimulating hormone

Jiang et al. purified recombinant human follicle-stimulating hormone (hFSH) into low-glycosylated hFSH

and fully-glycosylated hFSH.[39] Granulosa cells were then treated with either a high concentration of complete hFSH or low-glycosylated hFSH for 48 h. Those treated with low-glycosylated hFSH showed a more significant accumulation of cAMP, PKA activation and phosphorylation of the S133 site on CREB. Human follicle-stimulating hormone with low glycosylation also stimulated CREB response element-mediated transcription more effectively than that of hFSH with complete glycosylation. It implies that low-glycosylated hFSH exhibits higher biological activity than fully-glycosylated hFSH. These processes regulate the CREB signaling pathway and thus play a positive role in follicle stimulation in older patients using assisted reproductive technology.

Nucleotide receptor P2X (7)

Nucleotide receptor P2X (7), an immunomodulatory cation channel protein, is expressed in immune cells such as monocytes and macrophages. It is activated by extracellular adenosine 5′-triphosphate (ATP) after tissue injury or infection.[40] Ligand binding to P2X (7) can stimulate the production of ERK1 and transcriptional activation of CREB. It was found that P2X (7) is sensitive to Endo H and PNGase F, and is glycosylated at sites N187, N202, N213, N241, and N284. Mutations at the N187 site result in significantly decreased phosphorylation of ERK and CREB by a P2X (7) agonist, suggesting that residue N187 is essential for receptor transport and function.[41]

Signal transducer and activator of transcription

Signal transducer and activator of transcription (STAT) can bind to specific peptides containing phosphorylated tyrosine. Some studies have demonstrated that O-linked GIcNAc is the second modification necessary for STAT5-induced transcription. This glycosylation was only found in activated STAT5 within the nucleus. The STAT5 binds to CBP only after glycosylation.[42]

Sirtuin 1

The CREB functions show a close relationship with learning and memory, which is also related to AD. In this disease, Sirtuin 1 (SIRT1) has neuroprotective properties and the dysregulation of SIRT1 is associated with an aberrant accumulation of the key AD-associated tau protein. A recent study showed that SIRT1 could deacetylate CREB and decrease p-CREB levels. Then, inactivated CREB could attenuate the O-GlcNAcylation of tau by inhibiting OGT.[43]

Others

Drosophila NOT, human clone hNOT-1/ALG3-1 and yeast *ALG3* gene undergo N-glycosylation modification

and bind with the CREB3 precursor. However, there are no interactions with the CREB3 protein cleavage products in the ER and nucleus. A prerequisite for the interaction between these 2 chaperones is the proteolytic activation of CREB3.[44]

Regulatory factors of CREB glycosylation

The glycosylation of CREB is associated with several factors. As a result of a variety of regulatory mechanisms, CREB glycosylation levels and deglycosylation levels undergo constant dynamic adjustment. For example, micronutrients found in organisms are of vital importance in metabolic regulation and provide fuel and energy for protein glycosylation.[45] Therefore, dynamic changes in micronutrient levels in vivo may regulate target genes, and affect related protein glycosylation levels and the utilization of GlcNAcylated CREB. A recent study showed that the glycosylation of CREB is affected by the nutrient sensing pathway of iron by leptin gene regulation. In this study, researchers discovered that high iron intake changed the CREB occupancy pattern, increasing the occupancy of p-CREB and decreasing the occupancy of O-GlcNAcylated CREB on the leptin promoter.[46]

CREB-associated glycosylation and disease

The CREB is an important transcription regulator in eukaryotic cells and is involved in the development of multiple types of diseases, such as neurodegenerative diseases, diabetes complications, tumorigenesis, and neurogenesis (Fig. 3).

Alzheimer's disease

Of note, CREB is mostly related to the molecular mechanisms of learning and memory which are dysregulated in the degenerative disease. As mentioned above, the dysregulation of PKA-CREB signaling could lead to memory loss and cognitive decline. The O-GlcNAcylation of PKA promotes PKA kinase activity and might be a novel way of improving learning and memory deficits in patients with AD.[38] In addition, region-specific activation of CRTC1-CREB signaling mediates long-term fear memory.[47]

Metabolic disease

Previous studies have shown that CREB glycosylation levels and utilization rates are regulated by micronutrients. Induced nutrient sensing and glycolipid metabolism regulation play an important role in metabolic diseases such as obesity, diabetes and hyperglycemia.

Neurodegenerative disease

✓ Glycosylation affects the interaction between CREB-1 and TAFII130, which inhibits the transcriptional activity of CREB-1 involved in gene regulation and provides a link between O-GlcNAc and the information storage process in the brain
✓ O-β-N-acetyl-D-glucosamine-modified CREB weakened its relationship with the transcription coactivator CRTC and then repressed CREB-dependent transcription in neurons
✓ The blocking of CREB glycosylation changed the function and behavior of cells and enhanced the growth of neuron axons and dendrites, thus improving long-term memory

ER stress

✓ CREBH undergoes glycosylation in response to ER stress and then induces proteasome hydrolysation
✓ N-glycosylation modification is necessary for proteolysis-dependent full activation of CREBH
✓ CREBH undergoes deglycosylation and degradation via ER-related degradation pathways
✓ The heterodimer of CREBH, ATF6β contains 5 conserved N-linked glycosylation sites and is a key transcriptional inhibitor of ATF6α, which assists in regulating the intensity and duration of ATF6-dependent ER stress response.

CREB family Glycosylation

Metabolic diabetes disease

✓ High glucose levels increased the recruitment of the IL-1β promoter to CREB binding proteins
✓ Phenolic acid treatment interfere with chromatin remodelling and monocyte transcription, and can weaken protein glycosylation and high glucose levels stimulated the inflammatory response, acting as an anti-glycosylation agent

Reproductive development

✓ TISP40, a mouse spermatid-specific gene, encodes a CREB/CREM family transcription factor, and localizes to the endoplasmic reticulum (ER) via the Rip pathway
✓ Low-glycosylated hFSH has higher biological activity than that of fully-glycosylated hFSH, which affects the CREB signaling pathway and thus plays a positive role in follicle stimulation in elderly patients with assisted reproductive technology
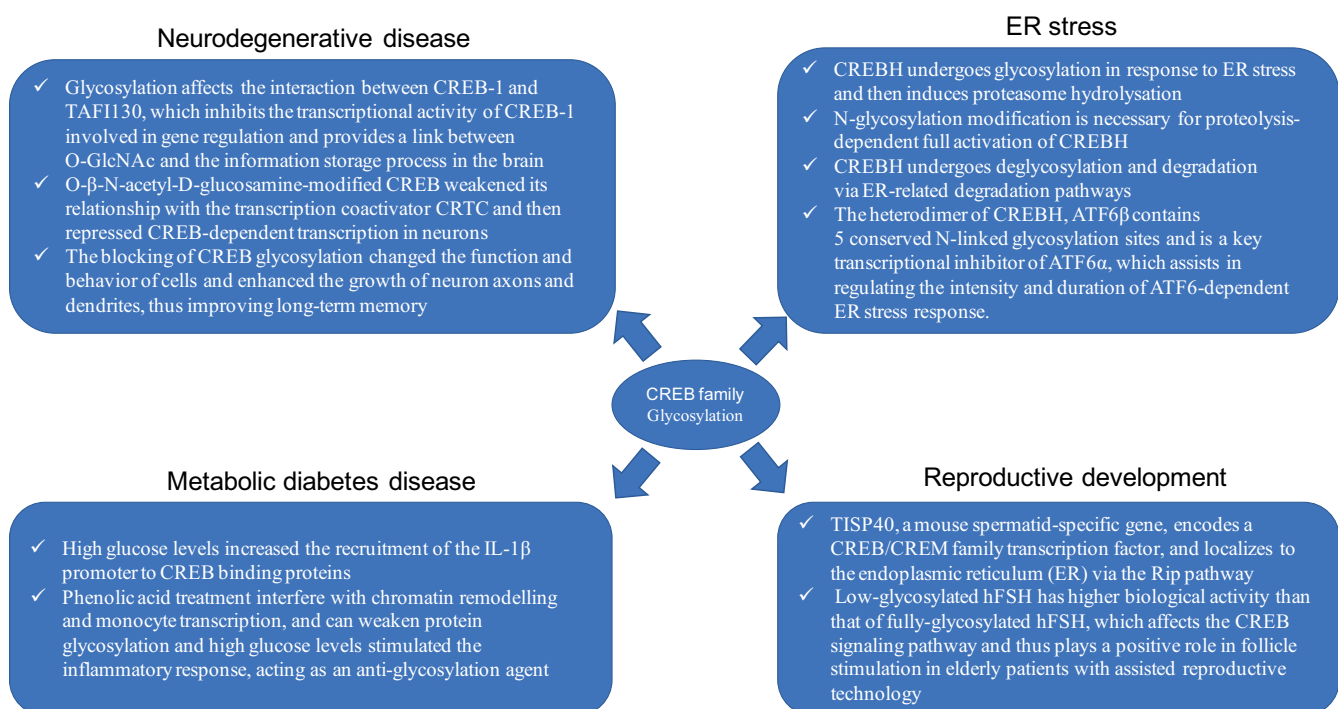
Fig. 3. The regulating mechanism of cyclic adenosine monophosphate (cAMP) response element-binding protein (CREB)-associated glycosylation in disease development, and the involvement of CREB glycosylation in different types of diseases including degenerative diseases, diabetes, reproductive diseases, and endoplasmic reticulum (ER) stress

CRTC – CREB transcription coactivator; IL-1β – interleukin-1β; ATF – activating transcription factor; CREM – cyclic adenosine monophosphate response element modulator; hFSH – human follicle-stimulating hormone.

In addition, CRTC and ATF are both involved in metabolic control. Interestingly, this protein family affects the response of the cell to different external stimuli by sensing extracellular signals such as nutrients, energy state and hormone levels. This results in the changing of the transcriptional activity in order to regulate homeostasis in a variety of important tissues and organs, especially the liver. Disorders of glucose and lipid metabolism can lead to severe metabolic diseases, such as fatty liver disease or hepatocellular carcinoma. It is important to determine how to reverse the disturbance of hepatocyte homeostasis induced by excess nutritional intake. However, protein O-GlcNAc mainly acts through the HBP and, based on its reversible property, might be a promising regulatory mechanism in glucose metabolism.

Reproductive development

Many studies have shown that CREB family genes are related to the development and maturation of germ cells, such as sperm development and follicular cell maturation. In CREB-associated genes, the bZIP-type transcription factors CREB and CREM are reported to play pivotal roles in the events that occur before the morphological changes in spermatogenesis.[48] In particular, CREM is essential for spermatogenesis. The glycosylation process regulates a subsequent signal transduction (such as the RIP pathway) and biological functions (ER degradation).[25]

Regarding female fertility and sex steroid hormone production-related diseases, glycosylation of hFSH changes the bioactivity of hFSH and stimulates the cAMP-PKA-CREB pathway in human granulosa cells. This study suggests that glycosylation of hormones may be the correct direction in the treatment of reproductive and developmental diseases.

Overall, clarifying the relationship between CREB-related glycosylation and diseases is helpful for further applications. By analyzing the glycosylation level of proteins and evaluating the occupancy and heterogeneity of glycans and glycosides, we can further assess the physiological and pathological role of protein glycosylation in diseases. Thus, glycoproteins may be worthy of further study as biomarkers of diseases.[49]

In the future

Glycosylation is one of the most important types of PTMs for CREB functional regulation. The study of the glycosylation of CREB at the proteomic level helps to understand the biological significance of the glycosylation of CREB in life processes. It is also helpful in analyzing the function and significance of CREB from the comprehensive level of genome proteome glycobiology, and enables a more comprehensive understanding of the role of CREB in the pathogenesis of diseases. On the other hand, this research provides scientific guidance for the early diagnosis and treatment of diseases. In conclusion, with the continuous development and improvement of protein glycosylation analysis technology, we will obtain more information on glycoprotein structure and gain a deeper understanding of the biological functions of protein glycosylation.

Admittedly, this review has several limitations. We only discussed CREB-associated glycosylation and its functional regulation, while the noncanonical cellular mechanisms of CREB-associated glycosylation are still unclear. Additionally, CREB-associated glycosylation is involved in a broad number of diseases and only a cursory summary of the most relevant diseases was provided in this study.

ORCID iDs

Ning Zhang https://orcid.org/0000-0001-8082-8219
Liu Shi https://orcid.org/0000-0002-1802-0603
Yuli Wang https://orcid.org/0000-0001-8349-3397

References

1. Zachara NE, Hart GW. The emerging significance of O-GlcNAc in cellular regulation. *Chem Rev*. 2002;102(2);431–438. doi:10.1021/cr000406u
2. Jackson SP, Tjian R. O-glycosylation of eukaryotic transcription factors: Implications for mechanisms of transcriptional regulation. *Cell*. 1988;55(1):125–133. doi:10.1016/0092-8674(88)90015-3
3. Comer FI, Hart GW. Reciprocity between O-GlcNAc and O-phosphate on the carboxyl terminal domain of RNA polymerase II. *Biochemistry*. 2001;40(26):7845–7852. doi:10.1021/bi0027480
4. Yang X, Zhang F, Kudlow JE. Recruitment of O-GlcNAc transferase to promoters by corepressor mSin3A: Coupling protein O-GlcNAcylation to transcriptional repression. *Cell*. 2002;110(1):69–80. doi:10.1016/S0092-8674(02)00810-3
5. Shaywitz AJ, Greenberg ME. CREB: A stimulus-induced transcription factor activated by a diverse array of extracellular signals. *Annu Rev Biochem*. 1999;68:821–861. doi:10.1146/annurev.biochem.68.1.821
6. Lonze BE, Ginty DD. Function and regulation of CREB family transcription factors in the nervous system. *Neuron*. 2002;35(4):605–623. doi:10.1016/s0896-6273(02)00828-0
7. Kornhauser JM, Cowan CW, Shaywitz AJ, et al. CREB transcriptional activity in neurons is regulated by multiple, calcium-specific phosphorylation events. *Neuron*. 2002;34(2):221–233. doi:10.1016/S0896-6273(02)00655-4
8. Jenuwein T, Allis CD. Translating the histone code. *Science*. 2001;293(5532):1074–1080. doi:10.1126/science.1063127
9. Bernstein BE, Humphrey EL, Erlich RL, et al. Methylation of histone H3 Lys 4 in coding regions of active genes. *Proc Natl Acad Sci U S A*. 2002;99(13):8695–8700. doi:10.1073/pnas.082249499
10. Jones SM, Kazlauskas A. Growth factor-dependent signaling and cell cycle progression. *Chem Rev*. 2001;101(8):2413–2423. doi:10.1021/cr000101f
11. Schimpl M, Schüttelkopf AW, Borodkin VS, Van Aalten DMF. Human OGA binds substrates in a conserved peptide recognition groove. *Biochem J*. 2010;432(1):1–7. doi:10.1042/BJ20101338
12. Rexach JE, Clark PM, Mason DE, Neve RL, Peters EC, Hsieh-Wilson LC. Dynamic O-GlcNAc modification regulates CREB-mediated gene expression and memory formation. *Nat Chem Biol*. 2012;8(3):253–261. doi:10.1038/nchembio.770
13. Nagel AK, Ball LE. O-GlcNAc transferase and O-GlcNAcase: Achieving target substrate specificity. *Amino Acids*. 2014;46(10):2305–2316. doi:10.1007/s00726-014-1827-7
14. Malaby LH, Kobertz WR. Molecular determinants of co- and post-translational N-glycosylation of type I transmembrane peptides. *Biochem J*. 2013;453(3):427–434. doi:10.1042/BJ20130028
15. Guan D, Wang H, Li VE, Xu Y, Yang M, Shen Z. N-glycosylation of ATF-6beta is essential for its proteolytic cleavage and transcriptional repressor function to ATF6alpha. *J Cell Biochem*. 2009;108(4):825–831. doi:10.1002/jcb.22310

16. Siddique H, Rao VN, Reddy ESP. CBP-mediated post-translational N-glycosylation of BRCA2. *Int J Oncol*. 2009;35:387–391. doi:10.3892/ijo_00000351

17. Chan CP, Mak TY, Chin KT, Ng IOL, Jin DY. N-linked glycosylation is required for optimal proteolytic activation of membrane-bound transcription factor CREB-H. *J Cell Sci*. 2010;123(Pt 9):1438–1448. doi:10.1242/jcs.067819

18. Lamarre-Vincent N, Hsieh-Wilson LC. Dynamic glycosylation of the transcription factor CREB: A potential role in gene regulation. *J Am Chem Soc*. 2003;125(22):6612–6613. doi:10.1021/ja028200t

19. Gewinner C, Hart G, Zachara N, Cole R, Beisenherz-Huss C, Groner B. The coactivator of transcription CREB-binding protein interacts preferentially with the glycosylated form of Stat5. *J Biol Chem*. 2004;279(5):3563–3572. doi:10.1074/jbc.M306449200

20. Wu CH, Yeh CT, Shih PH, Yen GC. Dietary phenolic acids attenuate multiple stages of protein glycation and high-glucose-stimulated proinflammatory IL-1β activation by interfering with chromatin remodeling and transcription in monocytes. *Mol Nutr Food Res*. 2010;54(Suppl 2):S127–S140. doi:10.1002/mnfr.200900395

21. Chan CP, Mak TY, Chin KT, Ng IOL, Jin DY. N-linked glycosylation is equired for optimal proteolytic activation of membrane-bound transcription factor CREB-H. *J Cell Sci*. 2010;123(Pt 9):1438–1448. doi:10.1242/jcs.067819

22. Bailey D, Barreca C, O'Hare P. Trafficking of the bZIP transmembrane transcription factor CREB-H into alternate pathways of ERAD and stress-regulated intramembrane proteolysis. *Traffic*. 2007;8(12):1796–1814. doi:10.1111/j.1600-0854.2007.00654

23. Zhong C, Li P, Argade S, et al. Inhibition of protein glycosylation is a novel pro-angiogenic strategy that acts via activation of stress pathways. *Nat Commun*. 2020;11(1):6330. doi:10.1038/s41467-020-20108-0

24. Wang X, Xu L, Gillette TG, Jiang X, Wang ZV. The unfolded protein response in ischemic heart disease. *J Mol Cell Cardiol*. 2018;117:19–25. doi:10.1016/j.yjmcc.2018.02.013

25. Hong M, Luo S, Baumeister P, et al. Underglycosylation of ATF6 as a novel sensing mechanism for activation of the unfolded protein response. *J Bio Chem*. 2004;279(12):11354–11363. doi:10.1074/jbc.M309804200

26. Nagamori I, Yabuta N, Fujii T. Tisp40, a spermatid specific bZip transcription factor, functions by binding to the unfolded protein response element via the Rip pathway. *Genes Cells*. 2010;10(6):575–594. doi:10.1111/j.1365-2443.2005.00860

27. Iourgenko V, Zhang W, Mickanin C, et al. Identification of a family of cAMP response element-binding protein coactivators by genome-scale functional analysis in mammalian cells. *Proc Natl Acad Sci U S A*. 2003;100(21):12147–12152. doi:10.1073/pnas.1932773100

28. Altarejos JY, Montminy M. CREB and the CRTC co-activators: Sensors for hormonal and metabolic signals. *Nat Rev Mol Cell Biol*. 2011;12(3):141–151. doi:10.1038/nrm3072

29. Dentin R, Hedrick S, Xie J, Yates J, Montminy M. Hepatic glucose sensing via the CREB coactivator CRTC2. *Science*. 2008;319(5868):1402–1405. doi:10.1126/science.1151363

30. Ravnskjaer K, Kester H, Liu Y, et al. Cooperative interactions between CBP and TORC2 confer selectivity to CREB target gene expression. *EMBO J*. 2007;26(12):2880–2889. doi:10.1038/sj.emboj.7601715

31. Chrivia JC, Kwok RP, Lamb N, Hagiwara M, Montminy MR, Goodman RH. Phosphorylated CREB binds specifically to the nuclear protein CBP. *Nature*. 1993;365(6449):855–859. doi:10.1038/365855a0

32. Heinrich A, von der Heyde AS, Böer U, Phu DT, Tzvetkov M, Oetjen E. Lithium enhances CRTC oligomer formation and the interaction between the CREB coactivators CRTC and CBP: Implications for CREB-dependent gene transcription. *Cell Signal*. 2013;25(1):113–125. doi:10.1016/j.cellsig.2012.09.016

33. Nagel AK, Schilling M, Comte-Walters S, Berkaw MN, Ball LE. Identification of O-linked N-acetylglucosamine (O-GlcNAc)-modified osteoblast proteins by electron transfer dissociation tandem mass spectrometry reveals proteins critical for bone formation. *Mol Cell Proteomics*. 2013;12(4):945–955. doi:10.1074/mcp.M112.026633

34. Impey S, Obrietan K, Wong ST, et al. Cross talk between ERK and PKA is required for Ca^{2+} stimulation of CREB-dependent transcription and ERK nuclear translocation. *Neuron*. 1998;21(4):869–883. doi:10.1016/S0896-6273(00)80602-9

35. Jung EL, Song HS, Park MP, Kim SH, Shim BS, Kim B. Ethanol extract of *Oldenlandia diffusa Herba* attenuates scopolamine-induced cognitive impairments in mice via activation of BDNF, P-CREB and inhibition of acetylcholinesterase. *Int J Mol Sci*. 2018;19(2):363. doi:10.3390/ijms19020363

36. Jin N, Ma D, Gu J, et al. O-GlcNAcylation modulates PKA-CREB signaling in a manner specific to PKA catalytic subunit isoforms. *Biochem Biophys Res Commun*. 2018;497(1):194–199. doi:10.1016/j.bbrc.2018.02.053

37. Liu F, Iqbal K, Grundke-Iqbal I, Hart GW, Gong CX. O-GlcNAcylation regulates phosphorylation of tau: A mechanism involved in Alzheimer's disease. *Proc Natl Acad Sci U S A*. 2004;101(29):10804–10809. doi:10.1073/pnas.0400348101

38. Xie S, Nana J, Gu J, et al. O-GlcNAcylation of protein kinase A catalytic subunits enhances its activity: A mechanism linked to learning and memory deficits in Alzheimer's disease. *Aging Cell*. 2016;15(3):455–464. doi:10.1111/acel.12449

39. Jiang C, Hou X, Wang C, et al. Hypoglycosylated hFSH has greater bioactivity than fully-glycosylated recombinant hFSH in human granulosa cells. *J Clin Endocrinol Metab*. 2015;100(6):E852–E860. doi:10.1210/jc.2015-1317

40. Dong L, Hu Y, Zhou L, Cheng X. P2X7 receptor antagonist protects retinal ganglion cells by inhibiting microglial activation in a rat chronic ocular hypertension model. *Mol Med Rep*. 2018;17(2):2289–2296. doi:10.3892/mmr.2017.8137

41. Lenertz LY, Wang Z, Guadarrama A, Hill LM, Gavala ML, Bertics PJ. Mutation of putative N-linked glycosylation sites on the human nucleotide receptor P2X7 reveals a key residue important for receptor function. *Biochemistry*. 2010;49(22):4611–4619. doi:10.1021/bi902083n

42. Cai L, Gu Z, Zhong J, et al. Advances in glycosylation-mediated cancer-targeted drug delivery. *Drug Discov Today*. 2018;23(5):1126–1138. doi:10.1016/j.drudis.2018.02.009

43. Lu S, Yin X, Wang J, et al. SIRT1 regulates O-GlcNAcylation of tau through OGT. *Aging (Albany NY)*. 2020;12(8):7042–7055. doi:10.18632/aging.103062

44. Hacker B, Schultheiß C, Döring M, Kurzik-Dumke U. Molecular partners of *hNOT/ALG3*, the human counterpart of the Drosophila NOT and yeast *ALG3* gene, suggest its involvement in distinct cellular processes relevant to congenital disorders of glycosylation, cancer, neurodegeneration and a variety of further pathologies. *Hum Mol Genet*. 2018;27(11):1858–1878. doi:10.1093/hmg/ddy087

45. Fernández-Real JM, McClain D, Manco M. Mechanisms linking glucose homeostasis and iron metabolism toward the onset and progression of type 2 diabetes. *Diabetes Care*. 2015;38(11):2169–2176. doi:10.2337/dc14-3082

46. Gao Y, Liu J, Bai Z, et al. Iron down-regulates leptin by suppressing protein O-GlcNAc modification in adipocytes, resulting in decreased levels of O-glycosylated CREB. *J Biol Chem*. 2019;294(14):5487–5495. doi:10.1074/jbc.RA118.005183

47. Nonaka M, Kim R, Fukushima H, et al. Region-specific activation of CRTC1-CREB signaling mediates long-term fear memory. *Neuron*. 2014;84(1):92–106. doi:10.1016/j.neuron.2014.08.049

48. Sassone-Corsi P. CREM: A master-switch regulating the balance between differentiation and apoptosis in male germ cells. *Mol Reprod Dev*. 2000;56(2 Suppl):228–229. doi:10.1002/(SICI)1098-2795(200006)56:2%2B<228::AID-MRD2>3.0.CO;2-B

49. Yang S, Chatterjee S, Cipollo J. The glycoproteomics-MS for studying glycosylation in cardiac hypertrophy and heart failure. *Proteomics Clin Appl*. 2018;12(5):e1700075. doi:10.1002/prca.201700075